Studies of Glacial and Periglacial Environments on Mars

Thesis

Studies of Glacial and Periglacial Environments on Mars

Jason David Ramsdale

MGeol

31st October 2016

A thesis submitted to the Open University in the subject of Planetary Geology and Geomorphology for the degree of Doctor of Philosophy.

Department of Physical Sciences

Open University

Abstract

This thesis presents the development and application of a grid-based mapping approach that provides an efficient solution to the problems of mapping small landforms over large areas. The approach allows the cataloguing of landform classes, of multiple sizes, efficiently in a single pass. The speed at which the data could be recorded allowed for the first continuous, full resolution mapping of decametre-scale landforms in CTX images on hemispherical-scale maps. The discrete, tabular nature of grid mapping opens up the possibility of citizen science meaning the grid mapping approach could have considerable future use and impact.

The main scientific goal of this thesis was to determine the distribution and origins of ice-related landforms in the northern plains, and provide insight as to whether these landforms are related to distinct geological or geomorphological units. To accomplish this, I used the grid mapping approach to explore a large tract covering the Arcadia Planitia region of the northern plains of Mars. In addition, I was able to compare these results to two other sister-studies performed in the Utopia and Acidalia Planitia regions of Mars.

To explore possible sources of ice I performed a detailed study of the Rahway Vallis system. This found an assemblage of terraces, channels and sinuous ridges in Rahway Vallis that are topographically and morphologically consistent with either a draining lake, or a melting, once liquid, ice-body, and is indicative of a flow of volatiles into the northern plains and large scale shifts in ground ice stability.

Overall, this thesis demonstrates the dominant effects of the deposition and sublimation of the Latitude Dependent Mantle in shaping recent landscapes on the northern plains of Mars. There was little evidence for thaw-related landforms, and evidence for a fluvial origin for ice in the near surface is circumstantial, or has been erased or covered.

Acknowledgements

This thesis was supported by a UK Science and Technology Facilities Council (STFC) studentship and a British Society of Geomorphology (BSG) Post Graduate Conference Grant. A special thanks to my supervisors Matt Balme, Susan Conway and Colman Gallagher for all you have done over the course of this project. Additionally I'd like to thank Axel Hagermann, John Bridges and Holly Hedgeland for a thought provoking examination and their corrections. Thank You!

For those of you that helped this work,
I ought to sing a song, dance and twerk,
But for fear of the trauma that could do,
I've made you this image and hope it'll do!

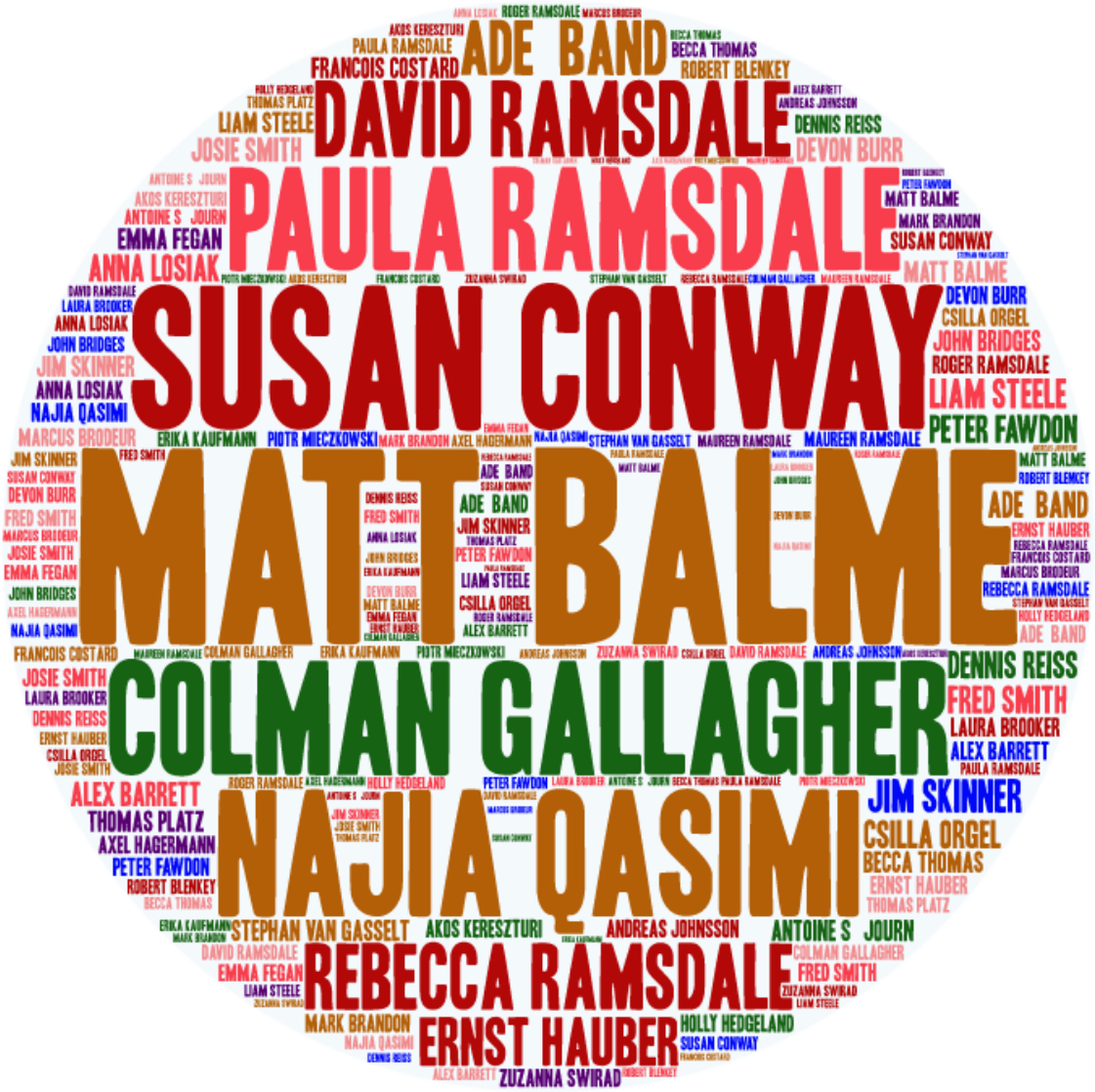

Contents

Table of Figures

1. Introduction

From polar craters on airless bodies like the Moon and Mercury (e.g. Ingersoll et al., 1992), through the icy bodies of Pluto and Charon (e.g. Stern, 1992) to the lonely comets of the Oort cloud (e.g. Stern, 2003) our solar system is rich in water-ice. Quantifying how much ice, where this ice is and understanding its history is key to learning about the evolution of our solar system and – because water is often seen as a prerequisite for life – the origins of life itself. Some of the most studied and Earth-like ice-rich environments in our solar system can be found on Mars. For example, each pole has both a permanent and a seasonal ice cap, and the high latitude areas contain abundant ground ice in the uppermost parts of the soil (Smith et al., 2009). The permanent ice cap at the Martian northern pole is about a kilometre thick, covers an area about the size of Britain and France combined, and is composed largely of water ice (James et al., 1992). The southern permanent cap only covers an area around the size of England and has a small component of carbon dioxide ice. However, of the seasonal caps, which are made from CO_2 and which occur in each hemisphere's winter, the southern cap is bigger due to Mars being furthest from the Sun during the southern hemisphere's winter. Like the Earth, Mars also holds ice beneath the surface in pore spaces between soil and rock particles. The contraction and expansion related to freeze-thaw cycles leads to the development of recognisable landforms that we can observe in high resolution images.

This introduction provides a brief overview of the state of research into the Martian volatile budget to highlight open questions. After identifying broad open questions, the chapter will identify the specific research questions tackled in the thesis before outlining how they will be answered. The final part of the chapter sets out the structure of the thesis and explains contributions made to certain areas by my collaborators.

1.1. **A Brief Overview of the Martian Geography**

Mars shows a dramatic topographic and geological contrast between the northern and southern hemispheres (see *Figure 1.1*). The northern hemisphere is flatter with few impact craters and much lower elevations than the southern hemisphere. The transition between the Northern Lowlands and Southern Highlands is referred to as the global dichotomy boundary. Sharp (1973) describes the global dichotomy boundary as being characterized by an abrupt, complex, planimetric escarpment separating smooth, flat lowland areas from the heavily cratered uplands.

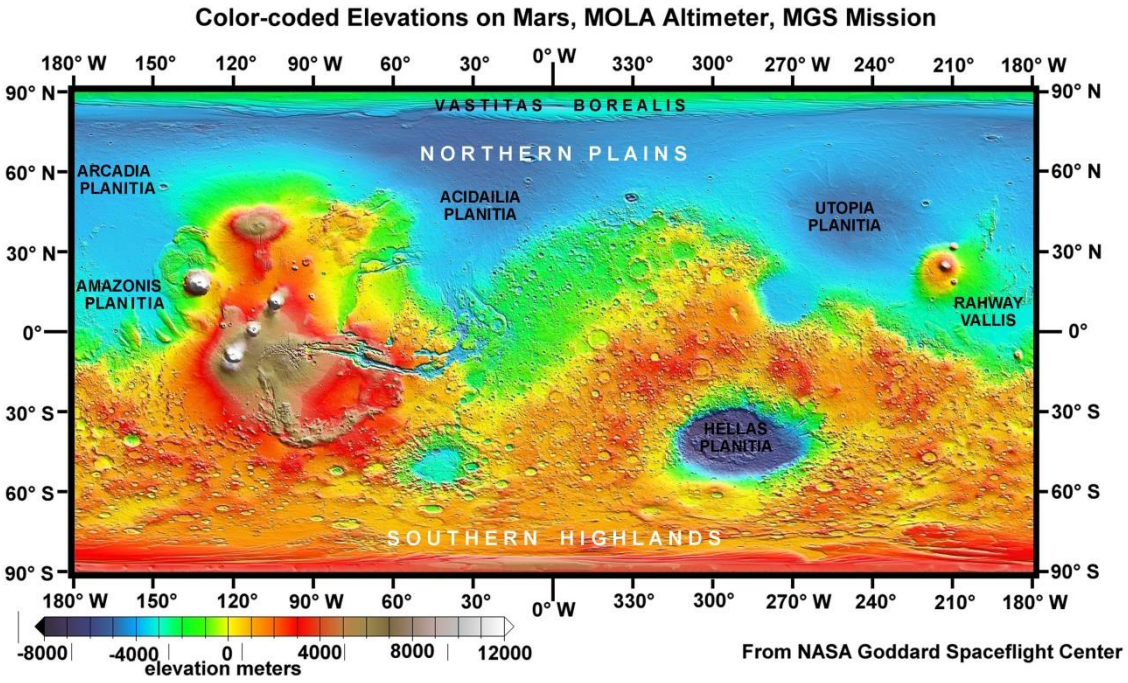

Figure 1.1 Shaded relief and colour topographic images from the Mars Orbiter Laser Altimeter (MOLA) were created by the MOLA team at Goddard Space Flight Center, NASA adapted to show key locations from this thesis. Image credits are to the MOLA team.

The crustal dichotomy implies a difference in crustal thickness of the two hemispheres and three types of explanations have been invoked including endogenetic causes, and single and multiple impacts. A possible endogenetic cause would be sub-crustal erosion over a large, long lasting mantle convection cell (Lingenfelter and Schubert, 1973; Wise et al., 1979). The single impact hypothesis was suggested by Wilhems and Squyres (1984); the

impact would have been gigantic and formed what is referred to as the Borealis basin. The multiple impact hypothesis was suggested by Frey and Schultz (1988, 1990) arguing that irregularity in the shape of the northern plains' margins better fits a hypothesis involving a number of large impact events, as opposed to one enormous one. The relative surface ages of geological units on Mars are well established through stratigraphic and crater density relationships (e.g. van-Gasselt and Neukum, 2011; Michael, 2013; Tanaka, 1986; Tanaka et al., 2014, 2005, 2003). The recent global geologic map of Mars shows that units of Noachian age cover roughly 45 percent of the Martian surface, Hesperian-aged units cover 29 percent and the Amazonian units cover about 26 percent (Tanaka et al., 2014). The distribution of surface ages are not uniform however, large portions of the southern hemisphere display Noachian surface ages significantly older than the northern hemisphere which is largely Amazonian (Tanaka et al., 2014).

The dichotomy is dissected by large valleys identified as outflow channels. The discovery of these large outflow channels on Mars was an important discovery from the Viking era of planetary science (the time when the Viking Orbiter and lander spacecraft were operational: 1975-1982). The outflow channels were the first indications that Earth was not the only planet in the solar system to possess large volumes of water. The outflow channels are enormous in scale, up to hundreds of kilometres in width and a few thousand kilometres in length and up to a few kilometres in depth. Largely originating at fractured chaos terrain regions of the Martian surface, containing streamlined islands and tracing consistently downslope suggests flow of liquid water (e.g. Lucchitta, 2001). The geomorphology and sources have led to the interpretation of cataclysmic outburst floods, but other interpretations include origin by glacial (e.g. Lucchitta, 2001), volcanic (Leverington, 2004) and debris flow activity (e.g. Nummedal and Prior, 1981).

The Viking era also saw the discovery of widespread valley networks (Masursky et al., 1977; Milton, 1973; Sharp and Malin, 1975). Initially these valleys systems were believed

to be immature and the product of groundwater release due to undissected regions, low stream orders and drainage density values (e.g. Carr, 1995; Pieri, 1980; Squyres and Kasting, 1994). However increased resolution datasets revealed many more valleys giving higher drainage density values indicative of precipitation and surface runoff (e.g. Craddock and Howard, 2002; Hynek et al., 2010; Hynek and Phillips, 2003) as shown by Figure 1.2. Mapping and crater density analyses show the vast majority of the valley networks formed around the Noachian-Hesperian boundary (~3.71 Ga; Hynek et al., 2010; Michael, 2013). If these valley networks are formed through precipitation they represent some of the best evidence for profound climate change and a transition from a warm, wet early Mars into the cold, relatively dry planet we see today.

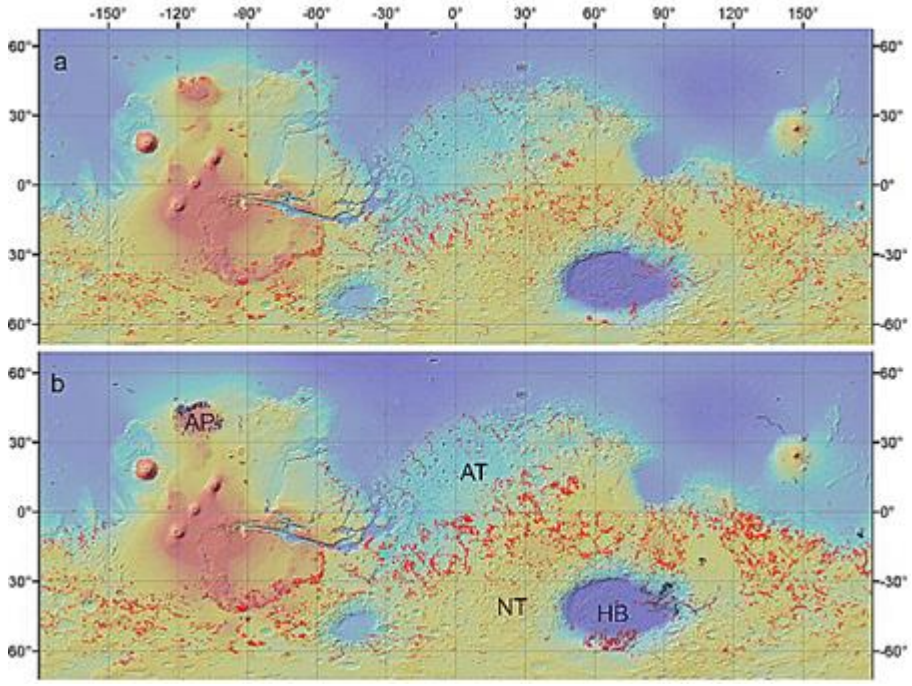

Figure 1.2 Global comparison of valleys identified by Carr (1995) from (a) Viking data and (b) Hynek et al. (2010) map using THEMIS data on top of a MOLA shaded relief map and MOLA topography from high (red) to low (blue).

1.1.1. **The Southern Highlands:**

The Southern Highlands of Mars (see *Figure 1.1*) are densely cratered and are, at the regional scale, reminiscent of the ancient cratered terrain of Mercury or the highlands of the Moon. Most of the highlands are between 0-5,000 m in elevation, except in the large impact basins of Hellas and Argyre. Large parts of the highlands contain smoother, less cratered inter-crater plains which are believed to be largely volcanic in origin (e.g. Bandfield et al., 2000). However, in complete contrast to the Moon or Mercury, the boundary between the Martian Highlands and Lowlands appears to be dissected by fluvial channels from what looks to be massive outburst floods (e.g. Baker, 1982). The Southern Highlands are also host to the vast majority of Mars' valley networks which are some of the best evidence for prolonged and at least quasi-stable water on the martian surface (Hynek et al., 2010). The main exceptions to the Southern Hemisphere being areas of high elevation are the impact basins of Hellas and Argyre (see *Figure 1.1*).

1.1.2. **The Northern Lowlands/Borealis basin**

The Northern Lowlands (see *Figure 1.1*), Northern Plains or Borealis basin covers the most northern 40% of Mars. The elevation of the Northern Lowlands is largely between --5000 to -4000 m. If the Northern Lowlands were formed by a single impact crater it would be the largest impact basin in the solar system (i.e. the Borealis basin). The northern lowlands are much less cratered than the Southern Highlands indicating much younger surface ages than that of the Southern Highlands (e.g. Barlow, 1990).

1.1.3. **Tharsis and Elysium**

Southern Arcadia and Amazonis Planitia are bounded by Tharsis to the east and Elysium to the west. Tharsis is the largest volcanic province on Mars including Arsia Mons, Ascraeus Mons and Pavonis Mons and is often associated with Olympus Mons to the north. Elysium is the second largest volcanic region on Mars and includes the volcanoes Albor Tholus,

Elysium Mons and Hecates Tholus. Both regions show lava flows with crater counts indicative of activity dating to the late Amazonian (Neukum et al., 2004).

1.1.4. Layered Polar Deposits

Both the southern and northern polar caps display layered features called polar-layered deposits. The layered deposits are believed to have formed from seasonal deposition of dust and ice (Laskar et al., 2002). The Martian polar layered deposits have been well mapped and characterised by previous studies (e.g., Blasius et al., 1982; Tanaka et al., 2014, 2005; Tanaka and Scott, 1987) and are not the main focus of this project. Instead this project focuses on mapping the presence of more difficult to identify water ice on Mars.

1.2. A Brief Chronology of the Martian Environment

It is widely thought that Mars was formed by the accretion of the solar nebula along with Earth and the other solar bodies. During the early formation of the solar system the high temperature gradient led to the partitioning of elements within the solar system. The degassing of volatile elements (such as hydrogen, helium and water) from the material composing the innermost part of the solar system left the so-called "rocky planets" dominated by refractory elements (i.e. silicates, iron and nickel). The elements transported outward from the inner solar system by prevalent solar winds are found within the volatile-rich gaseous and ice-rich outer planets. Radiometric dates obtained from primitive chondritic meteorites indicate that Mars and the other planets were formed 4.65 billion years ago, marking the start of the Martian geological period known as the Pre-Noachian (van-Gasselt and Neukum, 2011) which continued to about 4.5 Ga.

After the Pre-Noachian, was the Noachian (4.5 to 3.71 Ga; Michael, 2013). The Noachian (and its terrestrial counterpart, the Hadean) was characterised by intense meteorite bombardment and extensive surface volcanism (van-Gasselt and Neukum, 2011). Unlike the Earth, which undergoes intensive resurfacing due to plate tectonics and a highly active hydrosphere, Mars still hosts surface rocks dating from the Noachian, cropping out in the

rims of mega-impact basins such as Hellas, Isidis and Argyre (Carr and Head, 2010) and found across the southern highlands.

The transition from the Noachian Epoch into the Hesperian (around 3.71 Ga; Michael, 2013) was marked by a decrease in impact events to around present day rates (Mutch and Saunders, 1976). This decrease in impact rate left fluvial and volcanic activity as the dominant surface alteration processes (e.g. Head, 2007). The Hesperian is thought to have undergone a peak in volcanism with the emplacement of vast lava-flow flood deposits such as Hesperia Planum, Lunae Planum and Syrtis Major (e.g. Baratoux et al., 2013). The Hesperian surfaces provide evidence for tectonic activity with the uplift of Tharsis imposing tensional stresses on the Martian lithosphere and resulting in the formation of Valles Marineris (Mutch et al., 1976).

The last three billion years is accounted for by a single epoch, the Amazonian (around 3.0 Ga to present; Michael, 2013). This is an extraordinarily long period of time, and surface conditions varied enormously throughout the epoch. The early Amazonian is largely characterised by remnant volcanism declining from the peak during the Hesperian, but as volcanism waned towards the middle Amazonian, other processes began to dominate (Mutch et al., 1976). The prevalent factors in shaping the Martian surface since the middle Amazonian include aeolian activity (Leovy, 2001; Lorenz, 2009), fluvial processes (e.g. Dickson et al., 2009) and glacial and periglacial activity (Kargel et al., 1992; Madeleine et al., 2009; Morgan et al., 2009; Soare and Osinski, 2009). As on Earth, the relative balance between glacial, fluvial and aeolian processes varied with both time and space, with "ice ages" caused by variations in orbital parameters dominating geomorphological change in the last few million years (Baker et al., 2010; Head et al., 2003; Schon et al., 2009; Souness and Hubbard, 2012), and perhaps for millions of years before that.

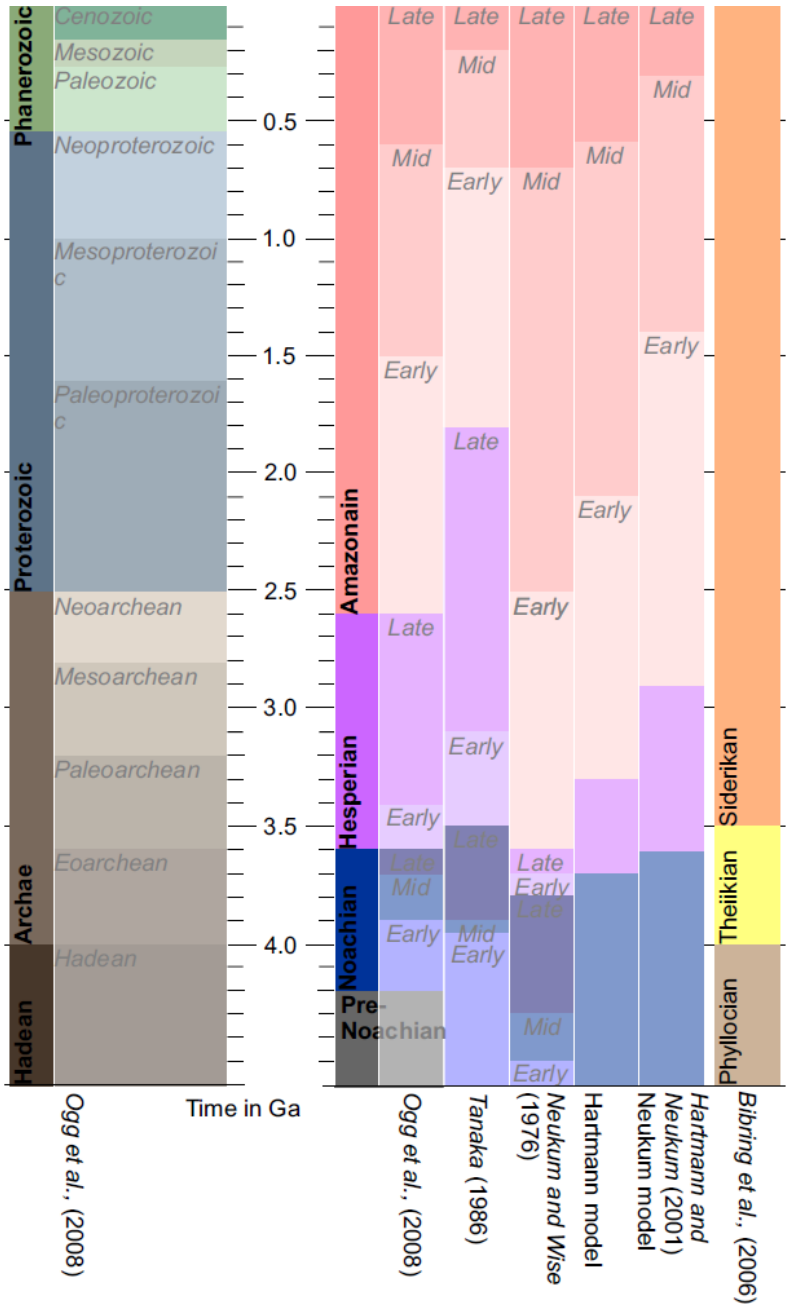

Figure 1.3 A chart to compare the time periods of Earth (left) and Mars (right) adapted from van-Gasselt and Neukum (2011) by Fawdon (2016).

1.3. **The Northern Ocean as a source of ice on Mars**

Otherwise dubbed as the Palaeo-Ocean or Oceanus Borealis, the existence of an ancient northern ocean on Mars is a hypothesis stating that the Vasitias Borealis basin has, on either a single or multiple occasions, been filled by an ocean of liquid water. If such an ocean existed, it would have covered around one quarter of the planet's surface with a depth of up to 1.5 km (Brandenburg, 1987). Initial observations of Viking images remark

the absence of possible cliffs and beaches on Mars (e.g. Masursky et al., 1977). However, Brandenburg (1987) presented observations of putative ancient shorelines and deltas around Shalbatana and Hrad Vallis (Brandenburg, 1987), and others noticed that large outflow channels (Masursky et al., 1977) and valley and delta networks (e.g. Di Achille and Hynek, 2010) were at the approximate zero elevation contour around the global dichotomy boundary. These observations lent evidence to a possible ancient northern ocean hypothesis, and were supported by calculations of Mars' original water inventory (McElroy et al., 1977) which gave maximum water values only twice that needed to fill the Vastitas Borealis basin and sedimentary deposits (Lucchitta et al., 1986). Parker et al. (1993, 1989) observed what appeared to be erosional and depositional strandlines in close proximity, and likened their geomorphology to terrestrial shoreline environments.

A new wave of analysis of the northern ocean hypothesis came with the availability of Mars Global Surveyor data (Albee et al., 1998). In particular Mars Orbiter Laser Altimeter (MOLA; Smith et al., 2001, 1993) data allowed for the testing of the palaeo-shoreline hypothesis. Head et al. (1998) found the elevations of the shorelines to be largely consistent with the presence of an equipotential surface. In contrast, though, Malin and Edgett (1999) report that the available MOC images at the time failed to support a shoreline hypothesis but conceded that palaeo-shoreline indicative landforms are difficult to identify even on Earth. However, other studies found that deviations from an equipotential surface, particularly on a long wavelength, appeared too great to be consistent with a palaeo shoreline (Head et al., 1999), but Perron et al. (2007) used a true polar wander model that accounted for the long-wavelength topography variations of the shorelines by taking into account deformation caused by changes in the geographical location of Mars' spin axis. These observations have since been supported by studies of the location of the termination of Martian valley networks and deltas (de Achille and Hynek, 2010) and by observations of possible mega tsunami deposits (Rodriguez et al., 2016). The

hypothesis of an extinct northern ocean is further supported by MARSIS radar data revealing dielectric constants consistent with low-density sedimentary deposits and ground ice (DiBiase et al., 2013). Atmospheric deuterium measurements suggests that there could be enough water present within the Northern Lowlands to form an ocean equivalent to Earth's Arctic Ocean (Villanueva et al., 2015).

1.3.1. **Could an ocean ever have existed on Mars?**

To understand whether early Mars could have supported an ocean we need to understand the thickness and composition of the primordial atmosphere, the heat output of the early Sun, and how the early atmosphere might have responded to other parameters. Constraining these variables for modelling is undoubtedly difficult as many of the parameters rely on largely untestable assumptions.

Mars' early atmosphere likely formed largely from impact related volatile release (e.g. Owen, 1992). This early atmosphere could have been relatively thick, with volatiles being released faster than they could be dissipated into space. However, much of these volatiles would have reacted with the surface and been reincorporated into the surface through weathering (Jakosky and Ahrens, 1979). Mars was believed to have taken longer to accrete than Earth and would have had more time for the atmosphere to be reincorporated between impacts meaning early Mars would still be considerably colder than early Earth (Jakosky and Ahrens, 1979). Degassing from large scale impact induced volcanism may have contributed to a thicker atmosphere on early Mars and Earth (Fanale, 1971). Although modelling of large impacts suggests impact erosion of the atmosphere, particularly given Mars' lower mass and surface gravity in comparison to that of Earth's (Melosh and Vickery, 1989).

When modelling Mars' early atmosphere it is difficult to parameterise the heat output of the Sun. Mars' distance from the Sun means that it receives roughly half as much sunlight as the Earth but it has also been suggested that the early Sun may have shone at 70% of its'

current luminosity (Endal and Schatten, 1982; Gough, 1981; Ulrich, 1975). A faint early Sun proves problematic when trying to model conditions that would provide a stable Martian ocean. Recent reviews (e.g. Feulner, 2012) highlight that the faint young sun hypothesis appears to have discrepancies with conditions inferred for early Earth. The exact output and timings of the Sun's luminosity are difficult to test suggesting that on their own they cannot dismiss a Martian ocean hypothesis.

It is possible that greenhouse gasses could have raised temperatures in the early Martian atmosphere but it has been argued that these gases are short-lived and lack a viable recharge mechanism (e.g. Anders and Owen, 1977; Kuhn et al., 1979; Kuhn and Atreya, 1979; Sagan and Mullen, 1972). It has been suggested that comets may have provided the volatiles needed to create the oceans on Earth and Mars (Carr, 1989; Chyba, 1987). Determining the timing and rate of build-up then loss to the atmosphere is difficult for four billion years ago but as a minimum estimate it is likely the Martian atmospheric pressure was 0.5 bar thick, and pressures greater than 1 bar do not seem unreasonable (Craddock and Howard, 2002). This is compatible with current day Earth and is in stark contrast to current Martian surface pressures which are around 0.006 bar. The decline in the Martian atmosphere was likely episodic with periods of higher and lower pressure due to the stochastic nature of volcanic outgassing and impact cratering (Craddock and Howard, 2002). Given the difficulties in calibrating various parameters, we should consider the Martian landforms collectively before attempting to force the interpretation of geomorphic features on Mars to fit the early Martian climate models.

1.4. **The influence of Climate on the distribution of ice on Mars**

The Martian average surface temperature at present is around -60°C ranging between +27 and -133°C, with atmospheric water levels three orders of magnitude lower than on Earth (Read and Lewis, 2004). The extreme cold, dry, low pressure conditions of Mars mean that water ice is unstable at the planet's surface, with the major exception of the

polar regions (Forget et al., 2006). Mars' environment is often compared to the Dry Valleys of Antarctica (Marchant and Head, 2007; Souness and Hubbard 2012). However, this is a limited analogy as Mars is far colder, dryer and has much lower atmospheric pressure that the Dry Valleys.

On 100 ka timescales, the spatial stability of water ice on Mars fluctuates due to changes in surface temperatures as a result of Mars' varying orbital obliquity and eccentricity, with increased polar insolation at high obliquity (up to 60 ° in the last billion years; see Laskar et al., 2004) allowing equatorward migration of ice (Jakosky and Carr, 1985; Mellon and Jakosky, 1995). The presence of possible glacial geomorphological forms in middle to high latitudes have led some authors to suggest Mars has undergone significant climate change and possibly Milankovitch style cyclical changes (Kargel, 2004; Read and Lewis, 2004; Ward, 1992). During the Amazonian, the most recent geological period on Mars (0-3 Ga), Martian obliquity is thought to have varied between 15° and 35° with a mean of around 24° for the last 3 million years (see *Figure 1.4*; Head et al., 2003; Laskar et al., 2004). Furthermore, orbital modelling suggests the overall mean obliquity for Mars is around 40° with a 63% probability that Mars reached an obliquity of 60° within the last billion years and 89% in the last three billion years (Laskar et al., 2004).

High resolution climate modelling and geomorphological evidence (Head et al., 2003; Kargel, 2004; Read and Lewis, 2004; Ward, 1992) suggest Mars undergoes low latitude ice growth when approaching higher obliquity as this configuration allows for increased solar radiation at the poles (Costard et al., 2002; Forget et al., 2006). Increased polar insolation increases polar sublimation, which in turn feeds equatorward moisture migration (e.g., Head et al., 2003) allowing for mid-latitude condensation and possible growth of permafrost and glaciers (Forget et al., 2006; Schon et al., 2009). Geomorphological (Carr and Head, 2010) and spectral (Vincendon et al., 2010a, 2010b) indications of ice present in the low latitudes today suggest that ground ice has equilibrated with high obliquity

conditions, under which the equator would receive lower levels of insolation and allow for the build-up of ice, and that the present configuration of ice deposition may be atypical of the Amazonian period.

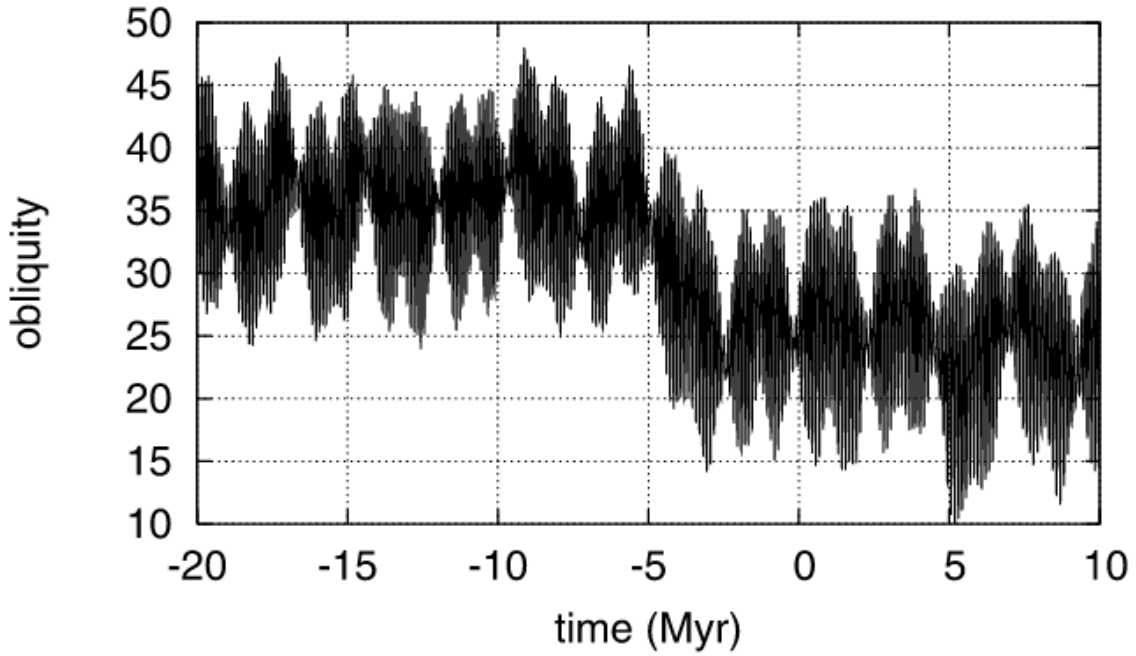

Figure 1.4 Obliquity (in degrees) from -20 to +10 Myr of Mars from (Laskar et al., 2004).

However, evidence of aqueous weathering and carbonate deposits seen in Martian meteorites (Fassett and Head, 2005; Hartmann and Neukum, 2001; McKay et al., 1996) have led some workers to put forward a model of a warmer, wetter early Mars than observed today (e.g., Kargel, 2004). Antagonists to the warmer, wetter model have argued that the absence of early atmospheric CO_2, a greenhouse gas, would have rendered the Martian surface too cold for stable liquid water (e.g., Bibring et al., 2005). Proponents have countered that, irrespective of liquid water's medium to long-term stability, fluvial processes are required to explain the surface forms of Noachian Mars, especially the valley networks (e.g., Kargel, 2004). Thus there appears to have been both a long term change in climate from (probably) warmer and wetter conditions in the Noachian, to drier colder conditions seen today, as well as shorter-period variations in Mars' recent climate driven

by orbital variations. The stability and distribution of ice could therefore be a function of processes that have operated over one or on both of these timescales.

It has been suggested that ice deposits shielded from the atmosphere by dust and debris (and hence from sublimation) could survive for many millions of years (Bryson et al., 2008; Smoluchowski, 1968; Touma and Wisdom, 1993). Direct imaging of water ice is rare due to the instability of water ice on the Martian surface, and without direct sampling the mode of formation and the proportions of ice and dust are difficult to determine. To combat this we study and attempt to identify landforms indicative of shallow sub-surface water ice. Despite the increasing number of highly successful planetary missions and a wealth of new orbital data, there is a lack of coordinated research and mapping programmes focussed on ice indicative landforms.

The northern hemisphere of Mars is of particular interest: there is the possibility of ancient ice surviving here, preserved from a putative ancient ocean, as well as recently deposited and modified ice, the spatial distribution of which is perhaps indicative of the processes that deposited it. This can be encapsulated in several broad research questions.

1.5. **Research Questions**

- What is the evidence for ground ice in the northern plains?
- What is the distribution of ground ice and can it be related to distinct latitudinal bands, different geological units, physiographic provinces, and/or topography?
- What insights can we gain from understanding the spatial distribution of the ground ice in the northern plains with regards to its origins and history?

1.5.1. **Context of this research**

This thesis reports my research related to these research questions. In part, it fits alongside an International Space Science Institute (ISSI) multi-collaborator project that both targets compelling research questions about Mars' Northern Plains, and creates a

coordinated European mapping project with the potential to foster future systematic mapping initiatives. I was an integral part of this team and provided both data and new methods and approaches to mapping.

1.5.1.1. *The ISSI Northern Plains Mapping Project*

The ISSI team used the latest mid- to high-resolution images of Mars to study its northern plains regions (Acidalia, Utopia, Arcadia) in order to compare and contrast the assemblages of landforms and their latitudinal distribution across the different regions, and to attempt to determine the origin of some of these materials. Our intent was to focus on surficial deposits related to ice and regolith, and to document landforms or features with unknown origins (e.g. small cones that might have formed by volcanic, mud-volcanic, or cryotic (ice-related) processes) and test hypotheses for their formation with our mapping data. We compared and contrasted the different basins and used impact crater statistics to find ages of the different surfaces.

The key questions that the ISSI project sought to address include:

- What is the distribution of ice-related landforms in the northern plains, and can it be related to distinct geological or geomorphological units?

- What does the distribution of these units and landforms tell us about the ice-content, sediment types, and environmental evolution of the northern plains?

- What is the type and source of this ice? Is the origin of the ice syngenetic or epigenetic? (i.e., was the ice deposited with the sediments, or later?)

- How old are landforms and surfaces in the northern plains and are the stratigraphic relationships and inferred surface ages consistent between the three plains regions?

- What is the relationship between the latitude dependent mantle and (i) the suite of landforms indicative of ground ice, and (ii) other geological units in the northern plains?

- What are the distributions and unit associations of very recent landforms thought to be indicative of thaw of ice or snow (e.g. gullies, clastic networks such as solifluction lobes, stone polygons, etc.)?

1.5.1.2. *How this thesis contributes to the ISSI project*

This thesis focuses on presenting the results and interpretations stemming from my observations made of the Arcadia and Amazonis Plantita regions. Arcadia Planitia forms one of the three study areas from the ISSI study, and Amazonis Planitia is an "upstream" region that might have contributed volatiles to the Arcadia region.

The observations and results/interpretations from these areas are my own unless otherwise stated (in chapter 5, for example, I compare my Arcadia data with the results of the two other study areas from the ISSI project, Utopia Planitia and Acidalia Planitia). I suggested and took a lead role in developing the grid mapping approach described in chapter 3, to which multiple team members provided test observations, before it was then implemented into the wider ISSI project.

1.6. **Thesis Structure**

This first chapter sets the theme of the thesis and highlights how current and past research have been the drivers behind this research.

Chapter 2 presents a review of the current Martian literature regarding the evidence for ground ice in the northern plains.

Chapter 3 outlines the methods used to tackle this project's research questions and includes an in-depth description and assessment of "Grid Mapping", an approach for mapping small features over large areas that I took lead the in developing and putting into practice as part of the ISSI team.

Chapter 4 presents results from my grid mapping of Arcadia Planitia and contextual mapping of a large channel system.

Chapter 5 discusses the implications of the grid mapping, the contextual study of Arcadia Planitia, and the northern plains as a whole.

Chapter 6 presents results from Rahway Vallis, a possible source of water and sediment for Arcadia Planitia. The large majority of Chapter 6 is comprised of a first authorship paper published in Icarus regarding various landforms suggestive of liquid water in Rahway Vallis.

Chapter 7 provides a discussion of the implications of the results of the work presented in this thesis and how they tie in with current martian literature and future projects.

Chapter 8 provides a synthesis of conclusions drawn from each of the interlinked studies that make up respective chapters.

1.7. **Published or to be submitted work**

Parts of this thesis have been published or have been prepared for publication in the peer reviewed literature. Table 1.1 shows the chapters for which this is the case and outlines the contribution each author has made to this work. The contents of these manuscripts remain unchanged with the exception of slight formatting alterations to allow for figure and table

numbers to run consecutively with the rest of the thesis and slight changes to tense and first person singular and plurals where appropriate.

Table 1.1 Author Contributions (in %) to Chapters.

Chapter	Title	Author	Concept and Design	Data Collection	Analysis and Conclusions	Manuscript Prep	Journal Status
3.5	Grid-based mapping: a method for rapidly determining the spatial distributions of small features over very large areas.	Jason Ramsdale Matt Balme Susan Conway Colman Gallagher Other authors	70 10 5 5 10	90 2 2 2 4	75 5 10 5 5	75 5 5 5 10	To be submitted to Icarus
6	Ponding, draining and tilting of the Cerberus Plains; a cryolacustrine origin for the sinuous ridge and channel networks in Rahway Vallis, Mars.	Jason Ramsdale Matt Balme Susan Conway Colman Gallagher	60 20 10 10	100 - - -	80 5 10 5	80 10 5 5	Published in Icarus DOI: 10.1016/j.icarus. 2015.03.005

2. Literature Review: ground ice in the northern plains

This chapter discusses past work related to the research covered in this Thesis. General information about the evolution of the martian surface and climate is found in Chapter 1. Here, I summarise key literature information about the various landforms and geological formations related to water-ice on Mars, and describe how this information is related to the research questions outlined in Chapter 1.

I begin by summarising the key landforms thought to have formed by ice or water related processes that exist in the northern plains of Mars. I have concentrated on landforms visible in 6 m/pixel CTX images, the highest resolution data that have a near-global coverage. Higher resolution data such as MOC NA or HiRISE can provide information, but as these data have very limited spatial coverage they cannot be used for comprehensive surveys of landforms.

I have grouped these ice-related landforms into three somewhat overlapping groups: (i) landforms that are most likely to have formed due to interactions between ice and regolith, or the deposition of ice onto or into regolith, with the origin of the ice usually being interpreted as being deposited from the atmosphere; (ii) landforms that formed as a result of the degradation via melt or sublimation of ice or ice-rich soils/bedrock; and (iii) other landforms that are commonly found in, or restricted to, the northern plains, and which have a more enigmatic origin, but which have been proposed to have formed as a result of ice or liquid water.

I then discuss what wider insights can be gained from the landforms collectively about the distribution of ground ice and the history of the northern plains. I finish this chapter discussing the possible implications of achieving a better understanding of the ice related landforms in the northern plains.

2.1. Landforms indicative of interactions between ice and the martian surface materials

2.1.1. (Not) The Polar Cap

When I refer to ground ice it is important to note that I am *not* referring to the Martian polar caps. The cap deposits each form a pole-centred mound with a maximum thickness of around 3 km (e.g. Carr and Head, 2010). Planum Boreum (the northern cap) can be subdivided into two main units; the first being a 1 km thick platy, low albedo unit that overlies the older Borealis basin fill deposits (Byrne and Murray, 2002 and Fishbaugh and Head, 2005) and the second being the younger, overlying laminations that comprise the bulk of the polar cap deposits (Tanaka et al., 2005). Planum Australe (the southern cap) appears more complex in structure but can be thought of as concentric rings with the youngest deposits in the centre (Byrne, 2009) and with older underlying layers being exposed outwards from the pole. The distinct layering displayed within the polar ice is widely attributed to alternating accumulations of dust and ice caused by alterations in Milankovitch-style orbital cycles (e.g. Toon et al., 1980), thereby giving the most complete record of recent geological events on the martian surface.

Interestingly, the average surface age between the two poles differs considerably (see *Figure 2.1*). The Boreum surface is about 100 ka, but the Australe surface is about 10 Ma (Herkenhoff and Plaut, 2000). An explanation offered by Herkenhoff and Plaut (2000) for the apparent age discrepancy is variations in the persistence of the residual CO_2 ice cap. It has been suggested that the entire northern polar ice cap may be lost during periods of high obliquity (Levrard et al., 2007) but the possibility that older layers may be protected by overlying dust deposits (Tanaka et al., 2005) has not been ruled out.

While these polar cap deposits are intriguing and are of great interest themselves they are not what we are referring to with regards to ground ice. Ground ice within the context of

this thesis is all water-ice that is found beneath Mars' subsurface either as discreet layers or within pore spaces of sediments and/or rock.

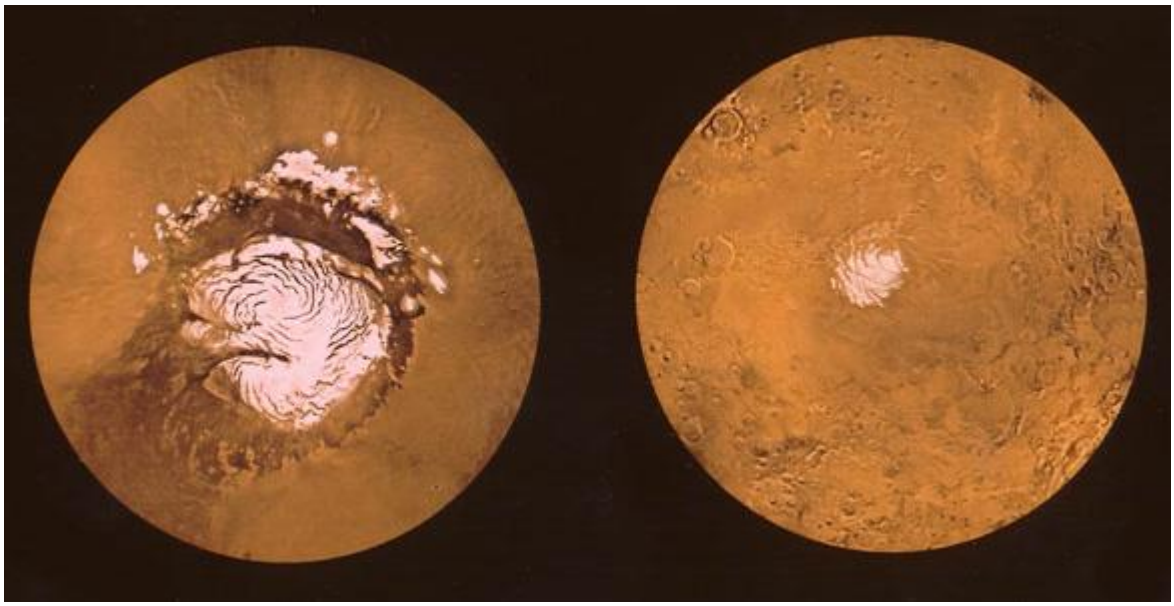

Figure 2.1 The extensive northern polar cap (left) and the smaller southern cap (right). These pictures are projections of images taken by the NASA Viking Orbiter spacecraft from Gierasch (2002).

2.1.2. **The Latitude Dependant Mantle (LDM) as evidence for ground ice**

Theoretical predictions of wide-scale ground ice on Mars (e.g., Mellon and Jakosky, 1993) and orbital spectrometer measurements of abundant near-surface water ice in the northern plains (e.g., Feldman et al 2007) are supported by the observation of a young, dissected mantle terrain present between latitudes 30° and 60° and covering 23% of the Martian surface (e.g. Costard and Kargel, 1995; Mustard et al., 2001; Kreslavsky and Head, 2002). This feature is commonly referred to as the latitude dependant mantle (LDM) and has both topographic and textural signatures. The LDM appears to be sedimentary, several metres thick, draping over and smoothing topography (Kreslavsky and Head, 2002a; Mustard et al., 2001; Schon et al., 2009). This is most apparent around ~ 100 m to 1 km-scale impact craters, whose margins appear 'softened', giving a subdued appearance. The pitted surfaces displayed by the LDM have been argued to suggest a cycle of dis-

aggregation and re-accumulation (e.g. Carr and Head, 2010). Linear, wrinkled, brain and "basketball" terrain textures have been associated with the LDM (see Figure 2.2; Kostama et al., 2006) – presumably due to degradation patterns. It is these textures that I will be refering to when I use the term "textured" or "textured terrain" when assessing distributions of such terrain in the later grid-mapping results (Chapters 3 and 4).

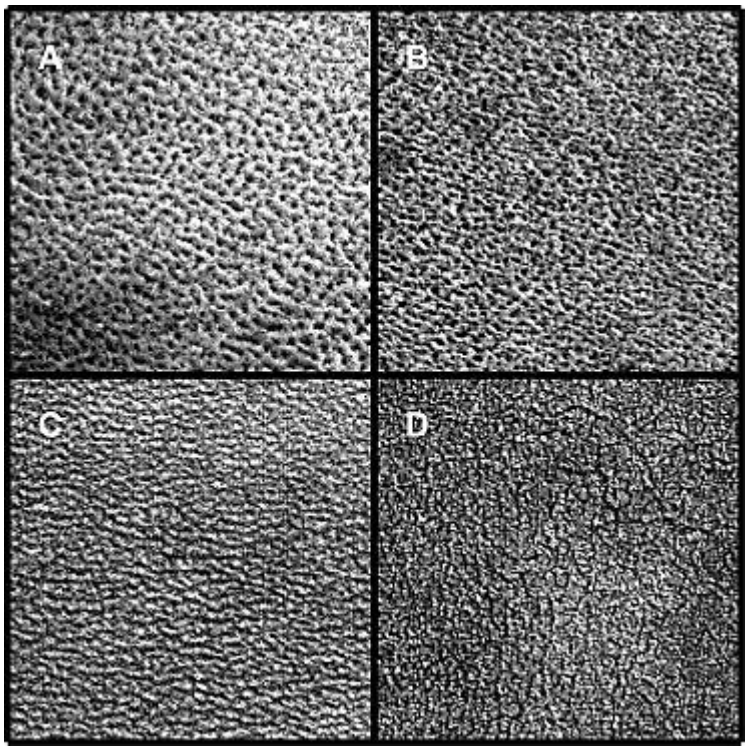

Figure 2.2 From Kostama et al., 2006. Typical textures of the mantle in the northern plains: (a) Basketball texture, (b) linear texture, (c) wrinkle texture, and (d) polygonal texture. Portions of E01/01975, E04/00026, E01/01868, and E04/00028, respectively. Each sub-image is 0.9 × 0.9 km, illumination is from lower left.

The LDM deposits have been interpreted as layers of ice-cemented dust, with each layer being formed during a glacial phase and being subject to ablation during interglacial phases (e.g. Mustard et al., 2001). Further evidence for an ice-rich mantling or near-surface deposit has been provided by the Odyssey spectrometers (Boynton et al., 2002; Feldman et al., 2004) and in-situ observations at the Phoenix landing site (Smith, 2009).

2.1.3. **Viscous Flow Features (VFFs) as evidence for ground ice, or buried ice**

Occurring largely on steep slopes in the mid-latitudes, viscous flow features (VFFs) were first identified by Squyres (1978) and displaying characteristics similar to that of terrestrial valley glaciers (Forget et al., 2006; Head et al., 2005). Where the LDM appears to be a thin draping deposit the VFFs are thicker, comparatively older and are confined to valleys (Souness and Hubbard, 2012). The diagnostic features for VFFs include primary and secondary lobes often displaying surface lineations, ridges and troughs (Berman et al., 2009; Milliken et al., 2003). Surface textures indicate flow away from the slopes with the debris often "wrapping around" obstacles to the flow (Lucchitta, 1981). Ridges, often described as “moraine-like” sometimes run both parallel and perpendicular to the VFF, and are inferred to be evidence for glacial sedimentation (Arfstrom and Hartmann, 2005; Souness and Hubbard, 2012). VFFs, unlike debris flow fans and landslides, have no associated headwall hollow and rarely rise above adjacent topography (Souness and Hubbard, 2012; van Gasselt et al., 2010).

The term VFFs stemmed from the multitude of evidence to suggest these features flowed over or around obstacles situated within high relief valleys (Milliken et al., 2003; Souness and Hubbard, 2012) with a preference for pole-ward facing slopes (Berman et al., 2009; Milliken et al., 2003; Souness and Hubbard, 2012) largely between the 30° and 60° latitudes (Head et al., 2010; Milliken et al., 2003; Souness and Hubbard, 2012; Squyres and Carr, 1986). Despite the use of repeat imaging no direct evidence for flow has yet been observed (Souness and Hubbard, 2012). However, given that terrestrial cold-based rock glaciers can have flow rates less than 1 mm per year (Rignot et al., 2002) this is not unexpected. VFFs have been interpreted as icy relics surviving in areas of relatively low insolation and protected from sublimation by a thick lag of dust or debris and surviving since the last high-obliquity driven ice age (possibly within the last few millions years; Forget et al., 2006; Levy et al., 2009; Page et al., 2009; Souness and Hubbard, 2012).

Crater density studies (Hartmann, 2005; Hartmann and Werner, 2010) and flow modelling (Milliken et al., 2003; Turtle et al., 2003) have suggested that the VFFs are geologically recent (within the last ten million years). The reliability of these dating techniques applied to VFFs has been questioned due to the complexities introduced by unknown geometries and composition alongside uncertain rates of sublimation, dissection and viscous relaxation (Pathare et al., 2005) leading Souness and Hubbard (2012) to conclude that the VFFs' age remains elusive, although certainly late Amazonian. VFFs can be divided into three distinct subtypes ; see *Figure 2.3*); lobate debris aprons (LDAs; e.g. Levy et al., 2007; Morgan et al., 2009; Squyres, 1979, 1978), glacier like forms (GLFs; e.g. Hubbard et al., 2011) and lineated valley fill (LVF; e.g. Levy et al., 2007; Morgan et al., 2009; Squyres, 1979).

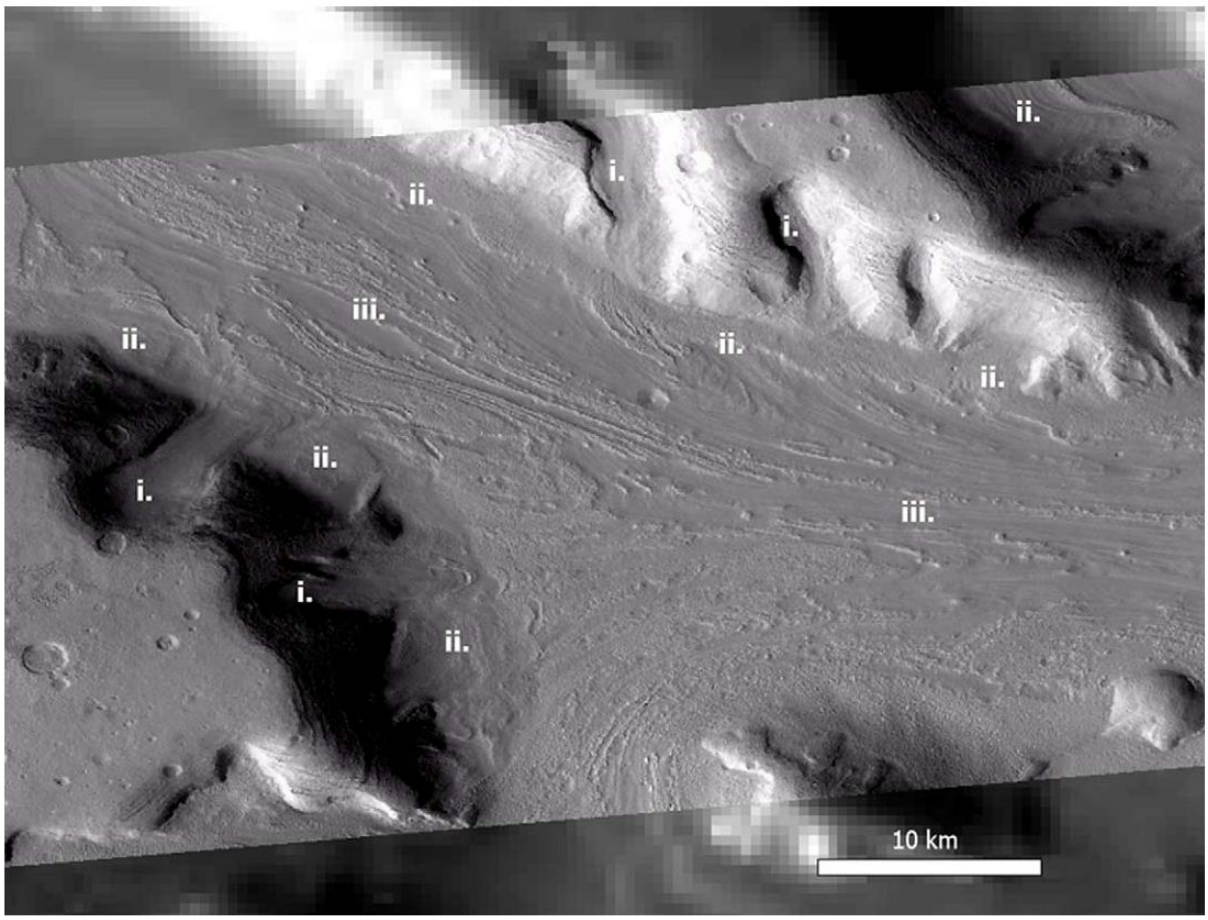

Figure 2.3 An integrated glacial landsystem on Mars of the type described by Head et al. (2010). After Souness and Hubbard (2012).Different components of this system are annotated as follows: Glacier-like forms (GLFs) (i.);Lobate Debris Apron (LDA) (ii.);

Lineated Valley Fill (LVF) (iii.). GLFs (i.) can be seen flowing from cirque-like alcoves (in the bottom left and top right of the frame) and contributing to the laterally extensive LDA (ii.) which line the valley. This LDA then converges in the valley centre to form LVF (iii.). This scene is a subset of CTX image P17_007715_2232_XN43N312W (detail centred at 47.477 E, 44.213 N in Protonilus Mensae), projected on a backdrop of THEMIS daytime infra-red (IR) imagery. The image is oriented north-up and illumination is from the left.

2.1.3.1. ***Lobate Debris Aprons (LDAs)***

LDAs were identified in the early Viking imagery (Carr and Schaber, 1977; Squyres, 1978, 1979) as distinct lobate bulges, with assumed rock and ice mix compositions, flowing down-slope from apparent cirque-like cliff faces (see *Figure 2.4*). The shallow radar (SHARAD) instrument on the MRO (Mars Reconnaissance Orbiter) gave estimates of several hundreds of metres thickness for LDAs (Holt et al., 2008; Plaut et al., 2009). Carr and Schaber (1977) interpreted LDAs as gelifluction lobes whilst Squyres (1978) argued that the LDAs' convex upper surface, a product of en-masse flow, and a lack of evidence for significant thawing at depth was more consistent with terrestrial rock glaciers. Recent work (e.g. Morgan et al., 2009) confirmed that both LDAs and LVF are comprised of the same material, display integrated flow patterns, and originate as glacier-like forms but largely have subsequently been resurfaced by a mantling material suggesting periods of both sublimation and accumulation during the Late Amazonian (Berman et al., 2015).

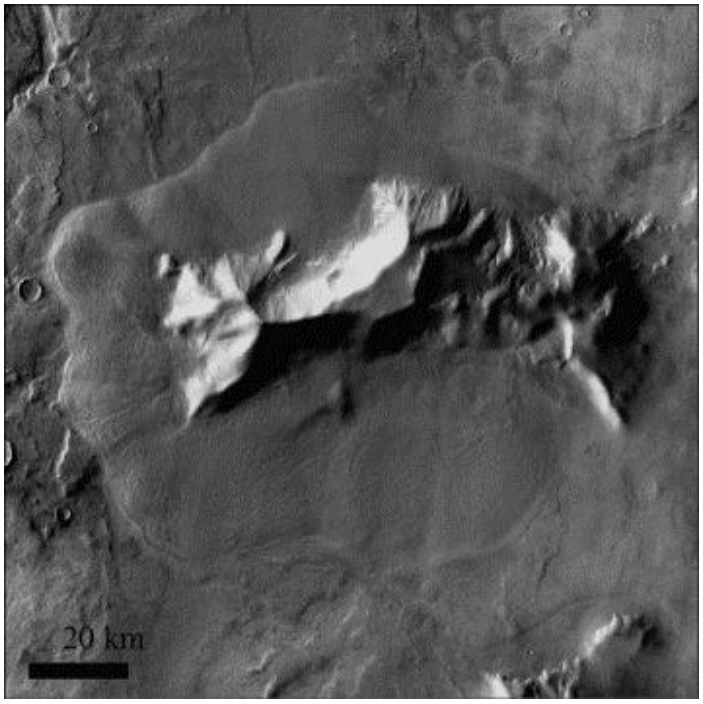

Figure 2.4 From Berman et al. (2015) martian debris apron surrounding rugged highland massif Euripus Mons in the eastern Hellas region, centred at 45°S, 105°E. THEMIS IR daytime 512 pixel/deg mosaic.

2.1.3.2. ***Lineated Valley Fill (LVF)***

The contorted surfaces of LVF were recognised alongside LDAs during the Viking era (Squyres, 1979, 1978), often forming with the convergence of LDAs. The long arcuate ridges and troughs seen to be running parallel to the valley sides point towards flow related strain (see *Figure 2.5*; Levy et al., 2016; Souness and Hubbard, 2012). The lineations likely occur due to faster down-valley flow rates in the centre of an ice/rock body away from the friction of the valley walls, with folds being elongated and stretched out over time (Baker et al., 2010). Other features including pits and hollows have led some authors to argue that the surface patterns of the LVF often appear to be the product of a thermokarst environment (van Gasselt et al., 2010) with increased sublimation and disaggregation inferring to a a similar episodic climate history as the dissected mantle terrain (Souness and Hubbard, 2012; van Gasselt et al., 2010). At the convergence of valleys, LVF typically becomes chaotic in appearance (Souness and Hubbard, 2012).

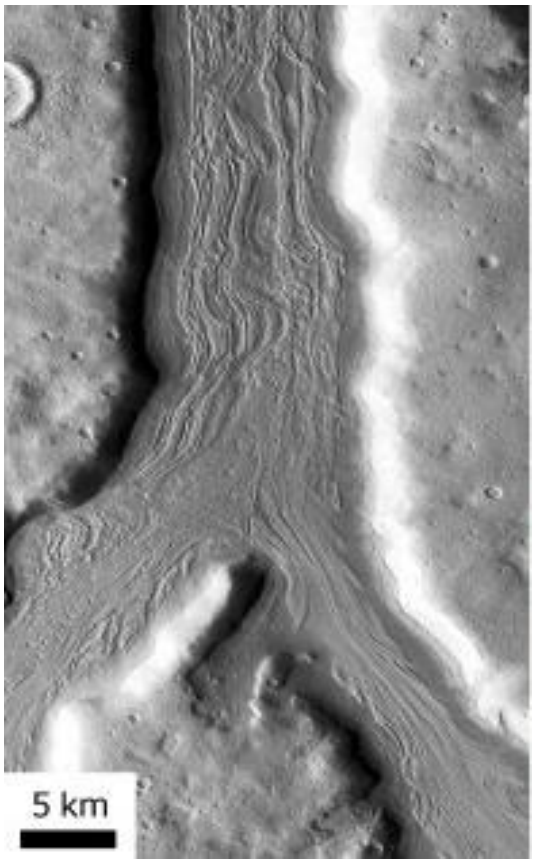

Figure 2.5 From Levy et al. (2016) showing LVF from CTX image P03_002375_2209 from the Ismeniae Fossae region; 40° N and 40° E. Flow appears to be downhill towards the north from a long valley to the SW and an alcove to the SE.

2.1.3.3. ***Glacier Like Flows (GLFs)***

GLFs were identified to begin in "cirque-like" alcoves, and then extend down-valley until they reach a natural terminus on lower slopes (see *Figure 2.6*). They are similar in appearance to terrestrial valley glaciers (Hartmann et al., 2003) when viewed in Mars Orbital Camera (MOC) images from the Mars Global Surveyor (MGS) spacecraft. A characteristic feature diagnostic of GLFs, and in accordance with the glacial theory, is the presence of a moraine-like ridge bounding the elongate tongue-shaped feature on the valley floor that gradually merges with the surrounding topography on the upper slopes (Arfstrom and Hartmann, 2005; Hubbard et al., 2011). Later studies (Head et al., 2010; Hubbard et al., 2011; Souness and Hubbard, 2012) have associated GLFs with en masse down-slope

transport of debris. GLFs have been observed to occur both in isolation and merging with LDAs to form part of an integrated glacial land system (Souness and Hubbard, 2012). Souness and Hubbard (2012) described GLFs as the lowest-order component of an integrated glacial land system, occurring at the highest elevations and often representing the source materials for VFFs. The moraine-like ridges have been used as evidence for episodic climate change with multiple ice advances and retreats (Hubbard et al., 2011). Other associated features such as the sinuous ridges described by Carr et al. (1980) lead to speculation of wet-based glaciers occurring at Martian mid-latitudes. Gallagher and Balme (2015) present the first identification of putative martian eskers that can be directly linked to their parent glaciers, offering particularly convincing evidence of glacial meltwater production and subglacial routing.

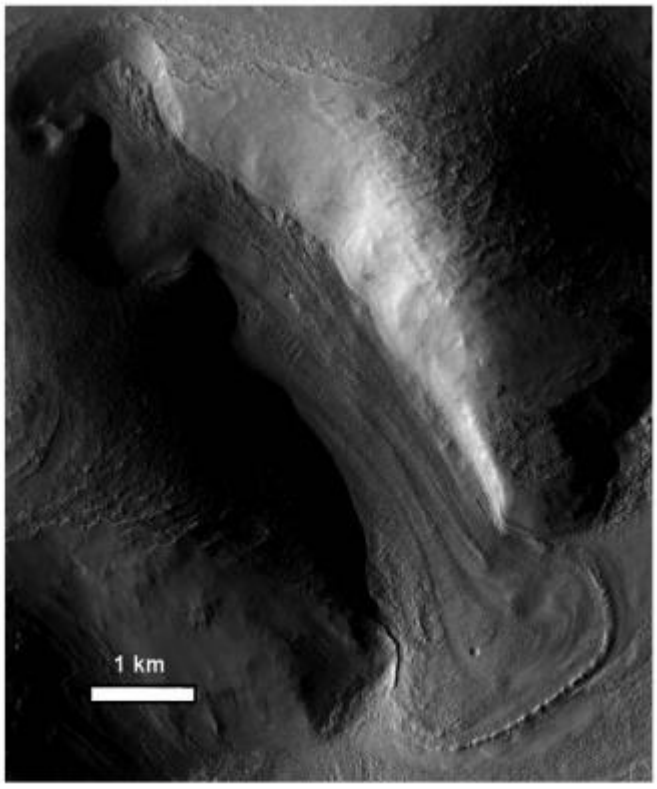

Figure 2.6 From Souness and Hubbard (2012) a GLF in Protonilus Mensae with lineated flow features and a moraine like ridge at the feature's terminus. Flow is from the NW towards the SE. CTX image is P22_009455_2214, at 41° N and 54° E.

2.1.4. **Patterned Ground**

The term patterned ground refers to non-random, often symmetrical, geometric textures displayed on the surface of drift material. Patterned ground has a variety of forms including polygons, circles, and stripes. Various landforms can be described as patterned ground; they can be clastic, ridges, troughs or a combination of all three and take a variety of shapes include polygons, circles, stripes and clastic lobes.

Polygonized ground is pervasive over the Martian surface (Levy et al., 2009) with polygonal textures being shaped by surface cracks and clast organisation. The scale of these polygons tend to range from tens of centimetres to tens of metres. A climatic control on formation is implied by a strong latitudinally dependent distribution (Levy et al., 2009; Mangold, 2005; Seibert and Kargel, 2001). Polygonized ground has been attributed to several processes including desiccation, jointing, cooling contraction in lavas, tectonic uplift and frost heaving due to freeze-thaw cycles (Balme et al., 2013; Levy et al., 2009). These forms could be indicative of liquid water if they are consistent with the ice-wedge polygons found in the terrestrial polar regions as suggested by Levy et al. (2010). However, after a survey of morphology, composition and spatial relationships Levy et al. (2010) concluded that formation due to sublimation or sand wedge processes were more likely than that of freeze-thaw. This conclusion is not undisputed: as highlighted by Ulrich et al. (2011) and Balme et al. (2013), the identification of the processes responsible for the formation of patterned ground from remote sensing data alone is unreliable on Earth and, presumably, more so on Mars.

The spatial sorting of clasts into both circle and striped domains has been observed on Mars (see *Figure 2.7*). With stripes, alternating bands of fine and coarse material are orientated down-slope and can be identified due to differences in albedo (Hauber et al., 2011; Mangold, 2005). Stone circles, varying in diameter from tens of centimetres to several metres, tend to display finer material in the centre surrounded by a circle of coarser

clasts. Circles and stripes have been identified in a number of locations including on impact crater slopes and the margins of what appears to be fluvial channels (Balme et al., 2009; Gallagher et al., 2011; Gallagher and Balme, 2011; Johnsson et al., 2012). Clastic circles and stripes could be symptomatic of liquid water if formed due to freeze-thaw processes (e.g., Balme et al., 2013) although several dry processes have also been proposed. The "dry" processes include gravitation slumping of clasts into thermal contraction cracks (Levy et al., 2009; Mellon, 1997) and a form of CO_2 frost heaving (Orloff, 2012). Solifluction lobes, tongue-shaped sedimentary features formed on slopes due to different rates of mass wasting, have also been identified on martian slopes also indicative of freeze-thaw cycles (Gallagher et al., 2011; Johnsson et al., 2012).

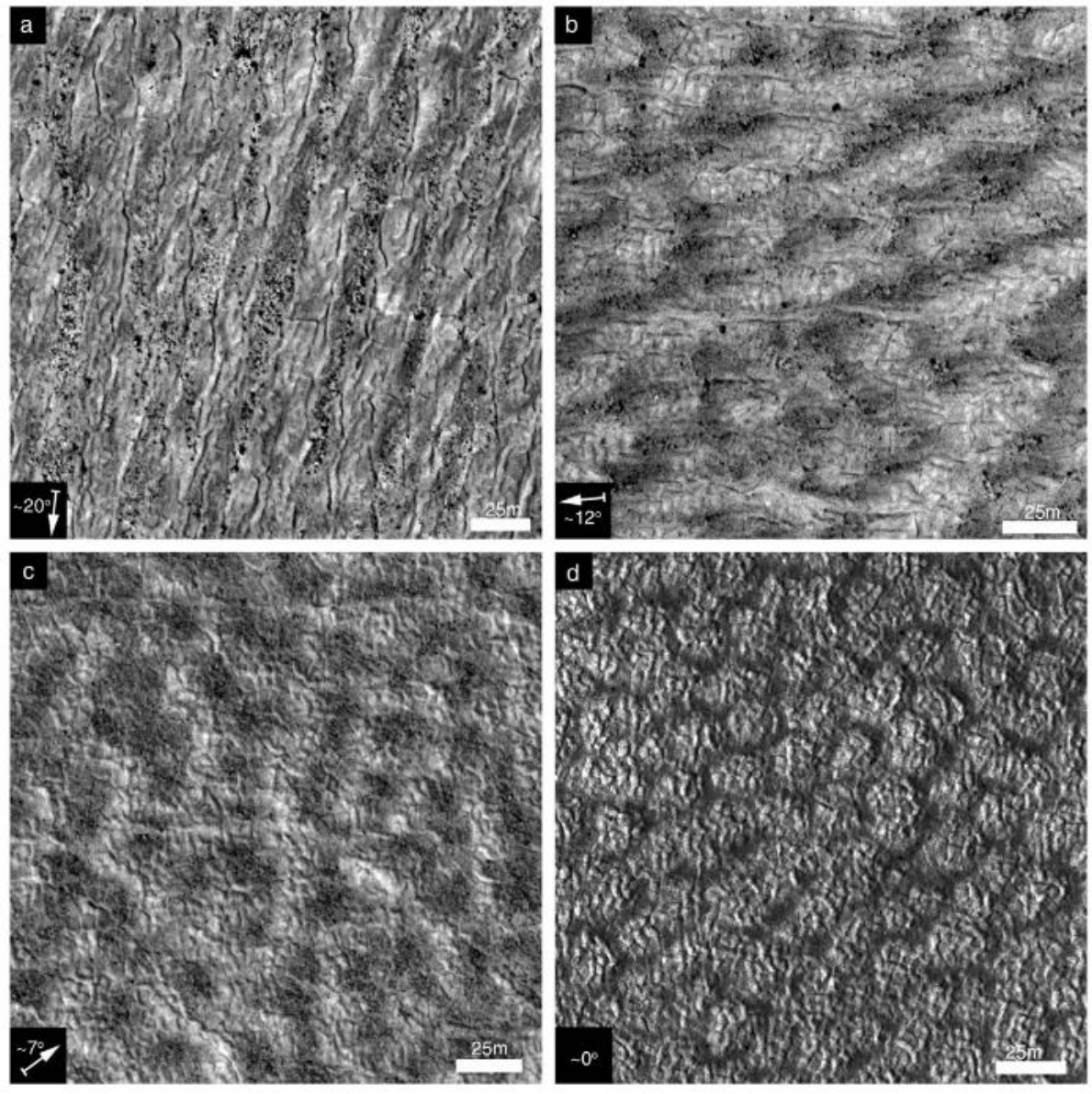

Figure 2.7 From Balme et al. (2013) sorted forms within and around Heimdal crater. (a) Clastic stripes HiRISE image PSP_009580_2485. (b) Clastic polygons trending into clastic stripes HiRISE image PSP_009079_2485. (c) Clastic rubble piles HiRISE image PSP_009778_2485. (d) Low-albedo high-centred polygons inferred to comprise sorted clasts below the image resolution HiRISE image PSP_009079_2485.

2.2. Landforms indicative of Ice Melt, Sublimation or degradation/erosion by flowing water

2.2.1. Does the ice ever melt?

Assuming the presence of water ice on Mars the obvious question to follow is whether melting occurs or has occurred under certain conditions. The answer to this question bears relevance on whether life could survive on Mars: if liquid water became available on Mars, even if only intermittently, it could provide a viable habitat for extremophiles such as those found in the harshest conditions of Antarctica (Torre et al., 2003). If melting does occur, such as in the form of wet-based glaciation, the resultant geomorphologies could be very different. Identification, mapping and analysis of potential wet-based glacial morphologies provide a sub-theme of this project.

2.2.2. Channel and Valley Networks

The origin of large scale channels of Mars has been a source of debate since their discovery in 1971 (Masursky et al., 1972; McCauley et al., 1972; Milton, 1973). Where outflow channels are formed through catastrophic outbursts of groundwater (e.g. Burr et al., 2009a), valley networks are formed through prolonged fluvial erosion, likely from surface runoff, though whether from precipitation (warm and wet early Mars) or melt of ice sheets (cold and dry early Mars) is still unknown (e.g. Ansan and Mangold, 2013; Gulick, 2001). Either way, these channels and valleys represent the removal of material by fluvial erosion and are indicative of liquid water on the surface of Mars and vary in appearance much like their terrestrial analogues (see *Figure 2.8*). Smaller, sub kilometre-

scale channel and valley networks have been observed to occur on top and down-slope of some VFFs (Dickson et al., 2009; Fassett et al., 2010; Howard and Moore, 2011) and consequently have been interpreted as fluvioglacial valleys (e.g. Balme et al., 2013). These small scale valleys point to the presence of liquid water during the Amazonian and Balme et al. (2013) attributed them to part of a mid-latitude ice-related assemblage.

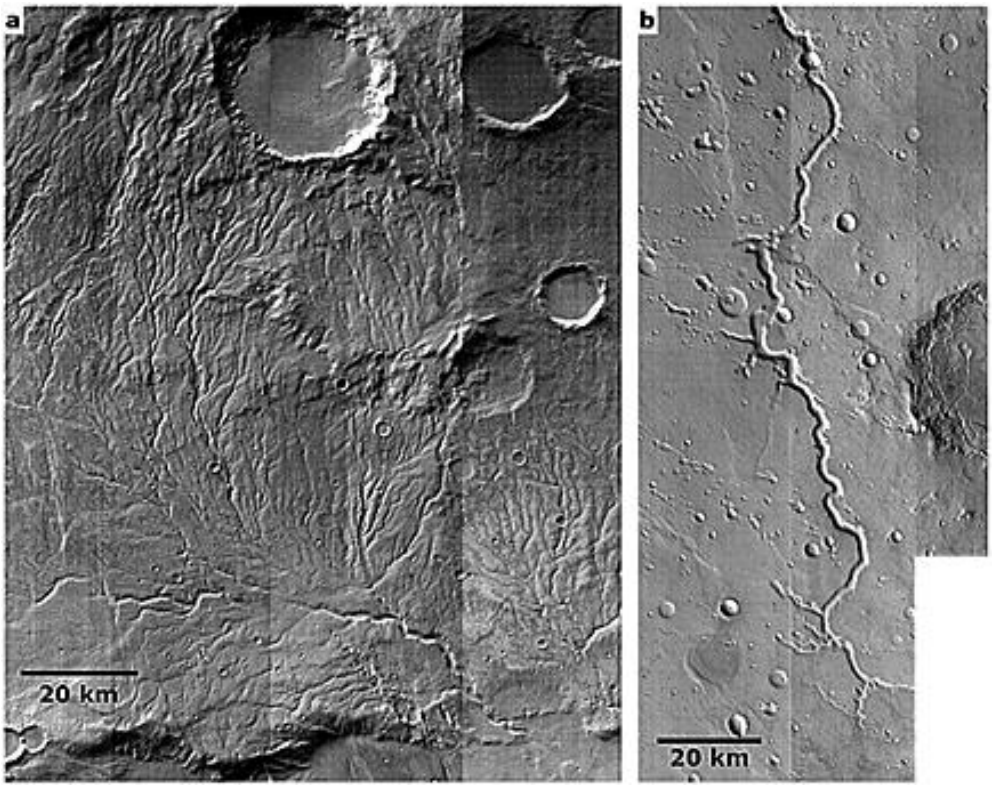

Figure 2.8 THEMIS images from Ansan and Mangold (2013). (a) Warrego Valles, 41° S and 93° W, on the southern boundary of the Thaumasia highlands with a densely dissected drainage basin and many, well-developed tributaries, (b) Eastern Nanedi Vallis in Xanthe Terra, 5° N and 48° W, with few tributaries and poorly developed source region.

Dickson et al. (2009) described a putative fluvial channel system in Lyot Crater (see *Figure 2.9*) dating to Middle or Late Amazonian, arguing that periods of high obliquity and low elevations could provide sufficient heating for melting of surface ice and fluvial activity. Other channel systems such as those found around the Galaxias Fossae (Wilson and Mouginis-Mark, 2003) have been attributed to phreatomagmatic (magma and

water/ice interaction) eruptions and resulting pyroclastic flows (volcanic debris flows with volcanic material suspended by steam) and lahars (volcanic mudflows). Importantly, Wilson and Mouginis-Mark (2003) comment that the deposits associated with these features show no signs of dewatering, this could be suggestive of either complete devolatisation during transportation or it could be indicative of deposition and burial of volatiles into the northern plains, in this case Utopia Planitia.

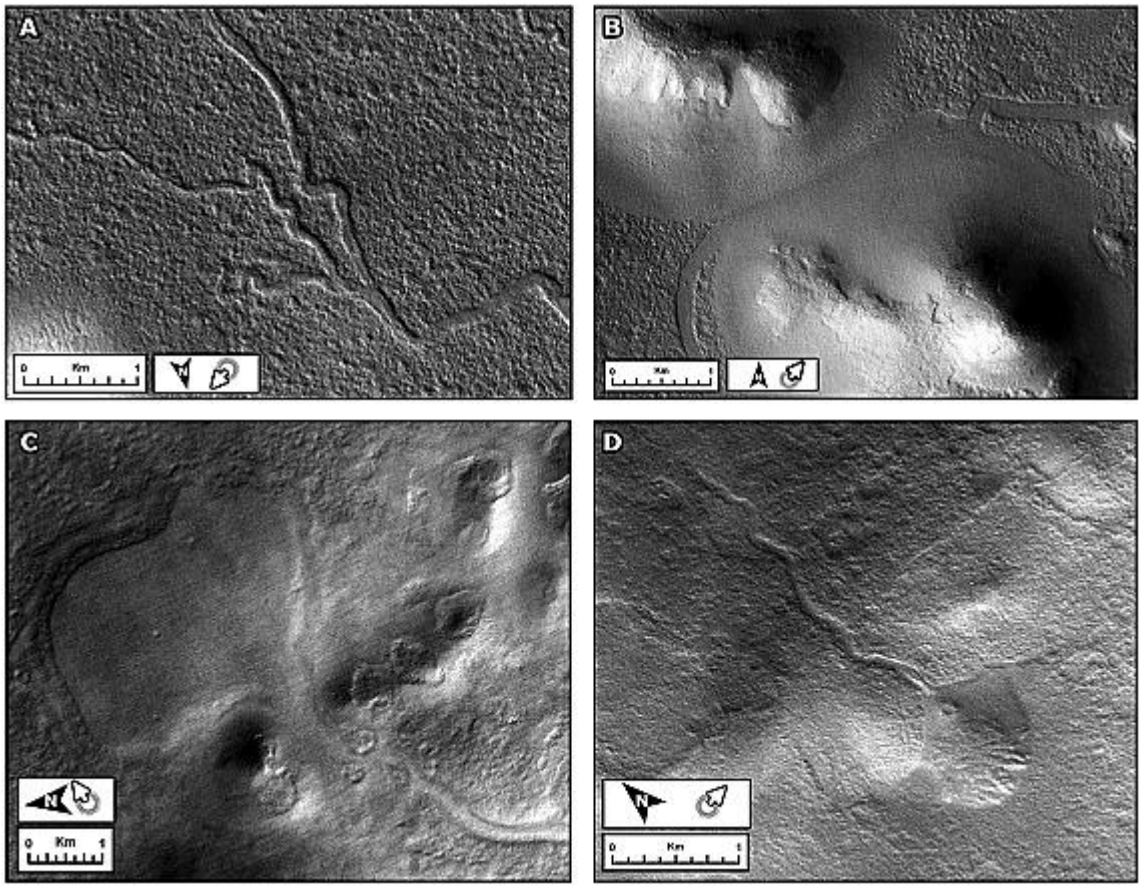

Figure 2.9 Lyot crater, 50° N and 30° E, fluvial valley systems and fans from Dickson et al. (2009) . (a) Valleys converging and trending downslope toward the lower right (CTX P04_002560_2309), (b) Smooth mantling deposits on knobs superposed on valleys. Direction of flow from topography was from upper-right to lower-left (CTX P04_002560_2309). (c) Broad fan sourced by a ~28 km valley (CTX P04_002494_2310). (d) Smaller dissected fan sourced by small channel from the north (CTX P04_002494_2310).

Fluvial channels are important both in that they indicate possible upstream melt of water-ice (degradation), and that they represent the transport of water and sediment. As liquid water is unstable on Mars currently, and probably has been throughout the Amazonian, fluvial transport could cease due to loss of water by boiling, freezing and evaporation. Some channels, though, do not appear to "fade out" in this way, and have abrupt termini. These, then, are likely depositional zones (perhaps even lakes) where a mixture of ice and sediment was deposited. If such regions are extensive in the northern plains, this could provide an important explanation for how ice came to be deposited here.

2.2.3. **Gullies**

Gullies on Mars are kilometre-scale features similar in form to small alluvial or debris flow fans on Earth (see *Figure 2.10*). They are defined as features that have an alcove, a channel and a debris apron (Malin and Edgett, 2000). Gullies are typically found at latitudes between 30° and 50° in both hemispheres, and preferentially on pole facing slopes (Balme et al., 2006; Dickson et al., 2007; Heldmann et al., 2007; Heldmann and Mellon, 2004; Kneissl et al., 2010; Malin and Edgett, 2000). The main exception to this trend is within the south polar pits (around 70° south) where many gullies are found and which have little pole-facing preference (Harrison et al., 2015). Gullies are also much more prevalent in the southern hemisphere, but this is likely due to the lack of steep slopes in the northern hemisphere (Kreslavsky and Head, 2000). Possible formation mechanisms include dry mass wasting (Treiman, 2003), liquid water flow (Malin and Edgett, 2000), flow of brines (Hartmann, 2001), debris flows (Balme et al., 2006; Conway et al., 2011; Costard et al., 2002) and flow of liquid CO_2 (Musselwhite et al., 2001; Pilorget and Forget, 2016). While formation on moderate to steep slopes is consistent with dry-granular flow, latitudinal and orientation preferences suggest that gully formation is linked to variations in insolation. These patterns would lean towards hypotheses that are dependent on

climatically controlled processes such as melt of ice to form liquid water and deposition and mobilisation of CO_2 to form dry flows.

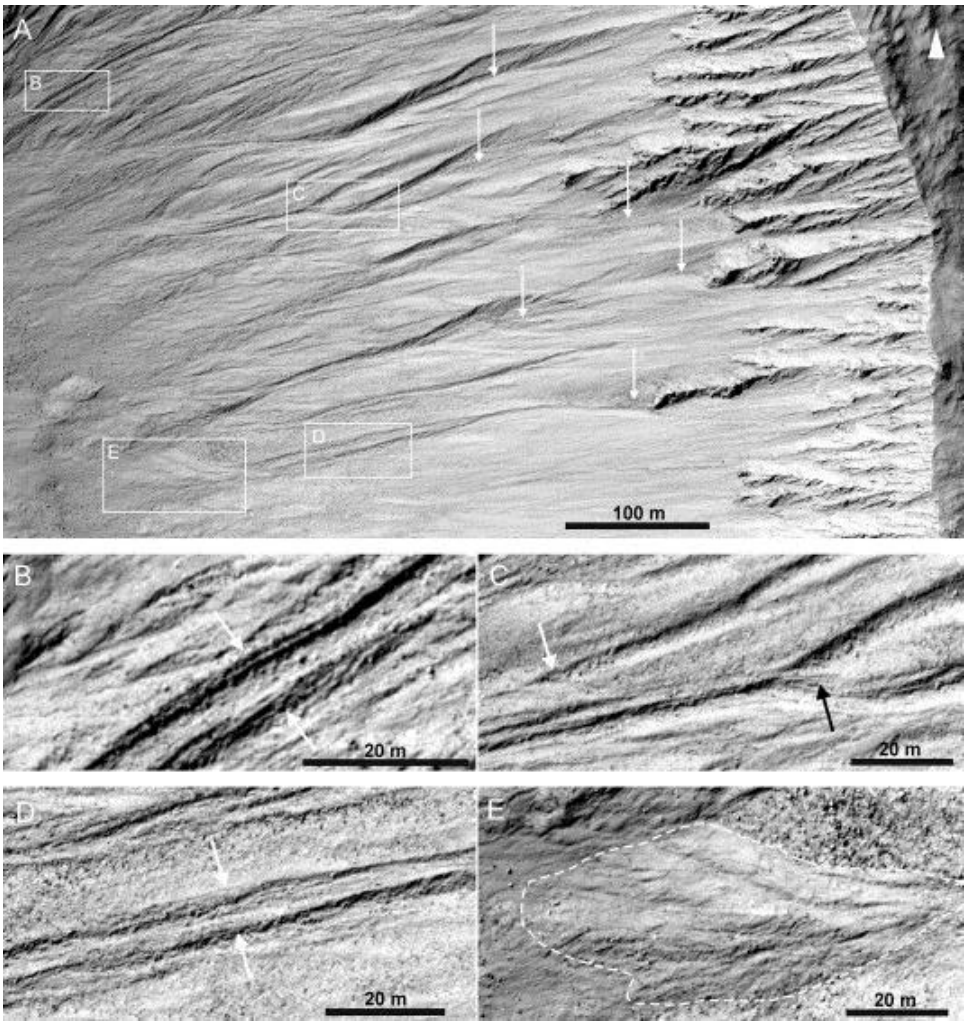

Figure 2.10 From Johnsson et al. (2014) (A) gullies on an interior west-facing crater wall. White boxes show the location of the sub-images. (B) Levée-like structure along gully channel. (C) Cut channels (white arrow) and hanging channels (black arrow) indicate multiple flow events. (D) Straight gully channels with levée-like structures. (E) Gully channels terminate in small fans. HiRISE image PSP_006837_1345 at 45° S and 85° W.

Similar features, displaying alcoves, channels and aprons, also occur on the slip faces of martian sand dunes and have been shown to be active during the winter (see *Figure 2.11*; e.g. Diniega et al., 2010; Pasquon et al., 2016). This winter activity occurs when seasonal CO_2 ice is present, with temperatures below -120° C, suggesting that they are unlikely to

be formed by the flow of liquid water but instead formed as a result of CO_2 processes (Diniega et al., 2010; Pasquon et al., 2016). The presence of non-dune gullies is controlled by local relief, so they require impact craters or other topography to form. It is also very likely that they form in, or in relation to, the LDM (Bleamaster and Crown, 2005; Schon and Head, 2012), so they appear to need a source of ground ice to form too. Thus, while they may be relatively uncommon in the northern plains due to the lack of relief, they do appear to be indicative of the current or recent presence of near-surface water ice.

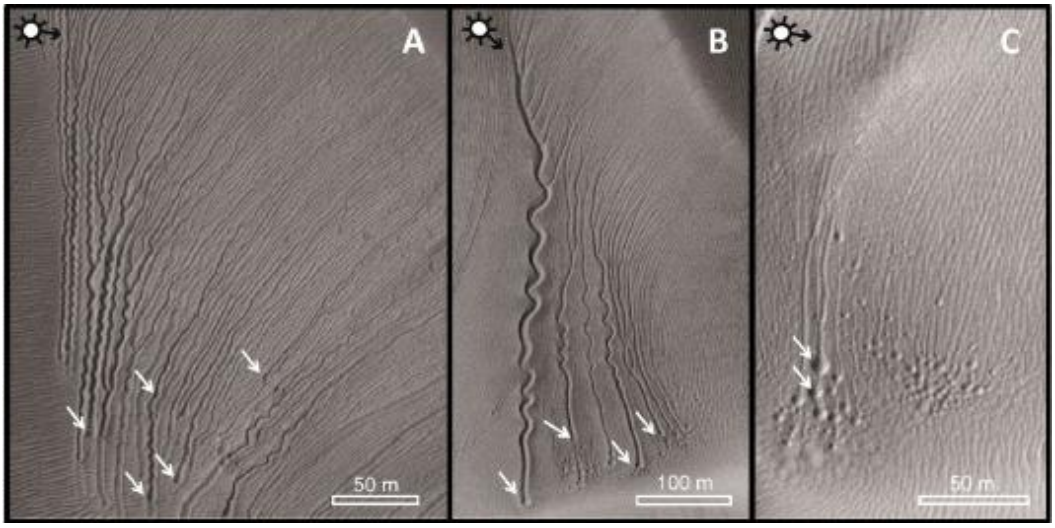

Figure 2.11 From Pasquon et al. (2016) Linear gullies on Kaiser and Matara crater dunefields ,at 46° S and 18° E. White arrows show the location of pits. (A) Highly sinuous linear gullies HiRISE Image: ESP_011,738_1325). (B) Sinuous linear gullies HiRISE image: ESP_030,528_1300). (C) Low-sinuosity linear gullies and non-aligned pit groups HiRISE image: ESP_038,255_1300).

2.2.4. **Pitted and Scalloped terrains**

Depressions and pits, often overprinted by patterned ground, are observed to occur in the draping mantle deposit in the mid-latitudes (Costard and Kargel, 1995; Lefort et al., 2009; Morgenstern et al., 2007; Zanetti et al., 2010). A commonly occurring morphology is "scalloped pits" which have a distinctive scallop-shaped, planview morphology, often merging to form larger depressions, but are generally shallow with respect to their area

(see *Figure 2.12*). These scalloped depressions often display steeper poleward facing scarps and have inner steps which have led some authors to suggest the scallops once contained thaw lakes which have since been subject to evaporation (Costard and Kargel, 1995; Soare et al., 2007, 2008). However, it is also possible that these pits formed through sublimation without the need for thawing of the ground ice (Lefort et al., 2009; Morgenstern et al., 2007; Séjourné et al., 2011; Ulrich et al., 2010; Zanetti et al., 2009). The cold, arid conditions of the current Martian surface (Morgenstern et al., 2007) and the lack of runoff channels or interconnected "tapping channels" support the hypothesis of formation by sublimation (Séjourné et al., 2011, 2012). However, at least one pit highlighted by Séjourné et al. (2011) contains channel-like forms, appearing similar to terrestrial thaw gullies, on the poleward facing slope which may represent localised conditions which permitted the thawing of ground ice. Again, although the formation mechanism of these pits is still not completely understood, they seem to be diagnostic of the presence and subsequent loss of ground ice due to either thermal disequilibrium (i.e., melting or enhanced sublimation) or changes in (or sudden exposure to) the humidity of the atmosphere (i.e. to enhance sublimation).

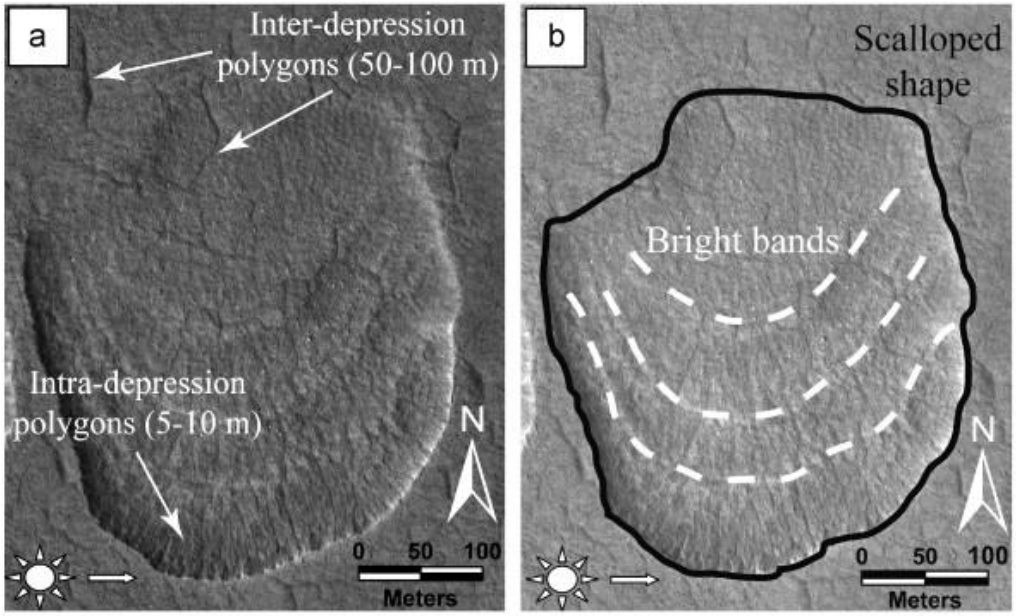

Figure 2.12 From Séjourné et al. (2011) morphology of scalloped depressions in Utopia Planitia, at 45° N and 93° E. (a) The depressions are elliptical with scalloped edges in HiRISE image PSP_001331_2260. (b) They show many bright bands whose origin is enigmatic. Their N–S profile is asymmetric, their pole-facing slope is steeper than their equator-facing slope.

2.3. **Other landforms thought to be formed by water/ice related processes**

2.3.1. **Thumbprint Terrain**

"Thumbprint terrain" is a term used to describe widespread distinctive patterns found on the northern plains of Mars. These terrains comprise sub-parallel curvilinear ridges and lines of mounds with summit pits (Tanaka et al., 2005). They are found almost entirely at the periphery of a geological unit termed the "Middle Amazonian lowland unit" (Skinner et al., 2012) and/or near the termini of large outflow channels (Schaefer, 1993).Thumbprint terrain can vary significantly in form (Rossbacher and Judson, 1981) and can be grouped into three sub-types: (i) ridges and depressions around 500 m to 2500 m wide (see *Figure 2.13*), (ii) chains of cones (with or without summit pits) up to a few hundreds of metres in diameter (see *Figure 2.14*), (iii) striped differences in albedo with little topographic expression.

Figure 2.13 From Rossbacher and Judson (1981). Thumbprint terrain; curvilinear forms with alternating positive and negative topography in Utopia Planitia (Viking frame 57B56 centred at 50°N, 287°W)

The origins of thumbprint terrain are enigmatic, with no obvious terrestrial equivalent. Processes suggested for their formation include volcanism, infill of depressions in, and subsequent removal of, a debris mantle resulting in topographic inversion, and glacial or periglacial processes such as kame formation with the build-up of sediment at the front of a

retreating glacier or ice sheet (Rossbacher and Judson, 1981; Tanaka et al., 2005). Proponents of a glacial hypothesis have argued that the ridges are recessional moraines (Kargel et al., 1992), ice-pushed ridges (Scott and Underwood, 1991), or that they have the ribbed appearance characteristic of rogen moraine (Lockwood et al., 1992). Others have suggested that the breakdown of surface material as a result of subsurface ice could form these patterns (Rossbacher and Judson, 1981) or mudflows (Costard et al., 2015).

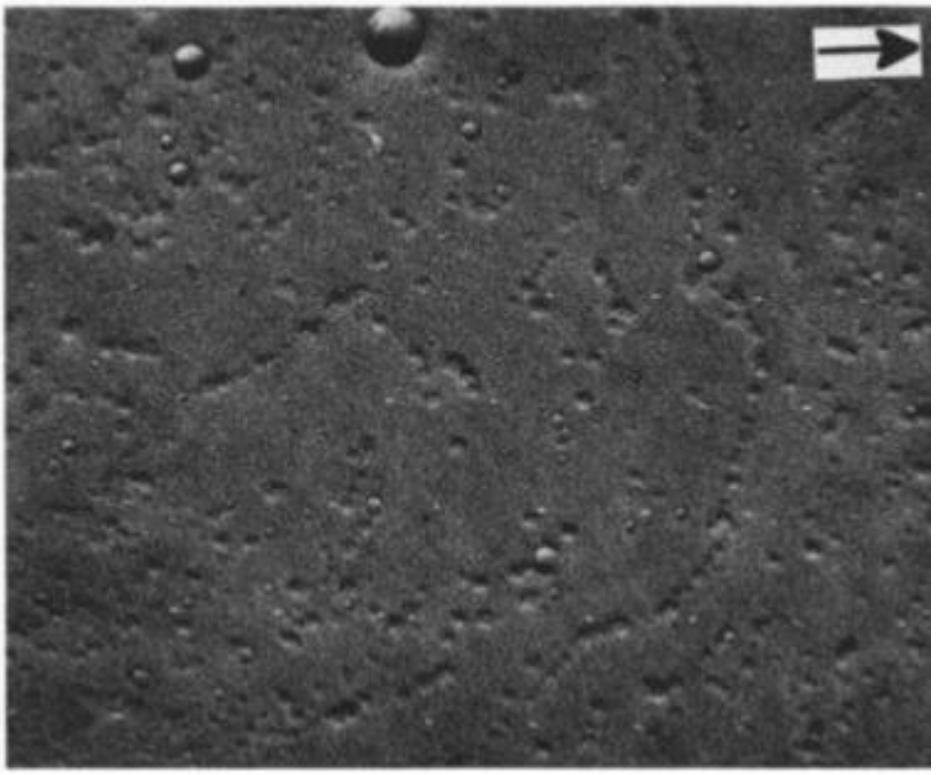

Figure 2.14 From Kargel et al. (1995) Thumbprint terrain comprised of arcs of disconnected hills and short ridges, many with summit pits. Viking Orbiter image 146S13, Isidis Planitia, 15° N, 90° E. Scene width ~32 km.

2.3.2. **Sinuous Ridges (SRs)**

The term sinuous ridge (SR) has been used by a number of authors (e.g. Kargel and Strom, 1990) to describe elongate, positive relief landforms that occur on the Martian surface (see *Figure 2.15*). These ridges occur both individually and as part of complex systems incorporating various patterns of cross-cutting, anastomosing and branching

ridges. The SRs described by Kargel and Strom (1990; 1991; 1992) in the Argyre Planitia are one of the most diagnostic glacial features found on Mars, as in this case they appear to be similar to terrestrial eskers, i.e. sediment ridges deposited by en/sub/supra-glacial channels. The SRs in the Argyre impact basin are typically 100-200 km long, 600-2400 m wide and around 40-160 m high (Kargel and Strom, 1991) thus falling well within the range of terrestrial esker scales of 100s of metres to 400 km long, metres to kilometres wide, and centimetres to a few hundreds of metres high (Lee, 1965; Price, 1973). Kargel and Strom (1991) describe the ridges as having internal bedding and occurring both as lone sinuous ridges and also in cross cutting en-echelon, anastomosing, dendritic, rectilinear and distributary systems, with forms varying from sharp crested through to flat-topped and rounded to double ridged (Kargel and Strom, 1991). Kargel and Strom (1992) note that the SRs are identified alongside features interpreted to be tunnel valleys, outwash plains, rock glaciers, kettle holes, kames and glacial grooves.

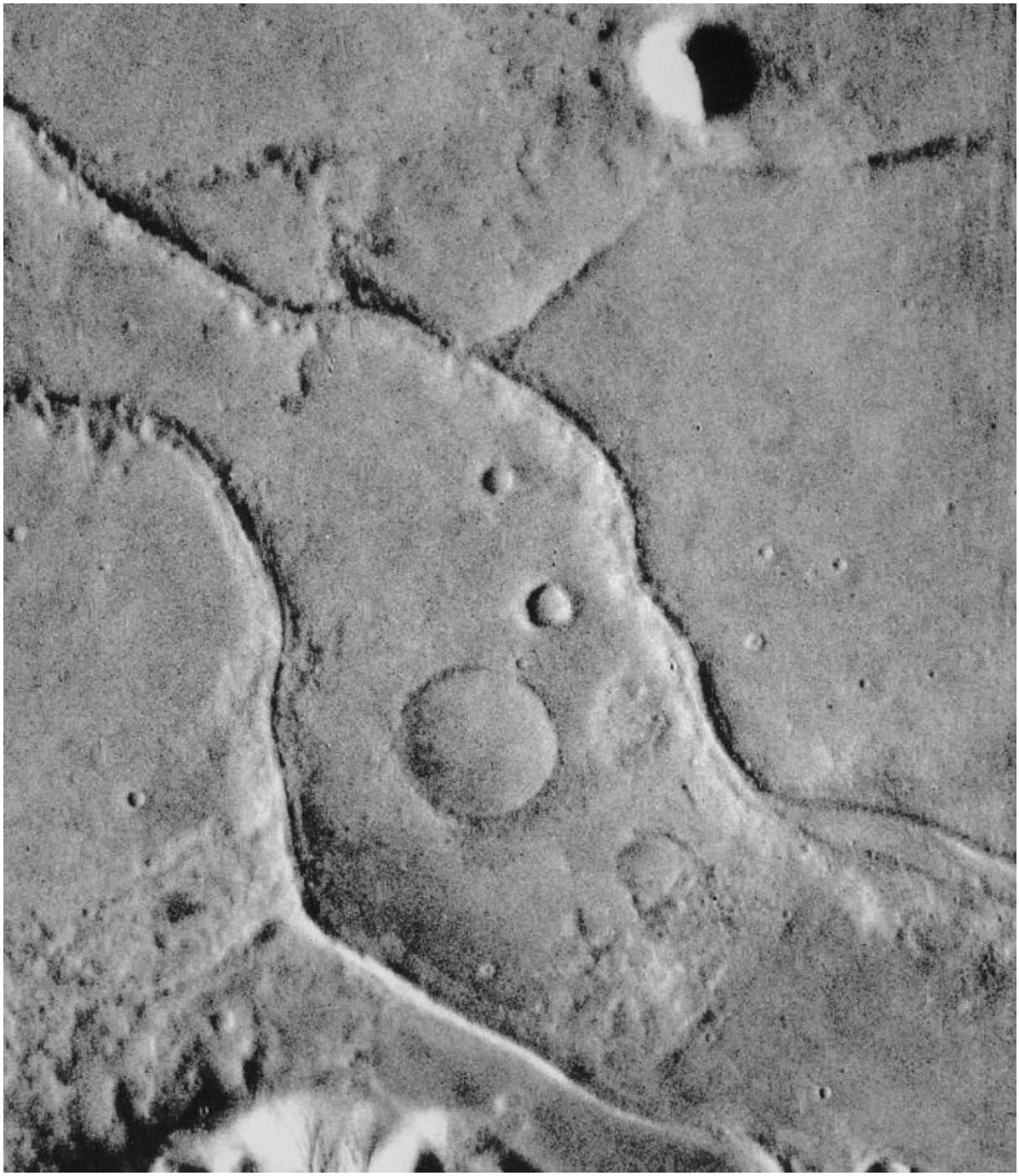

Figure 2.15 From Baker (2001) the esker-like ridges in southern Argyre Planitia, 56° S and 40° W. The Viking orbiter image (567B33) shows a scene about 50 km across. The ridges are sharp-crested and about 1,000 m in width.

Various other modes of origin have been proposed for these sinuous ridges including wrinkle ridges (Tanaka and Scott, 1987), exhumed igneous (Carr et al., 1980) and clastic (Ruff and Greeley, 1990) dykes, lava flow features (Tanaka and Scott 1987), linear sand dunes (Parker et al., 1986; Ruff, 1992), lacustrine spits or barrier bars (Parker et al., 1986;

Parker and Gorsline, 1992; Parker, 1994; 1996a; 1996b), glacial moraines (Hiesinger and Head, 2002; Kargel, 2004), inverted stream topography (Howard, 1981; Rice and Mollard. 1994), frozen waves within a mudflow (Jöns,1992). Interpretation as eskers has been suggested by various authors (Carr et al., 1980; Howard, 1981; Ruff and Greeley, 1990; Metzger, 1991; 1992; Kargel and Strom, 1990; 1992; Nussbaumer et al., 2000; Hiesinger and Head, 2002; Kargel, 2004; Lang, 2007).

The coexistence of SRs and interpreted tunnel valleys is discussed by Shaw and colleagues (1992). However, they argue that the term tunnel channel would be the more appropriate term due to the possibility that the water level may have surpassed the bank height. Tunnel channels on Earth are subglacially eroded drainage features that tend to be relatively large in scale than other drainage channels (Shaw et al., 1992). Shaw et al. (1992) note that the tunnel channels of south eastern Onatrio are found to contain eskers similar to those found in Argyre. Recent work (Gallagher and Balme, 2015) has identified a potential *in situ* esker complete with a glacier-like form in Phlegra Montes in western Arcadia. This could represent the first esker that can be directly linked to its parent body on Mars. Similarly Butcher et al. (2016) concluded that the Dorsa Argentea on Mars showed lengths, planar geometries, crest morphologies, and sinuosities consistent with terrestrial eskers.

2.3.3. **Mounds and Rimmed depressions**

2.3.3.1. ***Large Pitted Mounds***

Large pitted mounds range from a few hundred metres to a couple of kilometres across and are typically domes surrounded by a topographic moat (see *Figure 2.16*). Large pitted mounds can be found on the northern plains and have enigmatic origins. Oehler and Allen (2010) mapped 18,000 large pitted mounds in Acidalia Planitia noting that the features had a relatively high albedo in comparison to the surrounding material. They have been associated with mud volcanism (e.g. Davis and Tanaka, 1995; Farrand et al., 2005; Oehler and Allen, 2010; Skinner and Tanaka, 2007; Tanaka et al., 2003), pseudo-craters

(e.g. Frey et al., 1979) and volcanism (McGill, 1989). Skinner and Mazzini (2009) discuss several formation mechanisms that involve the burial of volatile rich sediments with expulsion occurring as a result of rapid sedimentation, crustal shortening, volcanic/geothermal destabilisation, long term subsidence or seismic liquefaction (see Figure 2.17). If these features do represent mud volcanism the sheer number of these features suggests at least somewhat long-lived expulsion of volatiles and a potential habitat for life.

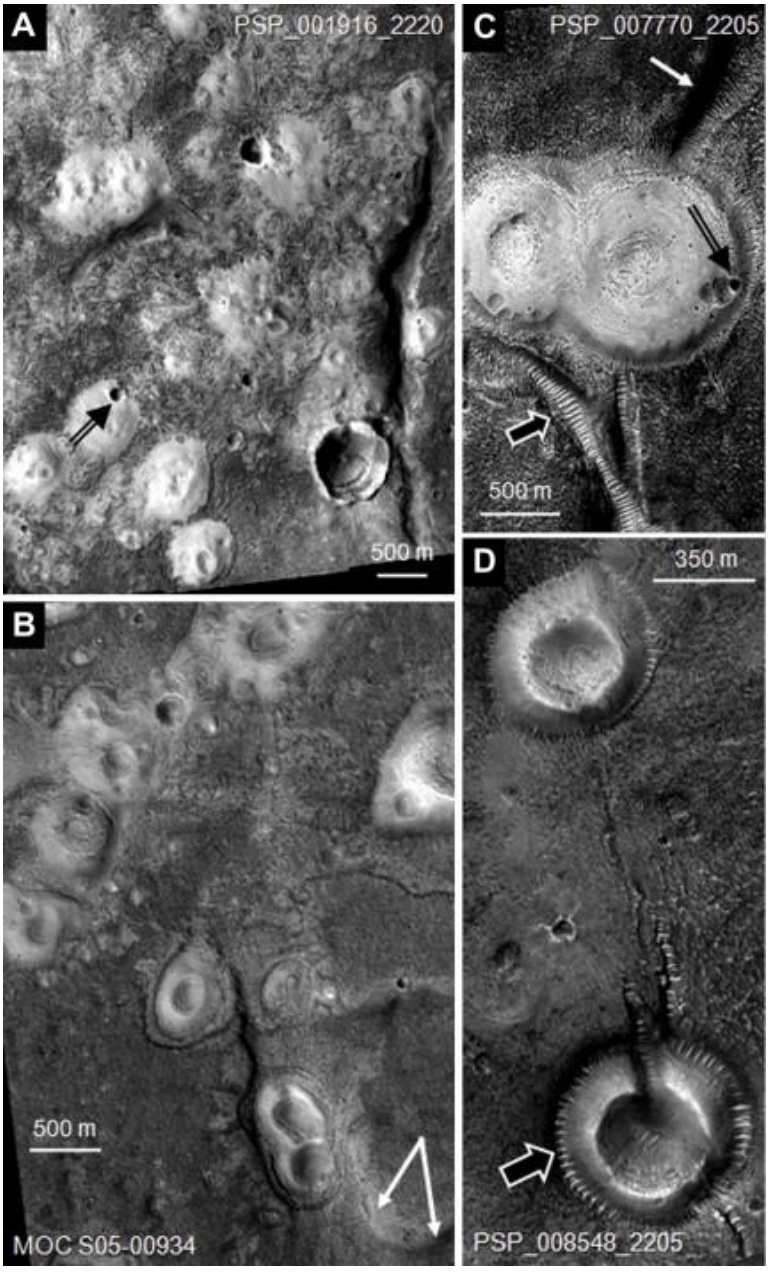

Figure 2.16 From Oehler and Allen (2010) High-albedo large pitted mounds in Acidalia, at 41° N and 27° W. (A) Large pitted mounds with irregular clustering. HiRISE image PSP_001916_2220. (B) Large pitted mounds with concentric crestal depressions and moats. MOC image S05-00934 (C) Mounds with marked concentric structures on their crests. HiRISE image PSP_007770_2205. (D) Large pitted mounds with pronounced moats and large crestal depressions. HiRISE image PSP_008522_2210.

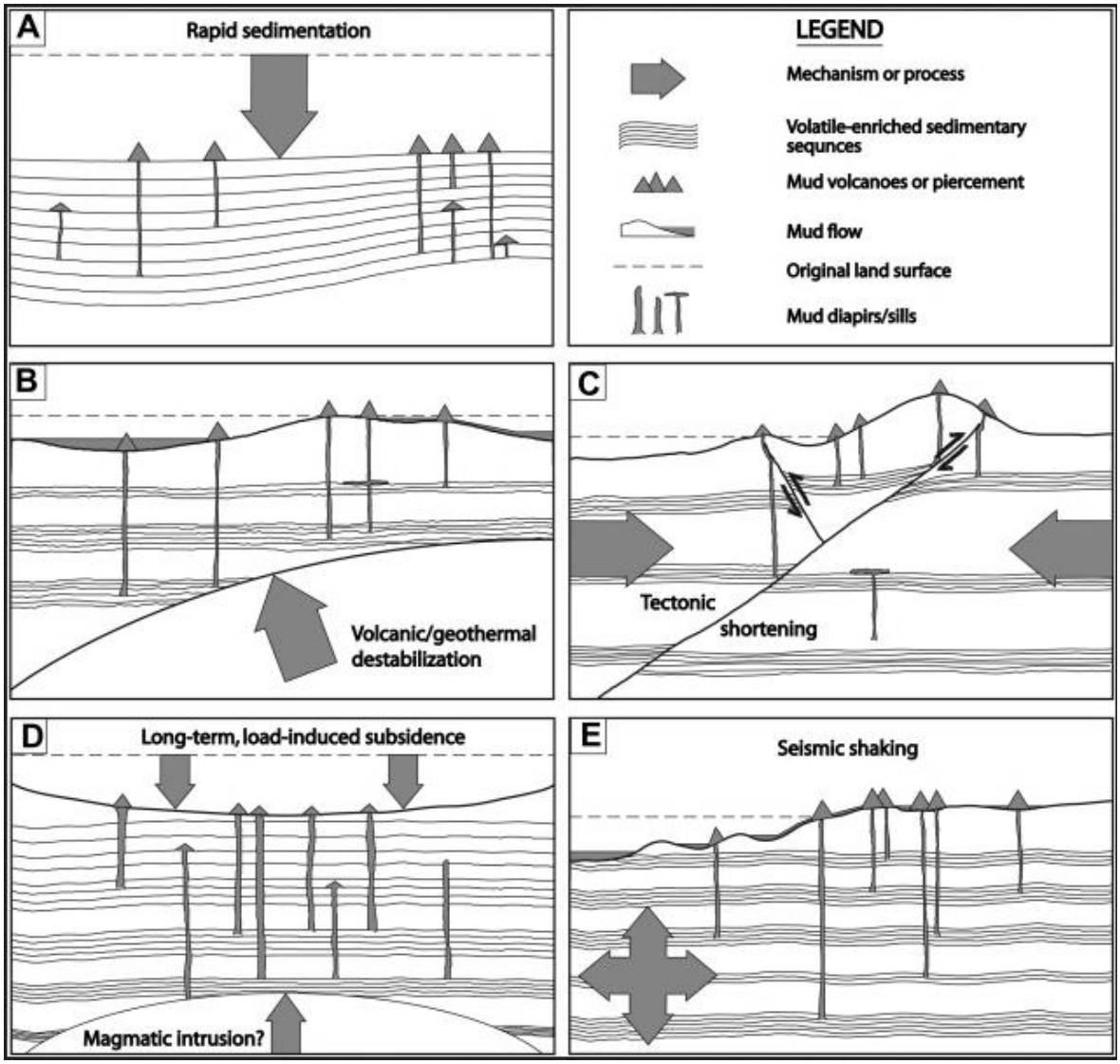

Figure 2.17 From Skinner and Mazzini (2009) showing mud volcanism formation scenarios. (A) Scenario A – vertical compaction of rapidly-deposited sediments, such as catastrophic flood deposits. (B) Scenario B – vertical compaction of subsurface units through volcano-related heating through the intrusion of magmatic dikes and sills. (C) Scenario C – lateral compaction through tectonic shortening. (D) Scenario D – vertical

compaction through long-term, load-induced subsidence. Mud volcanism due to the intrusion of magmatic dikes and sills may provide an alternative or supplemental condition. (D) Scenario E – vertical compaction through seismic shaking.

2.3.3.2. ***Mesoscale Raised Rim Deposits (MRRDs)***

Martian Mesoscale Raised Rim Deposits (MRRDs) is a term used to describe nearly circular mounds that often display central pits and circum moats (see *Figure 2.18*; e.g., Burr et al., 2009b) with often disputed origins. Due to the nature of remote sensing projects, large numbers of the Martian MRRDs can be organised and reviewed by latitude (e.g., Burr et al., 2009c). Utopia Planitia has been highlighted as an area containing MRRDs around 25-50 m across displaying radial cracks and summit depressions (Soare et al., 2005) alongside patterned ground, pitted cones, rounded depressions, elliptical mounds and local fractured rises indicative of water saturated sediments and an ice rich permafrost (e.g. Soare et al., 2005; Osinski and Soare, 2007; de Pablo and Komatsu, 2007, 2008; Dundas et al., 2008; Burr et al. 2009a). Skinner and Tanaka (2007) suggested the sediments these features occur in could be subject to inherited conditions such buried impact basin structures and topography. It has been suggested that Utopia Planitia may have constituted to a former ocean basin (Baker et al., 1991; Parker et al., 1993; Head et al., 1999) now infilled by the periglacial Vastitas Borealis sediments (Tanaka et al., 2005; Skinner and Tanaka, 2007). The inter-granular water inferred by Chapman (1994, 2003) could provide the ice-rich permafrost required for pingo, mounds of sediment covered ice, development and could help to explain the widespread patterned ground identified by Costard and Kargel (1995).

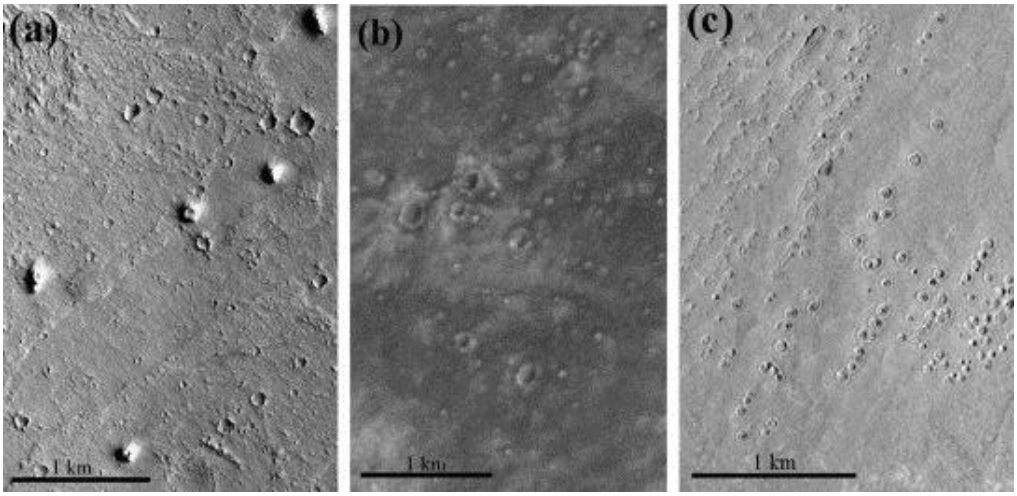

Figure 2.18 From Burr et al. (2009b) MRRDs on Mars. (a) Subset of MOC image M07-00373, located in western Amazonis Planitia, 12° N and 163° W. (b) Subset of MOC image E22-00813, located in Acidalia Planitia, at 44° N and 27° W. (c) Subset of MOC image R01-00365, in Athabasca Valles, at 9° N and 156° E.

Osinski and Soare (2007) and de Pablo and Komatsu (2007, 2008) discuss the different stages of pingo development with radial cracks forming as the pingos grow and depressions resultant of pingo collapse. MRRDs share much of their morphology with rootless cones and are often difficult to distinguish. Rootless cones were first identified by Thorarinsson (1953) in Iceland and are a product of a phreato-magmaic eruption caused when lava or pyroclastic flow material is deposited over wet or icy ground (Thordarson et al., 1992; Thordarson, 2000; Greeley and Fagents, 2001). The trapped volatiles evaporate, creating a localised pressure spike which can cause secondary eruptions on the surface of the flow deposit. Examples of rootless cones have been identified on Mars (Greeley and Theiling, 1978; Frey et al., 1979; Allen, 1980; Frey and Jarosewich, 1982; Wood, 1982; Mouginis-Mark, 1985; Greeley and Fagents, 2001; Lanagan et al., 2001; Meresse et al., 2006; Jaeger et al., 2007a, 2007b). However, due to the lack of evidence for volcanic material de Pablo and Komatsu (2007, 2008, 2009) concluded that pingo formation is more likely in the Utopia Planitia. This conclusion was supported by subsequent work by Dundas et al. (2008) where various geometric parameters were taken and compared with

terrestrial analogues. Burr et al. (2009a) argue that the research in Utopia Planitia is most consistent with terrestrial style pingo formation.

2.4. **The importance of contextual landforms**

Given the variety of interpretations proposed for each landform identified, it is entirely possible that there could be a number of processes occurring on Mars that are producing forms that look very similar when viewed from orbit. The inability to provide ground-truth with in-situ geological analysis on Mars favours an agnostic position when reviewing geomorphic interpretations. This means that, in practice, landforms must be viewed in a contextual setting, whereby the interpretation of several landforms in a context (both spatially and in terms of topography of stratigraphy) supporting the same mode of origin is more reliable than an interpretation based on a single form. It is worth noting that many interpretations formed during the Viking era, but since then, higher resolution images have become available, such as those taken by the Context Camera (CTX; Malin et al., 2007) and the High Resolution Imaging Science Experiment (HiRISE; McEwen, 2007) cameras have helped to narrow down interpretations for various landforms.

2.5. **The confirmation of ground ice on Mars by in-situ analysis and by observations of fresh impact craters**

A primary objective of the Phoenix lander, which landed 68° N and 124° W in the northern plains of Mars near Heimdal Crater in 2008, was to confirm the presence or ground ice on Mars and to try to elaborate on its origins. The lander found ice beneath a thin veneer of sediment at a mean depth of 4.6 cm, with the largest depth to ice being 10-15 cm (Mellon et al., 2009). Mellon et al. (2009) liken the ice deposits to the formation of ice lenses and needle ice formed through soil ice segregation (see *Figure 2.19*).

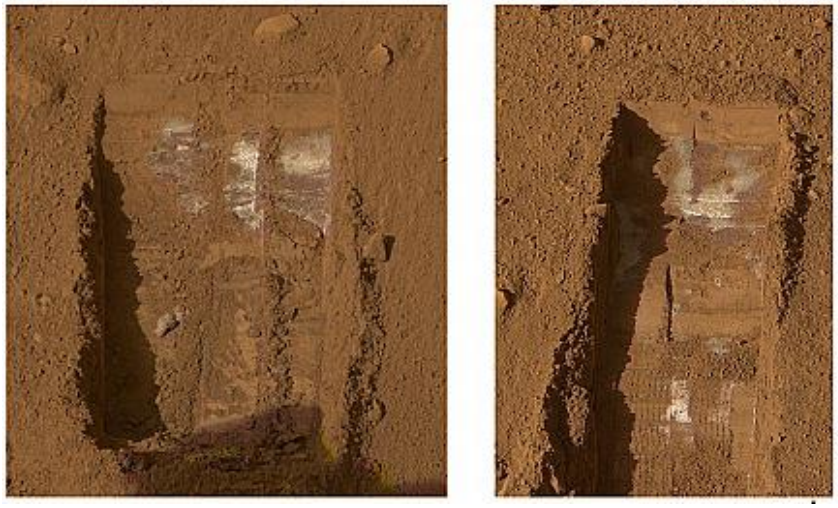

Figure 2.19 Examples of water ice found in soil exposed in a trench dug by the Phoenix lander (Mellon et al., 2009).Trench around 10 cm across. The landing site is located at 68° N and 125° W. Further observations confirmed that this ice quickly sublimated confirming that although ice maybe unstable at the martian surface a thin covering of sediment can protect it from sublimation.

The presence of widespread ground ice is also supported by observations of a bright white material found in recent impact craters in the northern plains (see *Figure 2.20*; Byrne et al., 2009). Of the five sites described by Byrne et al. (2009) one is in Amazonis Planitia and three occur on the Arcadia/Utopia boundary. Bryne et al. (2009) shows all five sites display excavated material from depths of decametres that displays a brightness and colour indicative of water ice with fading over the subsequent months as to be expected for sublimating ice.

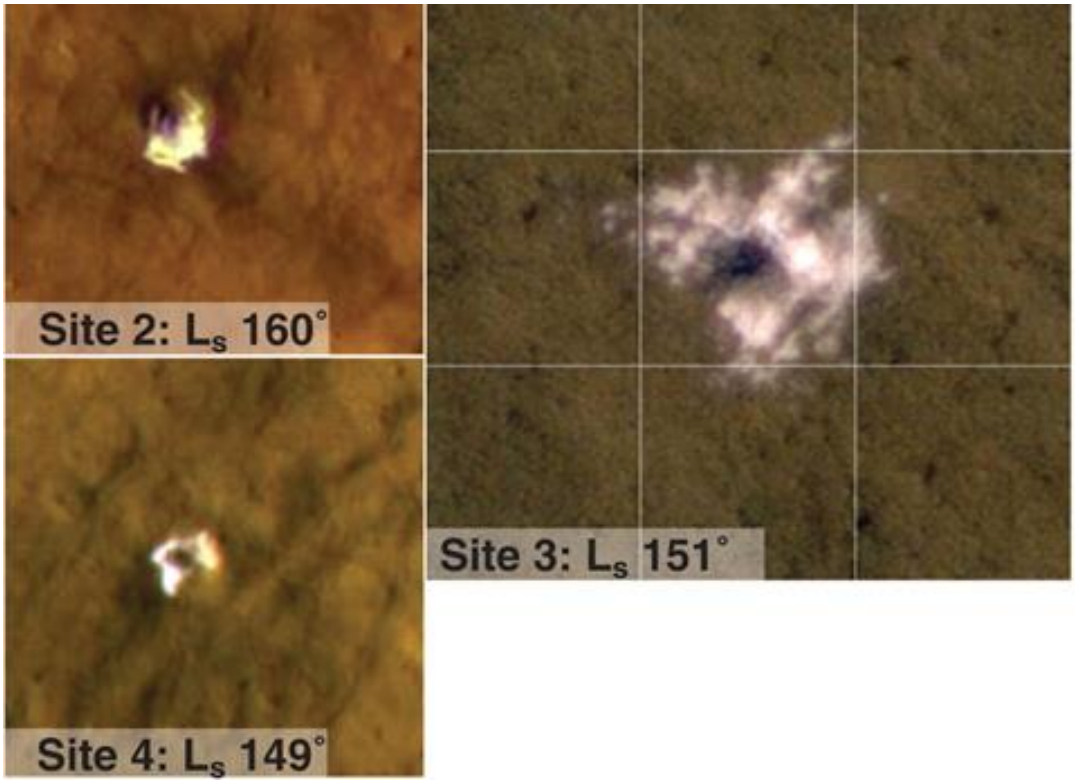

Figure 2.20 HiRISE false-color data of sites 2 to 4 from Bryne et al. (2009). Left panels are 35 m across; gridlines at site 3 show the scale (18 m). Images show icy material exposed by recent impact craters into the northern plains. Like the observations from the phoenix lander this shows that while ice maybe unstable at the martian surface sediment can protect it from sublimation.

2.6. **What is the distribution of ground ice and can it be related to distinct latitudinal bands, different geological units, physiographic provinces, and/or topography?**

The spatial distributions of some landforms indicative of ground ice have been measured and, to some extent, correlated with latitude (and therefore, perhaps, climatic processes). These include dissected terrains (where the LDM appear to be degrading; Milliken et al., 2003), gullies (Harrison et al., 2015; Milliken et al., 2003), VFFs (Levy et al., 2014; Milliken et al., 2003) and glacier-like forms, GLFs (Souness et al., 2012) all four of which occur in 30-60° N/S latitude bands (see Figure 2.21 and Figure 2.22).

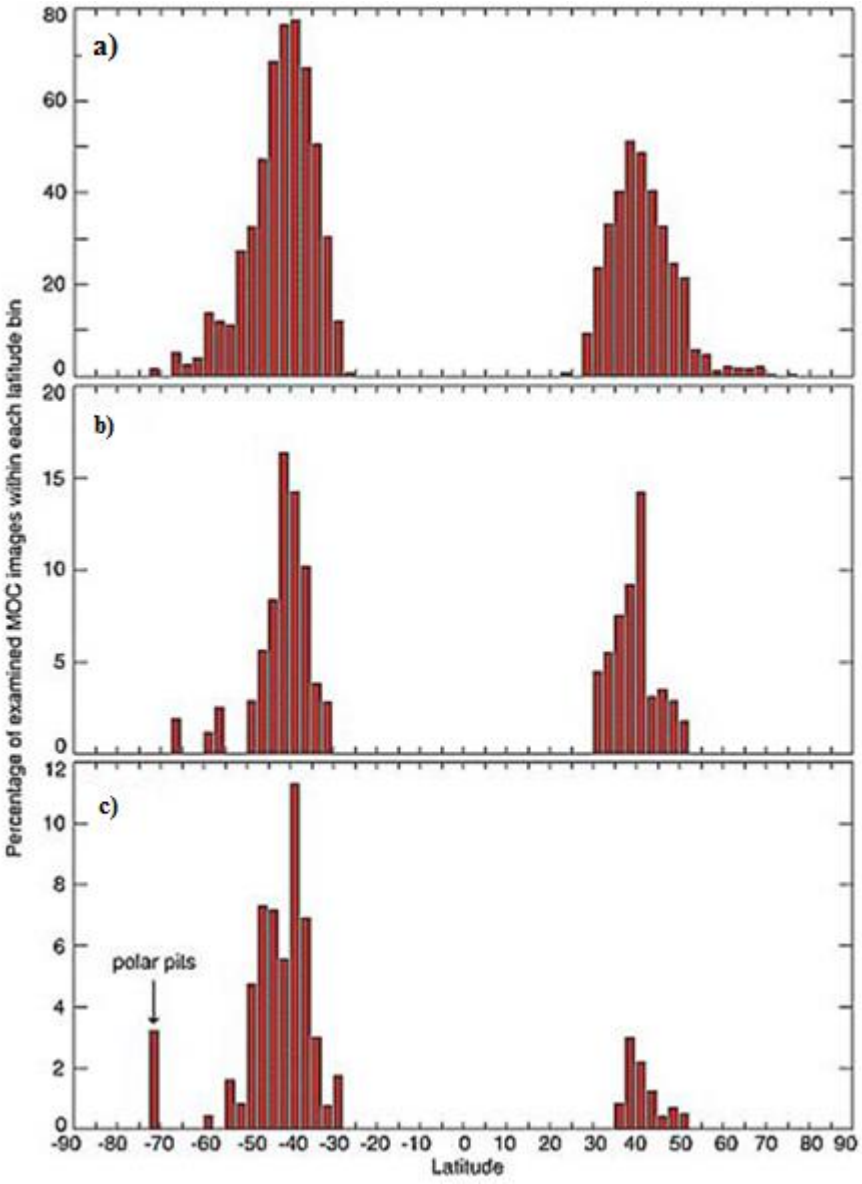

Figure 2.21 From Milliken et al., 2003: Location and distribution of (a) dissected mantle terrain, (b) viscous flow features (VFF), and (c) gullies. Note that all three features occur within the 30–60° N/S latitude bands. The data are in 2.5° latitude bins.

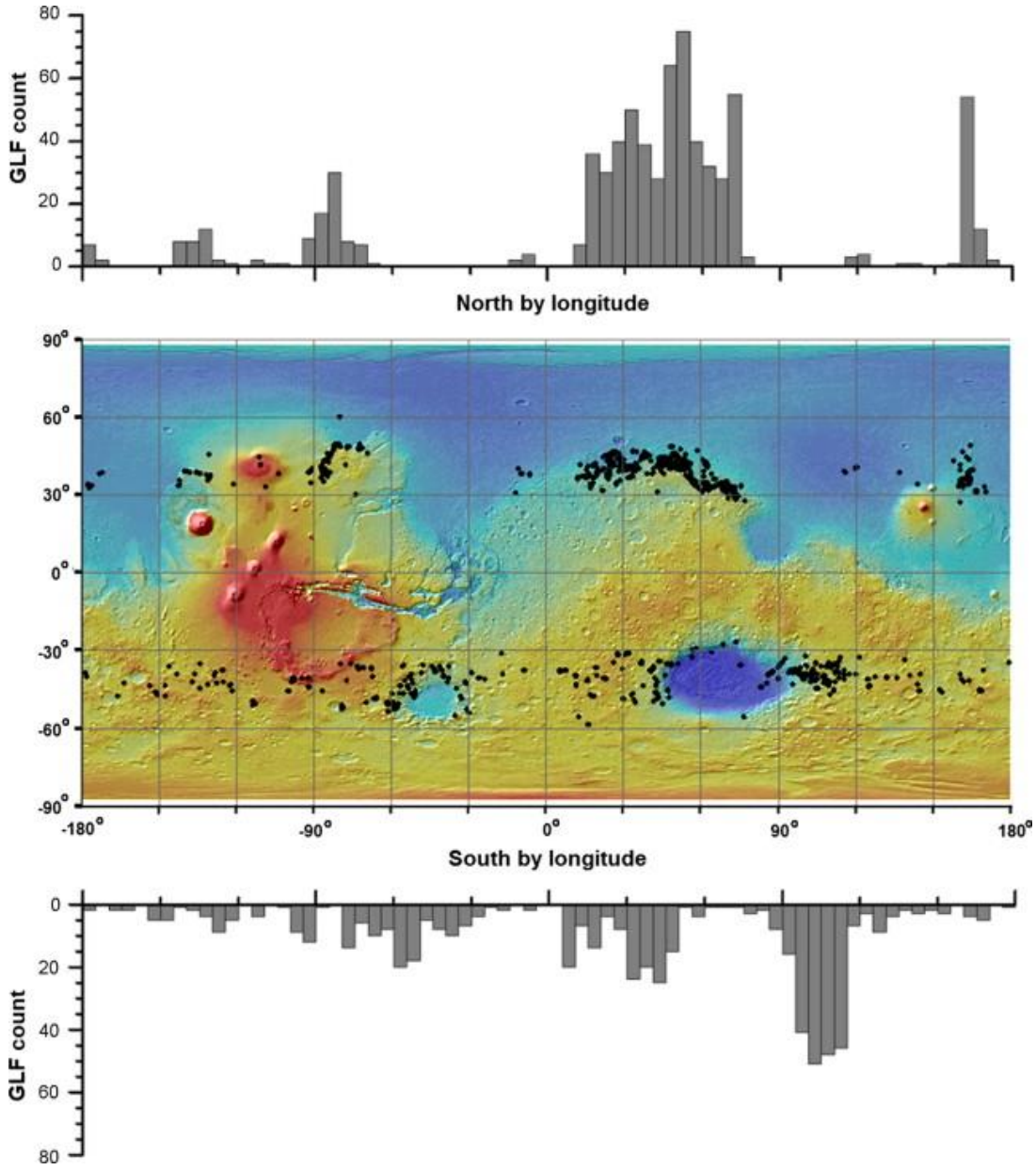

Figure 2.22 From Souness et al., 2012: Mars global map showing the mid-latitude distribution of glacier-like forms (GLFs). 1309 GLFs were identified globally. 727 were located in the northern hemisphere and 582 were located in the southern hemisphere. Histograms are displayed above and below the distribution map showing concentration of GLFs per 5° longitude. GLF locations are plotted on a MOLA hillshade projection.

Although broad latitudinal controls exist for some features, broad-scale heterogeneity in surface features exists within latitude bands (e.g. Geology; Tanaka et al., 2005, craters; Barlow and Bradley, 1990; Robbins and Hynek, 2012, latitude-dependent mantle, LDM; Kreslavsky and Head, 2002b, GLFs; Souness et al., 2012). This suggests that both local

controls and broad climate-related controls played a role in the evolution of the northern plains, which requires a more detailed understanding of the relationships between the geological units of the northern plains, the boundary conditions, and the resulting geomorphic landforms. While at first glance if may appear that heterogeneity in geology and crater morphology may have little to do with the distribution of ground ice it appears that crater morphology may provide an indication to the presence of ground ice (Barlow and Perez, 2003). Pedestal craters are believed to have formed through armouring ice deposits protecting them from ablation and subsequent erosion of the inter-crater regions (e.g. Kadish et al., 2008). Geology may play a part in whether ground ice is present. For example ice lenses are more freely able to form in loose sediments than solid rock. Systematic, targeted geomorphological mapping of the spatial distribution of landforms thought to be indicative of ice in the regolith must be completed if we are to understand the geological evolution, environmental changes, and astrobiological potential (particularly to understand whether sufficient liquid water was ever generated from ground-ice thaw; e.g., Ulrich et al., 2012) of the martian northern plains.

2.7. What insights can we gain from understanding the spatial distribution of the ground ice in the northern plains with regards to its origins and history?

2.7.1. How was ice in the northern plains emplaced?

There is ample geomorphological evidence showing ice-related landforms in the northern plain of Mars. But how was this ice emplaced? There appear to be three possible mechanisms: (i) ground ice in the northern plains is primordial ice that is the frozen remnant of a northern ocean; (ii) ground ice was fluvially emplaced into the northern plains, ending up either as buried frozen seas and lakes, or as icy sediments deposited from long lived fluvial activity, or more likely during floodwater outbursts onto the northern plains (Baker et al., 1991; Clifford and Parker, 2001; Head et al., 1999; Masursky et al., 1977); and (iii) atmospheric air-fall precipitation of snow or ice followed by burial and

mixing with dust, produced ice-rich deposits, protected from sublimation by auto-generated lag covers. Such a mechanism would explain both draping mantles (LDM) and VFFs, depending on the dust content or coverage of the deposited ice.

Some authors suggest that air-fall precipitation is unlikely under Mars' current climate (e.g. Read and Lewis, 2004) and that direct condensation into the pore spaces within the loose surficial materials is more probable (Mellon et al., 2008; Mellon and Jakosky, 1995; Mustard et al., 2001). However, Souness and Hubbard (2012) argued that this appears to be at odds with the results of SHARAD based studies (Holt et al., 2008; Plaut et al., 2009) of LDAs, which show them to be glacial landforms comprised largely of water ice with minimal lithic content and thereby supporting the air-fall hypothesis. Proponents to the air-fall model have argued also that snowfall may have been possible during Mars' recent past (Forget et al., 2006; Kite et al., 2011; Levy et al., 2009, 2014; Page et al., 2009) and that snow, if buried by significant dust or debris, could have been protected against ablation and have survived since the last Martian glacial phase (Bryson et al., 2008; Fanale et al., 1986).

In general, the origins of the ice in the northern plains remains an open question – although for some landforms, such as the LDM, which drapes topography, the origin seems more clear. Systematic mapping of the landforms present in the northern plains, and trying to establish what form the ice takes and how it has evolved over time, is required if we are to understand the origins of the ground ice in the northern plains. As a wealth of new data becomes available, more detailed observations will be made possible and will need to be compiled into the global or hemispherical datasets required to understand the Martian water budget. This thesis aims to clarify where the landforms indicative of ground ice occur and to shed light on the origins of this ice.

Ground ice on Mars could represent the largest reservoir of water on that planet (Rossbacher and Judson, 1981). If we are able to locate and identify landforms indicative

of ground ice we are able to better establish how much water ice may be present. Understanding the preservation states alongside the age of these landforms can provide insight on the processes and time frame of the Martian water cycle. Climate and thermal modelling predicts that ground ice should be present northward of 30-40°N (e.g. Fanale et al., 1986). However, modelling also shows at previous obliquities ground ice could have been stable globally, so we might expect to find relict ground ice structures south of 30-40°N (e.g. Mellon and Jakosky, 1995). These hypotheses are supported by observations of the latitude dependant mantle (northward of 40°N; e.g. Mustard et al., 2001) and patterned ground (northward of 55°N e.g. Mangold et al., 2004). Better understanding the geological evolution of the landforms indicative of water ice can provide insight into environmental change and potential astrobiology (if sufficient liquid water were ever generated from ground-ice thaw) of the martian northern plains.

The key aspect of this thesis are to explore what controls the distribution of ice-related landforms, and what is the origin of the ice that they represent. I will test the hypothesis that the spatial distribution of most ice-related landforms is based on latitude (as a proxy for climatic control) and also, therefore, that the origin of the ice is mainly by air fall deposition.

3. **Methodology**

Geomorphology is the scientific study of how physical, chemical or biological surface processes shape the landscape. This thesis uses a geomorphological approach to attempt to characterize the landscape of the northern plains of Mars. Practically, planetary geomorphology requires detailed observations taken from spacecraft in orbit, so to acquire detailed and repeat observations of the martian surface requires satellites in orbit around Mars (e.g. Figure 3.1).

The first spacecraft to successfully enter orbit around Mars, or any planet other than Earth, was Mariner 9 in 1971 (McCauley et al., 1972). At the time of writing, there are six active satellites (Mars Express, Mars Reconnaissance Orbiter, Mars Odyssey, MAVEN, Mangalyaan, and ExoMars Trace Gas Orbiter) returning data from Mars' orbit. All of Mars has been imaged from orbit, with around 90% of the planet being imaged at around 6 m/pixel resolution (Malin et al., 2007). Orbiters are able to make a variety of observations about a planet's surface including images (both visible images and those sensitive to other parts of the electromagnetic spectrum), topography (measured by laser altimeters or stereo imaging; e.g. Smith et al., 1993 and Neukum and Jaumann, 2004), gravitional and magnetic properties (e.g. Albee et al., 1998), and aspects of the near surface composition (based on various spectrometers and ground penetrating RADAR; e.g. Christensen et al., 2004 and Picardi et al., 2005). The successful Mars orbiter missions, and their related data products, are summarised in table 3.1, with those instruments/data that are widely used in this thesis shown underlined.

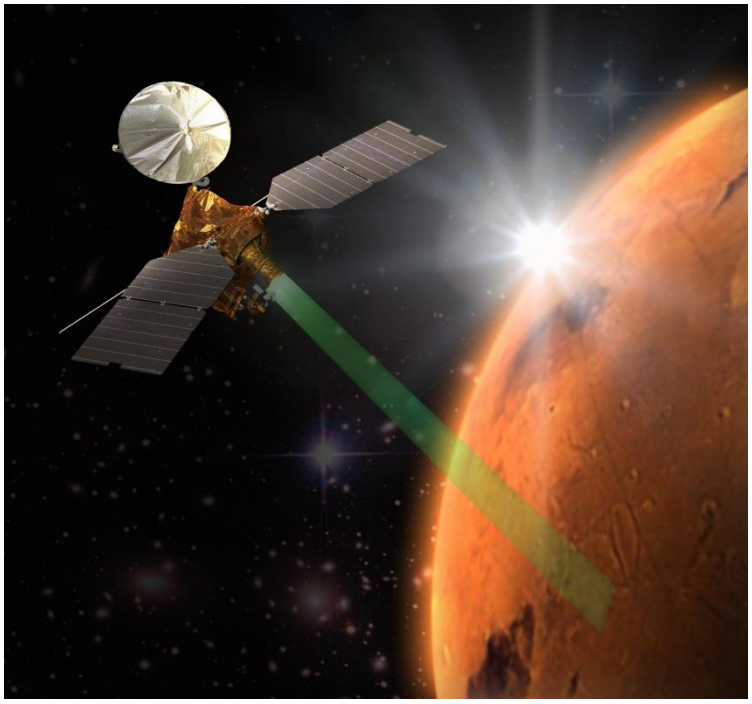

Figure 3.1 Mars Reconnaissance Orbiter (MRO) observing Rahway Vallis, Mars.

While conducting remote sensing geomorphological observations on Earth it is common practice – and in many cases a necessity – to conduct "ground truth" observation by visiting a sample of the sites observed. In almost all cases, this is an unavailable luxury with respect to Mars. However, conducting lander/rover based observations can allow in-situ observations and even chemical/physical examination of the surface. From the first shoebox-sized rover Sojourner in 1997 that wielded a small camera, Alpha Particle X-ray Spectrometer (APXS) and weather sensors to the car-sized Curiosity rover, the rover missions have progressively been getting bigger and better (Carr, 2015).

The Curiosity rover as part of the MSL (Mars Science Laboratory) Mission carries a small labs' worth of equipment with the objective of identifying both water and the chemical building blocks for life alongside high resolution cameras (see Figure 3.2; Grotzinger et al., 2012). The rationale for MSL mission is that of "following the water" to "seek signs of life" though identifying possible organics and life essential elements, for example carbon, hydrogen, nitrogen, oxygen, phosphorus and sulphur, in the hope of determining whether life could ever have arose on Mars. This, alongside characterising the climate, radiation

levels and geology of Mars are seen as necessary steps in paving the way for human exploration of Mars. These missions are shown in Table 3.2.

Table 3.1 Successful Mars orbiter missions and related data products; instruments used in this thesis are underlined. Adapted from the complete NASA Chronology of Mars Exploration http://nssdc.gsfc.nasa.gov/planetary/chronology_mars.html.

Agency	Mission	Year	Data Products (Surface Observing Instruments)
NASA	Mariner 9	1971-1972	Returned >7000 images covering 85% of the surface.
Soviet Union	Mars 2 & 3	1971-1972	Arriving together these orbiters returned around 60 images of the surface.
Soviet Union	Mars 5	1973-1974	Returned 43 useable images before failing due to a leak in the pressurised instrument compartment.
NASA	Viking 1	1975-1980	The scientific payload for the two Viking orbiters included visible light and infrared imaging and instruments of measuring atmospheric water vapour.
NASA	Viking 2	1975-1978	
Soviet Union	Phobos 2	1988-1989	Largely observed Phobos: VSK Imaging system ISM Thermal Infrared Spectrometer Lima-D Laser Experiment Thermal Imaging Camera Magnetometrs Gamma-ray Spectrometers X-Ray Telescope Radar and Laser Altimeters
NASA	Mars Global Surveyor	1996-2006	Mars Orbiter Camera (**MOC**) Mars Orbiter Laser Altimeter (**MOLA**) Thermal Emission Spectrometer (**TES**) Magnetometer and Electron Reflectometer (**MAG/ER**)
NASA	2001 Mars Odyssey	2001-Present	Thermal Emission Imaging System (**THEMIS**) Gamma Ray Spectrometer (**GRS**)
ESA	Mars Express	2003-Present	High Resolution Stereo Camera (**HRSC**) up to 2 m/pix Visible and Infrared Mineralogical Mapping Spectrometer (**OMEGA**) 100 m resolution Sub-Surface Sounding Radar Altimeter (**MARSIS**)
NASA	Mars Reconnaissance Orbiter	2005-Present	The High Resolution Imaging Science Experiment camera (**HiRISE**) The Context Camera (**CTX**) The Compact Reconnaissance Imaging Spectrometer for Mars (**CRISM**) Shallow Subsurface Radar (**SHARAD**)
ISRO	Mars Orbiter Mission	2013-Present	Thermal Infrared Imaging Spectrometer (**TIS**) Mars Colour Camera (**MCC**)
NASA	MAVEN	2013-Present	Imaging Ultraviolet Spectrometer (**IUVS**) Neutral Gas and Ion Mass Spectrometer (**NGIMS**) Solar Wind Electron Analyzer (**SWEA**) Solar Wind Ion Analyzer (**SWIA**) SupraThermal And Thermal Ion Composition (**STATIC**) Solar Energetic Particle (**SEP**) Langmuir Probe and Waves (**LPW**) Magnetometer (**MAG**)

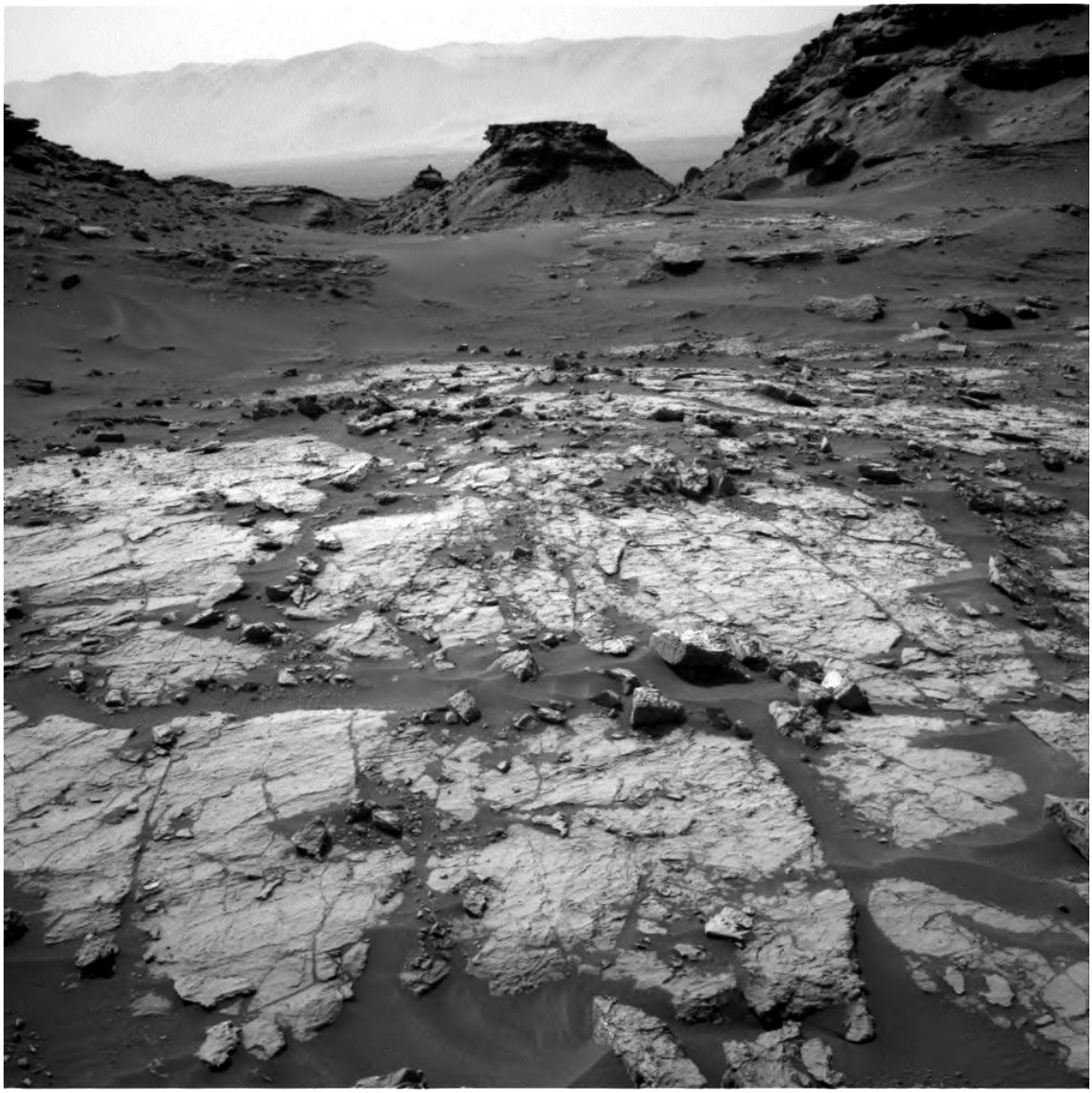

Figure 3.2 Mastcam image for Curiosity studying the stratigraphy of the Murray Buttes. This image shows the Murray Formation, deposits that are dominated by mudstones stratified at the millimetre scale. From http://mars.nasa.gov/msl/mission/mars-rover-curiosity-mission-updates/.

Table 3.2. Successful Mars lander/rover missions and related data products.

Agency	**Mission**	**Year**	**Data Products (Instrument)**
Soviet Union	Mars 2 & 3	1971-1972	The Mars 2 lander crash-landed. Mars 3 lander however managed to return the first ever image from the surface of another planet before communications ceased.
NASA	Viking 1	1975-1982	Two 360° cameras Seismometer Gas Chromatograph Mass Spectrometer X-Ray Fluorescence Spectrometer Pressure temperature and wind sensors.
NASA	Viking 2	1975-1980	
NASA	Mars Pathfinder and Sojourner Rover	1996-1997	Imager for Mars Pathfinder (**IMP**) and 3 Sojourner Cameras Atmospheric and Meteorological Sensors (**ASI**/**MET**) Laser Striper hazard detection system
NASA	MER-A Spirit	2003-2011	Panoramic Camera (**Pancam**) Navigation Camera (**Navcam**) Microscopic Imager (**MI**) Miniature Thermal Emission Spectrometer (**Mini-TES**) Alpha Particle X-ray Spectrometer (**APXS**) Mössbauer Spectrometer (**MB**) Rock Abrasion Tool (**RAT**) Two 120° Hazcams
NASA	MER-B Opportunity	2003-Present	
NASA	Phoenix	2007-2008	Surface Stereo Imager (**SSI**) Mars Descent Imager (**MARDI**) Meteorological Station (**MET**) Robotic Arm and Camera (**RA**) Thermal and Evolved Gas Analyzer (**TEGA**) Microscopy Electrochemistry and Conductivity Analyzer (**MECA**) Thermal and Electrical Conductivity Probe(**TECP**) Wet Chemistry Lab (**WCL**)
NASA	MSL *Curiosity*	2011-Present	Mast Camera (**MastCam**) Chemistry and Camera Complex (**ChemCam**) Mars Hand Lens Imager (**MAHLI**) Mars Descent Imager (**MARDI**) Alpha Particle X-ray Spectrometer (**APXS**) Chemistry and Mineralogy (**ChemMin**) Sample Analysis at Mars (**SAM**) Radiation Assessment Detector (**RAD**) Dynamic Albedo of Neutrons (**DAN**) Dust Removal Tool (**DRT**) Robotic Arm Navigation Cameras (**navcams**) Hazard Avoidance Camera (**hazcams**)

3.1. **Elevation and Topography data**

For elevation and topography measurements this thesis mainly uses Mars Orbiter Laser Altimeter (MOLA; Smith et al., 1993) data. This data product has a ~1 m vertical accuracy, based on averaging the heights within a ~150 m surface spot size. The individual spots (often called "point data") are situated along a spacecraft orbital track at ~300 m spacing. Elevations given throughout this thesis refer to the zero elevation being defined as Mars' mean planetary radius (Smith et al., 1999, 2001) unless otherwise stated. Topographical analysis was done along MOLA tracks to give the maximum resolution. Where elevation raster data were required, the official MOLA gridded data set was downloaded from Planetary Data Systems' Geosciences Node, Mars Orbital Data Explorer (ODE; http://ode.rsl.wustl.edu/mars/). This is an interpolated, gridded topography product, based on the MOLA point data, and has a resolution of ~460 m/pixel. MOLA elevation data was processed in ArcGIS to create hillshades, slope maps and hypothesised flow-direction maps. I used these maps to identify channel and valley networks. Kreslavsky and Head, (2000) used MOLA data to create kilometre-scale roughness maps. I used this dataset during the reconnaissance mapping in Chapter 4 to identify large-scale changes in surface roughness. Mean slope values were calculated for each grid square using ArcGIS and MOLA data. Approximate roughness values were approximated by calculating the difference between the surface area of each 20 km by 20 km grid square and the surface area assuming a flat surface.

3.2. **Imaging data**

The geomorphological analysis and mapping in this thesis was performed primarily using publically available Context Imager (CTX; ~6 m/pixel; Malin et al., 2007) and High Resolution Stereo Camera (HRSC;12 m/pixel; Neukum and Jaumann, 2004) images. CTX images were downloaded, pre-processed directly from the Arizona State University Mars Portal (http://global-data.mars.asu.edu/) and inserted into ArcGIS 10 software. THermal

EMission Imaging System (THEMIS; Christensen et al., 2004), HRSC, and High Resolution Science Imaging Experiment images (HiRISE; McEwen et al., 2007) were downloaded from the ODE. With around 90% global coverage CTX images were first choice for basemaps during this project. The majority of mapping and morphometrics were taken using CTX images. THEMIS images highlight differences in thermal inertia and aid in the identification of units. HiRISE images allowed for detailed sub-metre scale observations where available. This was useful in identifying individual clasts within the sinuous ridges described in Chapter 6.

3.3. **Geographic Information Systems (GIS)**

A Geographic Information System, or 'GIS', is a software framework used for capturing, storing, displaying, and analysing data related to some kind of spatial projection – usually a planetary surface. A GIS can show multiple data types in many map layers within the program. This makes viewing, analysing, and understanding spatial patterns and relationships much easier and is crucial for modern planetary geomorphology. The GIS system used in this thesis is primarily the commercial software package "ERSI ArcGIS 10.1".

A planet can be represented by various spatial reference systems, each of which may provide a different set of XYZ coordinates. For this research I have used the Mars 2000 spherical datum. On this sphere, we are able to project the data. Like paper maps, ArcGIS uses a flat surface to represent the globe rather than displaying an actual sphere. Projecting a 3D image onto a flat surface means that distortion is inevitable. However, each projection system distorts the surface differently. Understanding how different projections systems distort the surface is crucial to both making measurements and knowing how best to display the data. This thesis uses three main projection systems, equidistant cylindrical (also known as "equirectangular") projection – to minimise distortion along a line of

latitude (most commonly the equator), Cassini – to minimise distortion along a line of longitude, or polar projection North Pole Stereographic to display the northern hemisphere.

3.4. Northern Plains mapping: ISSI team approach

As described in Chapter 1, part of this thesis describes my contribution to an international project run under the auspices of an International Space Science Institute (ISSI) "international team". This project involved mapping three long cross-latitudinal strips of the northern plains of Mars, looking for geomorphological evidence of ice at (or near) the surface. My major contributions to this project included leading one mapping swath (the Arcadia Planitia study area – see Chapter 4) but also for designing, testing and communicating the mapping strategy, using a methodology that I have dubbed "grid-mapping". The remainder of this chapter is based upon a paper that is in the final stages of preparation to be submitted for peer-review with myself as lead author. The paper text, which commences at section 3.5, describes the grid-mapping approach, its implementation and testing and the advantages and disadvantages of the method.

3.4.1. Key Research Questions of the ISSI project

The top-level science questions (A-C) that drove the study are listed below, together with more focussed research questions or tasks that were used to make progress towards the top-level questions:

A. What is the distribution of ice-related landforms in the northern plains, and can it be related to distinct geological or geomorphological units?

• Where are ice-related landforms/surfaces in each mapping strip?

To address this question we decided upon the mapping of ice-related landforms, definable in CTX images in three long strips situated so as to cut across each of three major basins on the Northern Plains.

B. What is the relationship between the latitude dependent mantle (LDM;* Kreslavsky and Head, 2002) *and (i) the suite of landforms indicative of ground ice, and (ii) other geological units in the northern plains?

•Where is the latitude dependent mantle in each strip – can it be identified?

To begin with, we were unsure whether the LDM could be identified reliably in CTX images. However, during the reconnaissance mapping of Arcadia, I was able to show that it could be identified at between 1:10,000 and 1:20,000 scale in CTX images, allowing it to be mapped alongside other ice-related landforms.

C. What are the distributions and unit associations of very recent landforms thought to be indicative of thaw of ice or snow (e.g. gullies, clastic networks such as solifluction lobes, stone polygons etc)?

- Where are thaw related landforms?

We hoped to address both the question of thaw and of ice-related landforms simultaneously through the mapping of landforms visible in CTX. In addition to the ISSI work, Chapter 6 addresses a potential source of liquid water into Arcadia Planitia from Rahway and Marte Vallis.

From these, questions we produced the following hypotheses that we sought to test:

- There is intact ground ice north of ~40° N.
- There are relict ground ice structures south of ~ 40°N.
- The distribution of landforms indicative of ground ice will be controlled primarily by latitude.
- Evidence for thaw and sublimation will be more prevalent south of 40°N.

3.4.2. **Selection of the ISSI Strips**

The northern lowlands can be broken down into; Planum Borum, Acidalia Planitia, Amazonia Planitia, Arcadia Planitia, Utopia Planitia, and the Isidis basin (see Figure 1.1). Planum Boreum can be described as the northern polar plain of Mars and it extends northward of roughly 80°N, containing Mars' northern ice cap. The northern ice cap is centred within the northern plains and is roughly 1.2 million km^3 in size (Tanaka et al., 2005) and consists largely of water ice with a thin CO_2 deposit during the winter (Kieffer, 1979). The ice cap is surrounded by vast dune fields called the Olympia Undae (Hayward et al., 2007). The ice cap is dissected by spiral troughs that expose the layers and extend almost to the full depth of the northern cap (Tanaka et al., 2005).

Amazonis Planitia is located between Elysium and Olympus Mons and is remarkably smooth and flat. These plains show very few craters and are amongst the youngest on Mars, approximately 100 million years old (e.g. Tanaka et al., 2005). The landscape is hypothesised to have been created by large scale effusive volcanism (e.g. Plescia, 2003). The Amazonis plains host much of the Medusa Fossae formation, an easily eroded deposit found close to the Martian dichotomy boundary (Bradley et al., 2002), which often has yardangs suggesting its primary agent of erosion is wind. Arcadia Planitia is located north of and connected to Amazonis Planitia. Large areas of Arcadia Planitia display thumbprint terrain, sand dunes and polygons (e.g. Tanaka et al., 2005).

Utopia Planitia is located northeast of the Isidis basin and has been suggested to be the largest impact basin in the solar system with an estimated diameter of 3300 km (McGill, 1989). Previous work has identified large areas of scalloped topography (e.g. Séjourné et al., 2012). Acidalia Planitia is named after a corresponding albedo feature on a map by Giovanni Schiaparelli (Schiaparelli, 1882) and is located between the Tharsis volcanic province and Arabia Terra. The Isidis basin is an impact basin around 1500 km in diameter that lies over the dichotomy boundary and is located at the western edge of Utopia Planitia.

To test for latitudinal trends in landform abundance the ISSI team decided to map three long narrow strips through the three major planitia, with one strip going through Utopia, one through Acidalia and another going through the joint planitias of Arcadia and Amazonis. The exact longitudinal locations of the ISSI strips within each designated area were chosen to maximise CTX latitudinal coverage. Where CTX availability was evenly distributed, the priority was to produce a representative strip, not to intentionally target the most interesting features of the area. For example, the Arcadia strip was selected based upon the reconnaissance mapping (see below). The southern boundary is at 30°N, well into the platy-ridge material, proposed to comprise effusive volcanic materials (Tanaka et al., 2005), which dominate the Amazonis basin (Plescia, 2003; Tanaka et al., 2005). The northern boundary at 80°N is well into the dunefields that dominate the most northern part of Arcadia where the plains meet the north polar cap (Tanaka et al., 2005). This allows the strip to cover full range of latitudes that have potential for ground ice-related landforms. The centre longitude of 170° W was selected to optimise CTX image coverage.

3.4.3. **Reconnaissance**

The ISSI team adopted a two-stage strategy. The first stage was reconnaissance mapping to provide context for the landform mapping to be conducted in the second stage. The planned map scale was 1:10M (i.e. the Arcadia map would be about 4cm wide by 40 cm tall if printed). The reconnaissance mapping had a digital scale of 1:2M following a USGS rule of thumb of mapping at approximately 5 times the desired printed scale. We used a vertex spacing (when digitising using lines or polygons) of 2 km.

The approach was to digitise the basic structures and features within the strip. This provides topographic and regional context for the later, detailed maps of landform spatial distribution. The context mapping included:

- Major tectonic features such as wrinkle ridges, faults, fractures (etc.) that are at least 10km in length.

• Impact craters visible at 1:10M (i.e. craters with indistinct ejecta that have diameters > 10km or craters with distinct ejecta that have ejecta > 10km in diameter).

• Large regions (>10 km across) of distinctive surface morphology (dunes, polar caps, lava flows etc).

• Channels, valleys etc (inverted or otherwise) that are > 10km in length.

• North polar cap outliers and dunefields.

• Where possible, broadly defined units (perhaps defined by previously published maps in the first instance) should be included.

Large parts of this reconnaissance mapping were completed by adapting previous global or regional maps and by including data from other studies (see Chapter 5). In addition to mapping the large scale features, during the reconnaissance stage, we compiled an inventory of which ice-related landforms could be identified in CTX images within our areas in preparation for the thematic landform mapping.

3.5. Grid-based mapping: a method for rapidly determining the spatial distributions of small features over very large areas.

Ramsdale, J.D.[(1)], Balme, M.R.[(1)], Conway, S.J. [(1)], Gallagher, C.J., van Gasselt, S.A., Hauber, E., Orgel, C., Séjourné, A., Skinner, J.A., Jr., Costard, F., Johnsson, A., Losiak, A., Reiss, D., Swirad, Z., Kereszturi, A., Platz, T.

This rest of this chapter forms one of five proposed papers to be submitted to Icarus by the ISSI group. It is to provide an introduction and standardised methods to the grid mapping approach developed as part of this thesis. Section 3.5 discusses the need for a standardised approach with regards to planetary geomorphology and outlines the problems of trying to incorporate high resolution images into hemispherical mapping efforts. Section 3.5 covers

the approach through preliminary reconnaissance, landform and grid selection, testing and refinement, normalisation and finalisation. Section 3.5 gives insight on how to analyse grid mapping data and how it can be compared with other datasets. The discussion attempts to provide and argument for the advantages and disadvantages of the approach and provide guidance on how the approach can be adapted or implemented in future work.

3.5.1. **Abstract**

The increased volume, spatial resolution, and areal coverage of high-resolution images of Mars over the past 15 years have led to an increased quantity and variety of small-scale landform identifications. Though many such landforms are too small to represent individually on regional-scale maps, determining their presence or absence across large areas helps form the observational basis for developing hypotheses on the geological nature and environmental history of a study area. The combination of improved spatial resolution and near-continuous coverage significantly increases the time required to analyse the data. This becomes problematic when attempting regional or global-scale studies of metre and decimetre-scale landforms. Here, we describe an approach for mapping small features across large areas, formulated for a project to study the northern plains of Mars, and provide context on how this method was developed and how it can be implemented.

Rather than “mapping” with points and polygons, grid-based mapping uses a “tick box” approach to efficiently record the locations of specific landforms. A grid of squares (e.g. 20 km by 20 km) is created over the mapping area. Then the basemap data are systematically examined, grid-square by grid-square at full resolution, in order to identify the landforms while recording the presence or absence of selected landforms in each grid-square to determine spatial distributions. The result is a series of grids recording the distribution of all the mapped landforms across the study area. In some ways, these are equivalent to raster images, as they show a continuous distribution-field of the various landforms across

a defined (rectangular, in most cases) area. When overlain on context maps, these form a coarse, digital landform map.

We find that grid-based mapping provides an efficient solution to the problems of mapping small landforms over large areas, by providing a consistent and standardised approach to spatial data collection. The simplicity of the grid-based mapping approach makes it extremely scalable and workable for group efforts, requiring minimal user experience and producing consistent and repeatable results. The discrete nature of the datasets, simplicity of approach, and divisibility of tasks, open up the possibility for citizen science in which crowdsourcing large grid-based mapping areas could be applied.

3.5.2. **Introduction**

With increasing coverage of high-resolution images of the surface of Mars (e.g. Context Imager – CTX, ~ 6 m/pixel, Malin et al., 2007, covering ~ 90% of the surface) we are able to identify increasing numbers and diversity of small-scale landforms. Many such landforms are too small to represent individually on regional maps, yet determining their presence or absence across large areas can form the observational basis for developing hypotheses on the geological nature and environmental history of a study area. The combination of improved spatial resolution with near-continuous coverage in spatial data means that sub-sampling of a study areas is no longer needed when identifying landforms, but significantly more time is required to analyse the data. This becomes problematic when attempting regional or global-scale studies of metre and decimetre-scale landforms. Here, we describe an approach for mapping small features across large areas formulated for a project to study the northern plains of Mars and provide context on how this method was developed and how it can be implemented.

This project aimed to detail the geological and stratigraphic character of the martian northern plains, with particular regard to the role that near-surface ice has played in their evolutionary history through the mapping of surface ice-related features. It is thought

(Kreslavsky and Head, 2002; Lucchitta et al., 1986; Tanaka et al., 2005) that the uppermost layers of the northern plains are largely sediments that have been shaped by processes involving water-ice, but no consensus has emerged on the origin and emplacement mechanism of the ice. Kargel et al. (1995) discuss several proposed mechanisms of emplacement including freezing of fluvial, lacustrine or marine wet sediments, air-fall deposition/condensation, shallow groundwater processes, or a combination of these different processes. Furthermore, although the spatial distributions of some landform types have been measured and correlated with latitude-controlled climatic processes (transverse aeolian ridges, TARs; Wilson and Zimbelman, 2004, viscous-flow features, VFFs; Milliken et al., 2003, glacier-like forms, GLFs; Souness et al., 2012, dunes; e.g. Hayward et al., 2007), broad-scale heterogeneity in surface features exists within latitude bands (e.g. Geology; Tanaka et al., 2005, craters; Barlow and Bradley, 1990; Robbins and Hynek, 2012, latitude-dependant mantle, LDM; (Kreslavsky and Head, 2002). This suggests that regional geology and climate have played a dominant role in the evolution of the northern plains, which requires a more detailed understanding of the relationships between the geological units of the northern plains, the boundary conditions, and the resulting geomorphic landforms.

Systematic, targeted geomorphological mapping of the spatial distribution of landforms thought to be indicative of ice in the regolith must be completed if we are to understand the geological evolution, environmental change and astrobiological potential (particularly whether sufficient liquid water was ever generated from ground-ice thaw; e.g., Ulrich et al., 2012) of the martian northern plains. The project aimed to answer the following science questions: (1) What is the distribution of ice-related landforms in the northern plains and can it be related to distinct latitude bands, different geological units, physiographic provinces, and/or topography? (2) What is the relationship between the LDM and (a) landforms indicative of ground ice and (b) other geological units in the

northern plains?, (3) What are the distributions and associations of recent landforms indicative of thaw of ice or snow? This paper deals with the method used to answer these questions.

Previous work on the Martian northern plains includes the first global geologic map of Mars, which was produced at a 1:25,000,000 scale on a photomosaic of 1–3 km/pixel Mariner 9 visible wavelength images (Scott and Carr, 1978). Viking images with spatial resolutions of up to 100 m/pixel were analysed, leading to the production of three 1:15,000,000 scale maps (Greeley and Guest, 1987; Scott and Tanaka, 1986; Tanaka and Scott, 1987). These maps were combined and digitised for surface age reconstruction (Tanaka et al., 1988) and later updated to a GIS format (Skinner et al., 2006). Later, MOLA (Mars Orbiter Laser Altimeter; Smith et al., 1993) global topographic elevation data with 463 m/pixel spatial resolution or better and 1 m vertical precision (Smith et al., 1993), THEMIS (Thermal Emission Imaging System) near-infrared (IR) day and night-time images at 100 m/pixel (Christensen et al., 2004) and CTX images provided an excellent base for the next generation, 1:15,000,000 scale northern hemisphere map (Tanaka et al., 2005). A new global geological map at 1:20,000,000 scale with up to date chronostratigraphy and resurfacing ages has recently been published (Tanaka et al., 2014).

The early Mariner 9- and Viking-based geological maps were drafted by hand onto image mosaics or air brushed onto manually produced shaded relief bases (Batson et al., 1979). With the development of geographic information system (GIS) software, planetary mapping has become increasingly digital with older maps being scanned and digitised to allow for direct comparisons with the modern maps and bases that are developed almost entirely within GIS software (Tanaka et al., 2014). Both, the early and modern geological maps focus on boundary and unit mapping, recording the distribution of units and landforms on the planet’s surface and placing them within a chronological framework.

Where geological maps focus on placing observations into stratigraphic units, geomorphological maps can be considered graphical inventories of landscape that catalogue landforms, surface, and subsurface materials (Otto and Smith, 2013). Geomorphological maps can be categorised as either basic/analytical or derived/specialized. While basic maps are more generic and display the observed features of a landscape, derived or thematic maps are topically focused for a specific study or application. Traditionally, the basis for constructing a geomorphological map has been the drawing of points, lines, and polygons to represent landforms and surface types onto a topographic and/or image base map. For example, the northern plains of Mars are generally divided into allostratigraphic (unconformity-bounded) units based upon their inferred primary (emplacement) physical features, areal extent, relative ages, and geologic associations (Tanaka et al., 2005). However, small-scale (large area) geological and geomorphological maps are only capable of representing the largest features and the regional basement materials, and cannot consistently include decametre-scale landforms or thin surficial covers of materials. Previous martian geomorphological studies of small features have generally incorporated a survey-style approach and identified single landforms (TARs; Wilson and Zimbelman, 2004, VFFs; Milliken et al., 2003, GLFs; Souness et al., 2012, dunes; e.g. Hayward et al., 2007, craters; Barlow and Bradley, 1990; Robbins and Hynek, 2012, latitude-dependant mantle, LDM; Kreslavsky and Head, 2002). In most cases, these studies have used high resolution images that do not have a continuous spatial extent over the study area but instead are only small 'windows' sampling a subset of the true population of the features.

Where basic geomorphological mapping has been conducted on Mars, it has tended to be, at best, regional in scale (e.g. Valles Marineris; Peulvast et al., 2001, Hellas Basin; Kargel and Strom, 1992, Hale Crater; Jones et al., 2011) and there has been no global basic geomorphological mapping effort aimed at the sub-kilometre scale landforms. This is

largely due to the question of scale. The majority of identifiable ice-related landforms and terrain types are of meter to decametre scale and mapping them requires observations at 1:10,000 scale. This makes cataloguing their global spatial occurrence on a traditional 1:15,000,000 scale geomorphological global map an enormous task, first requiring the identification and classification of all visible, thematically relevant landforms in 1500 separate 1:10,000 mapping areas. However, a compromise between basic and derived thematic geomorphological mapping can be found in the grid-based mapping approach described in this manuscript. While not a replacement for geological mapping, grid-based mapping is a powerful approach that allows for systematic identification of the distribution of multiple landform types across very large continuous areas. We find that this approach provides a viable alternative – or pre-cursor supplement – to traditional geological and geomorphological mapping on regional to global scales.

3.5.3. **An overview of the grid-based mapping approach**

Rather than delineating discrete geological or geomorphological units and features using points, lines, and polygons on a continuous mapping base, (i.e., "traditional" mapping approach), our grid-based mapping approach uses a simple identifier for the presence of a specific landform in each cell of an overlain grid. This work demonstrates the first example of grid mapping used on Mars, although earlier similar methods have been used for the Earth in few cases, for example, mapping of glacial bedforms and erosional zones in NW Scotland (Bradwell, 2013) and various statistical analyses in hydrometeorology (Greene and Hudlow, 1982). The first (reconnaissance) stage of the approach is to conduct context/reconnaissance mapping using regional or global scale datasets. For Mars, this could be a combination of MOLA terrain and, for example, THEMIS daytime IR image mosaics. In addition, the formal basemap for the study area must also be constructed. Importantly, the basemap data type must be of sufficient resolution to identify all the required landforms reliably, and must have continuous (or near continuous) image

coverage. For the Martian northern plains study, we used CTX mosaics that had nearly complete coverage for each study area and that, with 6 m/px resolution, allowed decametre-scale landforms and surface textures to be identified. The aim of the context mapping is to: (i) identify large-scale features such as impact craters or large scale relief that provide topographic context, and (ii) to identify which specific landforms and terrain types will be systematically catalogued during the grid-based mapping. This suite of landforms can be either generic and include all the landforms seen within the area, or targeted in the context of a thematic geomorphological mapping programme. Either way, an important part of the reconnaissance stage is to study the basemap in detail and to produce a full inventory of the landforms types that will be catalogued. If previous studies have identified the diversity of landforms that are present, the reconnaissance should be used to select, group, and sub-divide the landforms into a workable list of features. One advantage of the grid-based mapping approach is that it enables the efficient identification of multiple landform types through a single, systematic pass through the overlain grid; repeated passes to augment or refine landform types effectively undercuts this efficiency. Thus, we emphasize that the reconnaissance step is critical to the grid-based mapping approach.

In the second (mapping) stage, the mapping area is divided into a grid, which should offer a labelling and divisional system for ease of identification of data and for communication between mappers. This is best performed in a GIS setting using a shapefile or feature class. The shapefile is given an attribute table, with a separate attribute for each landforms type to be studied and a unique identification code for each grid-square. The basemap imaging data are then systematically examined, grid-square by grid-square at full resolution (between 1:10,000 – 1:20,000 depending on the landforms present), in order to identify the landforms. Then, to record the spatial distribution of each of these landforms, their presence (or absence) in each grid-square is recorded in the grid-square shapefile attribute

table. In our northern plains study, landforms were recorded as being either “present”, “absent” or “dominant.” The “dominant” classification was used when a single landform type covered the entire grid-square to such an extent that other landforms could have been obscured. Where relevant, each grid-square can also be recorded as “null” (meaning “no data”) or “possible” if there is uncertainty in identification, either when the mapper is unsure or when the image quality is poor but there is some evidence to suggest that the landform is present.

The result is a series of grids recording the distribution of all thematically relevant mapped landforms across the study area. In some ways, these are equivalent to raster images, as they show a continuous distribution-field of the various different landform types across a defined (rectangular, in most cases) area. When overlain on context maps, these form a coarse, digital landform distribution map.

In section 3.5 we describe in detail how we applied the approach to one area in Arcadia Planitia during the Mars’ northern plains mapping project. This provides both contextual discussion about the effectiveness of the approach and in-depth methods for the results stemming from this project.

3.5.4. **Mapping the northern plains of Mars – the Arcadia Planitia Study area**

The northern plains project required mapping the spatial distribution of many ice-related landforms and surface types, in order to compare and contrast their distribution and generate hypotheses concerning their genesis. The northern plains comprise three main basin floors: Acidalia Planitia, Arcadia Planitia, and Utopia Planitia. A study area, consisting of a long latitudinal swath, was defined in each of these basins, with the precise location of the strips being selected largely based on the availability of high resolution images.

3.5.4.1. *Cartographic Projection*

The study area in Arcadia is a 300 km wide strip extending from 30° to 80° N latitude, centred on the 170° West line of longitude. We opted to use a Cassini projection centred on the 170° West meridian. The Cassini projection, is the transverse aspect of the commonly-used plate carrée, or equirectangular projection, with the equator at true scale. Where the plate carrée projection is based on a cylinder wrapped around the globe and tangent to the equator, the Cassini projection is a cylinder wrapped around the globe tangent to a chosen meridian. The advantage of this projection is that regions along the central meridian, and at right angles to it, have minimal distortion, making this projection ideal for long narrow north-south strips, like that of the three northern plains areas in this study.

3.5.4.2. *Data and Methods*

Geomorphological analysis and mapping were performed primarily using publically available CTX images. CTX images were downloaded pre-processed, directly from the Arizona State University Mars Portal and ingested into a GIS (ArcGIS 10.1). MOLA gridded data and hill-shade products with around 1 m vertical accuracy, MOLA track data with around 150 m surface spot size point data and around 300 m along-track spacing (Smith et al., 1993), and THEMIS images were downloaded from the Planetary Data Systems' Geosciences Node, Mars Orbital Data Explorer (ODE) and also ingested into the GIS.

The ESRI (Environmental Systems Research Institute, Inc. Redlands, CA) ArcGIS software package was used to display and manipulate the available datasets. Symbols were adapted from standard map drafting conventions (Federal Geographic Data Committee, 2006) and were provided as a package from the U.S. Geological Survey.

A simple reconnaissance map was created to give context to major relief and geological units. It used some of the line work from the published geological map of the northern

plains of Mars (Tanaka et al., 2005), with additional features based on our reconnaissance. The map scale of our context mapping was at 1:10,000,000 (i.e., the Arcadia strip would be about 3 cm wide by 30 cm tall if printed at this scale). The digital scale is around 1:2,000,000 with approximately 2 km vertex spacing for digitised lines and polygons; these scales are incapable of conveying the occurrence of local decimetre scale landforms individually. To identify the variety of landforms in the area, CTX images and THEMIS IR daytime images were overlaid onto MOLA hill-shade and elevation products. The suite of landforms identified within the Arcadia strip can be seen in *Figure 3.3* and the motivation for mapping these landforms in Table 3.3.

The mapping strip was divided into a 15 x 150 grid of squares, each 20 by 20 km. In ArcGIS, a polygon feature-class shapefile was produced, in which each grid-square was represented by a single square polygon object. In the attribute table of this shapefile, a new attribute for each landform type was added. The THEMIS IR day and CTX images were then viewed systematically at up to 1:10,000 scale for each grid-square and the presence or absence of each of the suite of landforms (described in section 3.5.4.3) was recorded.

3.5.4.3. ***Landform Selection***

The choice of landforms to include within a suite for thematic grid-based mapping is highly project-dependant; when deciding which landforms to include, scale, thematic relevance and grouping of related landforms must be considered. For the northern plains project we chose landforms that have been cited as providing evidence of past or present ground ice, including viscous flow features (VFFs; Hubbard et al., 2011), glacier like forms (GLFs; Hubbard et al., 2011), ~100 metre polygons (Mangold, 2005), scalloped and non-scalloped pits (which might have a thermokarstic origin; Costard and Kargel, 1995), and linear, wrinkled, brain and "basketball" terrain textures associated with the LDM (Kostama et al., 2006), which we have grouped under the class "Textured" for this study. In addition to searching for the textural signatures of the LDM, we also recorded instances

of topographic infilling and relief softening that provided a topographic (rather than textural) indication of a draping mantle (likely the LDM; Kostama et al., 2006)). We also chose to include landforms potentially indicative of thaw, such as gullies (e.g., Mellon and Phillips, 2001) and channels (e.g., Sharp and Malin, 1975).

Owing to their potential links with water/ice processes, the locations of kilometre-scale polygons, thumbprint terrain, large pitted mounds, and small mounds were recorded. The formation mechanism of the thumbprint terrain and associated large pitted mounds or cones is enigmatic and has been interpreted to be debris left behind after the removal of a static ice sheet (Grizzaffi and Schultz, 1989), rogen moraine - underwater glacial push moraine (Lockwood et al., 1992), mud volcanism (Davis and Tanaka, 1995), and various volcanic and lava/ice interaction features (Bridges et al., 2003; Bruno et al., 2004; Ghent et al., 2012; Plescia, 1980). Kilometre scale polygons or "giant polygons" are thought to be a product of tectonic, volcanic, dessication or compaction processes and could be a result of faulting and rebounding following the removal of a water/ice load (e.g. El Maarry et al., 2010; McGill and Hills, 1992; Pechmann, 1980). These kilometre-scale forms were mapped using a combination of THEMIS and CTX, as they can often be more easily seen in THEMIS than when 'zoomed-in' using CTX. Reconnaissance mapping revealed the presence of small mounds, typically small, featureless hills less than 30 metres in diameter that are morphologically similar to rootless cones (e.g. Lanagan et al., 2001), pingos (Burr et al., 2009), or erosional remnants. Finally, we chose to include landforms that might obscure or explain the absence of other landforms, obscuring landforms include dune fields, massive ice ("massive" in the spatial sence, not referring to geological layering) and continuous "bedrock" formations . An example of bedrock is the platy-ridged material inferred to be lava flows in Southern Arcadia/North Amazonis Planitia (Keszthelyi et al., 2000).

Gullies

Ravines carved into hill-slopes that show alcove, channel and debris apron morphology.

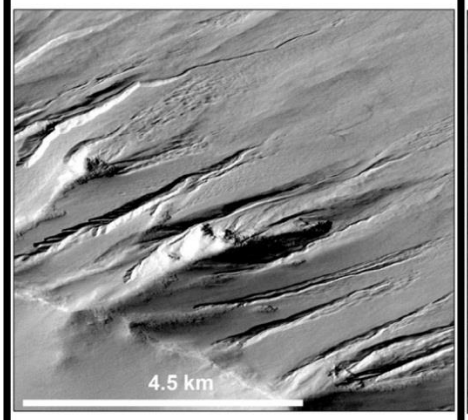

CTX: B11_013958_1222_XN_57S108W

Channels

Lineations that can be identified, either by topographic grooves or by albedo.

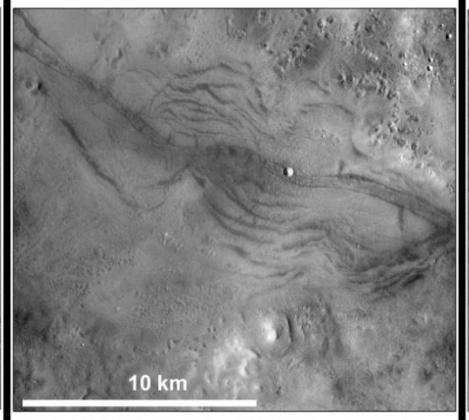

CTX: B20_017309_2278_XN_47N167W

Textured

Terrain fits into one of the categories described as etched terrain, includes linear, wrinkled, brain and basketbal sub-types i.e. Kostama et al., 2006.

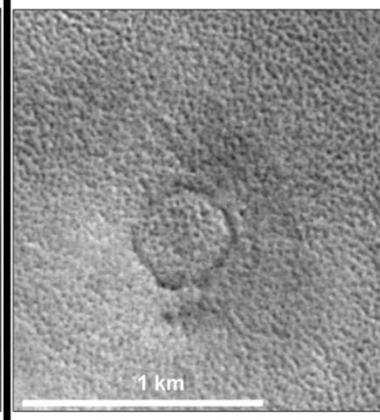

CTX: G23_027251_2528_XN_72N1

Scalloped

Negative relief features, steep headwall, often have concentric terraces, can form complex merged forms.

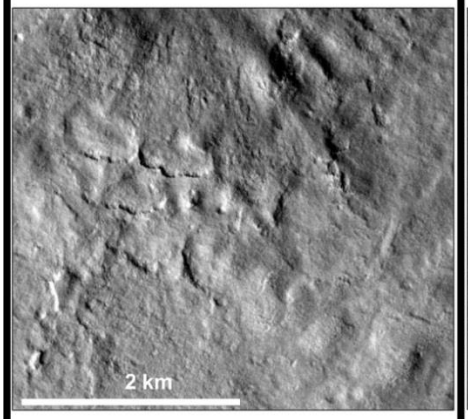

CTX: G01_018720_2312_XN_51N171W

Pitted

Small, simple pits. Pits that are not "scalloped" style.

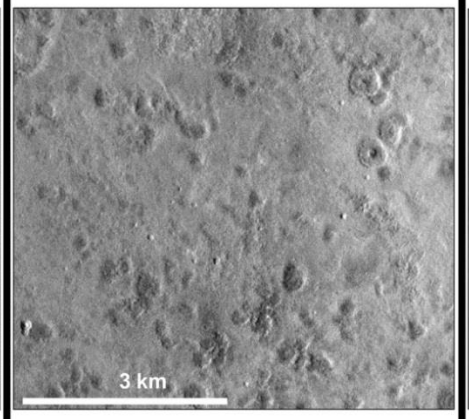

CTX: G22_026645_2285_XN_48N172W

100m Polygons

4-6 sided polygonal patterns. Occur across large areas. Can include sma junction pits.

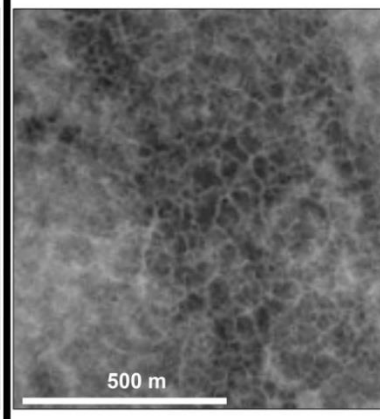

CTX: B18_016531_2540_XN_74N17

Viscous Flow Features

Including lineated valley and concentric crater fill, and lobate debris aprons.

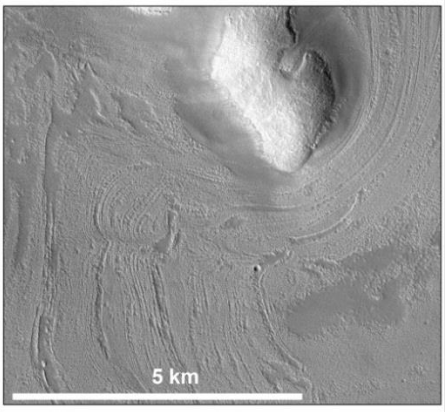

CTX: P15_006932_2181_XN_38N171W

Glacier Like Forms

Topographically confined, valley-glacier like forms.

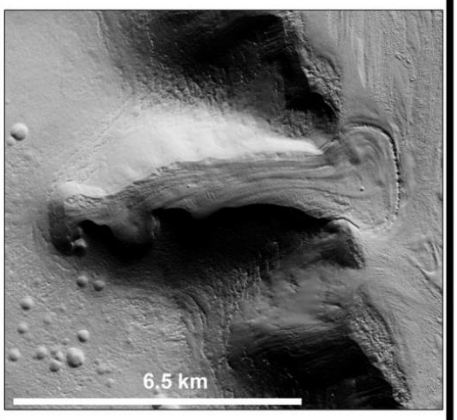

CTX: P01_001570_2213_XI_41N305W

Km Polygons

High centred, trough bounded polyg

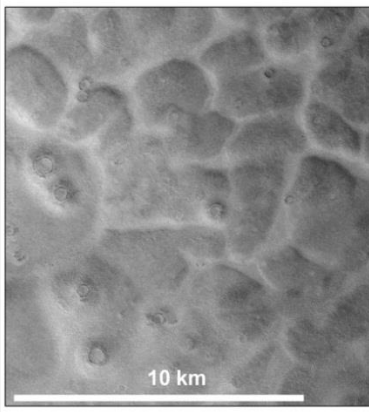

CTX: G23_027251_2528_XN_72N1

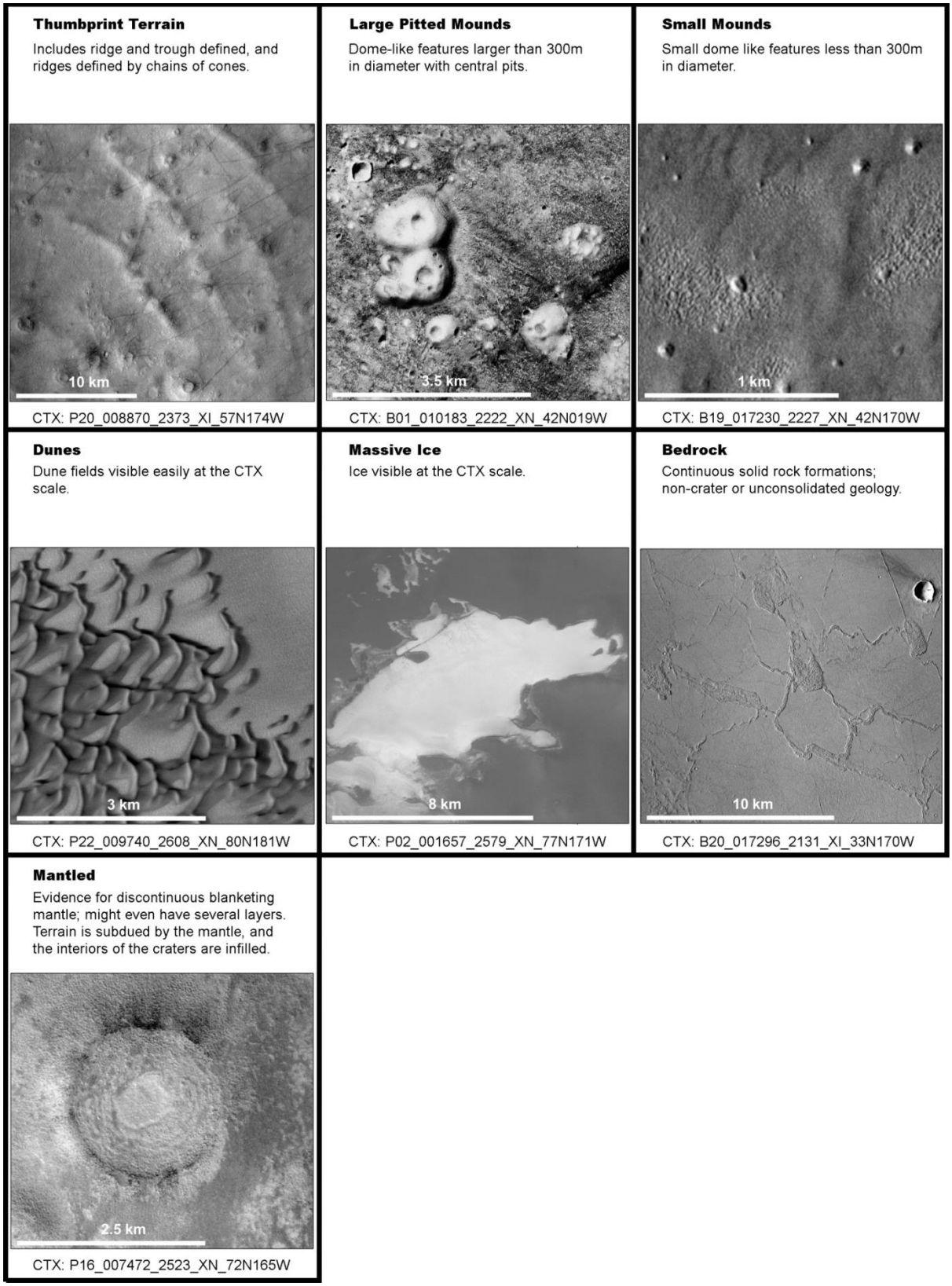

Figure 3.3 Images showing examples of landforms selected of the ISSI mapping project. North is up and illumination from the south-west in all images. The last part of each CTX label gives the latitude and longitude.

Table 3.3 showing the motivations for mapping the selected landforms with the scale of observations needed.

Landform	Approximate Observation Scale	Motivation	References
Mantled	Visible in CTX 1:20k	Evidence for ground ice, mantling deposit.	Kostama et al., 2006
Textured	Visible in CTX 1:20k	Evidence for degradation of ground ice.	Kostama et al., 2006
Pitted	Visible in CTX 1:20k	Evidence for degradation of ground ice.	Costard and Kargel, 1995
Scalloped Pits	Visible in CTX 1:20k	Evidence for degradation of ground ice.	Costard and Kargel, 1995
100m Polygons	Visible in CTX 1:20k	Evidence for possible ground ice processes.	Mangold, 2005
Km Polygons	Visible in CTX/THEMIS 1:100k	Unknown origin, possible evidence for ground ice/ water expulsion processes.	El Maarry et al., 2010; McGill and Hills, 1992; Pechmann, 1980
Viscous-flow Features	Visible in CTX/THEMIS 1:200k	Evidence for flow of ice-rich material.	Hubbard et al., 2011
Glacier-like Forms	Visible in CTX 1:20k	Evidence for deposition, flow and reworking of ice-rich material against topographic obstacles.	Hubbard et al., 2011
Thumbprint Terrain	Visible in CTX/THEMIS 1:200k	Unknown origin, possible evidence for glacial flow.	Grizzaffi and Schultz, 1989; Lockwood et al., 1992; Davis and Tanaka, 1995; Bridges et al., 2003; Bruno et al., 2004; Ghent et al., 2012; Plescia, 1980
Large Pitted Mounds	Visible in CTX 1:100k	Unknown origin, possible evidence for mud volcanism.	
Small Mounds	Visible in CTX 1:20k	Unknown origin, possible mud volcanism/ground ice processes/erosional remnants.	Lanagan et al., 2001; (Burr et al., 2009)
Channels	Variable CTX 1:20-200k	Evidence for liquid water, thaw.	Sharp and Malin, 1975
Gullies	Visible in CTX 1:20k	Evidence for liquid water, thaw.	Malin and Edgett, 2000; Mellon and Phillips, 2001
Massive Ice	Visible in CTX/THEMIS 1:200k	Ice visible at the surface. Obscures possible evidence for ground ice.	Tanaka et al., 2005
Dunes	Visible in CTX/THEMIS 1:200k	Evidence for wind-blown sand, Obscures possible evidence for ground ice.	Hayward et al., 2007 Tanaka et al., 2005
Bedrock	Visible in CTX/THEMIS 1:200k	Evidence for solid rock, or no evidence for ground ice processes/landforms.	Tanaka et al., 2005

3.5.4.4. *Verification of landform selection and the grid-based mapping approach: test mapping*

To determine whether the grid-based mapping approach was viable for multiple mappers, and that the landforms we had selected were consistently identifiable, six mappers with varying levels of experience, both with the martian datasets and ArcGIS, were selected to apply the method to a test sample. The test sample had nine different areas, each with four 20 km by 20 km grid-squares. As per the grid-mapping protocol, each mapper analysed the CTX and THEMIS sample data to estimate the relative frequency of occurrence of each member of a predefined set of landforms by recording if each landform type was "present", "dominant", "absent" or "possible", or if the availability of usable data was "null". The six mappers each completed the attribute table in the shapefiles of their grid-based mapping results for these areas, hence allowing an estimate of how consistent the approach could be when applied to a larger scale project.

For each landform type in each square, we assigned a consistency rating based on the number of mappers agreeing on the relative frequency class describing each landform type in a given area. To calculate the consistency value, we recorded each mapper's classification for each landform type. We interpreted the categories "present" and "dominating" as both meaning that a landform type is present. With 6 mappers, there were 28 possible outcomes, which can be seen in *Figure 3.4*. The consistency ratings ranged from Consistent through Semi-Consistent to Inconsistent. For the evaluation of consistency, we counted entries of "possible" to be split between present and absent and hence that they were half in agreement with both "present" and "absent". To be considered "consistent" at least five out of six mappers needed to agree on either the presence or absence of a landform. To be "inconsistent" less than four mappers had to agree on the presence or absence of a landform. Finally to be "semi-consistent" between four and five mappers had to agree on the presence or absence of a landform. Note that if five or six

mappers were to assign a “possible” for a landform this would be evaluated as inconsistent in this evaluation. While it could be argued that the mappers were consistent in that they agreed on the difficulty to say whether a specific landform was present or not, we took a more conservative approach, because no decision was made.

Present or Dominating	Possible	Absent
6	0	0
5	1	0
5	0	1
4	2	0
4	1	1
4	0	2
3	3	0
3	2	1
3	1	2
3	0	3
2	4	0
2	3	1
2	2	2
2	1	3
2	0	4
1	5	0
1	4	1
1	3	2
1	2	3
1	1	4
1	0	5
0	6	0
0	5	1
0	4	2
0	3	3
0	2	4
0	1	5
0	0	6

Consistent

Semi-Consistent

Inconsistent

Figure 3.4 A look-up table to show the 28 possible combinations of mappers’ responses for the test mapping with our consistency rating. “Present” and “dominating” are both have been groupe,. we counted entries of “possible” to be split between present and absent. We deemed “consistent” as five out of six mappers agreeing, “inconsistent” as less than four mappers agreeing and “semi-consistent” as between four and five mappers agreeing.

The results of the test mapping are shown in *Figure 3.5*. Note that the suite of landforms types in this test mapping was somewhat different from the final suite described above but the refinements to the final suite were made as a result of the test mapping. Our tests showed the rank classification of spatial frequency to be 70% consistent, 20% semi-

consistent and 10% inconsistent. However, *Figure 3.5* highlights that some landform and terrain types are more difficult to identify than others. For example, the difficulties in distinguishing between brain terrain and basketball terrain in the tests resulted in us finally grouping the two types together with etched and linear terrains into a more inclusive "textured" terrain type. We found that loosely defined attributes such as "rough" and "smooth" were inconsistent and these labels were dropped following the test mapping.

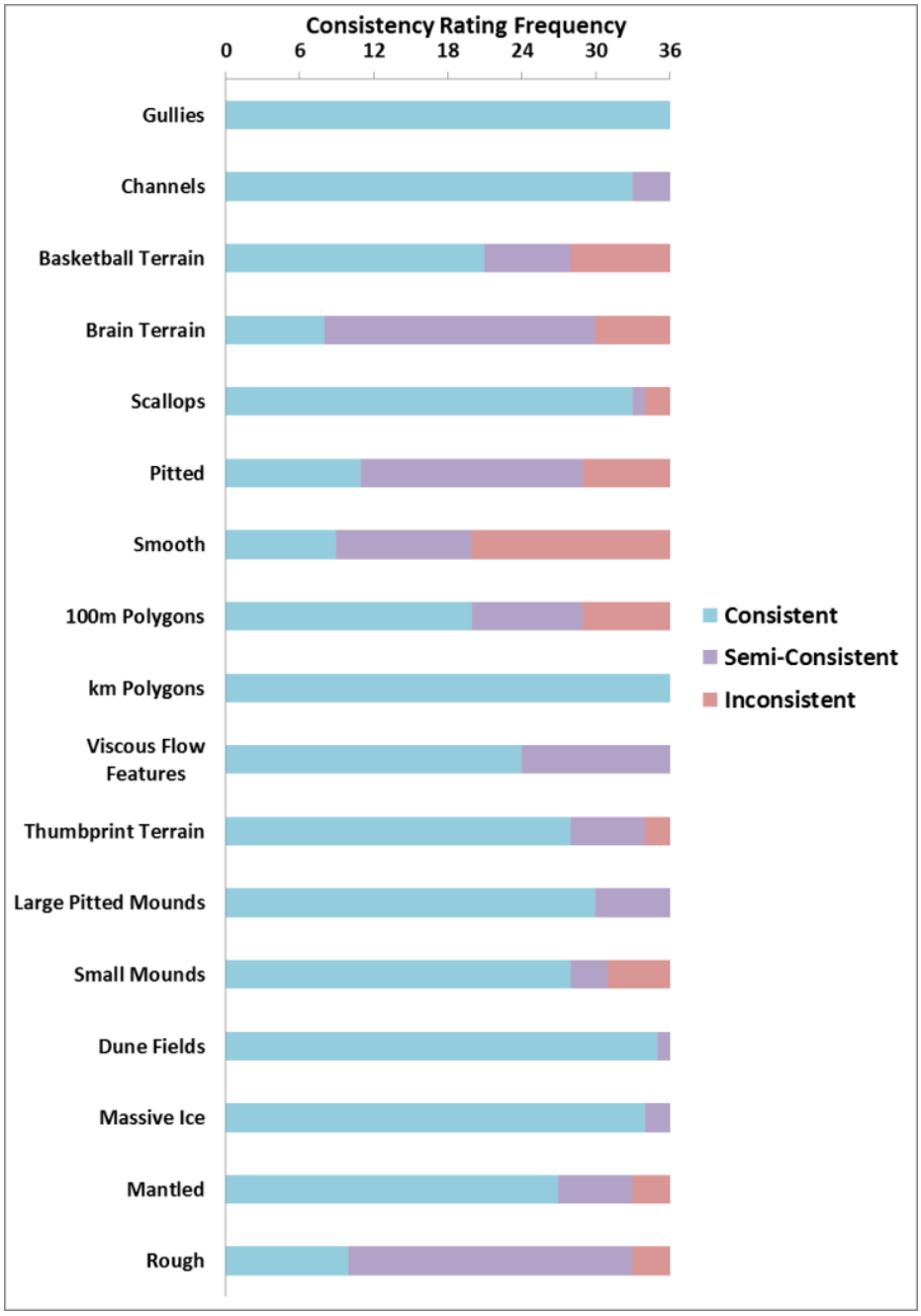

Figure 3.5 Stacked-bar chart showing the consistency rating frequency for each landform or terrain type. 9 × 4 (=36) individual grid squares were mapped.

3.5.5. **Grid-mapping results**

The results from the grid-based mapping are stored as attributes in a GIS shapefile. This data can be manipulated within a GIS to output a variety of products. The most basic of these products is shown in *Figure 3.6c*, where the different shades represent the presence or absence of a single landform type in each grid-square. Dual landform type maps can be constructed by manipulating the data so that the grid-squares are coloured to show where two landforms overlap, occur singularly or not at all, as shown in *Figure 3.6*d. Compilation landform type maps can be created by overlaying symbologies, as shown in *Figure 3.6b*, to show multiple landforms types and compare their distributions within and between grid-squares. As the data are gridded, summary statistics can quickly be generated, tabulated, and manipulated using statistical software such as *R*. Consistently-sized grids also allow for rapid inter-area comparisons, both within and between entire mapping strips.

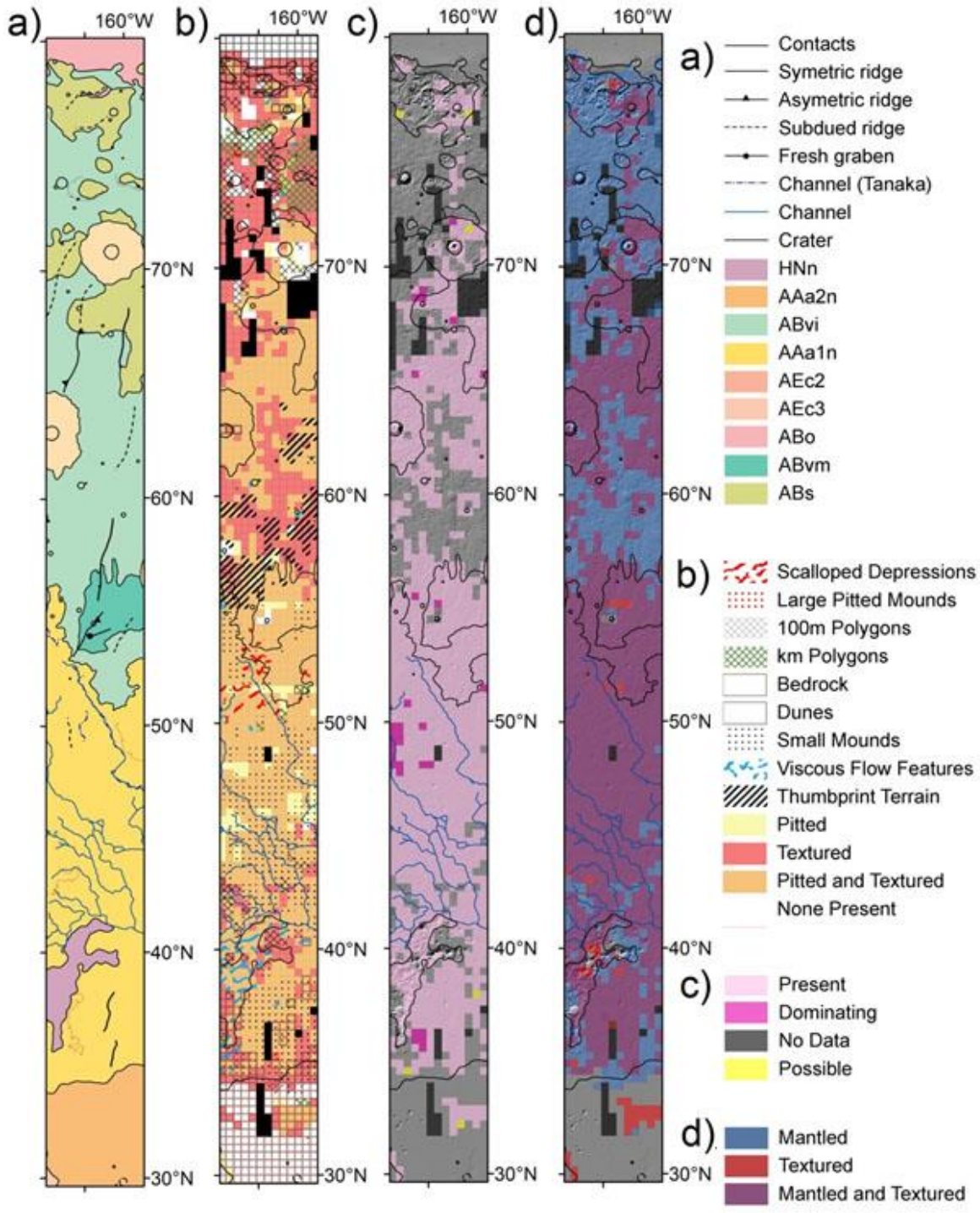

Figure 3.6 Results from grid-mapping in Arcadia Planitia. a) An adaptation of the Geological Map of the northern plains of Mars (Tanaka et al., 2005) used as our reconnaissance map. b) Geomorphic Map using a compilation of grid-based mapping data. c) Grid-based mapping data showing the location of pits only. d) A dual landform map comparing and contrasting the presence of mantled and textured geomorphic

signatures. b, c, and d, are all overlain onto a MOLA hillshade and outline extracts from the geological map in a.

3.5.6. **Comparison with other data**

The gridded data show where certain landform types occur, without consideration of age or landform density. These data can be extremely useful in delineating between surface units, determining contacts, and deriving geological maps. Equally, they can be used to generate statistical datasets for determining spatial associations between landform types and contextual attributes, such as topography, latitude, albedo or mineral/elemental abundances. Comparing the grid-based mapping results with other spatial datasets allows the identification of possible localised controls influencing the occurrence of specific landform types. For example, certain landforms are predisposed to occur only in certain topographic contexts; gullies require a slope or free face at the edge of morphological units, whereas polygons occur in flatter terrain within morphological units. As each entry in the dataset refers to a specific mapping grid-square, with a predefined size, other metrics such as terrain elevation mean, minimum, maximum and range, slope type (concave, convex, rectilinear) and steepness, surface roughness and compositional properties (e.g. hydrogen and phyllosilicate abundance) can be added to the table, allowing for multivariate analysis of the effect of a range of local surface properties on the presence of each landform type.

3.5.7. **Discussion**

3.5.7.1. ***Advantages and disadvantages of grid-based mapping***

There is a wide variety of both academic and applied studies that requires the acquisition, handling and analysis of large spatial datasets. While final map products are largely standardised, reconnaissance mapping is largely performed ad hoc. Standardising and converting reconnaissance data into a standardized map requires tremendous time and effort, meaning that the majority of data collected are not included in a formalised map.

Grid-based mapping allows for efficient collection of large datasets that can be output in a consistent and easily comprehensible manner, complete with nominal to ordinal scale statistics. Moreover, an efficient, consistent and standardised approach to spatial data collection makes it easier to share data and collaborate with partners and end users.

While the grid-based mapping approach is not a replacement for traditional mapping, it does provide an effective means of cataloguing multiple geomorphological landforms over large areas. This is due to the way interpretations are made through discrete decisions for small areas but mapping the extent of each landform type over large areas without having to physically locate and digitise boundaries or individual landforms. The technique becomes particularly advantageous when looking at vast and continuous high-resolution datasets, where there is a disparity between the scale of the final mapping output and the scale of data required to identify the landforms. Examples of high-resolution planetary datasets that can be used for landform identification include the terrestrial Landsat images, the Martian CTX and HRSC (High Resolution Stereo Camera; Neukum and Jaumann, 2004) images, and potentially images from the SIMBIO-SYS (Spectrometers and Imagers for MPO BepiColombo Integrated Observatory System; predicted global coverage at 50 m/pixel; Flamini et al., 2010) instruments on the yet to be launched BepiColombo mission to Mercury. For the northern plains of Mars mapping project, we catalogued potentially cryospheric landforms. However, this technique could be applied to a wider range of thematic data collection, targeting other genetic landform assemblages. The approach is particularly useful as first-pass reconnaissance as it provides both location and complementary contextual data and statistics to inform a more detailed study.

The main advantage of grid-based mapping is efficiency. For each area, a mapper has only to scan the image for the landforms in each of a range of landform types and record whether or not they are visible, removing the individual's decision about where to draw boundaries and what to include. This makes the process easier to implement for non-

specialists. On average, we found it took around 2-3 minutes to complete the attribute table for each individual grid-square (20 km x 20 km). At the suggested grid sizes, it would take around an hour to complete 25 grid-squares (100 km x 100 km). If further resolution was needed, finer grids could be added. These would be able to carry the null and zero values forward from the coarser grids, meaning only areas with positive values for that landform would need to be examined, so that to increase the resolution for the whole strip, the whole map would not need to be re-examined. Therefore, it is a scalable approach. Similarly, if a landform type needs to be split into two or more different sub-categories, then only those grid-squares that contain the parent category need to be re-examined. Hence, a hierarchy of high spatial resolution and detailed classifications could be built up by employing smaller and smaller grids, and sub-classifying individual landform types, where needed.

Unlike traditional landform mapping, grid-based mapping enables a set of landforms, of multiple scales, to be catalogued efficiently in a single pass, minimising the time spent looking over the same images. However, if an additional landform type needed to be added later, it would require re-examining the whole dataset, meaning that starting with more landforms and combining classes afterwards if needed, is preferential. This also reinforces the need for good reconnaissance work, aimed at determining the total range of thematically relevant landform types in a study area.

As each grid-square is systematically searched, for each individual landform type, grid-based mapping rapidly ensures the whole mapping area is covered at full resolution, actively marking negative results. Thus, it is possible to distinguish between absence of landforms and absence of data. Both the mapping squares and the data collected by grid-based mapping are discrete meaning that grid-based mapping is scalable with group efforts. Transitions between colleagues are simpler to merge than using traditional mapping methods, as there are no contact lines or units to match up. However, to provide a consistent result, all mappers need to be able to come to a consensus on which individual

landforms are going to be recorded under which landform type. This is where reconnaissance and test mapping comparisons between mappers are advantageous. Note that this sort of checking system can be added to the approach to maximise inter-operator consistency by requiring certain grid-squares throughout the overall study area to be mapped by all mappers. With the grid-based mapping method there is the potential problem of double accounting of large discrete landforms. If large landforms occur on overlapping cells, they would likely be recorded twice. This is not a major issue for most situations but it is important to consider that some large landforms could be over represented by double counting.

The discrete data outputs for each landform type make it easy for comparisons between multiple landform types. This is particularly highlighted by the dual landform maps such as Fig. 5d. The dual maps make it relatively easy to see where landforms appear to be mutually exclusive and where they consistently overlap, allowing landform assemblages to be constructed. The clearly defined grid also makes wider comparisons relatively easy, as multiple strips can be aligned alongside one another to check for spatial patterns and relationships, such as latitudinal trends.

The tabular nature of the dataset allows for effective statistical manipulation. Summary statistics can be produced through batch coding and quickly plotted to look for trends in large datasets. As each entry in the dataset refers to a specific area, with a predefined size, the resulting data are easily comparable with pre-existing datasets. To allow for direct comparison between the results of grid-based mapping and other data products it may be desirable to display other data in the grid-based mapping format. These can be used to compare results with, for example, mean, minimum, maximum and ranges of elevation, slope geometrics, surface roughness, surface concavity/convexity and compositional properties. This is particularly useful for assessing correlation between relief and landform types.

The main disadvantage of grid-based mapping is that it is an imprecise approach. The current method assigns the same weight to one landform as it does to a hundred. This could be easily modified, however, by entering a "percentage of the surface covered" estimate, or "number in the grid-square" when recording each landform type in the attribute table for each grid-square. On the other hand, this increases the time taken both to make decisions about the landforms and to enter the data, so a cost-benefit analysis must be made when modifying the approach.

3.5.7.2. ***Best practices for grid-based mapping.***

3.5.7.2.1. Selecting the landforms, cell size and approach

Grid-based mapping is most efficient when each image is only viewed once, meaning that a project-specific "standardized" work plan, developed through reconnaissance, is essential. Key considerations when performing grid-based mapping are outlined in *Figure 3.7*. The first considerations are whether multiple classes of data are required and whether high resolution, continuous datasets are available. If either is not, then a more traditional style of mapping or surveying may be more appropriate as the main benefit of grid-based mapping is being able to map the spatial distribution and relative spatial frequency of multiple landform types, and different sizes, over large spatial extents in one pass of the data. If the primary focus of the data collection is density information, grid-based mapping may not provide sufficient detail although it may be used initially to identify specific study areas. Once the approach has been decided upon, and the relevant datasets have been acquired, the suite of thematically relevant landform types needs to be predefined. To complete this vital stage, reconnaissance covering each mapping strip is required to confirm if the selected landform types are both relevant and consistently identifiable in the dataset(s). Subsequent to the definition of the thematically relevant suite of landform types, a projection that minimises distortion over the mapping strip must be chosen to allow for

test mapping a sample of grid-squares. The purpose of the test mapping is to determine whether the landform types can be consistently identified over the entire mapping strip.

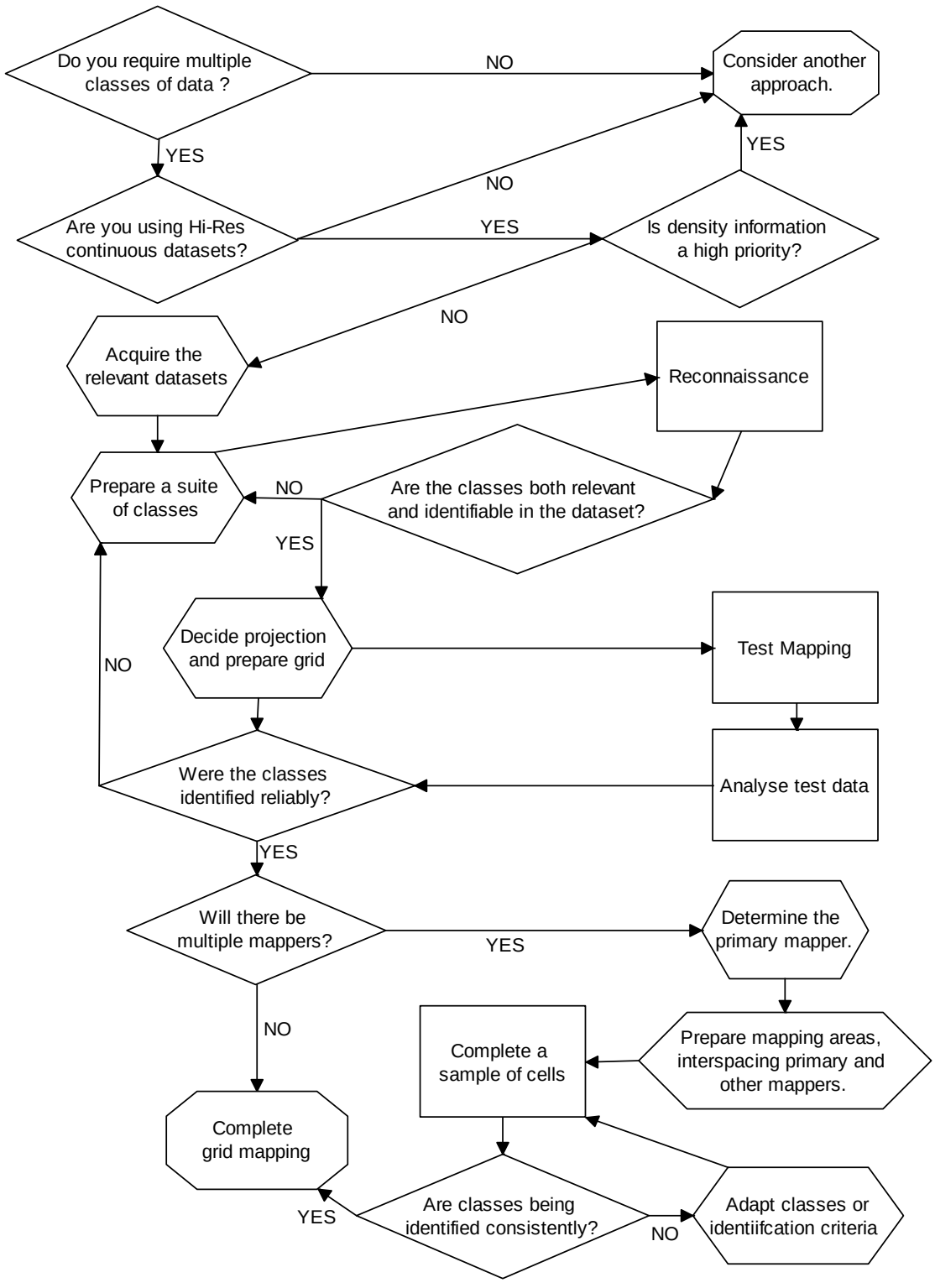

Figure 3.7 Flow chart demonstrating an idealised work process for grid-based mapping. Diamonds represent decisions to be made by the mappers, hexagons for preparation steps, quadrangles for mapping stages and octagons for endpoints.

3.5.7.2.2. Cell Completion Order and Possible Shortcuts

When adopting a grid-based mapping approach, it is important to consider the order in which the cells will be completed. The most obvious approach might be to start systematically at one end of the grid and sequentially complete each cell before moving to the adjacent cell (See. *Figure 3.8*). A sequential approach has the advantage of it being immediately obvious how much of the project has been completed and how much is left to go. However, a sequential approach is very inflexible and leaves the mapper no option but to complete the whole study area before even the most basic analysis can occur. A sequential approach can also lend to a cell completion order bias, if grids are completed systematically in one direction the mapper is more likely to carry decisions on whether a landform is present, or absent, forward, particularly for landforms that are difficult to identify. Where landforms extend over or cover more than one grid-square, a sequential approach could also lead to decisions on landform presence being cumulative, rather than being taken on a square by square basis. While this can dramatically speed up the completion of grids, it prevents the identification of mistaken or outlying cell entries, which removes an opportunity to check for self-consistency. Another option would be to complete grid-squares randomly, perhaps having them served through a random number generator. While this is an excellent way to minimise the problem of decisions made for one grid-square affecting the decisions made for surrounding grid-squares, it requires the mapper to complete the grid before being able to do any systematic analysis.

The mechanism we found to be most effective is to complete equally spaced grid-squares (such as every 2^{nd} or every 3^{rd} square) first, which can then be used to produce a coarse resolution landform map by extrapolating the results to surrounding grid-squares. This allows the mapper to review progress and assess the suitability of the grid dimensions and predefined thematically relevant attribute classes and, in addition, can be used to determine whether all grid-squares need to be populated to adequately represent the categorical range

and distribution of landform types within the mapping strip. This equal spacing method also limits multi-cell decision making, as no completely adjacent grid-squares are analysed sequentially. This is likely to increase reliability but at the expense of time required to populate each grid-square.

It is important to note that increasing the size of a grid-square does not significantly decrease the time it takes to complete the grid-based mapping but does produce a coarser map. This is because the time taken to enter the data into the GIS is small compared to the time required to examine the data at full resolution and make decisions about the landforms. If full resolution is not required to classify the features, however, then use of larger grid-squares is appropriate and can speed up the task. However, there is a compromise to be made between the time spent completing attribute tables, time spent observing the images, and the resolution of the classified dataset.

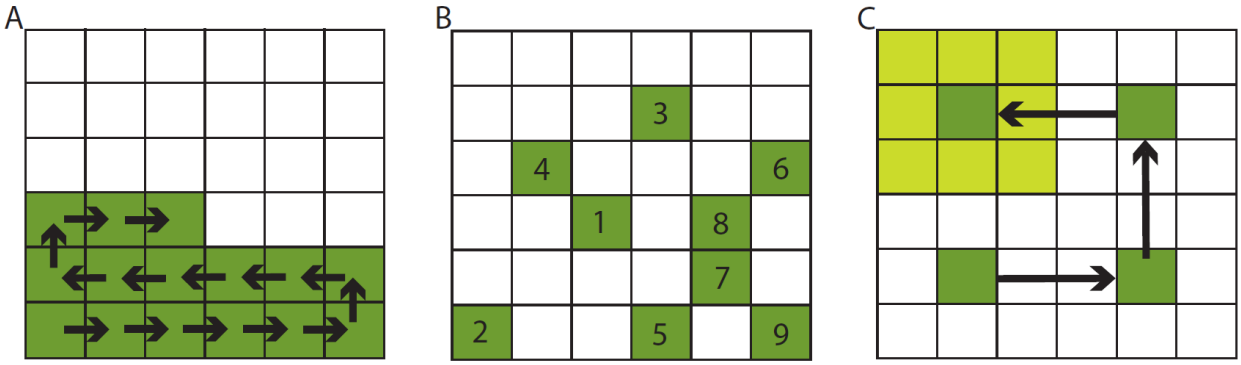

Figure 3.8 A) Adjacent cell completion; cells are completed row by row sequentially. B) Randomised completion; each cell is assigned a random number and completed sequentially. C) Coarse resolution first completion; every third cell (dark green) is completed allowing results to extrapolated to adjacent cells (light green) to produce a coarse resolution raster.

3.5.7.2.3. Dividing the mapping

Considerations should be made when dividing the mapping between multiple mappers on how best to maintain consistency across the whole mapping strip (see *Figure 3.7*). This can

involve using overlapping areas to promote discussion and consolidation on how landforms are mapped. An alternative approach is to interweave regions to be mapped by secondary mappers with smaller areas to be mapped by a primary mapper, ensuring that all mapper boundaries are between the primary mapper and one secondary mapper. This allows for inter-operator consistency to be checked by one individual, helping to improve overall reliability.

3.5.7.3. *Possible Modifications to the Approach*

Grid-based mapping, as presented, provides little to no spatial density information on landform types. As the method is described, there is no mechanism to discriminate between a single instance of a landform type in a grid-square and many such landforms, perhaps covering a significant proportion of the grid-square. It is possible to produce a variation on how the data are recorded to include some density information; however this would come at the cost of both speed and ease of data collection. While not providing a definitive study on each individual landform type, which would require morphometrics of individual landforms in the type, this technique does provide an excellent way of cataloguing where landform types occur and could be used to target more focused and detailed research questions. It is worth noting that reclassifying the data to include spatial density information afterwards would not require looking through the entire dataset again, but only where landform types had been positively catalogued; and perhaps even then a sampled approach could be taken. One such approach could be to provide two attributes per landform type to be recorded for each grid-square, the first being confidence level on identification (i.e., present, probable or absent) the other a first order estimation of the number of landform of each type occurring in the grid-square. For point and linear landforms this could be recorded as an estimate of the population size of each landform type within each grid-square, for surface terrain types (*cf.* landcover classes) as estimated percentage coverage. This approach could provide an effective compromise between

collecting density data and the time required to record each individual occurrence of a landform type.

3.5.7.4. *Applications of the Approach*

The grid-based mapping approach has been developed to be applied to the Arcadia, Utopia and Acidalia regions of the martian northern plains. Other applications of the grid-based mapping method since include geomorphological mapping of Hellas (Voelker et al., 2015) and Lyot (Brooker et al., 2015) crater.

The discrete nature of the datasets also opens up the possibility for citizen science, crowdsourcing large mapping areas. Mapping areas can be divided and distributed to large numbers of participants. To improve reliability, individuals' results could be weighted against "experts" using control squares, experts being members of the appropriate science community who survey a sample of the mapping area. Searching for landforms in this manner would make possible the prospect of cataloguing landform types over the entire surface of Mars at CTX resolution. Crowdsourcing the task would be advantageous in that individuals could be selected as "specialists" in certain landforms, who could then perform more in-depth measurements on landform types that have been located by other users, providing an additional layer of information. Additional metrics such as the average time taken by the mapper to complete each grid-square could be recorded and provide an interesting and perhaps useful insight into the complexity of different regions.

With regard to a crowdsource grid-mapping effort, somewhat comparable studies are being performed by NASA's "Be a Martian" and "ClickWorkers" projects and Zooniverse's "Moon Zoo" project (Joy et al., 2011). These three projects utilized the advantageous numbers in citizen science largely to count and classify craters on planetary bodies. Although the data are largely yet to be published, preliminary observations and analysis (e.g. Kanefsky et al., 2001) are promising. The data collected by citizens in Kanefsky et al. (2001) was shown to be reliable against that collected by Nadine Barlow, an "expert" with

several years of experience in crater counting. This encourages the consideration of applying a “grid-based mapping by citizen science” approach to map landforms across the northern plains and, potentially, the entire surface of Mars. The aim of expanding the study would be to improve extent to which we can test latitude dependence hypotheses. Opening up the study to citizen science would also allow the suite of landforms identified to be expanded.

3.5.8. **Conclusions**

A grid-based mapping approach provides an efficient solution to the problems of mapping small landforms over large areas by providing a consistent and standardised approach to spatial data collection. Moreover, it makes data sharing and collaboration easier, more consistent, flexible, and effective. Unlike with traditional landform mapping, grid-based mapping is able to catalogue a set of landform types, of multiple sizes, efficiently in a single pass, minimising the time spent looking over the same images. The discrete, tabular nature of the dataset allows for effectual statistical manipulation for assessing correlation between landform types, relief, relationships and trends. The simplicity of the approach makes grid-based mapping extremely scalable and workable for group efforts, requiring minimal user experience and producing consistent and repeatable results. The discrete nature of the datasets, simplicity of approach, and divisibility of tasks, open up the possibility of citizen science, in which crowdsourcing large grid-based mapping areas could be applied. A potential application of a “grid-based mapping by citizen science” approach would be to map landforms across the entire surface of Mars.

4. Grid Mapping results from Arcadia.

Increased availability of high-resolution images of the surface of Mars (e.g. CTX, ~ 6 m/pixel, covering ~ 90% of the surface) means that sub-sampling of a study area is no longer needed when identifying landforms of decametre-scale, but analysing the data takes significantly more time. This becomes problematic when attempting regional or global-scale studies of landforms, as many landforms are too small to represent on regional maps, yet mapping their occurrence can form the observational basis for developing hypotheses on the geological nature and environmental history of a study area.

In detailing the geological and stratigraphic character of the Martian northern plains, this project aimed to answer the following science questions. (i) What is the distribution of ice-related landforms in the northern plains and can it be related to distinct latitude bands or different geological or geomorphological units? (ii) What is the relationship between the LDM and (a) landforms indicative of ground ice and (b) other geological units in the northern plains? (iii) What are the distributions and associations of recent landforms indicative of thaw of ice or snow? In Chapter 3, I described an approach for mapping small features across large areas formulated for this project to study the northern plains of Mars.

Here I present the full results and implications of the study in the Arcadia Planitia mapping strip (see Figure 4.1). The main aims and objectives of this chapter are to address how specific landforms are associated with regional geology and topography and to identify whether landforms occur within specific latitude bands in Arcadia. The chapter also aims to clarify how specific landforms in Arcadia relate to each other and whether individual landforms come together to form landform assemblages. If landforms appear to occur within specific bands then I hope to test for latitude dependence by comparing my results in Arcadia with results gained from other ISSI team members who have mapped in Utopia and Acidalia. This will be addressed in Chapter 5.

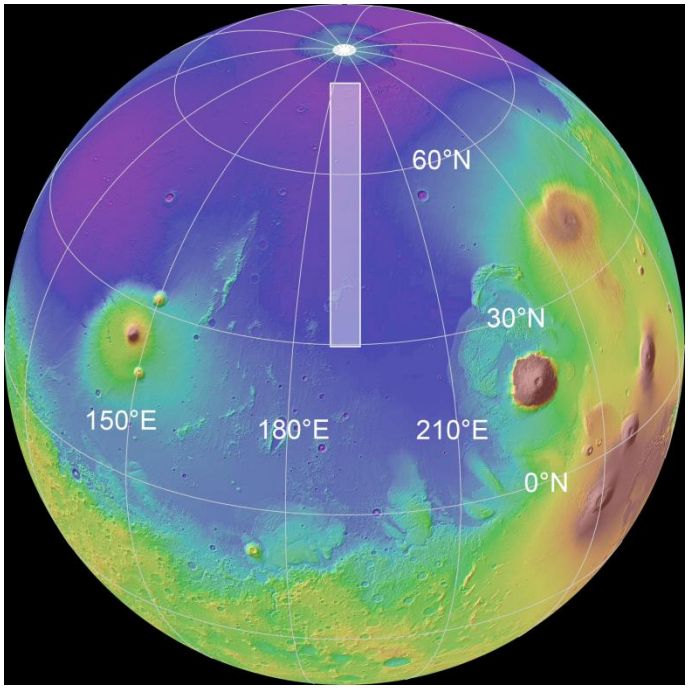

Figure 4.1 Colourised MOLA elevation map showing the location of Arcadia grid mapping strip. Blue colours represent low elevation and red, high.

4.1. What is known of the ice-related landforms and dominant surface processes in Arcadia Planitia

Although the spatial distributions of some landform types have been measured and correlated with latitude-controlled climatic processes (e.g. transverse aeolian ridges, TARs; Balme et al., 2008; Wilson and Zimbelman, 2004, viscous-flow features, VFFs; Milliken et al., 2003, glacier-like forms, GLFs; Souness et al., 2012, dunes; e.g. Hayward et al., 2007), broad-scale heterogeneity in surface features exists within latitude bands (e.g. geological units see Figure 4.2; Tanaka et al., 2005, craters; Barlow and Bradley, 1990; Robbins and Hynek, 2012, latitude-dependant mantle, LDM; Kreslavsky and Head, 2002). This suggests that both regional geology and climate play a role in controlling the distribution of landforms, requiring a more detailed understanding of the relationships between the geological units of the northern plains, the bounding conditions, and the resulting geomorphic landforms.

Arcadia Planitia is dominated by Hesperian to Amazonian-aged lavas and sediments (e.g. Tanaka et al., 2005) overlying a Noachian basement (Hoogenboom and Smrekar, 2006). The underlying

basement is believed to have undergone widespread alteration by liquid water, as implied by phyllosilicate outcrops in the rims of large impact basins (Carter et al., 2010). The uppermost layers of the northern plains are largely sediments that have been shaped by processes involving water-ice (Kreslavsky and Head, 2002; Lucchitta et al., 1986; Tanaka et al., 2005), but no consensus has emerged on the origin and emplacement mechanism of the ice. Kargel et al. (1995) discuss several proposed mechanisms of emplacement including freezing of fluvial, lacustrine or marine wet sediments, air-fall deposition/condensation, shallow groundwater processes, or a combination of these different processes.

The mapped dielectric characteristics suggests that the widespread Vastitas Borealis Formation, dominant in northern Arcadia like much of the northern plains, consists of low density deposits and/or massive ground-ice (Mouginot et al., 2012). It is these massive units of sediments and potentially ground-ice that is believed to be possible remnants of a Late Hesperian ocean (Carr and Head, 2003). It has been inferred that the Vastitas Borealis Formation comprises at least 100 m of stacked ice-rich outflow-channel deposits, formed through successive outpourings of sediment and water onto the northern plains (Kreslavsky and Head, 2002; Tanaka et al., 2003). The deposits in Arcadia have an estimated volume of up to $2x10^7$ km^3 and probably also reflect erosion of surrounding uplands followed by transport of fluidised debris into the depocentre (Tanaka et al., 2001).

Double layered ejecta and pedestal craters in Arcadia have led to the inference of the presence of near surface ground-ice, with their raised form being as a result of the ejecta blanket protecting the impact site as the surrounding ice-rich terrain down-wastes through sublimation (Barlow and Perez, 2003; Kadish et al., 2008). Hamilton et al. (2010) interpreted groups of pits and cones in Elysium Planitia, near southern Arcadia Planitia, as Late Amazonian volcanic rootless constructs (VRC), produced by lava- ground-ice phreatic interactions, and thermokarst modification. Rampey et al. (2007) interpreted larger km-scale domical structures in southern Arcadia as cryptodomes and lava-domes implying that volcanic processes alone could account for at least some of the large dome features without having to evoke ground-ice.

Tanaka et al. (2003) also identified several landform types which they associate with geological units and they interpret to be representing key environmental processes and contexts: (1) Contraction (wrinkle) ridges are the dominant landform type in the plains, and cross-cutting relations indicate that ridge development spanned the period from the late Early Hesperian to the Early Amazonian; (2) The linear to arcuate assemblages of ridges, hummocks, knobs and cones that characterize thumbprint terrain (TPT) and considered to possibly result from multiple episodes of near-surface fluidisation, discharge and eruption; (3) Hectometre to kilometre-scale polygonal networks consisting of intersecting linear troughs, 10s of metres deep and up to 1 km wide that are often buried by younger materials, possibly as a result of contraction of thick, volatile-rich sediments or the isostatic rebound following loss of a local waterbody or ice mass.

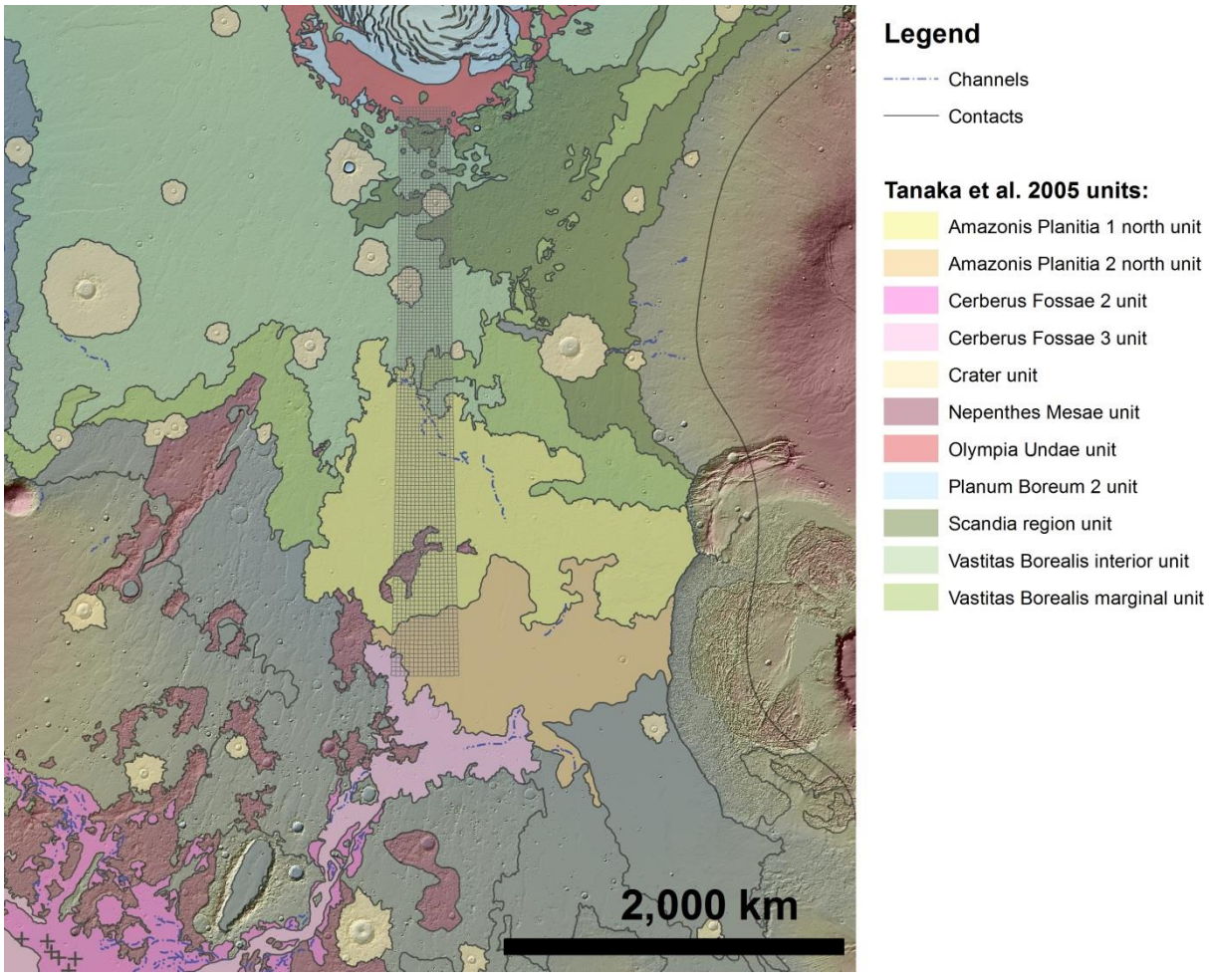

Figure 4.2 Geological Map of Acradia adapted from Tanaka (2005) overlain onto a MOLA DEM and hillshade. Location of the Arcadia grid mapping strip is shown (hatched).

The northern extent of ISSI strip overlaps the Olympia Undae unit. The Olympia Undae unit displays distinct alternating bright and dark stripes as result of an illumination pattern over vast dune fields. The dune fields are thought to be several tens of metres thick (Lancaster and Greeley, 1990), displaying both barchan and transverse forms, and have been shown to be active by observation of time-separated HIRISE images (Ewing et al., 2010; Hansen et al., 2011). Although the surface is likely to be continuously renewed, it is thought that the unit could have existed since the Early Amazonian (Tanaka et al., 2005).

South of the Olympia Undae unit, the strip overlaps patches of Scandia region units and Vastitas Borealis units. The Scandia region unit is a complex of mesas, knobs and patches of material ranging from a few hundred metres to a kilometre thick (Tanaka et al., 2005). The Vastitas Borealis units cover most of the northern plains and in parts displays polygonal troughs and the parallel arcuate ridges and cones referred to as thumbprint terrain. The Vastitas Borealis marginal unit appears smoother and brighter, therefore warmer, in THEMIS daytime images suggesting that the marginal unit is comprised of finer grained material than the surrounding units (Tanaka et al., 2005). The marginal unit contains thumbprint terrain, complex systems of sinuous troughs and ridges up to tens of kilometres long and a few kilometres wide; these features have been compared to glacial moraines and kame deposits (Lucchitta, 1982), glacial tunnel valleys and eskers (Kargel et al., 1995), and soft sediment deformation features (e.g. Tanaka, 1997).

Tanaka et al. (2005) mapped the Amazonis Planitia 2 north unit as lava flows displaying broad arcuate, low relief channels. The Amazonis Planitita 2 south unit displays hundreds of kilometre long lobate flows, flowing northwest from the south-eastern Amazonis Planitia margin. Both Amazonis units appear to embay large impact craters. The Cerberus Fossae units are mapped as extensive lobate, channelized lava flows and flow fields sourced from Elysium Planitia (Plescia, 2003; Tanaka et al., 2005). The unit likely consists of lavas and sediments resulting from large scale lava and water outbursts (e.g. Burr et al., 2002; Plescia, 2003; Tanaka et al., 2005). The Nepenthes Mensae unit comprised of individual kilometre-scale knobs and mesas and plains deposits (Tanaka et al., 2005). Tanaka et al. (2005) suggested that the plains material could be

talus slide and flow materials from the mesas. Parker et al. (1993) suggested that knobs and mesas could be eroded coastlines from the hypothesised ancient ocean.

4.2. **Choice of mapping area/strip**

The study area in Arcadia is a 300 km wide strip extending from 30° to 80° N latitude, centred on the 170° West line of longitude. The location of the strip was chosen primarily to maximise the availability of CTX images. We opted to use a Cassini projection centred on the 170° West meridian.

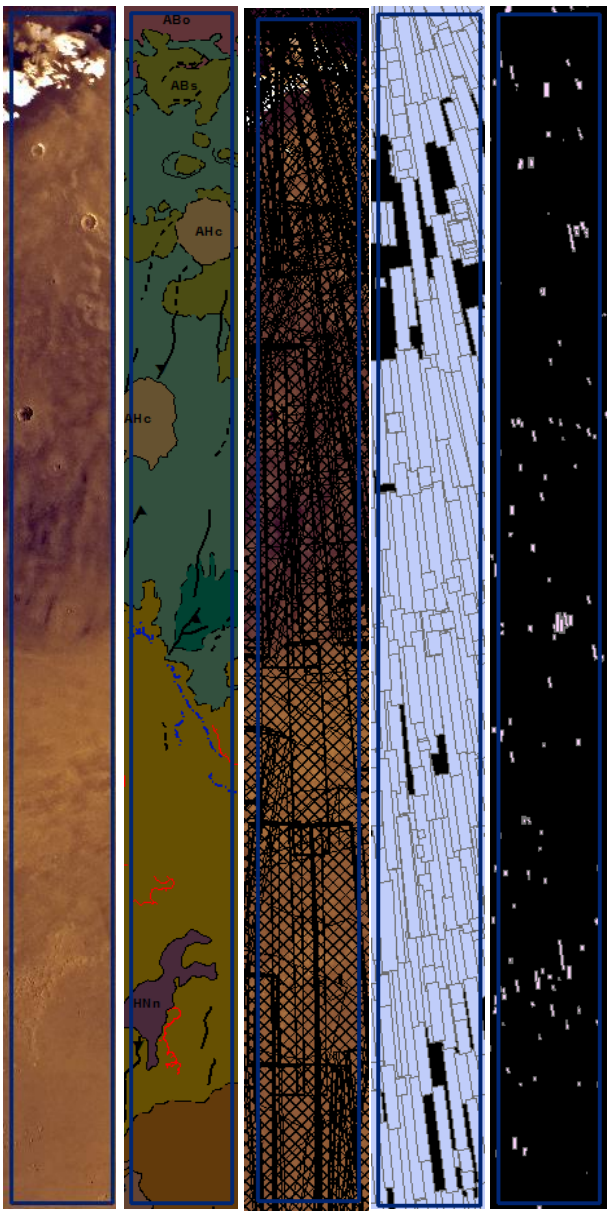

Vik. Ima. Geol. Map HRSC CTX HiRISE

Figure 4.3 (From left to right) Viking image mosaic of the 300 km wide Arcadia strip; geological map from Tanaka et al., (2005); HRSC; CTX; and HiRISE coverage. HRSC coverage is essentially 100%, but image resolution is poor and many images are noisy. CTX coverage is approximately 95% and of good quality. HiRISE is less than 10% of the area.

4.3. **Methods**

A full methodology is provided in Chapter 3. The first step was context mapping, identifying large scale relief to provide topographic context and identifying which specific landforms and terrain types would be studied to produce a full inventory of the landform types to catalogue. The context map used some of the line work from the published geological map of the northern plains of Mars (Tanaka et al., 2005), with additional features based on my reconnaissance study. The map scale of the context mapping was at 1:10,000,000 (i.e., the Arcadia strip would be about 3 cm wide by 30 cm tall if printed at this scale).

4.3.1. **Landform Selection**

As discussed in Chapter 3, many of the landforms that we chose to map have been cited as providing evidence of past or present ground ice, including viscous flow features (VFFs; Hubbard et al., 2011), glacier like forms (GLFs; Hubbard et al., 2011), ~100 metre polygons (Mangold, 2005), scalloped and non-scalloped pits (which might have a thermokarstic origin; Costard and Kargel, 1995), and linear, wrinkled, brain and “basketball” terrain textures which we grouped under the class “Textured” as they have all been associated with degradation or modification of the LDM (Kostama et al., 2006). We also catalogue topographic infilling and relief softening that provided a topographic indication of a draping unit. We include landforms potentially indicative of thaw, such as gullies (e.g., Mellon and Phillips, 2001) and channels (e.g., Sharp and Malin, 1975).

Kilometre-scale polygons, thumbprint terrain, large pitted mounds, and small mounds have been associated with water/ice processes and were recorded. The formation mechanism of the

thumbprint terrain and associated large pitted mounds or cones is enigmatic and has been interpreted to be debris left behind after the removal of a static ice sheet (Grizzaffi and Schultz, 1989), rogen moraine - underwater glacial push moraine (Lockwood et al., 1992), mud volcanism (Davis and Tanaka, 1995), and various volcanic and lava/ice interaction features (Bridges et al., 2003; Bruno et al., 2004; Ghent et al., 2012; Plescia, 1980). Kilometre scale polygons or "giant polygons" are thought to be a product of tectonic, volcanic, dessication or compaction processes and could be a result of faulting and rebounding following the removal of a water/ice load (e.g. El Maarry et al., 2010; McGill and Hills, 1992; Pechmann, 1980). These kilometre-scale forms were mapped using a combination of THEMIS and CTX, as they could often be more easily seen in THEMIS than when 'zoomed-in' using CTX. Reconnaissance mapping revealed the presence of small mounds, typically small, featureless hills less than 30 metres in diameter that are morphologically similar to rootless cones (e.g. Lanagan et al., 2001), pingos (Burr et al., 2009) or mesa-like erosional remnants. Finally, we chose to include landforms that might obscure or explain the absence of other landforms. Obscuring landforms include dune fields, massive ice ("massive" in the spatial sense, not referring to geological layering) and continuous "bedrock" formations. An example of bedrock is the platy-ridged material inferred to be lava flows in Southern Arcadia/North Amazonis Planitia (Keszthelyi et al., 2000).

4.3.2. **Defing the grid**

The mapping area was divided into a 15 x 150 grid of squares, each 20 by 20 km. In ArcGIS, a polygon feature-class shapefile was produced, in which each grid-square was represented by a single square polygon object. The shapefile is given an attribute table, with a separate attribute for each landforms type to be studied and a unique identification code for each grid-square. For a basemap, we used a CTX mosaic that had ~95% coverage (see Figure 4.3) for Arcadia and hence allowed decametre-scale landforms and surface textures to be identified.

4.3.3. **Populating the grid**

The CTX images and THEMIS IR daytime images were overlaid onto MOLA hill-shade and elevation products and systematically examined, grid-square by grid-square at full resolution (between

1:10,000 – 1:20,000 depending on the landforms present), in order to identify the landforms. The landforms were recorded as being either “present”, “absent” or “dominant.” The “dominant” classification was used when a single landform type covered the entire grid-square to such an extent that other landforms might have been obscured. Where relevant, each grid-square could also be recorded as “null” (meaning “no data”) or “possible” if there is uncertainty in identification, either when the mapper is unsure or when the image quality is poor but there is some evidence to suggest that the landform is present. The suite of landforms identified within the Arcadia strip can be seen in and the motivation for mapping these landforms is discussed in Chapter 3.

4.4. **Results**

Landforms were recorded as being either “present” (labelled-1; colour-red), “absent” (labelled-0; colour-white/hollow) or “dominant” (labelled-2; colour-purple). The “dominant” classification was used when a single landform type covered the entire grid-square to such an extent that other landforms could have been obscured. Where relevant, each grid-square can also be recorded as “null” (labelled-NA; colour-black; meaning “no data”) or “possible” (labelled-P; colour-orange) if there is uncertainty in identification, either when the mapper is unsure or when the image quality is poor but there is some evidence to suggest that the landform is present. To compare the occurrence of multiple landforms with respect to latitude, the grid mapping data can be grouped into bins of latitude where positive values (2,1,P) count towards the total frequency. The data in the graphs below are grouped into one degree bins unless otherwise specified. The landforms with the most frequent occurrences throughout the strip are mantled, textured and pitted. The landforms are discussed below and are loosely grouped by possible landform assemblages.

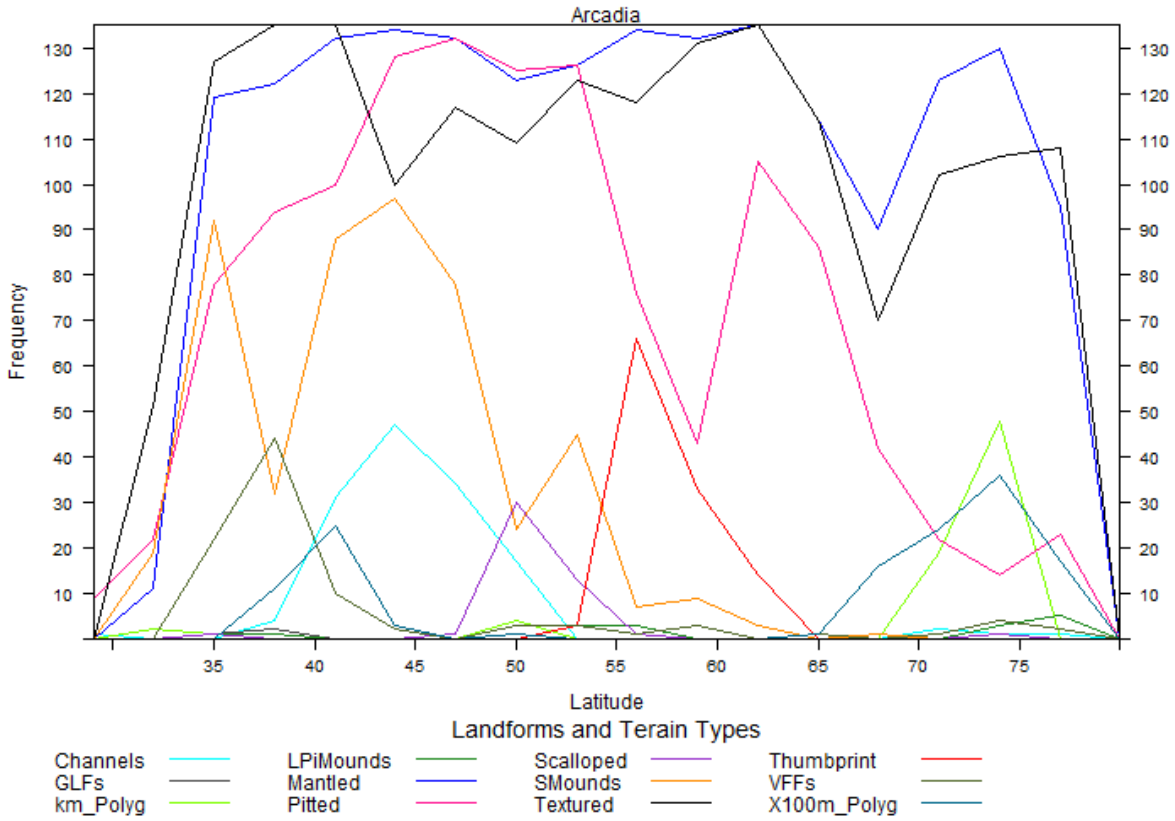

Figure 4.4 Frequency of landform occurrence by latitude in the Arcadia strip. The grid mapping data is grouped into one degree bins of latitude where positive values (2,1,P) count towards the total frequency.

4.4.1. **Latitude Dependant Mantle**

As shown in Figure 4.4 and Figure 4.5 approximately 86% of the grid squares are either mantled, textured or both. Mantled and textured have around 87% correlation, with 75% of the squares being both mantled and textured. The trends in abundance by latitude of mantled and textured surfaces are almost uniform from 78-35°N. The areas that are mantled but not textured have a smooth appearance and underlying topography appears to be more subdued as shown in Figure 4.6. The areas that are textured but not mantled are typically flat lying areas with little to no features that could show evidence of mantling. These observations are consistent with the presence of a ubiquitous mantle that has been degraded to form the textured appearance. The most prominent textural signatures occur between 60-65°N as shown by the purple patch as shown by Figure 4.10.

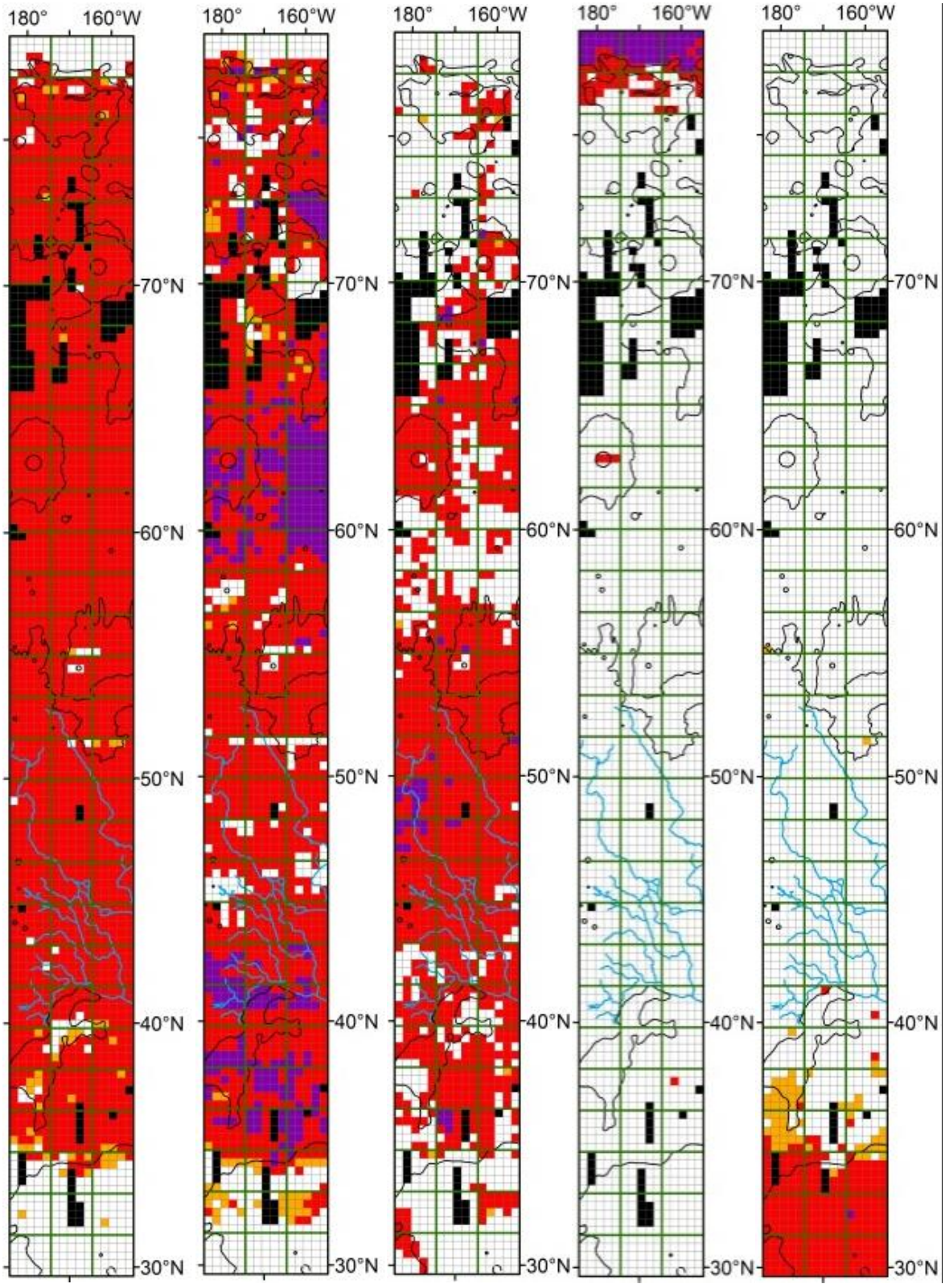

Figure 4.5 Grid maps of (left to right) mantle terrain, textured, pitted, dunes and bedrock.

Red is present, purple dominating, orange possible, black no data and white not present.

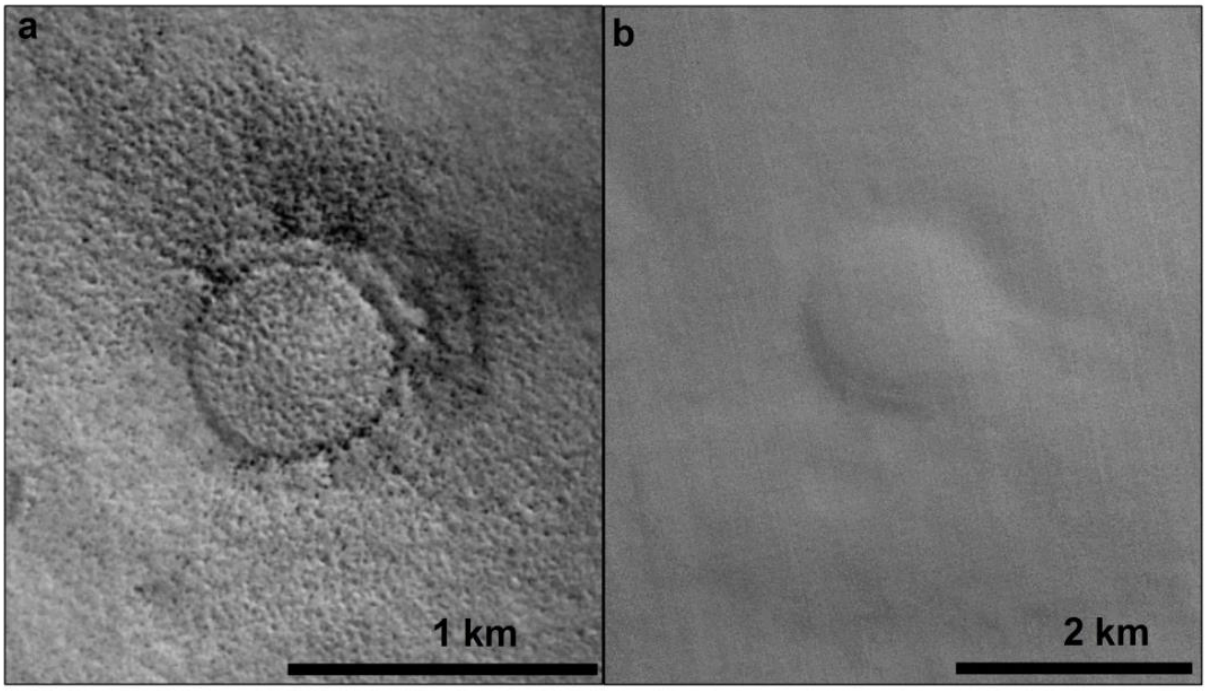

Figure 4.6 a) CTX image P17_007696_2568, at 76° N and 168° W, showing a mantled and textured surface. b) CTX image P16_007248_2558, at 75° N and 170° W, a mantled but not textured surface.

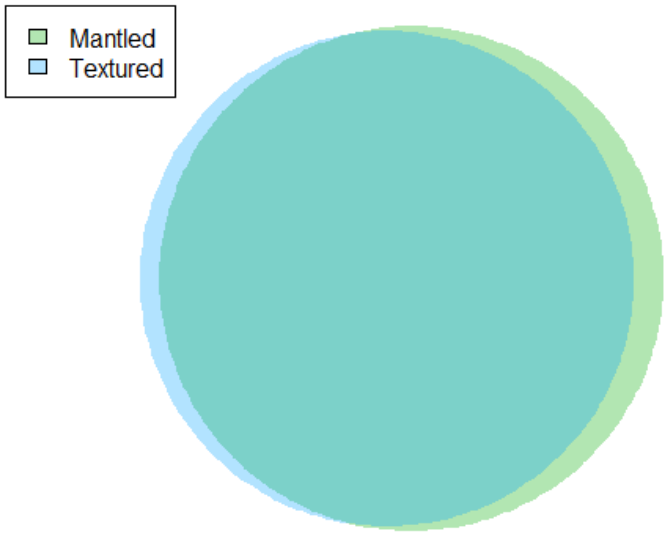

Figure 4.7 A proportional Venn-Euler diagram of the frequency of grid squares with positive Mantled and Textured identifications.

In addition to consistent texture at the CTX-scale, in HiRISE images the LDM has metre-scale polygons (see Figure 4.8) which are below the resolution of CTX images Figure 4.9). As HiRISE image coverage is discontinuous, these features cannot be mapped in full and a “random

selection" survey approach would be more applicable. Figure 4.8 shows how these metre-scale polygons can vary from being high-centred (e.g. g and h) to low-centred (e.g. c and f).

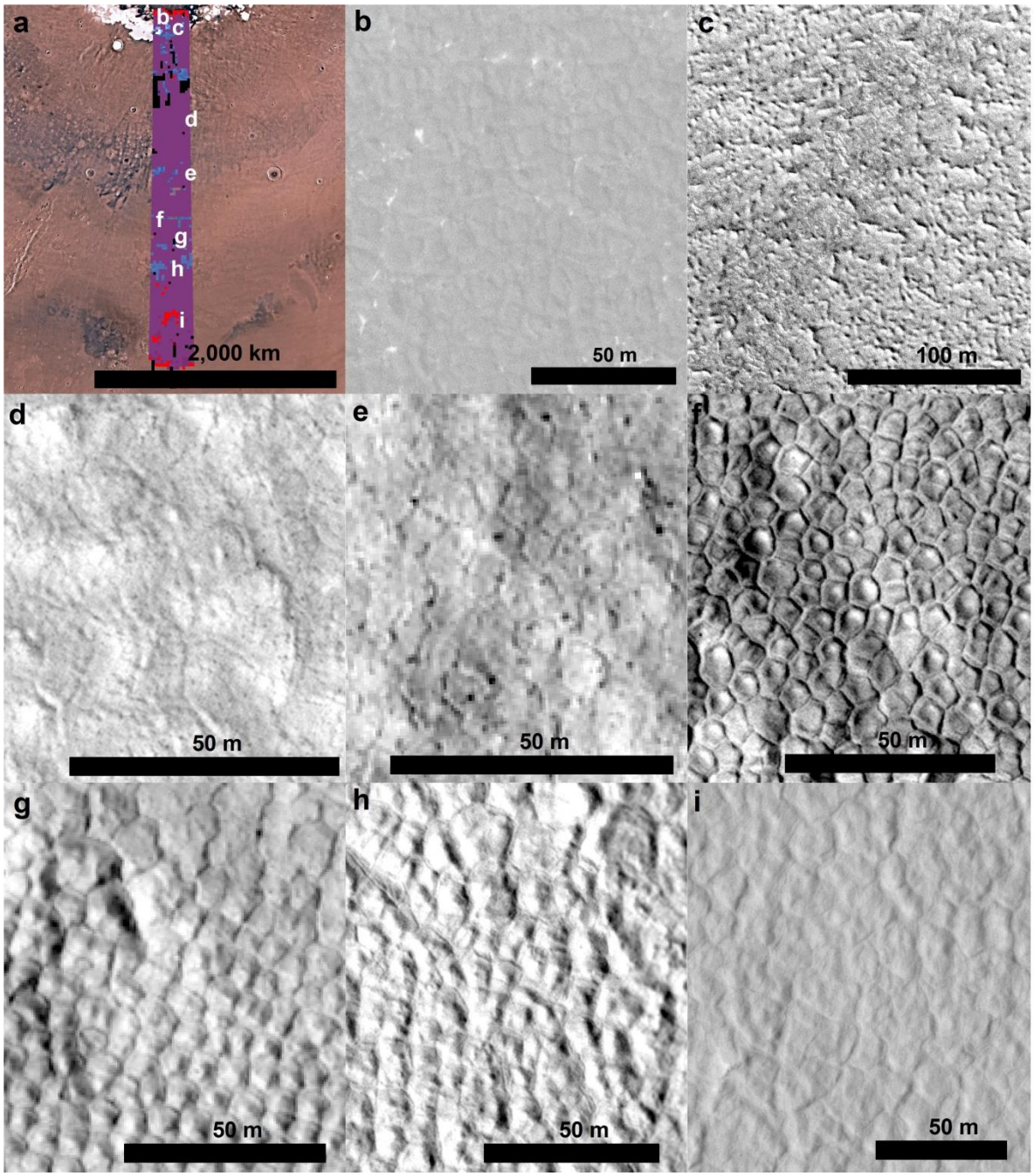

Figure 4.8 (a) Viking image showing the locations of b-i with grid mapping of textured (red), mantled (blue) and both (purple) overlain. (b) HiRISE image ESP_035255_2590 of subtle metre-scale high-centred polygons. (c) HiRISE image PSP_007248_2550 of putative low-centred metre-scale polygons made up of ridges (or sub-resolution clasts). (d) HiRISE image ESP_027093_2425 of subtle metre-scale high-centred polygons. (e) HiRISE image

ESP_028847_2360 of subtle metre-scale high-centred polygons and metre-scale boulders. (f) HiRISE image ESP_016940_2300 of metre-scale polygons with low centres, high margins and troughs between polygons. (g) HiRISE image ESP_036350_2280 metre-scale high-centred polygons. (h) HiRISE image ESP_016241_2240 high-centred polygons. (i) HiRISE image ESP_026579_2180 high-centred polygons.

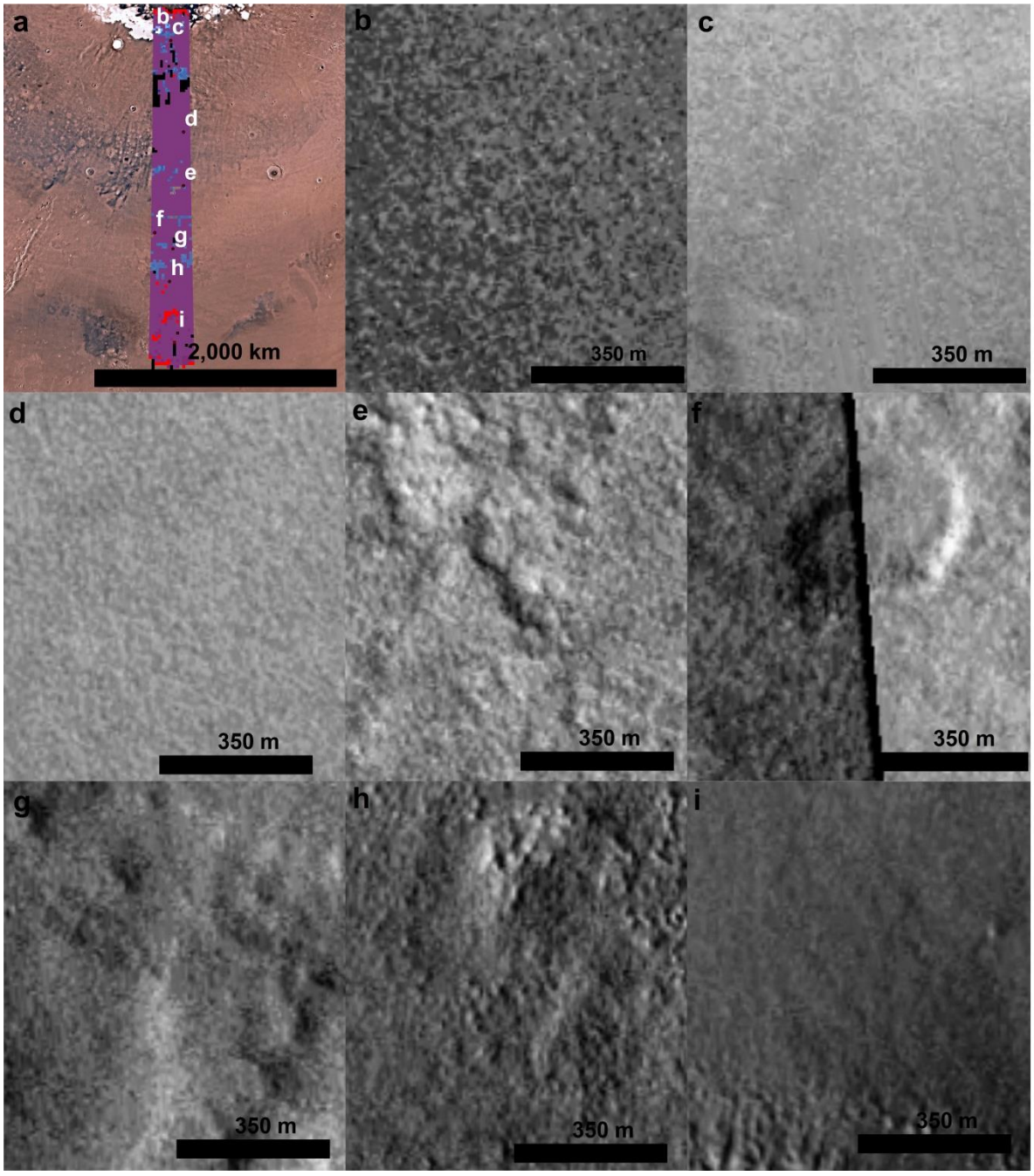

Figure 4.9 (a) Viking image showing the locations of b-i. Grid mapping of textured (red), mantled (blue) and both (purple) overlain. (b-i) CTX images centred at the same location as in Figure 4.8.

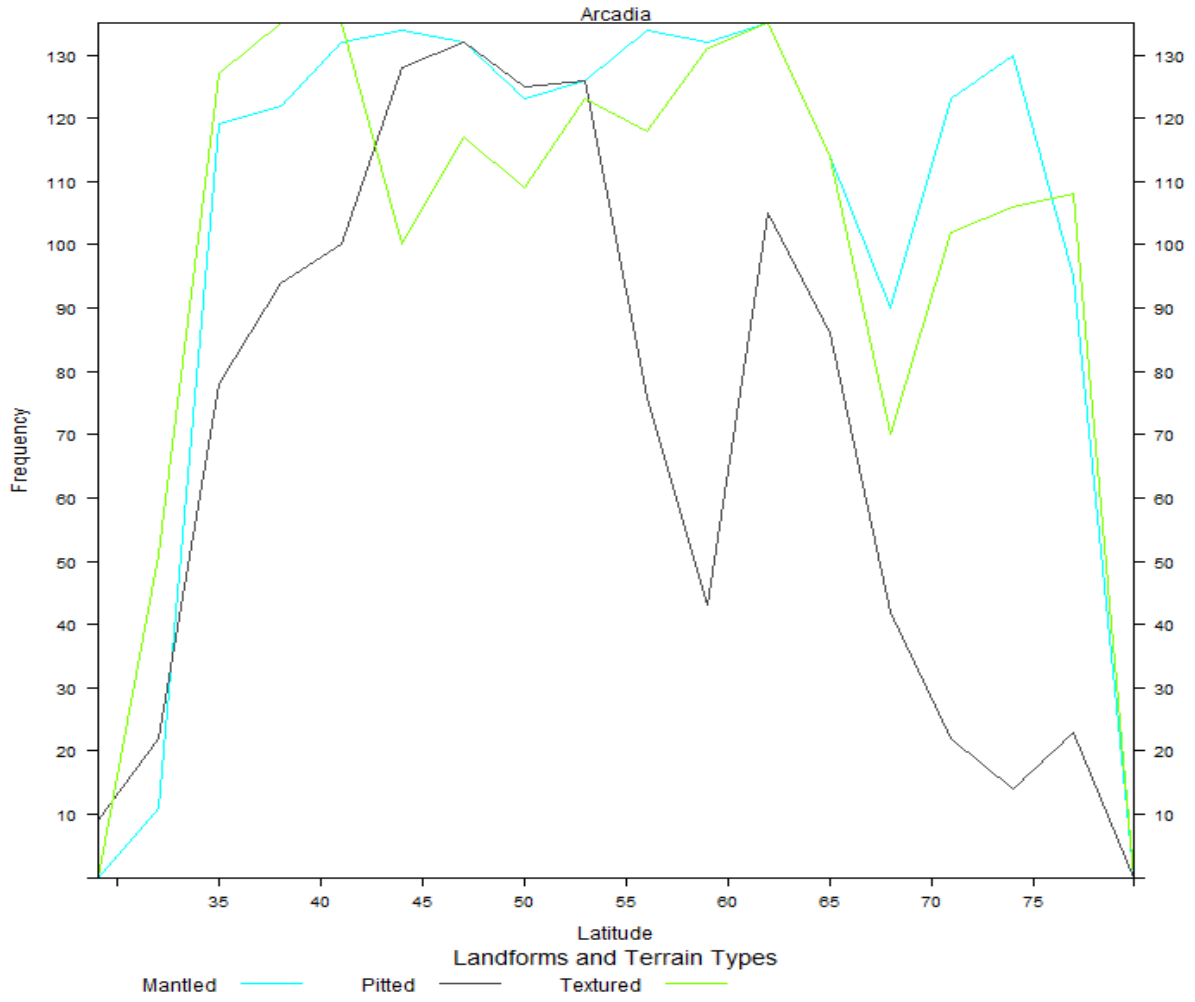

Figure 4.10 Frequency of mantled, textured and pitted terrain occurrence by latitude. The grid mapping data is grouped into one degree bins of latitude where positive values (2,1,P) count towards the total frequency.

The surface appears to be pitted consistently from 60-68°N and from 36-56°N with one significant gap between 56-60°N as shown by Figure 4.5 and Figure 4.10. The low points in the mantled and textured lines around 56-70° N in Figure 4.10 are a result of gaps in CTX availability as shown by the black squares in Figure 4.5. The pitted texture is usually comprised of circular to irregular and often overlapping depressions tens of metres across (see Figure 4.11). The pitting tends to occur

on mantled and textured surfaces supporting the hypothesis of a sublimating mantle. 70-80°N is largely not pitted; however the surface still shows both textural and topographic mantle signatures. At first glance it appears that the thumbprint terrain (see *Chapter 4.4.3*) coincides with the gap in pitting as shown in Figure 4.12 a and b. This initially lends to the interpretation that the thumbprint terrain and pitting are mutually exclusive; however 50% of the squares with pitted surfaces overlap with thumbprint terrain as shown in Figure 4.12 c. Figure 4.13 shows a CTX image of overlapping pitted and thumbprint terrain textures demonstrating that the two landforms types are not mutually exclusive.

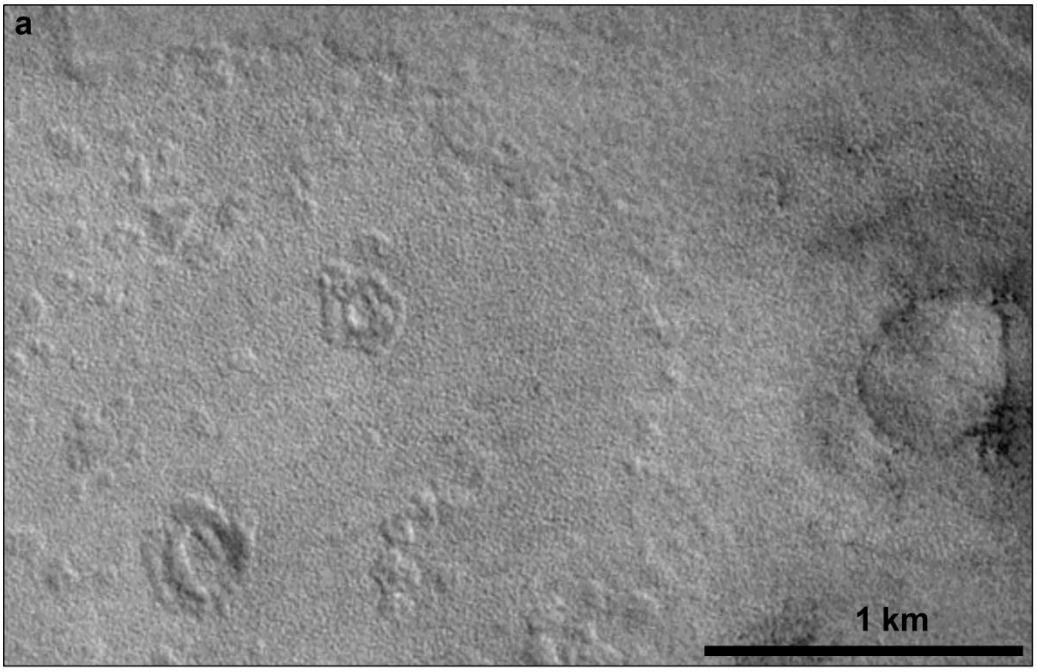

Figure 4.11 CTX image P16_007248_2558 showing a pitted texture at 75° N and 170° W.

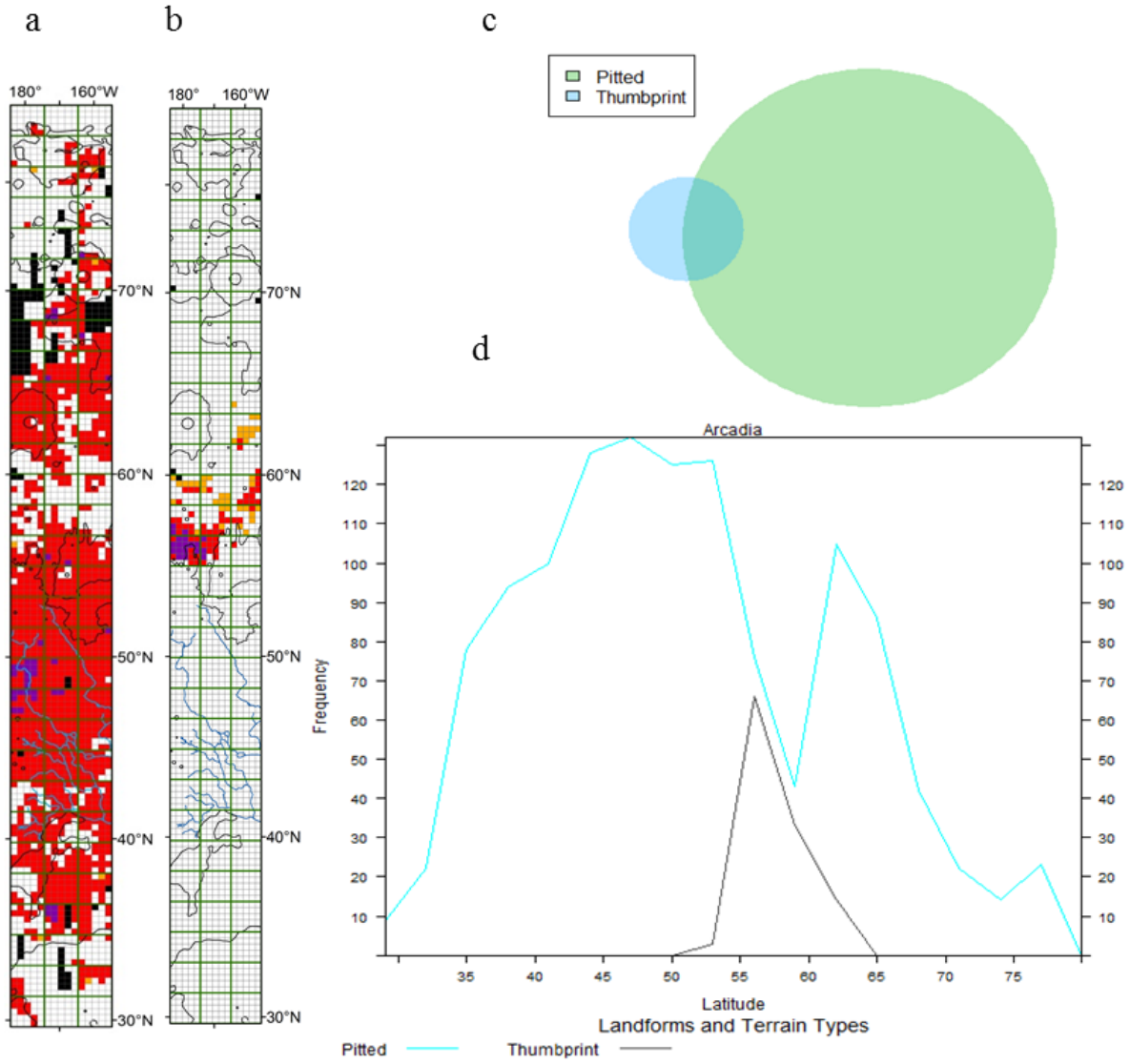

Figure 4.12 (a) Grid map of pitted terrain. (b) Grid map of thumbprint terrain. Red is present, purple dominating, orange possible, black no data and white not present. (c) Venn diagram showing the spatial overlap between thumbprint and pitted terrain. (d) A line chart showing the frequency of both pitted and thumbprint terrain per 1 degree latitutde bin.

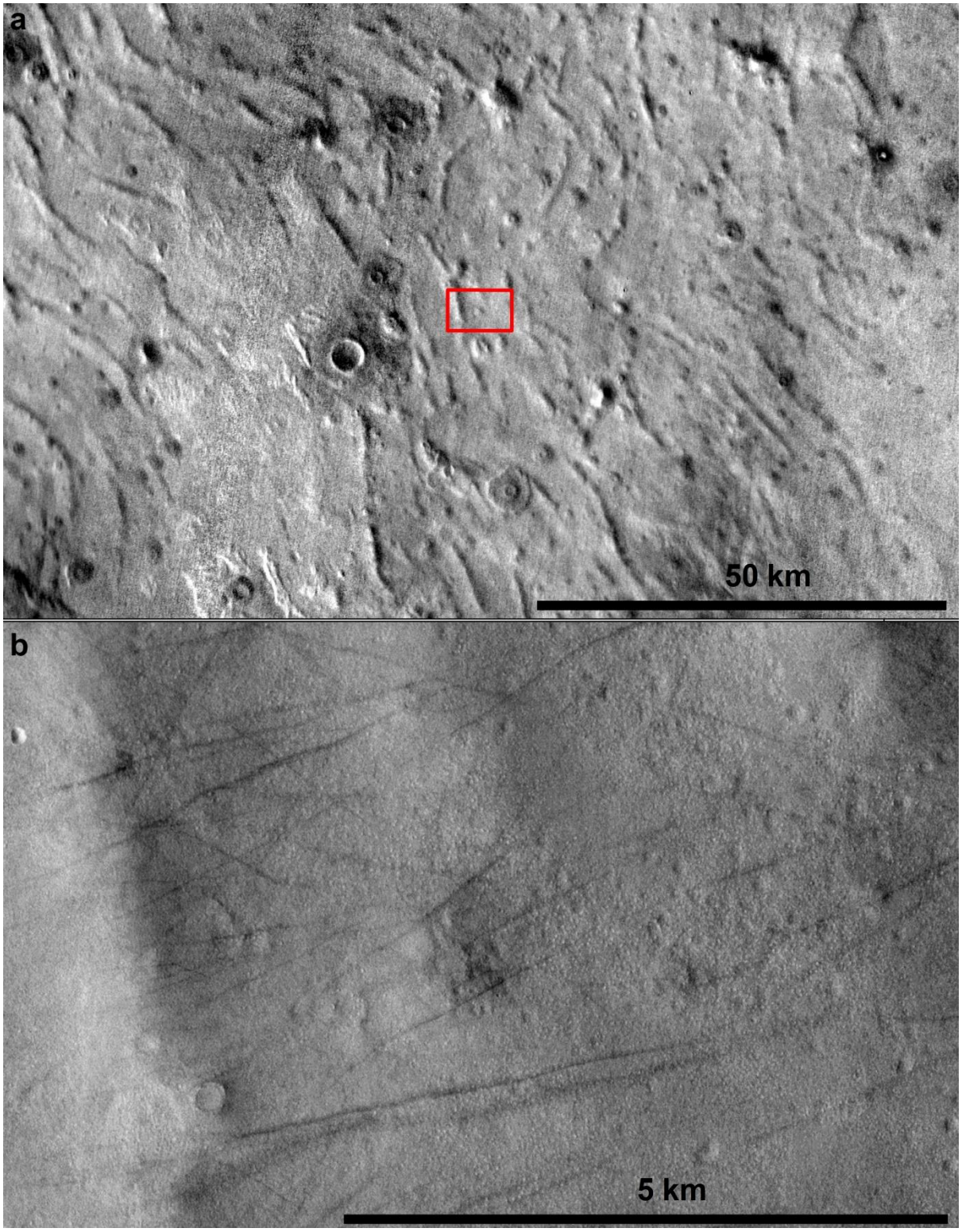

Figure 4.13 (a) THEMIS daytime infrared showing thumbprint terrain; red outline shows location of (b). (b) CTX image P21_009305_2377 showing both pitted textures and thumbprint terrain, at 57° N and 172° W.

4.4.2. **LDM margins, dunes and bedrock**

The northern-most part of the strip overlaps the Olympia Undae unit and dunefields dominate the nothern extent of the Arcadia mapping strip, between 76-80° N. Individual dunes are tens to hundreds of metres across and up to several kilometres in length and have a lower albedo than the surrounding material particularly in the summer months, during the winder they are covered in seasonal frost lowering the albedo contrast (see Figure 4.14). The dunes tend to have crisp edges and do not appear to be mantled. The surrounding material tends to be particularly smooth, lacking textures, and impact craters into this material tend to be subdued, suggesting that a relatively undegraded mantle could continue beneath the dunes.

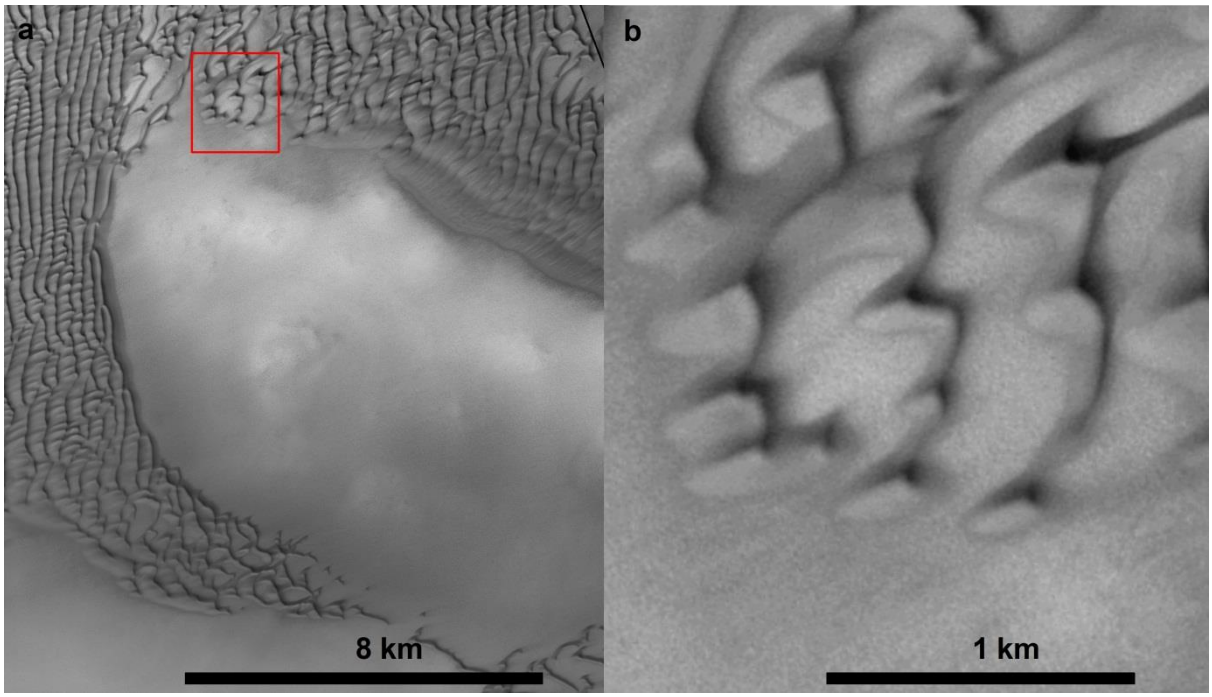

Figure 4.14 (a) and (b) CTX image P22_009779_2581 of dunes in Arcadia Planitia, at 78° N and 163° W.

Bedrock becomes dominant south of 35° N. The “bedrock” in Southern Arcadia/North Amazonis Planitia is the platy-ridged material inferred to be lava flows in Keszthelyi et al. (2000). The transition between the “bedrock” and the textural and mantled signatures appears to be gradational rather than a distinct boundary. The transition to non-mantled topogaphy shows

platy-ridge material that has softened edges and textural signatures in the inter-ridge zones as shown in Figure 4.15.

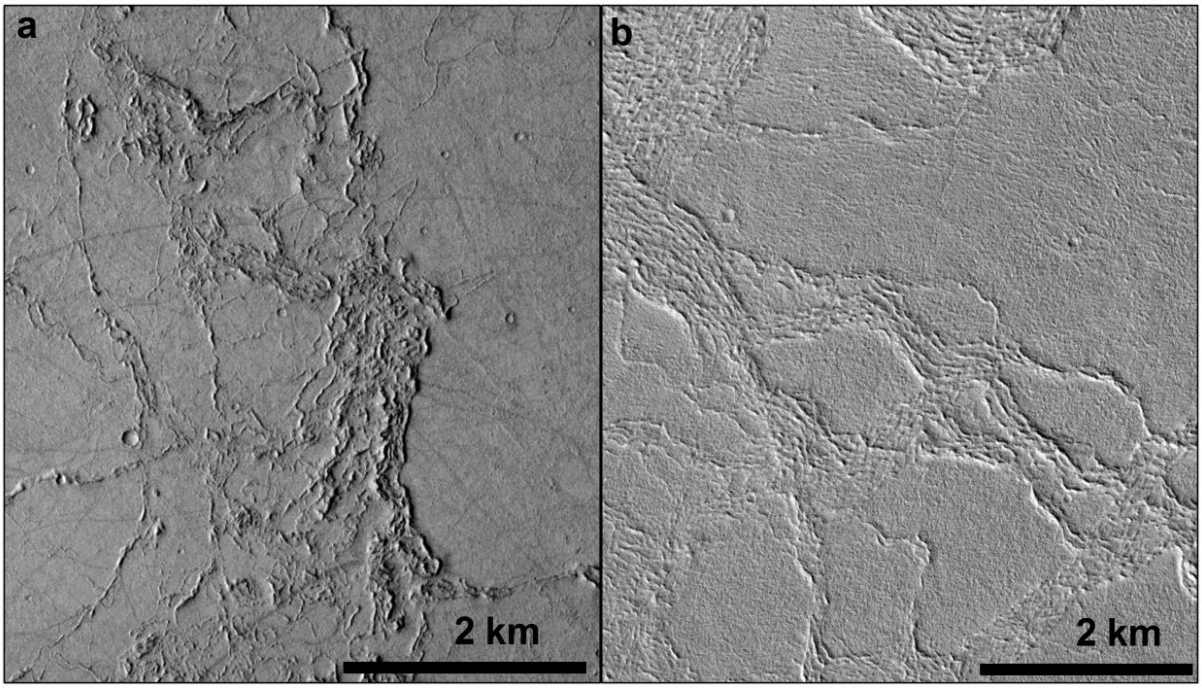

Figure 4.15 (a) CTX image B19_017151_2116, at 31° N and 171° W, showing unmantled/untextured platy-ridge material. (b) CTX image P15_006866_2147, 34° N and 168° W, platy-ridge material with a softened appearance and a "textured" signature.

4.4.3. **Thumbprint Terrain**

The thumbprint terrain identified in the Arcadia grid mapping is found between 55-65°N and is comprised largely of km-scale ridges. It appears much smoother that the conical chains that comprise the thumbprint terrain in Acidalia and Utopia. The thumbprint terrain in Arcadia overlaps with the mantle and textured signatures suggesting the thumbprint terrain is buried by the LDM in Arcadia.

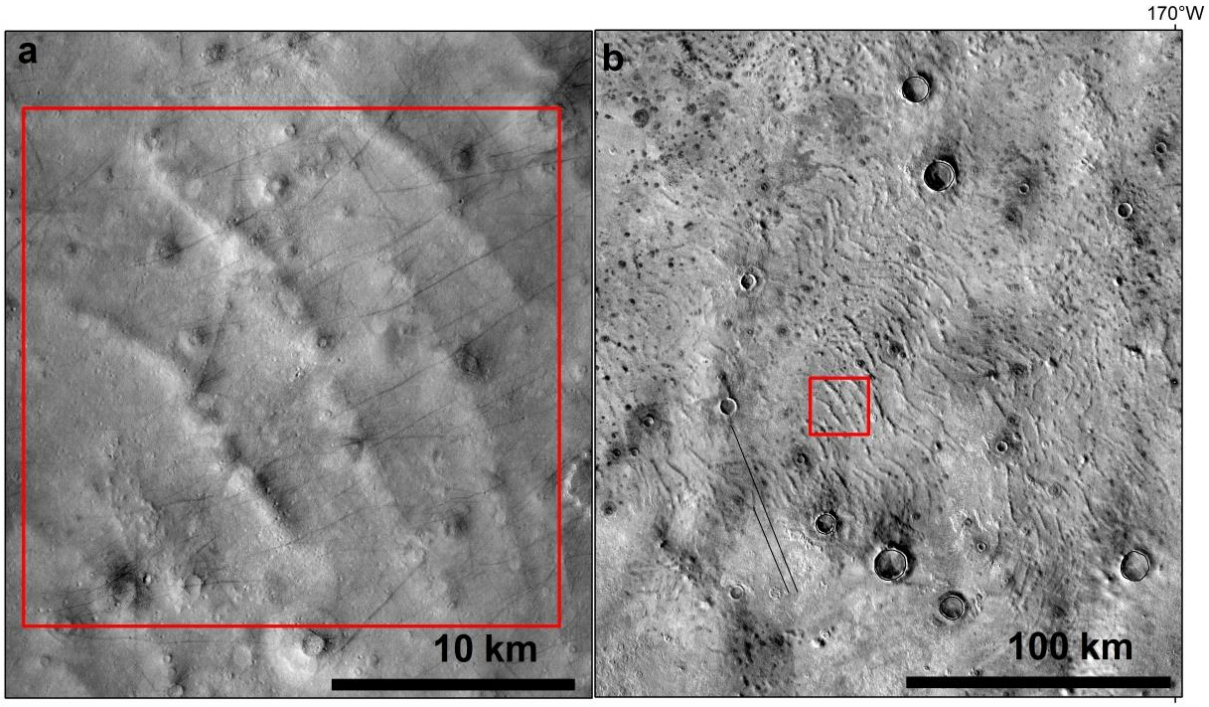

Figure 4.16 (a) CTX image P20_008870_2373 and (b) THEMIS daytime image of Arcadia thumbprint terrain, at 57° N and 174° W.

The thumbprint terrain appears to act as a boundary between different landform assemblages. South of the thumbprint terrain (approx. 60° N) we can identify a terrain assemblage of channels, scallops and small mounds (see Figure 4.17), but these are lacking further north.

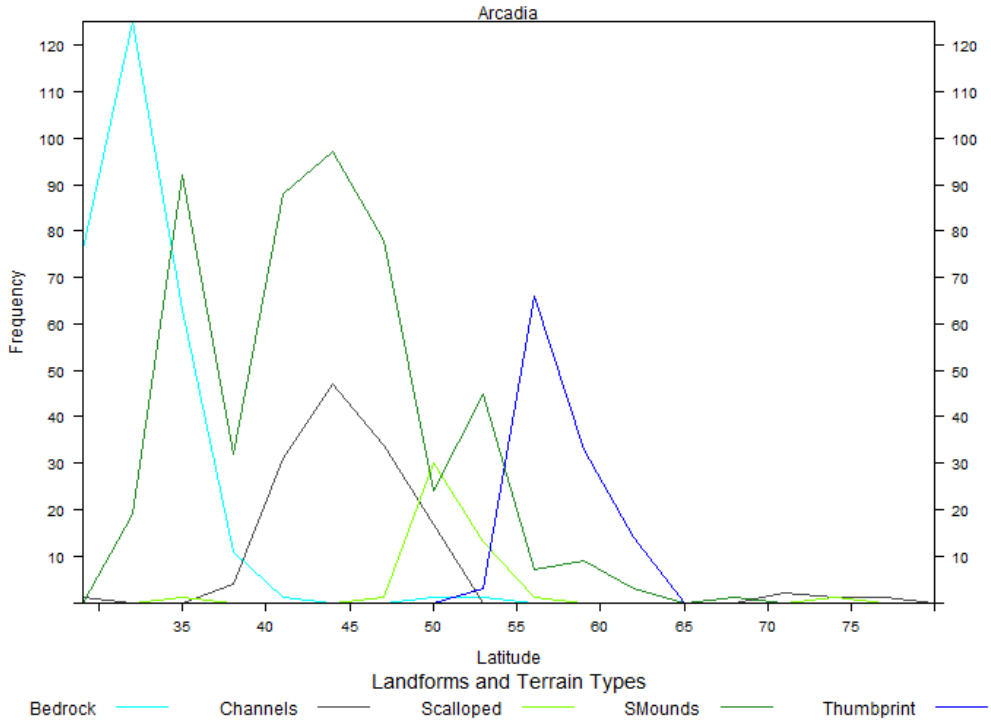

Figure 4.17 Frequency of bedrock, channels, scalloped, small mounds (SMounds) and thumbprint terrain occurrence by latitude. The grid mapping data is grouped into one degree bins of latitude where positive values (2,1,P) count towards the total frequency.

North of the thumbprint terrain we see a different set of landforms including km scale polygons, large pitted mounds (rarely), massive ice and dunes (see Figure 4.18).

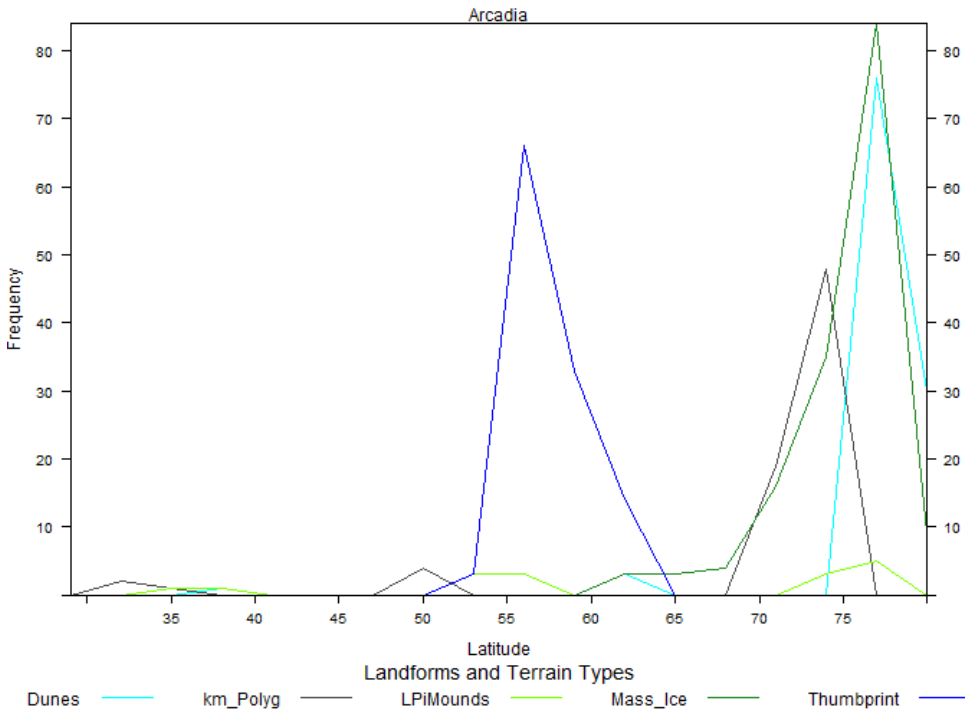

Figure 4.18 Frequency of dunes, kilometre scale polygons (km_Polyg), large pitted mounds (LPiMounds), massive ice (Mass_Ice) and thumbprint terrain occurrence by latitude. The grid mapping data is grouped into one degree bins of latitude where positive values (2,1,P) count towards the total frequency.

4.4.4. **Scalloped terrain, small mounds and channels**

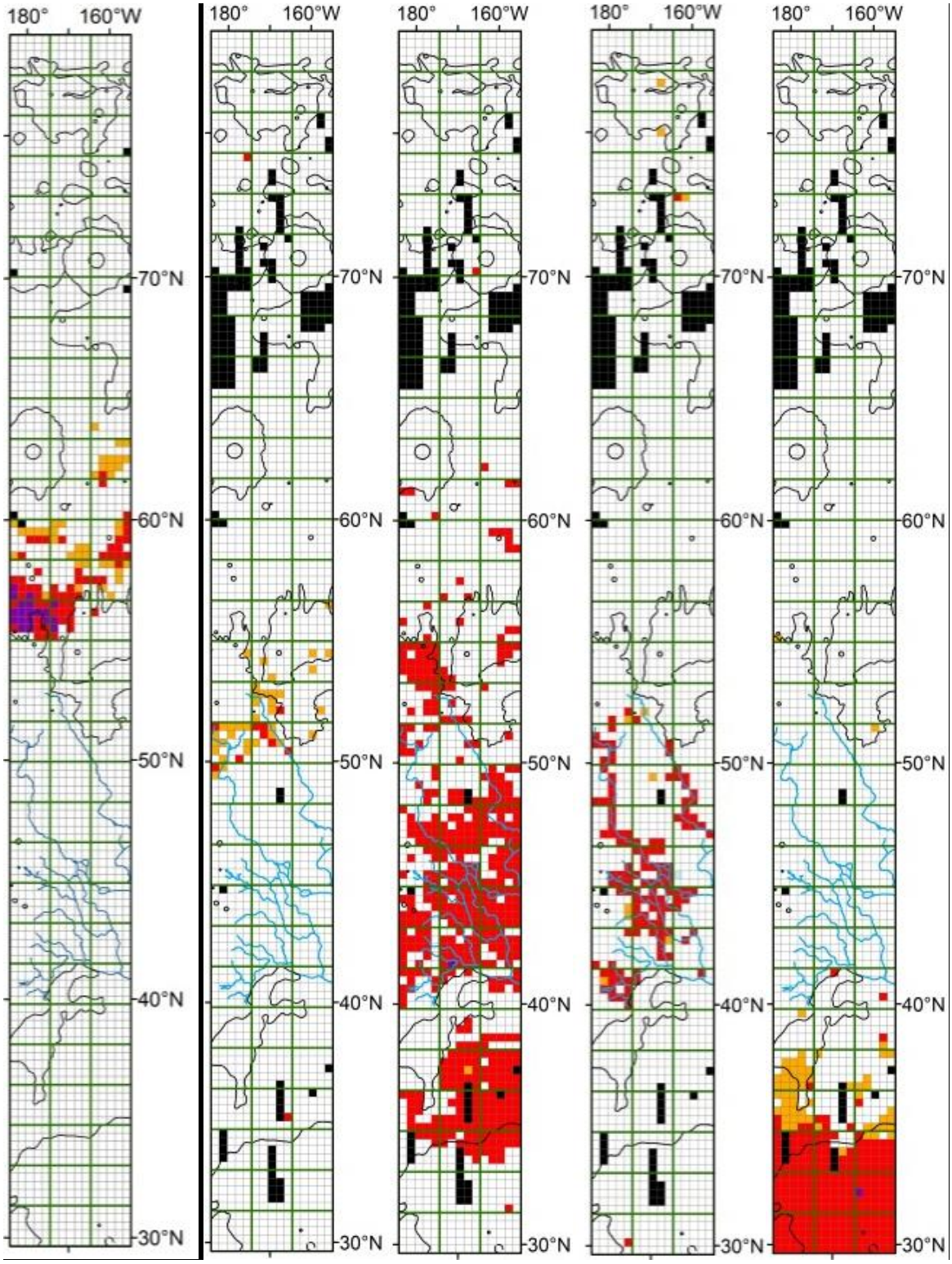

Figure 4.19 Grid Mapping results for landforms (Left to Right) Thumbprint Terrain, Scalloped pits, Small Mounds, Channels and Bedrock. Red is present, purple dominating, orange possible, black no data and white not present.

The scalloped terrain occurs in a narrow band in Arcadia between 50-55°N, and is much less prevalent than the large assemblages described in Utopia Planitia (e.g. Séjourné et al., 2012). The individual scallops in Arcadia are around a few hundred metres across with cuspate edges, like those found in Utopia, and they show consistent asymmetry with steep poleward facing scarps on their southern boundary (see *Figure 4.20*). However, where individual Utopian scallops can often be delineated (see *Fig. 2.12 from Séjourné et al. (2011)*), the scallops in Arcadia often have no obvious northern extent (see *Figure 4.20*). *Figure 4.20* also shows that the area around the scalloped terrain is also heavily pitted by more generic roughly circular depressions. The area immediately south of the scalloped terrain in Arcadia is heavily channelised. These channels are not apparent in Utopia so it is possible that the scalloped terrain previously extended further south and has been removed through the process that formed the channels. Alternatively, the surface materials south of 50°N may not be susceptible to scallop formation, whether due to different mechanical properties or ground-ice content. The scallops of Arcadia are poorly formed in comparison with those found in Utopia and do not display the inter depression polygons described by Séjourné et al. (2011) supporting a hypothesis of less prevalent conditions for scalloped pit formation in Arcadia.

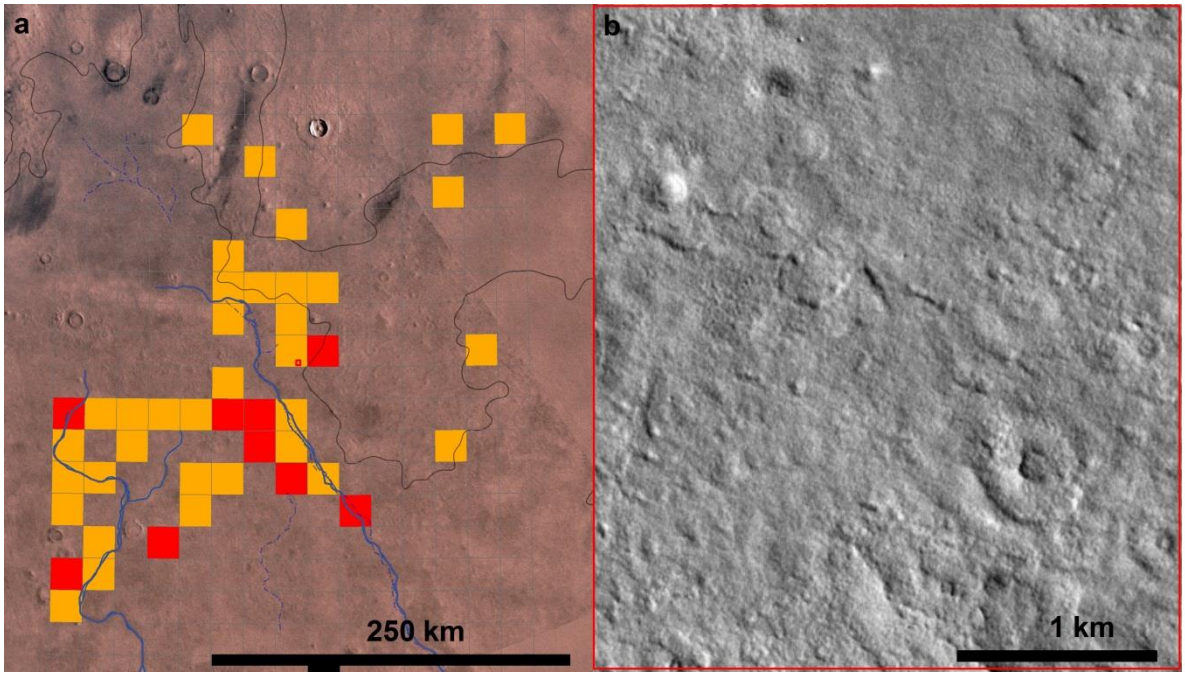

Figure 4.20 (a) Scalloped grid mapping results overlain onto Viking image mosaic, red outline shows location of (b), blue lines are channels, black lines contacts from Tanaka et al. (2005) geological map. Red is present, orange possible, and hollow not present. (b) CTX image G03_019221_2327, at 53° N and 170° W, showing the morphology of scalloped terrain in Arcadia Planitia.

The area between 35-55°N displays small featureless mounds around 100 m across. The mounds are smooth in appearance, with no obvious features in either CTX or HiRISE images (see Figure 4.21). There is no obvious difference in the albedo or colour between the mounds and the surrounding material. These mounds are very sparsely populated with roughly a few to a dozen mounds per 20 km by 20 km grid square.

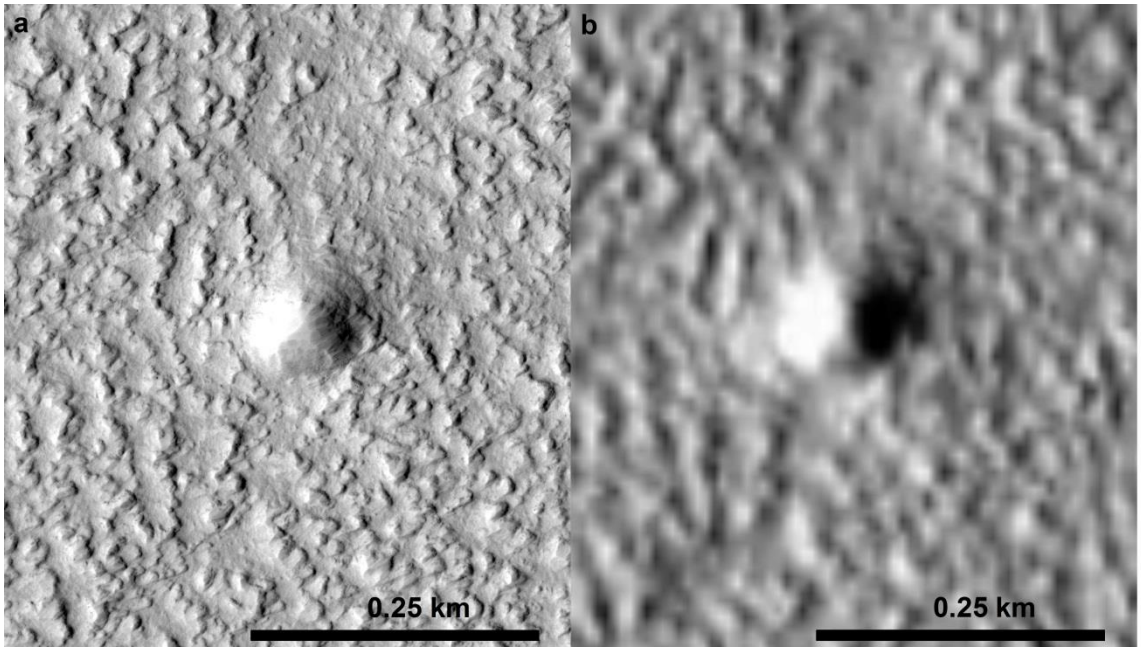

Figure 4.21 (a) HiRISE image ESP_026856_2160 of a small mound at 25 cm/pixel. (b) CTX image G22_026856_2148, at 35° N and 172° W showing the same small mound at 6 m/pixel. The small mound is around 100 m across and surrounded by textured terrain.

While I mapped channels using the grid mapping method, this was largely to identify small channels on the decametre scale. Many of channels identified in the context mapping of Arcadia were on the order of 20 km across and too large to identify when viewing individual 20 km grid

squares. There appears to be only one major channels system within the Arcadia grid mapping area, extending between 40-52° N with a NW-SE trend. The source and terminations of this system seems to lie outside of the grid mapped area. Assuming current topography and downhill flow, the source would be southeast of the mapped area, and the termination on the western boundary of the mapped area. More detailed observations of the channels and their source and termination can be found in Chapter 5.

4.4.5. **Kilometre-scale polygons, large pitted mounds and massive ice.**

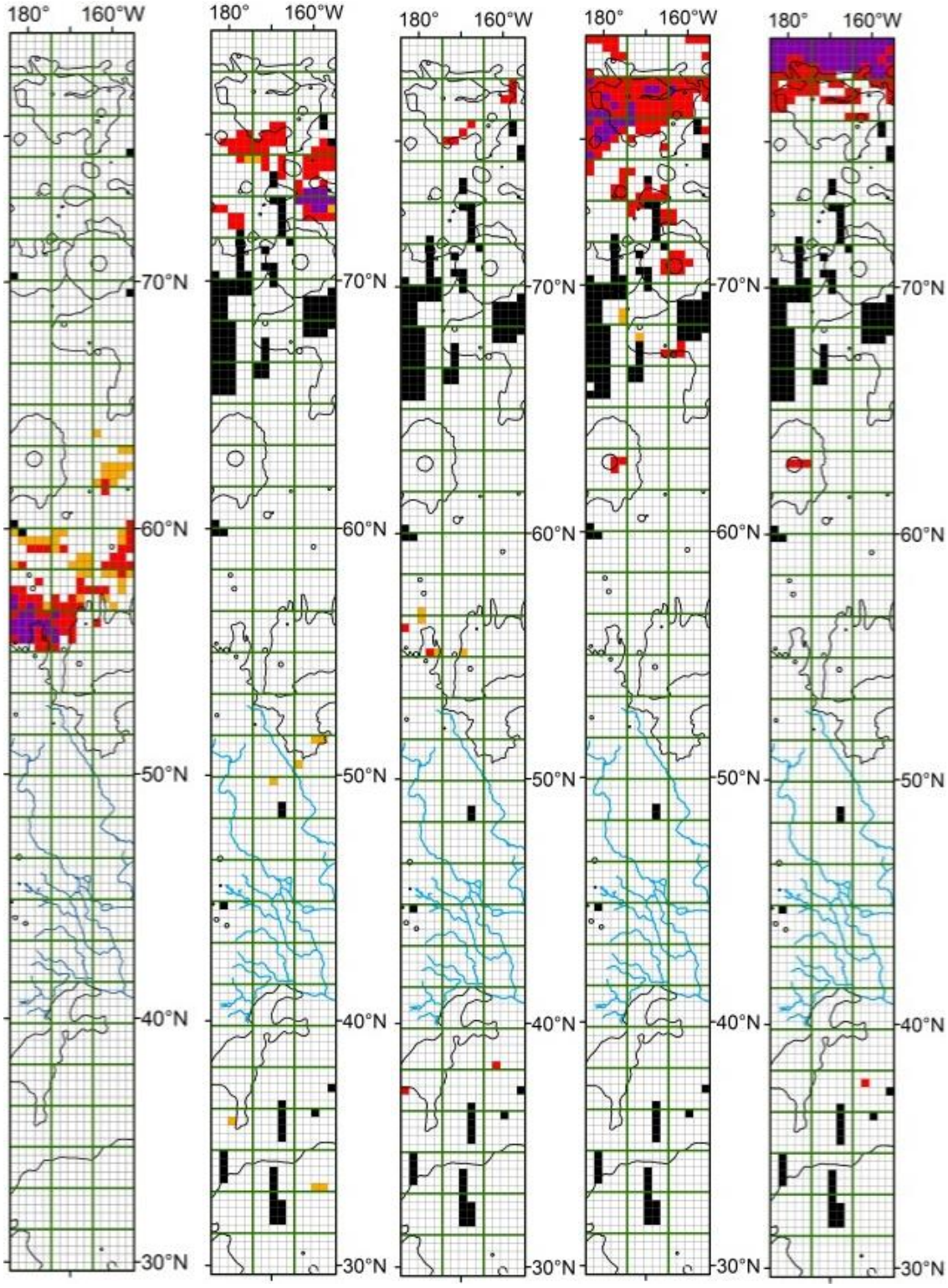

Figure 4.22 Grid Mapping results for landforms (Left to Right) Thumbprint Terrain, kilometre scale polygons, large pitted mounds, massive ice and dunes. Red is present, purple dominating, orange possible, black no data and white not present.

Kilometre-scale polygons occur between 72-76° N as shown by Figure 4.22. The kilometre-scale polygons in Arcadia are high centred and between 1-3 km across. The polygons appear to have rounded edges and form irregular, non-geometric, shapes. Multiple impacts into kilometre-scale polygons have been mantled suggesting that these features relate to sub-mantle geology, predating the mantle emplacement (see Figure 4.23).

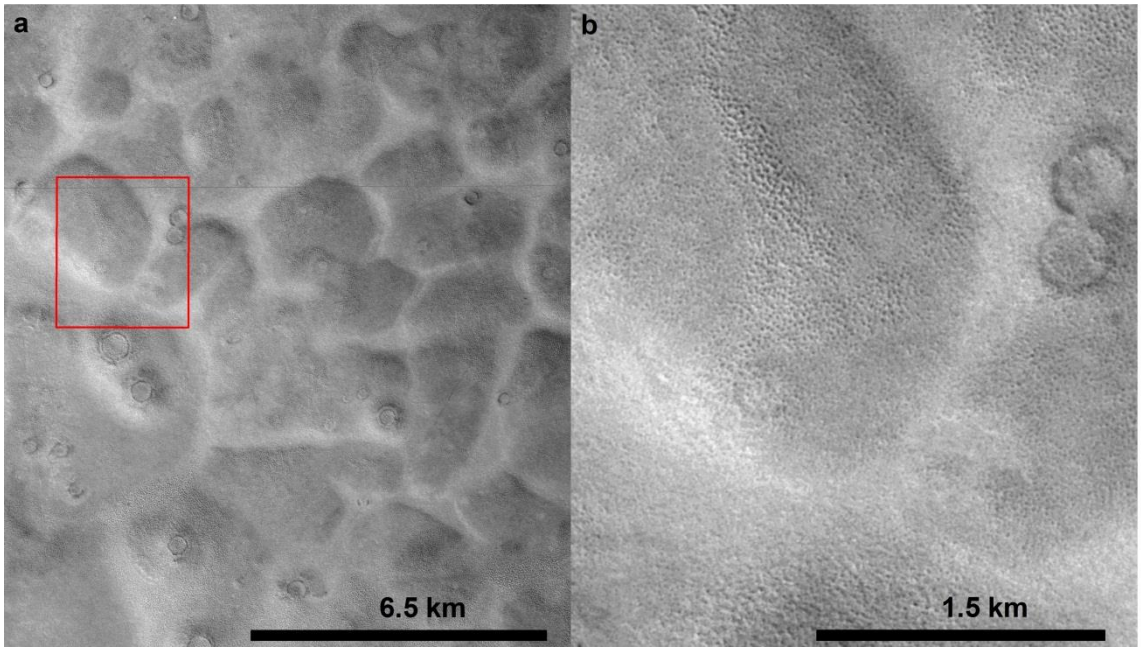

Figure 4.23 (a) CTX image G23_027251_2528, at 72° N and 163° W, showing high centred kilometre-scale polygons in Arcadia, red outline shows location of (b). (b) CTX image G23_027251_2528 close up of a kilometre-scale polygon. Note the textured appearance and the mantling of impact craters.

When identifying large pitted mounds I was looking for specifically kilometre-scale hills with a summit depression (see Figure 4.24). Large pitted mounds are found in <1% of the Arcadia strip, and putative examples lack the distinct albedo contrast of those found in Acidalia (Orgel et al., 2016). Given that the features identified are also mapped as mantled, the albedo contrasts could be subdued. However, it is likely that at least some of the large pitted mounds that I identified in the grid mapping of Arcadia are just degraded and buried impact craters e.g. Figure 4.24b.

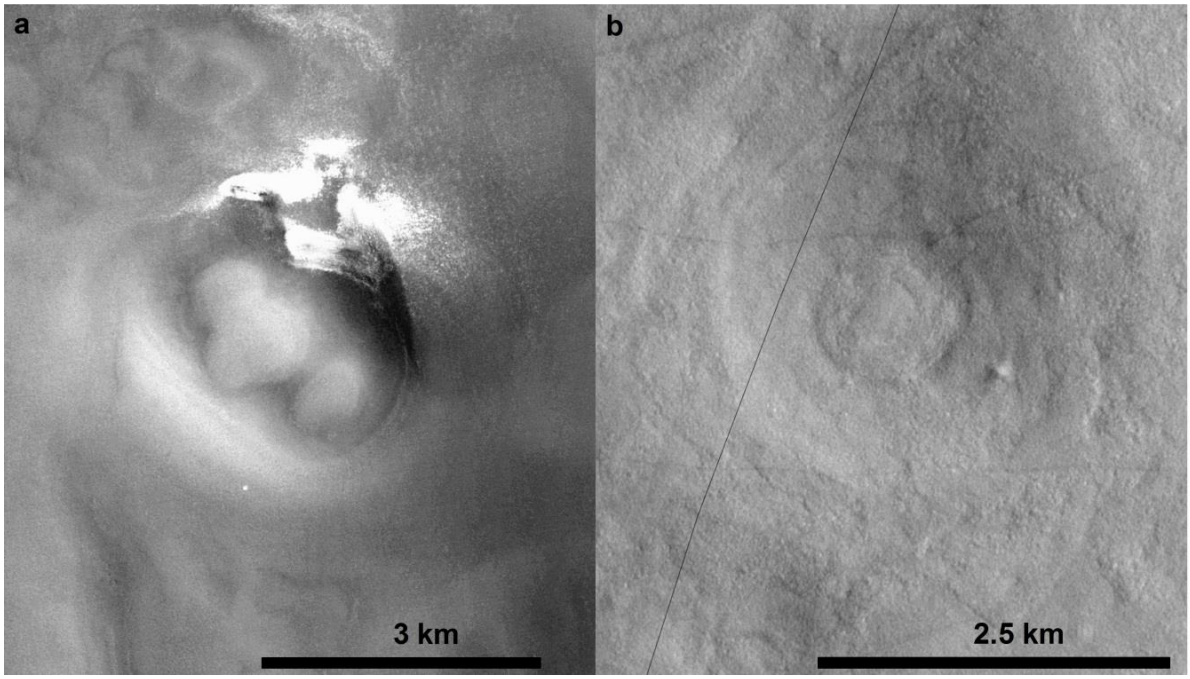

Figure 4.24 CTX images (a) P21_009318_2572, at 77° N and 174° W, and (b) P21_009305_2377, at 57° N and 172° W, showing large pitted mounds in Arcadia.

The massive ice observed in Arcadia is largely polar cap outliers found between 72-80° N, but also ice deposits around the rims of large impact craters down to 60° N. They range in size from tens of metres across to few hundred kilometres across. The massive ice deposits, see Figure 4.1) are easily identified by their high albedo and smooth uncratered surfaces. These deposits do not appear to be mantled or textured and likely post-date the mantle deposits.

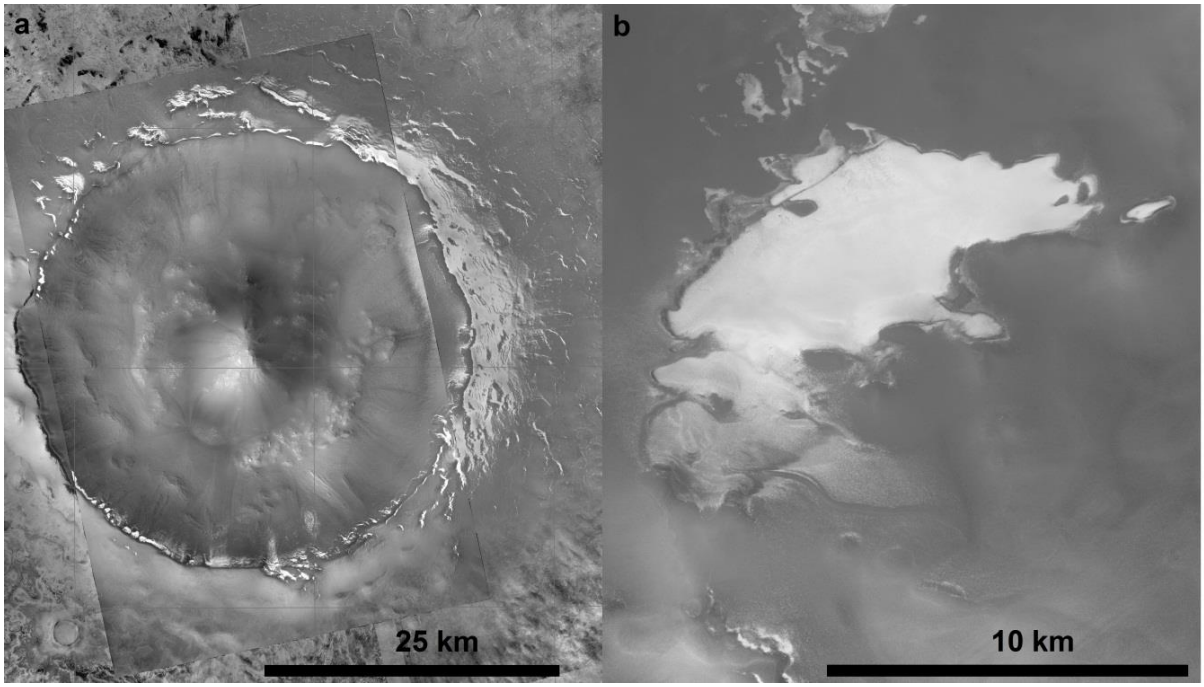

Figure 4.25 (a) CTX images G20_026117_2511, at 71° N and 165° W, and G22_026816_2510 showing massive ice deposits around a large crater rim in Arcadia. (b) CTX image P02_001657_2579, at 77° N and 171° W, showing an example of a massive ice polar cap outlier in Arcadia.

4.4.6. **Viscous Flow Features, Glacier-like Forms and Gullies**

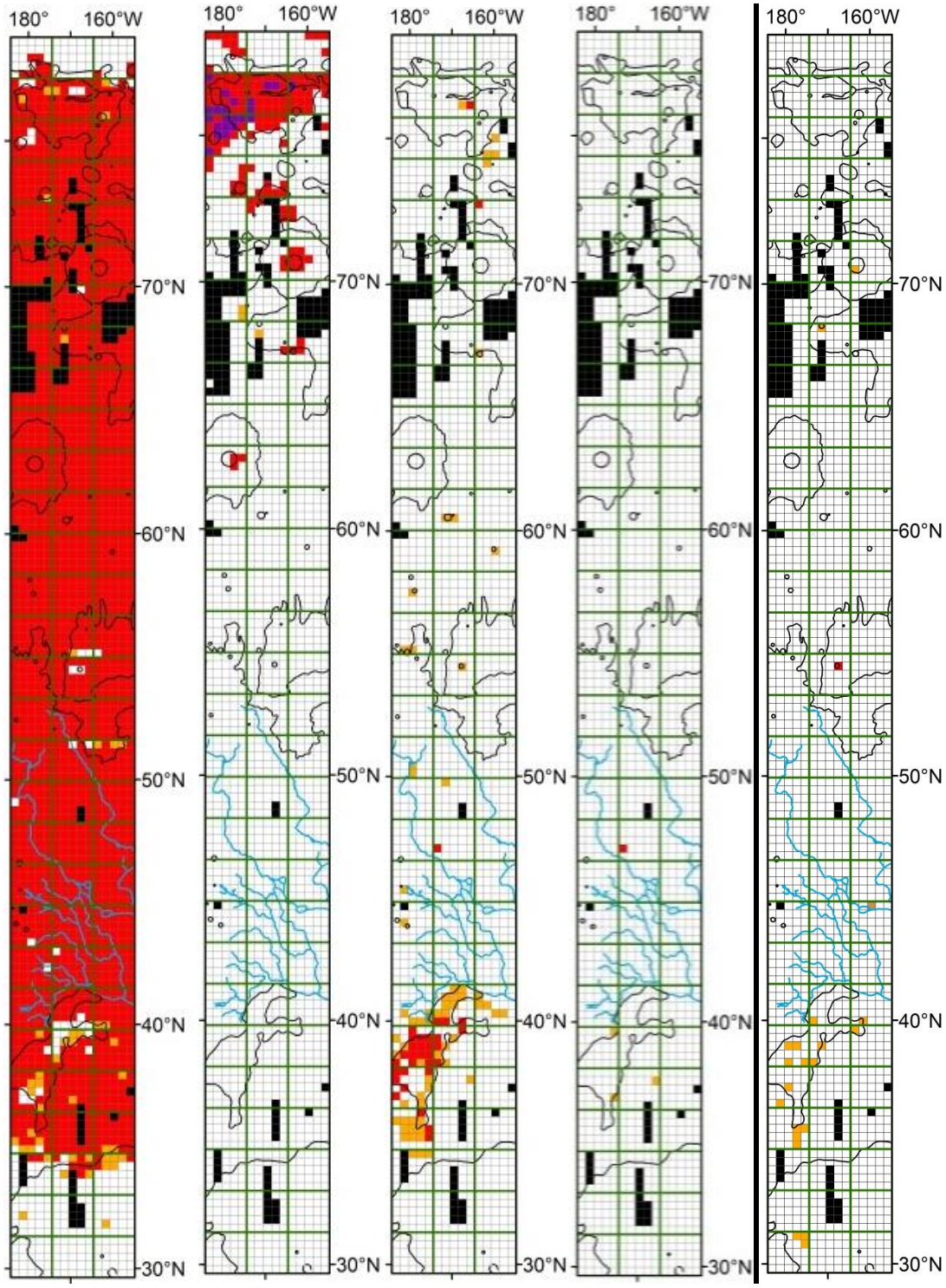

Figure 4.26 Grid Mapping results for landforms (Left to Right) mantled, massive ice, VFFs, GLFs, and gullies. Red is present, purple dominating, orange possible, black no data and white not present.

VFFs are largely restricted to one small area within the Arcadia strip between 35-42° N. The VFFs between 35-42° N are largely LDAs around inliers of Nepenthes Mensae unit. Other examples of VFFs in Arcadia include putative LDA's around topographic highs and concentric crater fill. No convincing gullies or GLFs were found in the Arcadia strip.

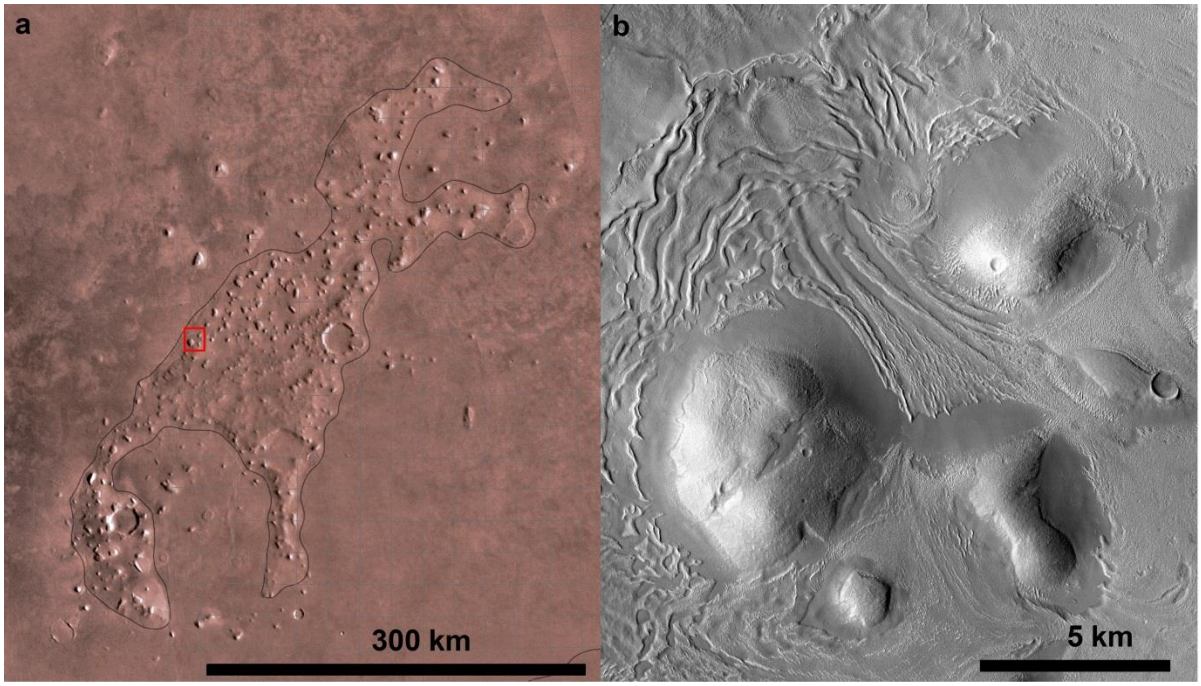

Figure 4.27 (a) Viking image with Tanaka et al. 2005 geological contacts shown by black lines. Red outlines shows location of (b). (b) CTX image P17_007644_2187, at 38° N and 172° W, showing VFFs overlying the Nepenthes Mensae unit in Arcadia.

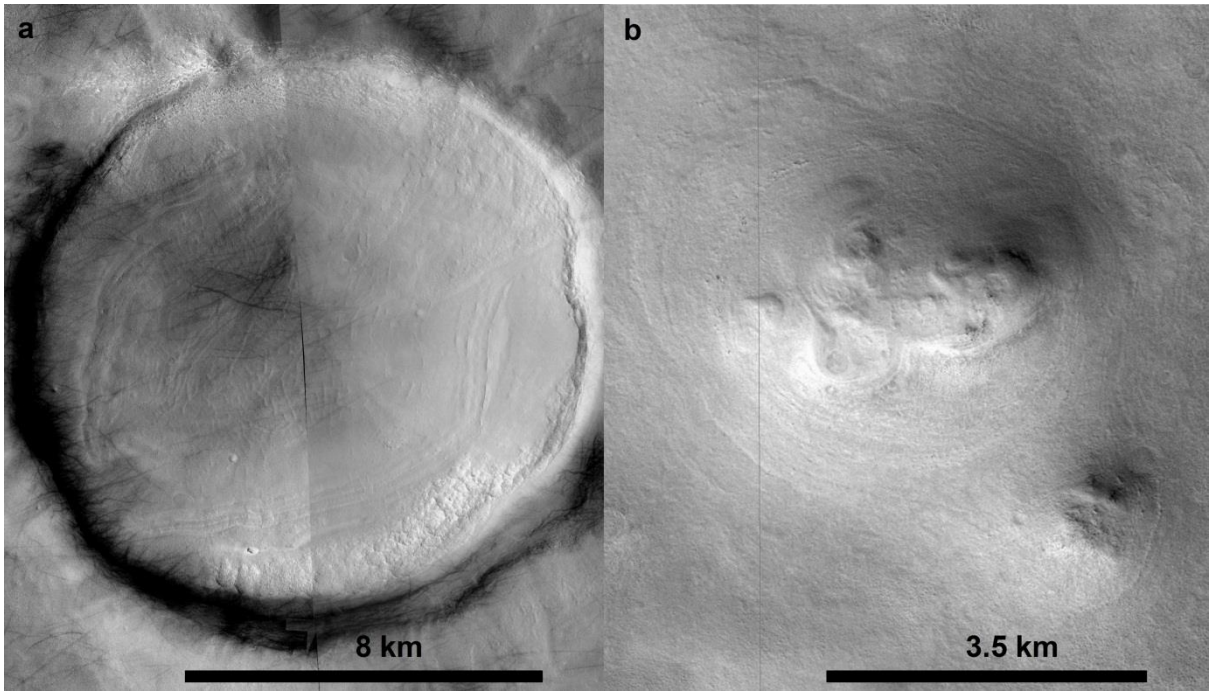

Figure 4.28 (a) CTX images P21_009371_2346 and P20_008870_2373, at 54° N and 172° W, showing putative concentric crater fill in Arcadia. (b) CTX image P17_007696_2568, at 76° N and 165° W, showing putative LDA in Arcadia, it is likely both the LDA and hill have been mantled given the subdued appearance and continuous texture.

4.4.7. **Small 100 metre-scale Polygons**

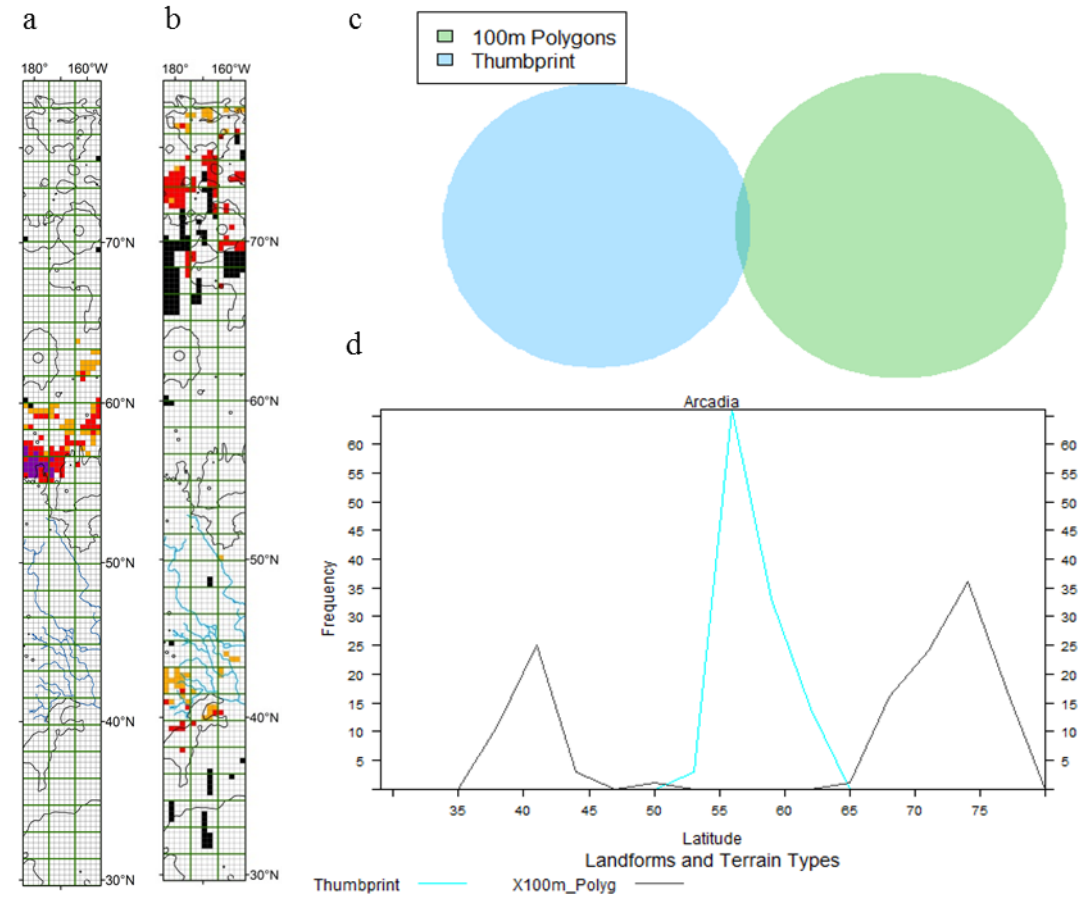

Figure 4.29 (a) Grid map of thumbprint terrain. (b) Grid map of 100m polygons. Red is present, purple dominating, orange possible, black no data and white not present. (c) Venn diagram showing the overlap between thumbprint terrain and 100m polygons. (d) A line chart showing the frequency of both 100m polygons (X100m_Polyg) and thumbprint terrain per 1 degree latitude bin.

Two groups of 100 metre-scale polygons can be observed in the Arcadia strip (see Figure 4.29). The northern group of polygons found between 66-78° N is generally characterised by high albedo contracts with dark centres (see Figure 4.30b). These northern polygons are reminiscent of snow filled, and ice-wedge polygons on Earth, marked by high albedo contrasts and irregular shapes. The southern group of polygons found between 38-45° N are generally angular high centred polygons (see Figure 4.30a). The southern polygons have clear topographic steps and appear more like fracture nets than clastic or ice related polygons.

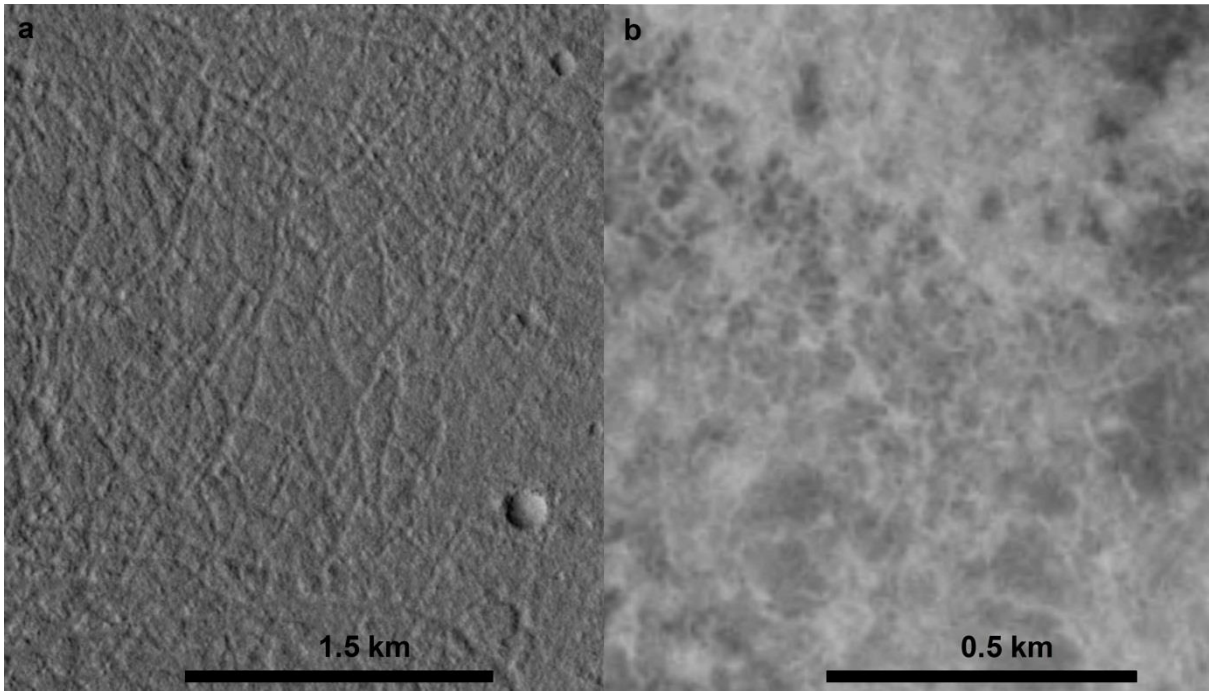

Figure 4.30 (a) CTX image P16_007433_2181, at 38° N and 171° W, showing high centred 100 metre scale polygons from the southern set in Arcadia. (b) CTX image B18_016531_2540, at 74° N and 174° W, showing high albedo contrast 100 metre scale polygons from the northern set in Arcadia.

4.4.8. **Further observations of the large channel system in Arcadia**

One of the most prominent features in Arcadia is a large channels system between 35-50° N and 150-175° W. Assuming downhill flow (see Figure 4.31), flow is from the south-east to the north-west (see Figure 4.32a). The channels are darker in appearance to the surrounding material and vary in width from tens of metres to several kilometres. Cross-profiles of the channels show varying morphology, from “V” (see Figure 4.32b) and “U” (see Figure 4.32c) shaped to ridges with twin parallel channels (see Figure 4.33 Figure 4.32e). The channels are typically 20-30 metres in depth and 500-1000 kilometres long. The channels for the most part are singular, however in some regions they appear to be anastomosing (see Figure 4.34).

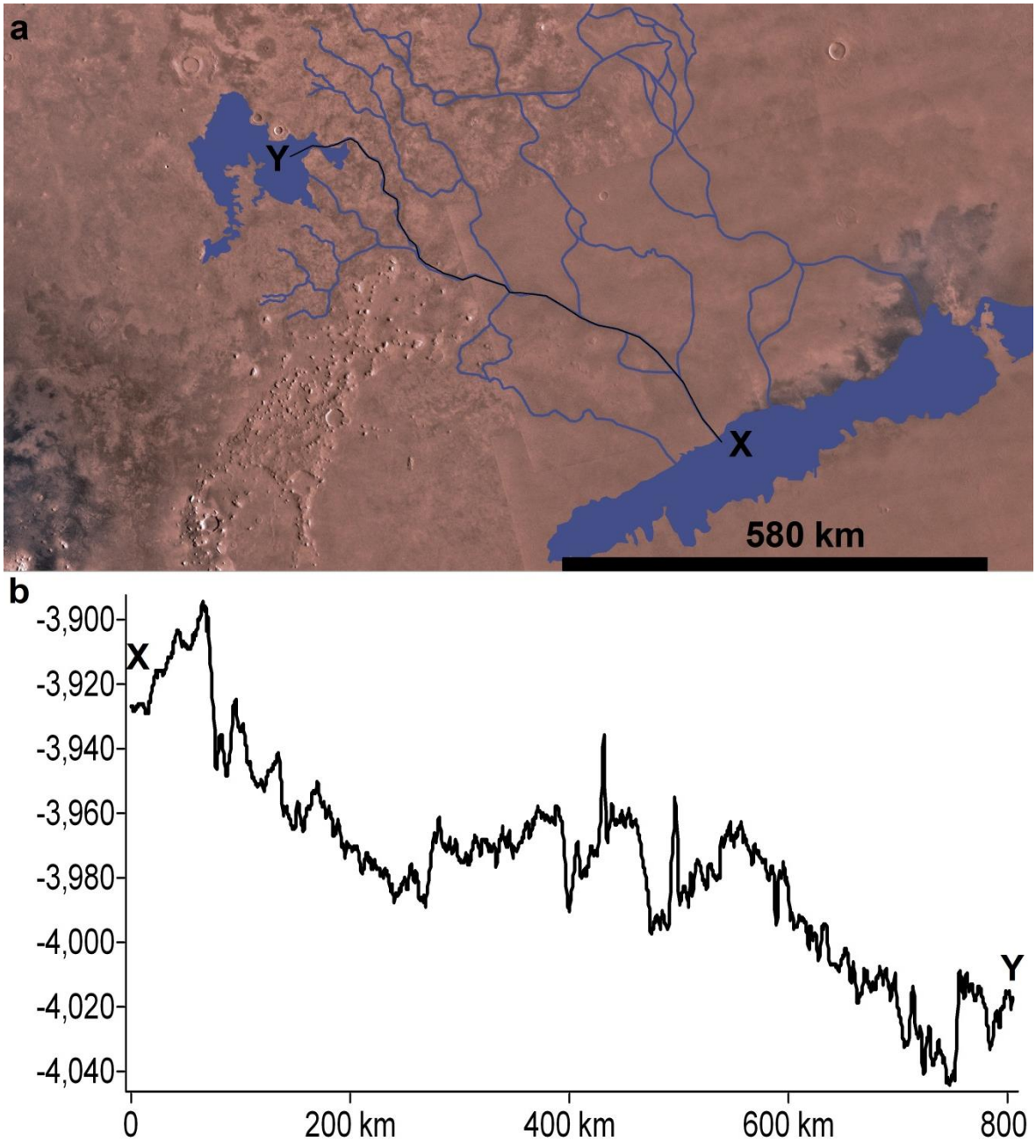

Figure 4.31 (a) Viking image, around 40° N and 170° W, showing the location of example channel long profile (b X-Y) and channel system (blue).

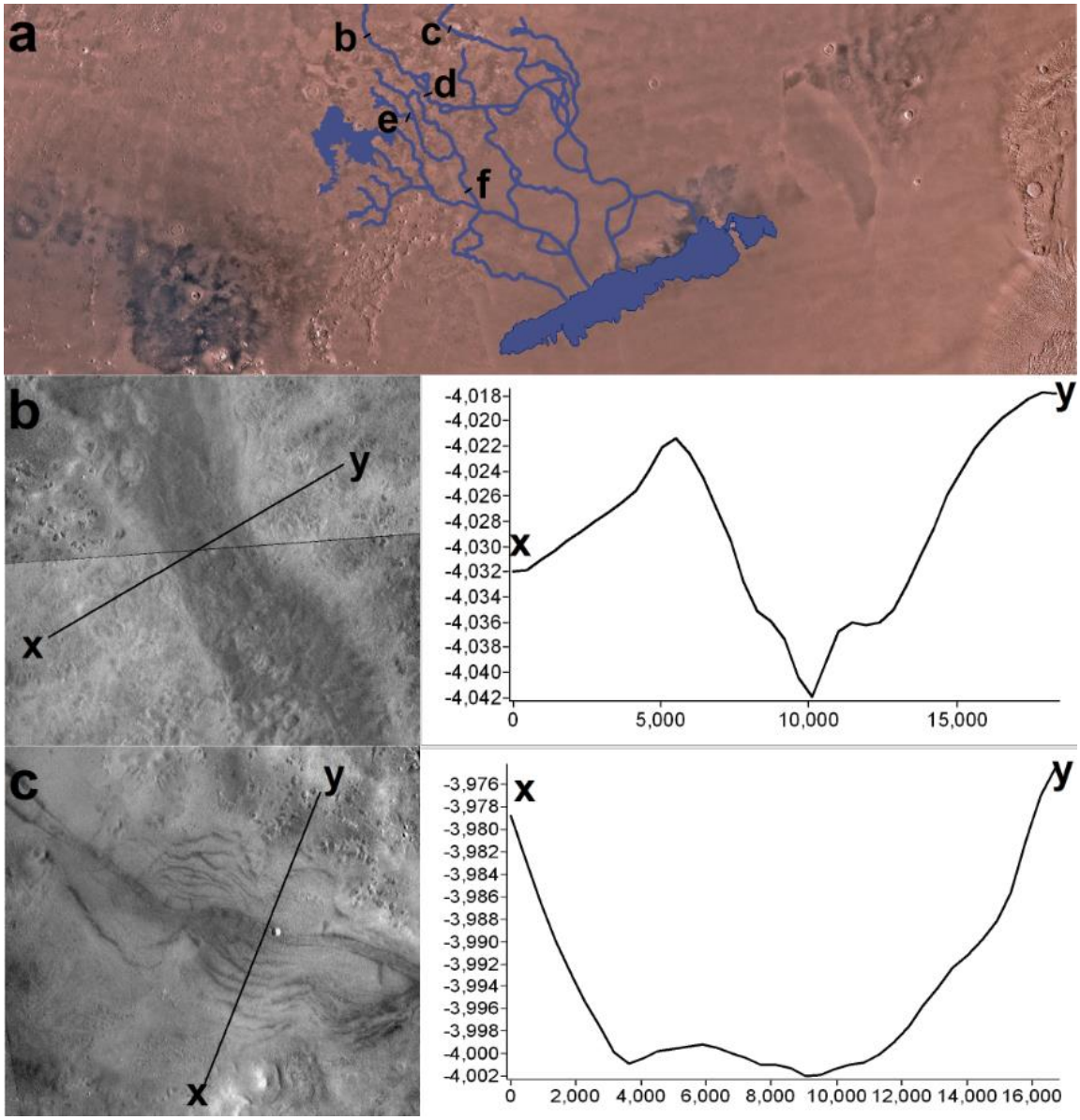

Figure 4.32 (a) Viking image, around 40° N and 170° W, showing the locations of the channels in (b-c) and (Figure 4.33 d-f). (b-c) Left – CTX images showing channels and X-Y location of cross profiles - Right.

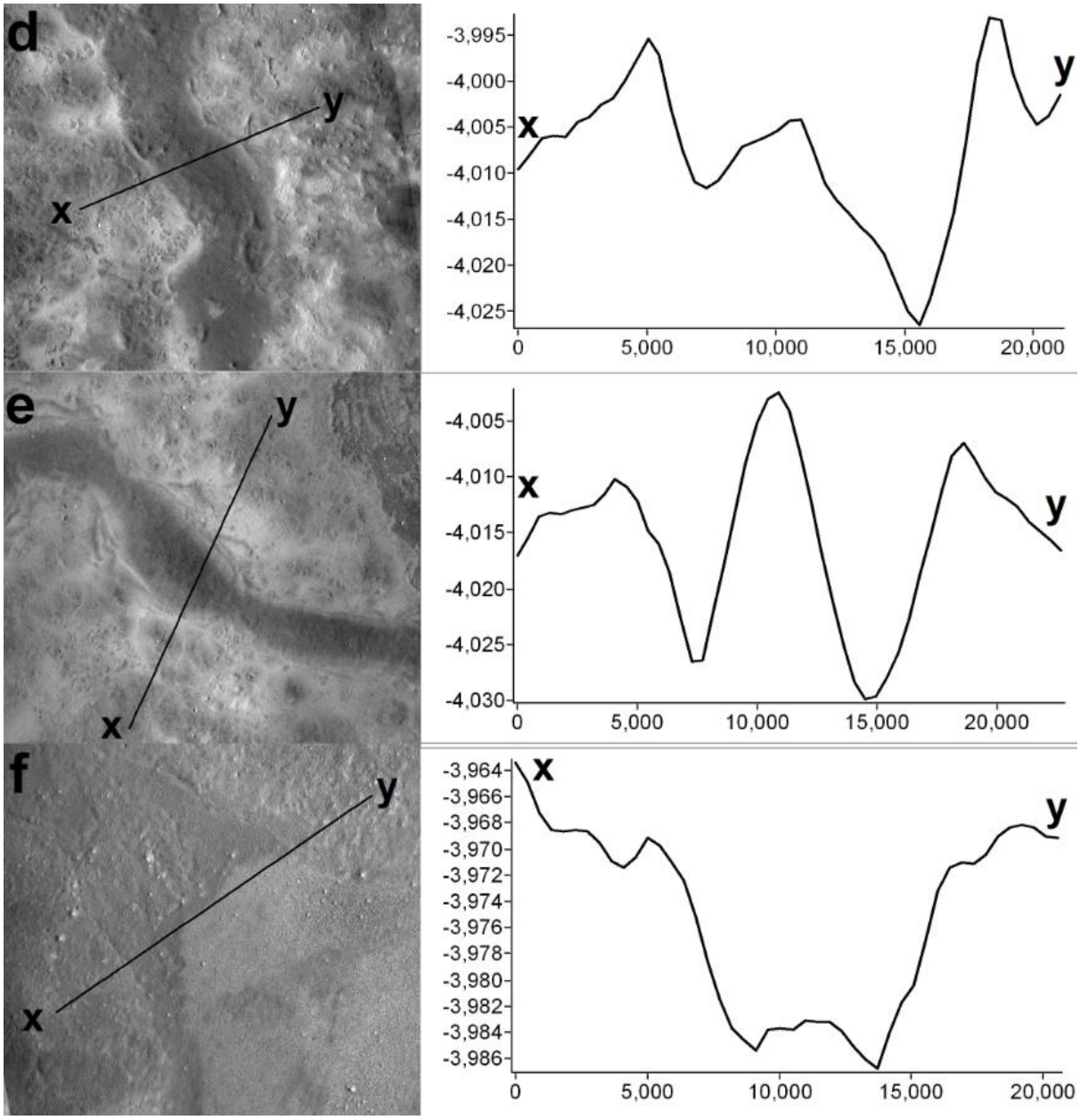

Figure 4.33 (d-f) Left – CTX images showing channels and X-Y location of cross profiles - Right. Locations of (d-f) shown in Figure 4.32a.

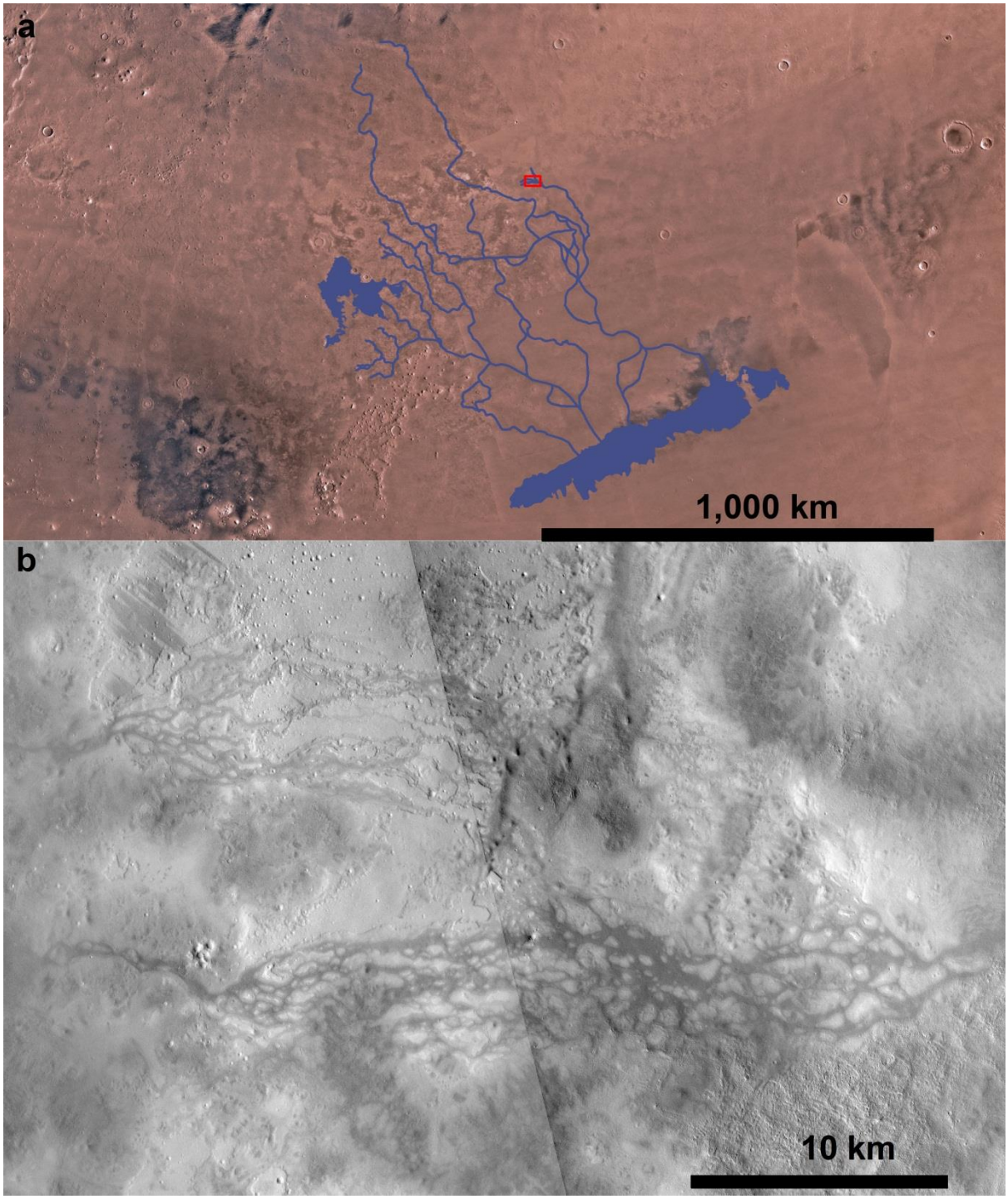

Figure 4.34 (a) Viking image, around 40° N and 170° W, showing the location of the channels in blue and (b) and red.

The channels appear to all be sourced from one dark (in visible light) patch (see Figure 4.34 and Figure 4.35). There is no obvious vent to source the fluid that formed the channels and the area is flat-lying. For the most part the channels and the source region appear to be largely infilled and

mantled, suggesting that they either predate the emplacement of the LDM or that the LDM emplacement is ongoing and thus the channels and LDM would be syngenetic.

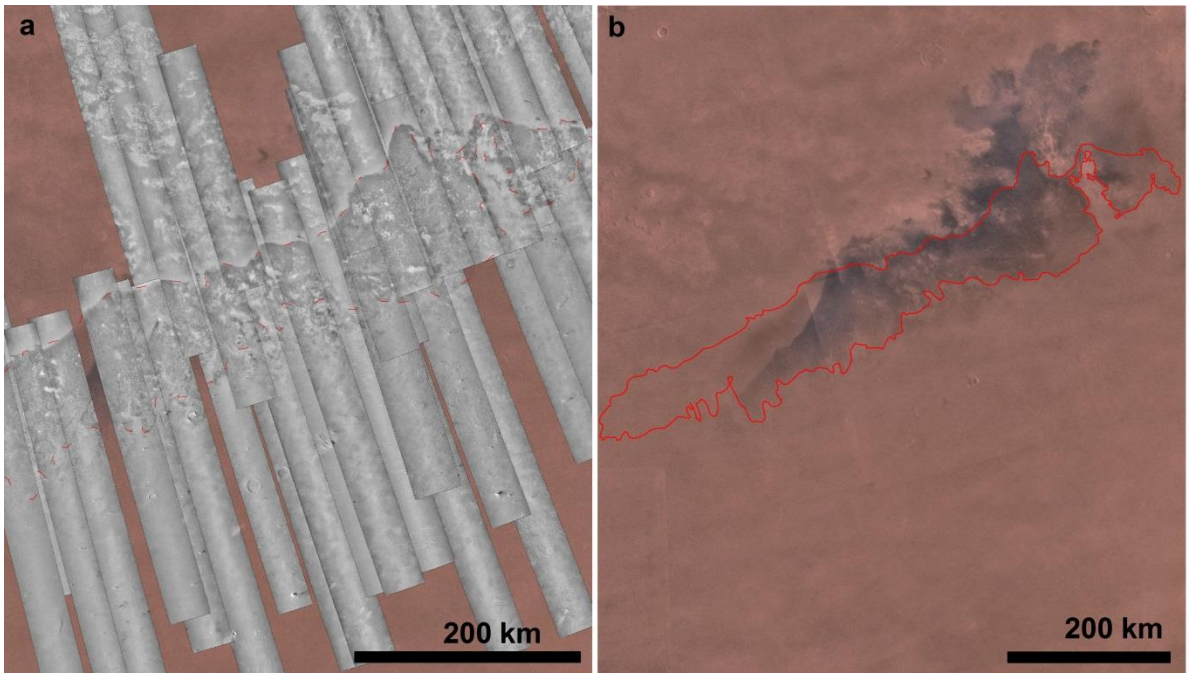

Figure 4.35 (a) CTX images showing the dark patch that the channels appear to be sourced from. (b) Viking image, around 38° N and 179° W, showing the location of the dark patch and red outline showing the location of the dark patch outlined in CTX (a).

The boundary between the dark patch and the surrounding lighter material has shifted significantly up to 200 km between the Viking era and the CTX era (see Figure 4.35). The western half of the boundary appears to have moved north whereas the eastern side of the boundary appears to have migrated south. The dark patch does not appear to be mantled whereas the lighter surrounding material appears to be mantled. This suggests that this boundary might represent a distinct edge to the mantle boundary as opposed to the gradual transition found within the grid mapping strip. Recent observations (see Figure 4.36) show similar albedo changes to the west of the grid mapping strip in the Propontis Region and successive images show that these changes occur due dust storm activity (Lee et al., 2013).

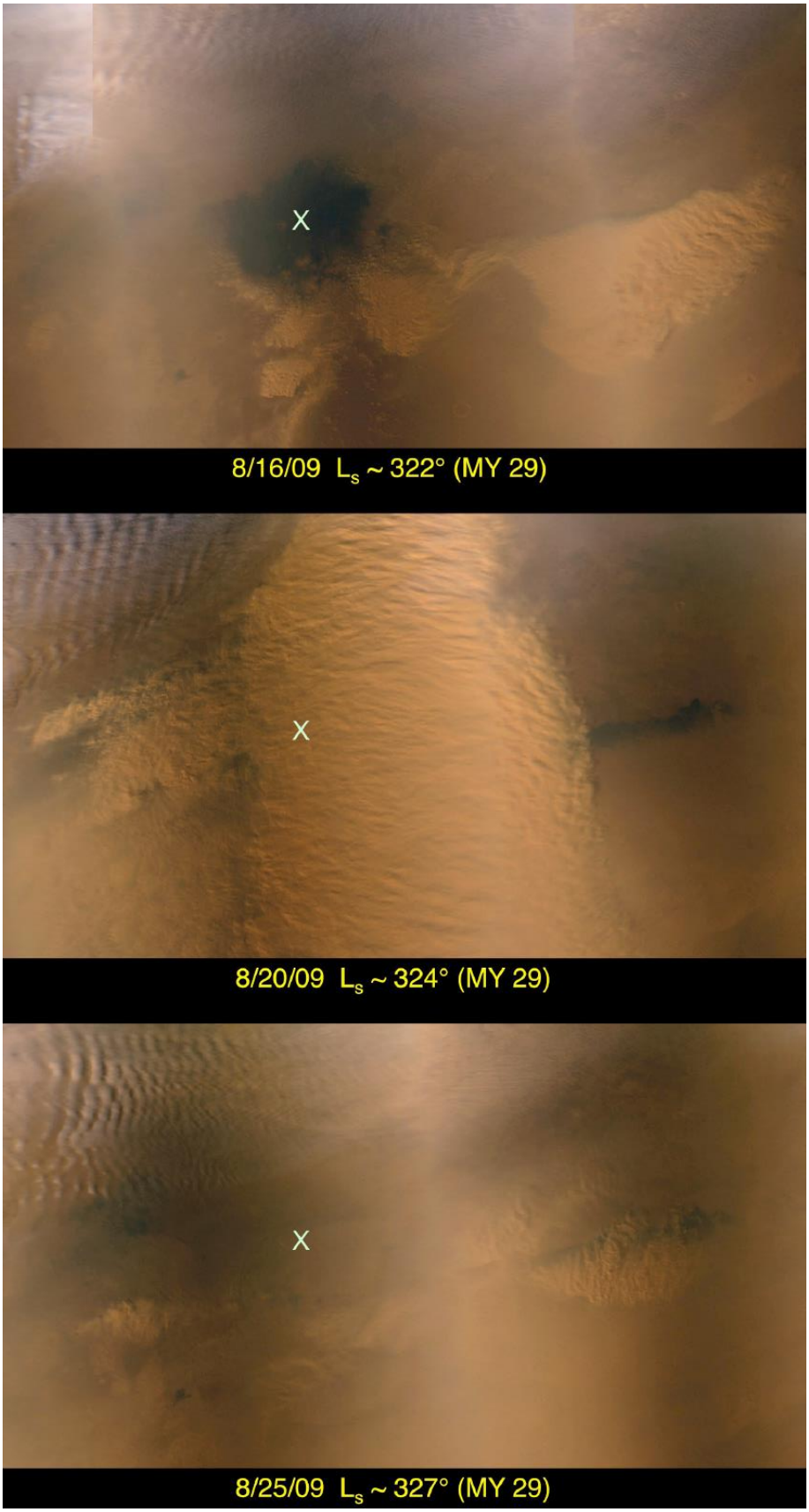

Figure 4.36 MARCI colour images showing repeated local dust storms sweeping over southern Arcadia. "X" is approximately 38°N, 179°W from Lee et al., 2013.

The channels largely thin and come to an end at a point. However, two channels terminate at a flat dark (in visible light) patch (see Figure 4.37) that is similar to the source region (assuming downhill flow). The channels, source and terminations appear bright in both day and night THEMIS images indicating they are comprised of a material with higher thermal inertia than the surrounding material. This higher thermal inertia suggests that the channels contain coarser or solidified material than the surrounding material.

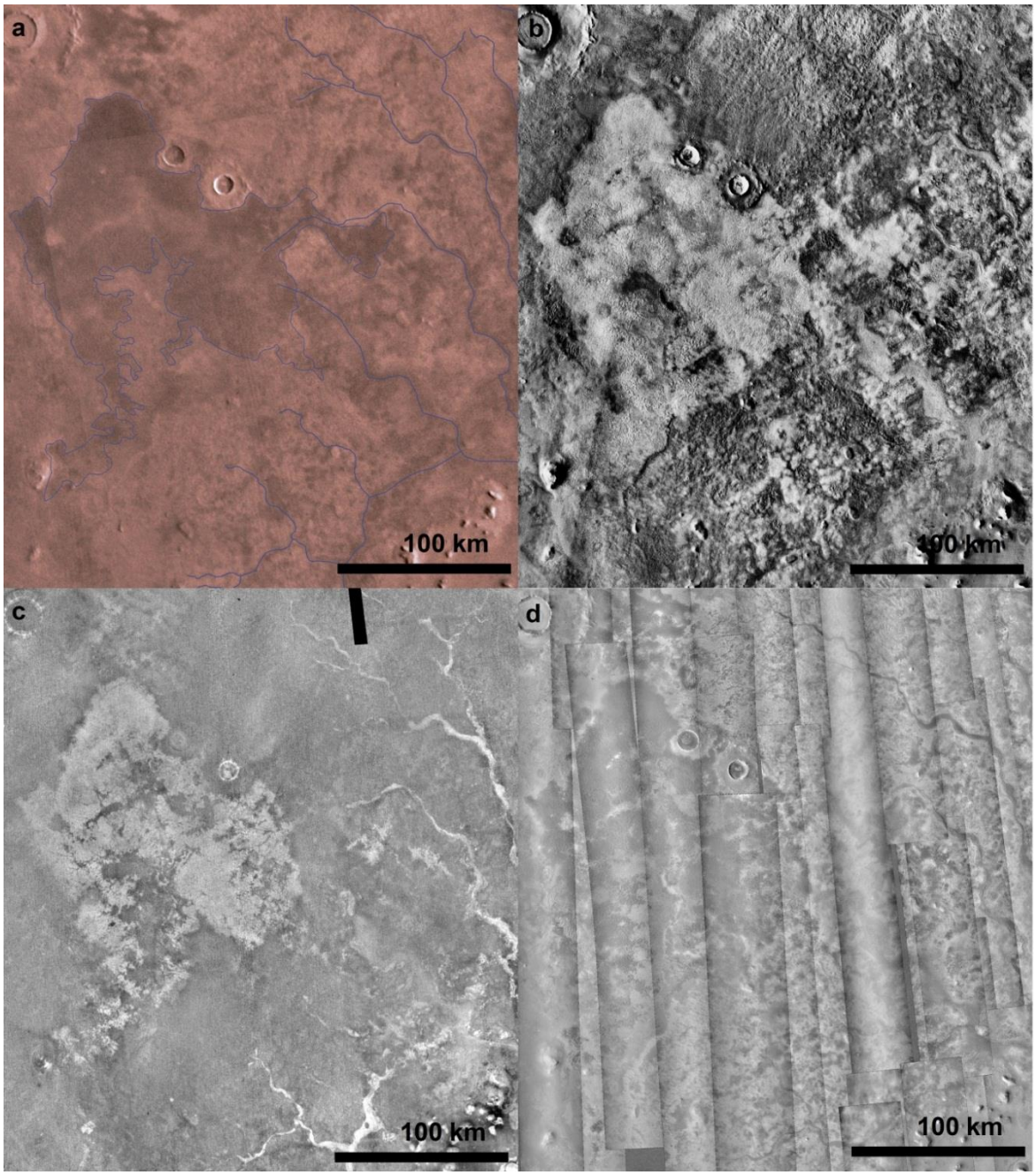

Figure 4.37 (a) Viking (b) THEMIS Day (c) THEMIS Night (d) CTX images of channels and terminations.

4.5. **Key Observations**

- In Arcadia, there is evidence for ground ice down to 35° N, and south of 35° N I see little to no evidence for ground ice processes. A transitional zone is found between 35-40° N.
- Both the mantled and textured signatures are widespread from around 35-78° N suggesting that the LDM is ubiquitous down to 35° N. Below which bedrock (platy-ridge material) dominates.
- Widespread pitting supports the idea that the LDM has at least in the past contained volatiles and has been subjected to subsequent volatile loss between 35-75° N. Scalloped pits are found between 50-55°N but are much less pervasive than in Utopia Planitia.
- VFFs are confined to areas of high relief. Large pitted mounds, gullies and GLFs are generally not found within the Arcadia mapping strip.
- Dunes dominate between 78-80° N, masking any underlying landforms indicative of ground ice, and WEH values suggest that these dunes are relatively ice-free.
- 100 m polygons can be divided into two groups in Arcadia, a northern group that are reminiscent of snow-filled, and ice-wedge polygons and likely to be a product of ground ice processes, and a southern group which appear to be more fracture related and are not likely to be a product of ground ice processes.
- Kilometre-scale polygons occur between 72-76° N and are high centred and between 1-3 km across. The polygons appear to have rounded edges and form irregular, non-geometric shapes, and appear to relate to sub-mantle geology, predating the mantle emplacement.
- The thumbprint terrain is found between 55-65°N and is comprised largely of km-scale smooth ridges and appears to be buried by the LDM in Arcadia.
- Both channels and small mounds are largely confined to the southern region of Arcadia between 35-60° N and are in areas of low relief.
- The channel system appears to be largely infilled with coarser or more solidified material and varies in cross-sectional morphology from “U” and “V” shaped to ridges with twin parallel channels.
- The channels are sourced in a dark region with boundaries that appear to shift as a result of dust storm activity.

5. **Implications of the Grid Mapping results in the context of the Northern Plains.**

In Chapter 4 I presented the full results obtained for the study in the Arcadia Planitia mapping strip. In this chapter I aim to convey what insights can be gained from comparing the grid mapping results from Arcadia with other available data. I also aim to test for latitude dependence by comparing my results in Arcadia with results gained from other ISSI team members who have mapped in Utopia and Acidalia. More specifically I aim to clarify the relationship between the LDM and landforms indicative of ground ice with respect to other geological units and direct observations of the northern plains.

5.1. **Insights from comparing the Arcadia grid mapping with other available data.**

In Arcadia, the distribution of the morphological "textured" designation matches the topographical "mantled" regions (e.g. Figure 4.7 and Figure 5.1), demonstrating that the textured surface morphology, designated from 100 m-scale observations, is essentially the morphological expression of a mantling deposit that drapes the relief. The mantled and textured signatures also continue over multiple geological and topographical boundaries (Figure 5.2). Large areas of the LDM are covered in pits (see Figure 4.10, Figure 4.11 and Figure 4.12), or depressions indicative of collapse, which has potentially occurred as a result of the removal of volatiles. This is consistent with both "textured" and "mantled" being signatures of an ice-rich, ubiquitous mantle extending in latitude from 34-78° N. The gradational boundary between textured and bedrock (see Figure 4.18) is supportive of an icy mantle that thins towards the south, possibly being removed by ablation, with more of the underlying solid rock (platy-ridge material; e.g. Plescia, 2003) becoming visible as the LDM thins out. This is consistent with the hypothesis that there is intact ground ice north of ~40° N (which potentially could be extended to ~35° N in Arcadia) and an absence of ground-ice related features south of ~35° N, with potential relict ground ice-related features being found in the transition zone 30-40° N. This hypothesis is also supported by the LDM metre-scale polygons observed in HiRISE images (see Figure 4.8). These

polygons are remarkably similar to thermal contraction cracks and ice-wedge polygons (Earth; e.g Lachenbruch, 1962; Mars; e.g. Levy et al., 2009; Mangold et al., 2004; Mellon, 1997) found in permafrost on Earth (see Figure 5.3).

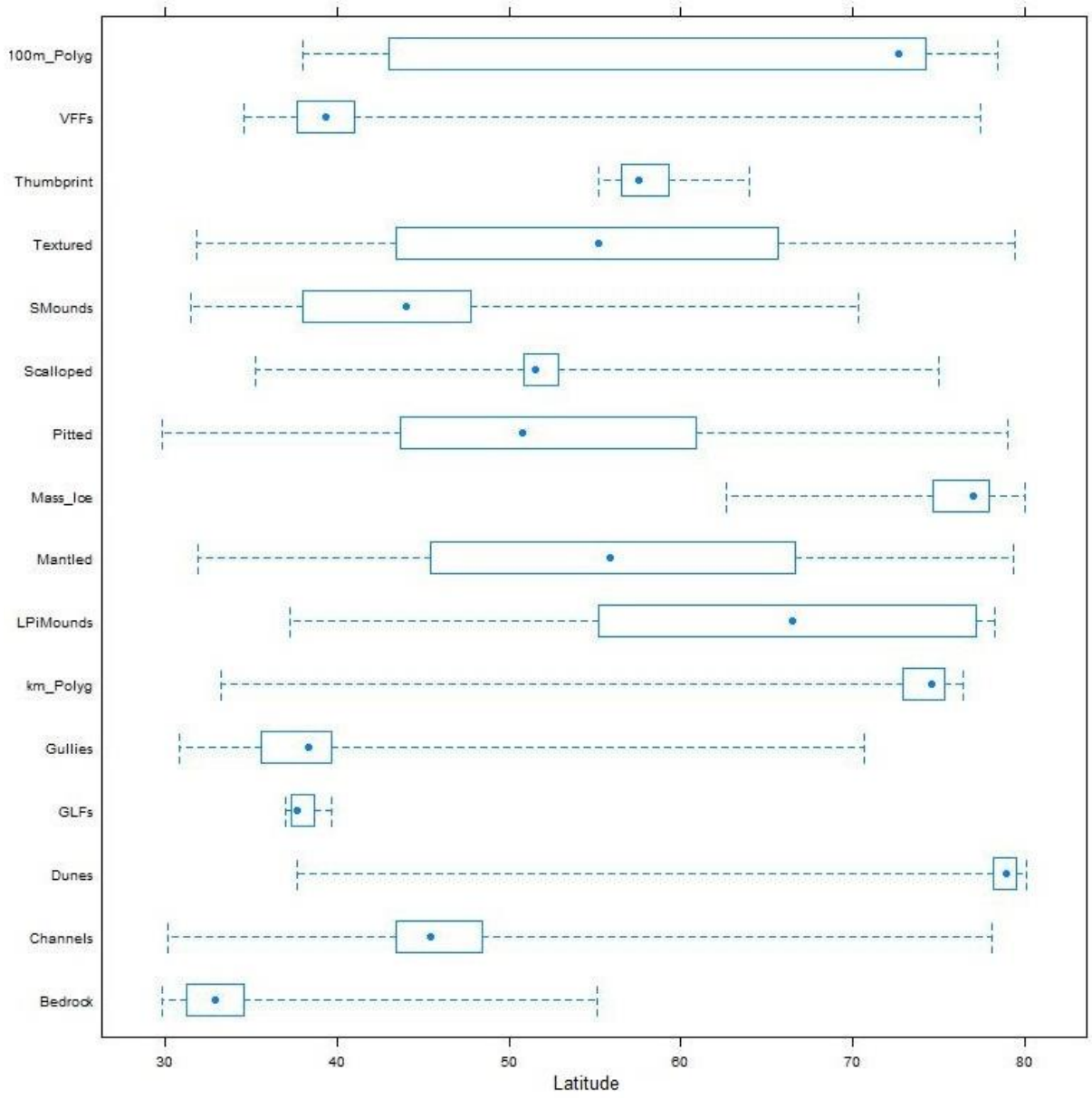

Figure 5.1 Boxplot of the distribution of landforms by latitude in Arcadia. Dots show median, boxes show interquartile range, whiskers mark extremes.

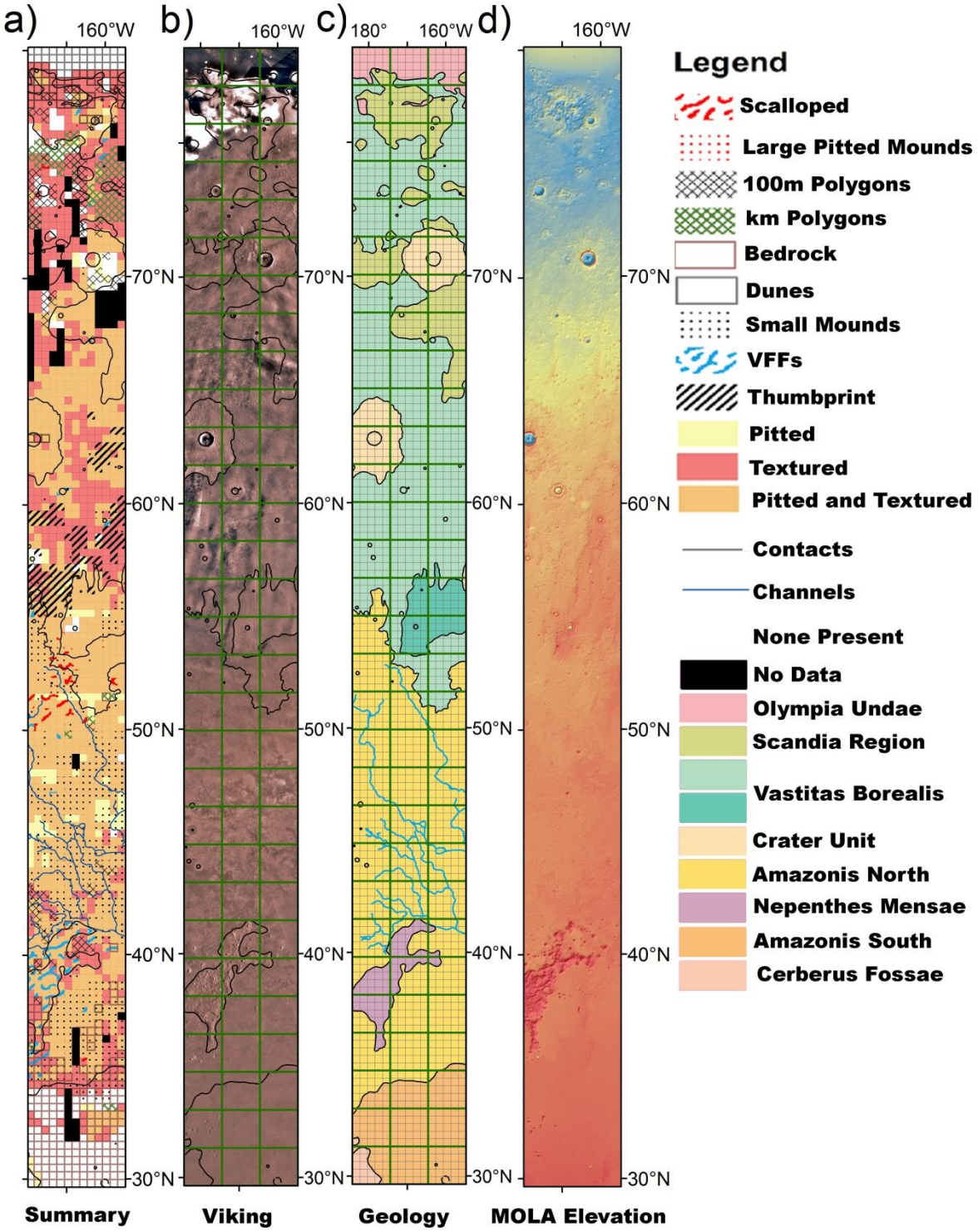

Figure 5.2 (a) Composite map showing the grid mapping results from Arcadia.(b) Viking image of the Arcadia grid mapping strip. (c) Adapted Tanaka et al., (2005) geological map of the Arcadia grid mapping strip. (b) MOLA topography of the Arcadia grid mapping strip ranging from ~-3000 m (red) to ~-6000 m (blue).

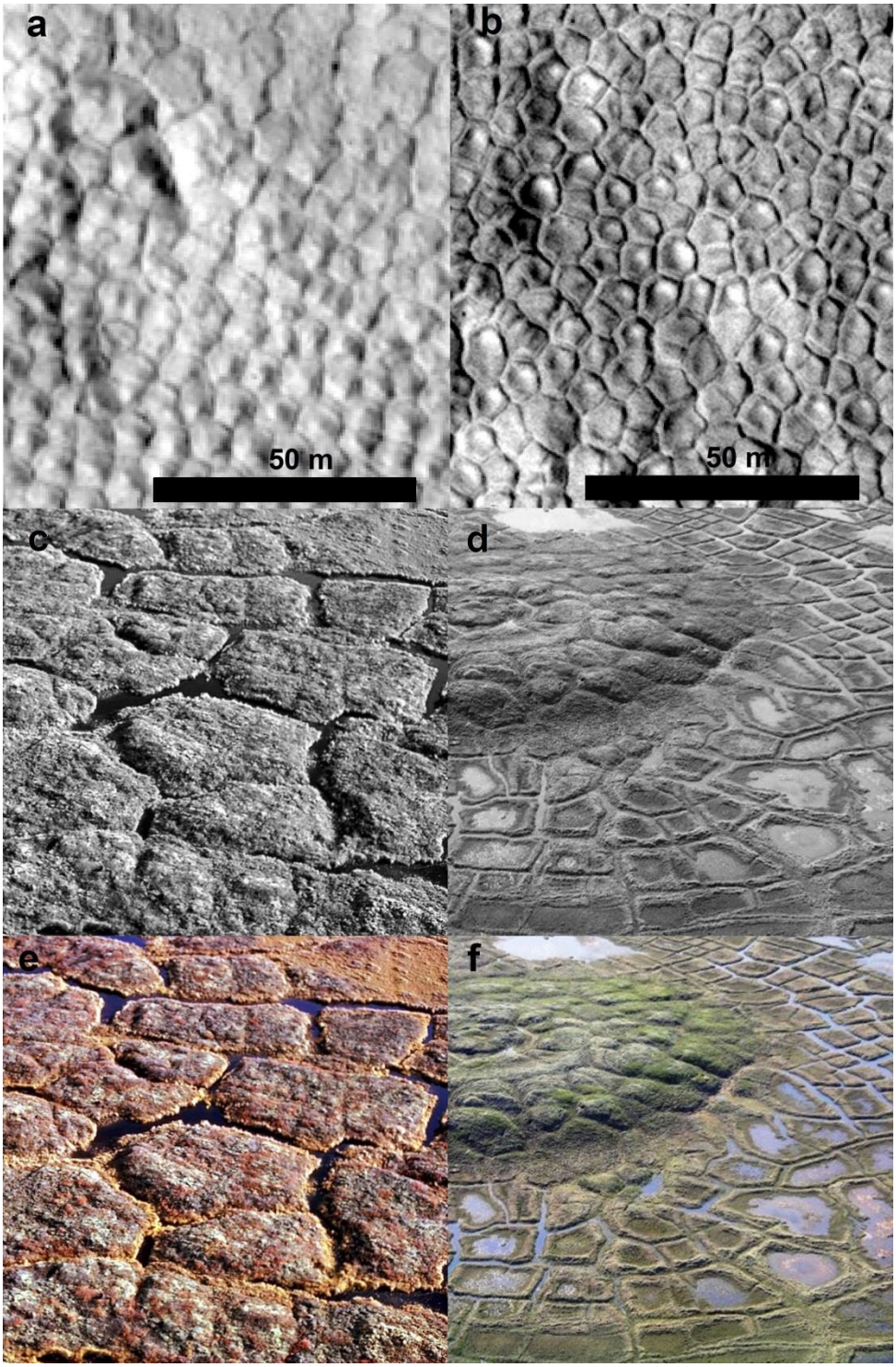

Figure 5.3 (a) HiRISE image ESP_036350_2280 metre-scale high-centred polygons. From Figure 4.8g (b) HiRISE image ESP_016940_2300 of metre-scale polygons with low centres, high margins and inter-polygon troughs. From Figure 4.8f (c-d) Desaturated images of ice-wedge polygons, that are metres to tens of metres across in Canada. (c) From http://sis.agr.gc.ca/cansis/images/nt/peri/index.html. (d) From

https://en.wikipedia.org/wiki/File:Melting_pingo_wedge_ice.jpg. (e-f) Original photographs of (c-d).

Given that ice is generally unstable at the martian surface (see Figure 5.4; e.g. Chamberlain and Boynton, 2007; Read and Lewis, 2004), it is expected (Costard and Kargel, 1995; Lefort et al., 2009; Morgenstern et al., 2007; Zanetti et al., 2010) that depressions would form in the LDM as a result of collapse due to the loss of volatiles to the atmosphere through ablation. The grid mapping shows large expanses of pitted terrain (see Figure 4.5) and scalloped terrain (see Figure 4.19) is formed into the LDM, as can be easily seen in CTX images (Figure 4.11). These observations support the idea that the LDM has at least in the past contained volatiles and has been subjected to subsequent volatile loss between 35-75° N. Between 70-75° N, pitting appears to be much less consistent and pervasive (see Figure 4.5). This could be as a result of decreased insolation and temperatures and a resulting increase in ice stability at the surface. This hypothesis is further supported by the smoother, less textured appearance of the mantle at these high latitudes (see Figure 4.6) which is consistent with the persistent stability of ground ice at high latitudes even under higher obliquities (see Figure 5.5).

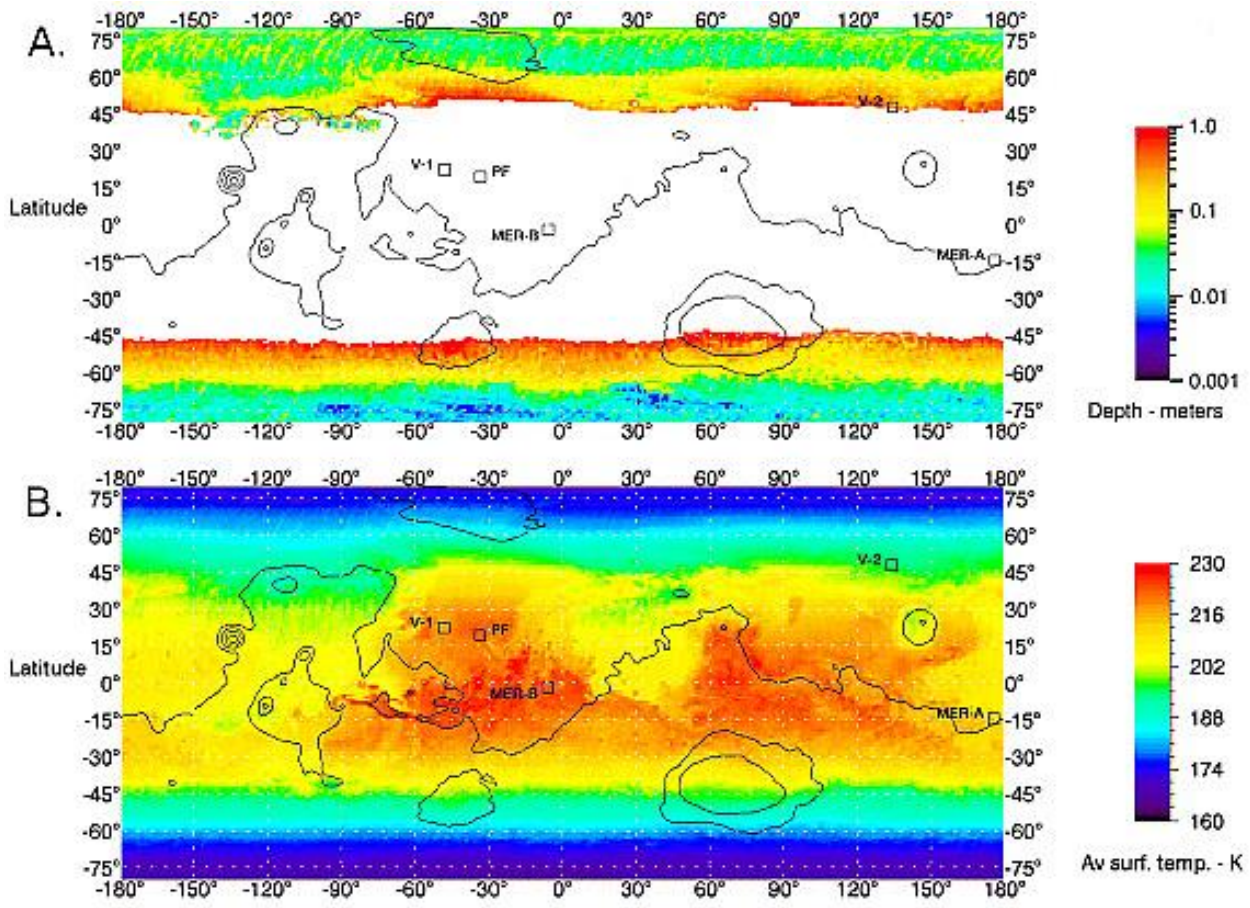

Figure 5.4 From Chamberlain and Boynton (2007) thermal model results for the present epoch. (a) The depth to stable ground ice. . (b) The average surface temperature. 5-km-elevation contours and lander sites shown for orientation.

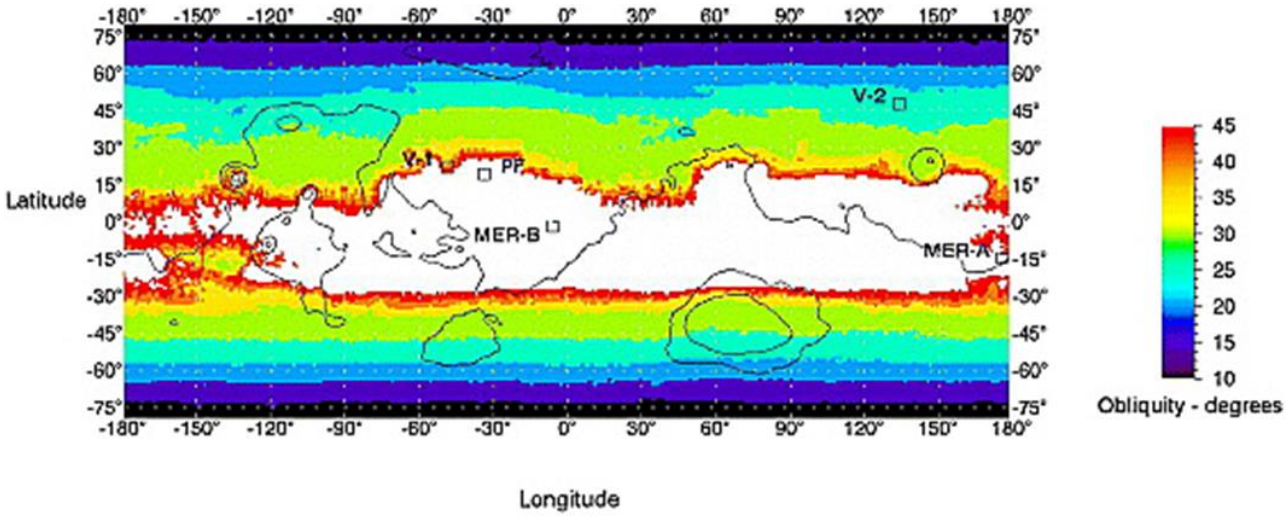

Figure 5.5 From Chamberlain and Boynton (2007): distribution of ground ice for different obliquities with zero eccentricity.

As the source of the ice and material that forms the LDM is believed to be airfall (e.g. Kreslavsky and Head, 2002) it is reasonable to assume for the most part the sediment-part of the LDM is fine enough for aeolian transportation and suspension. This would suggest that variations in the size and composition of lag deposits are less likely to be responsible for the different pit morphologies. On the other hand, the area immediately south of the scalloped terrain in Arcadia is heavily channelized, and contains few scalloped terrains, yet is at the same latitude as scalloped terrain in Utopia. These channels are not apparent in Utopia and Acidalia, so it is possible that these channels represent a source of sediment that would be harder to remove through aeolian activity and could provide a thicker lag that might curb scalloped-pit formation. If it is indeed the presence of a lag deposit that has prevented scalloped pit formation, this suggests that significantly more ice could still be present at this latitude in Arcadia than in Utopia.

Comparisons (e.g. Figure 5.6) between my grid mapping results and recent gamma-ray spectroscopy (GRS) studies showing water-equivalent hydrogen by measuring neutron return from the surface of Mars (Wilson, 2016), further suggest the idea that more volatiles exist in the northern extents of the Arcadia strip than in Utopia and Acidalia. However, the GRS also shows water ice to be detected at a low level over the vast majority of the Arcadia strip, supporting the hypothesis of a ubiquitous ice-rich mantle (Boynton et al., 2002; Feldman et al., 2002; Wilson, 2016). The return of non-zero values over almost the entire length of the strip, but with an obvious gradient of more water/ice in the north, and less water/ice in the south, together with widespread pit development, is supportive of the hypothesis that there has been widespread loss of ground ice in the northern plains, with intensity being dependent on latitude. Alternatively, as GRS is only sensitive to the top 50 centimetre to 1 metre (Wilson, 2016), the gradient could also be explained by progressively thicker lag deposits from north to south. The low WEH values at the very north of strip are expected, as the dunes are likely to mask any underlying ground ice and their surfaces are relatively ice-free. Given that the WEH shows a gentle gradient from

north to south it is difficult to say whether any landforms occur only within a specific WEH band from this strip alone. However, this is something I test further using the addition of Utopia and Acidalia data in section 5.2.

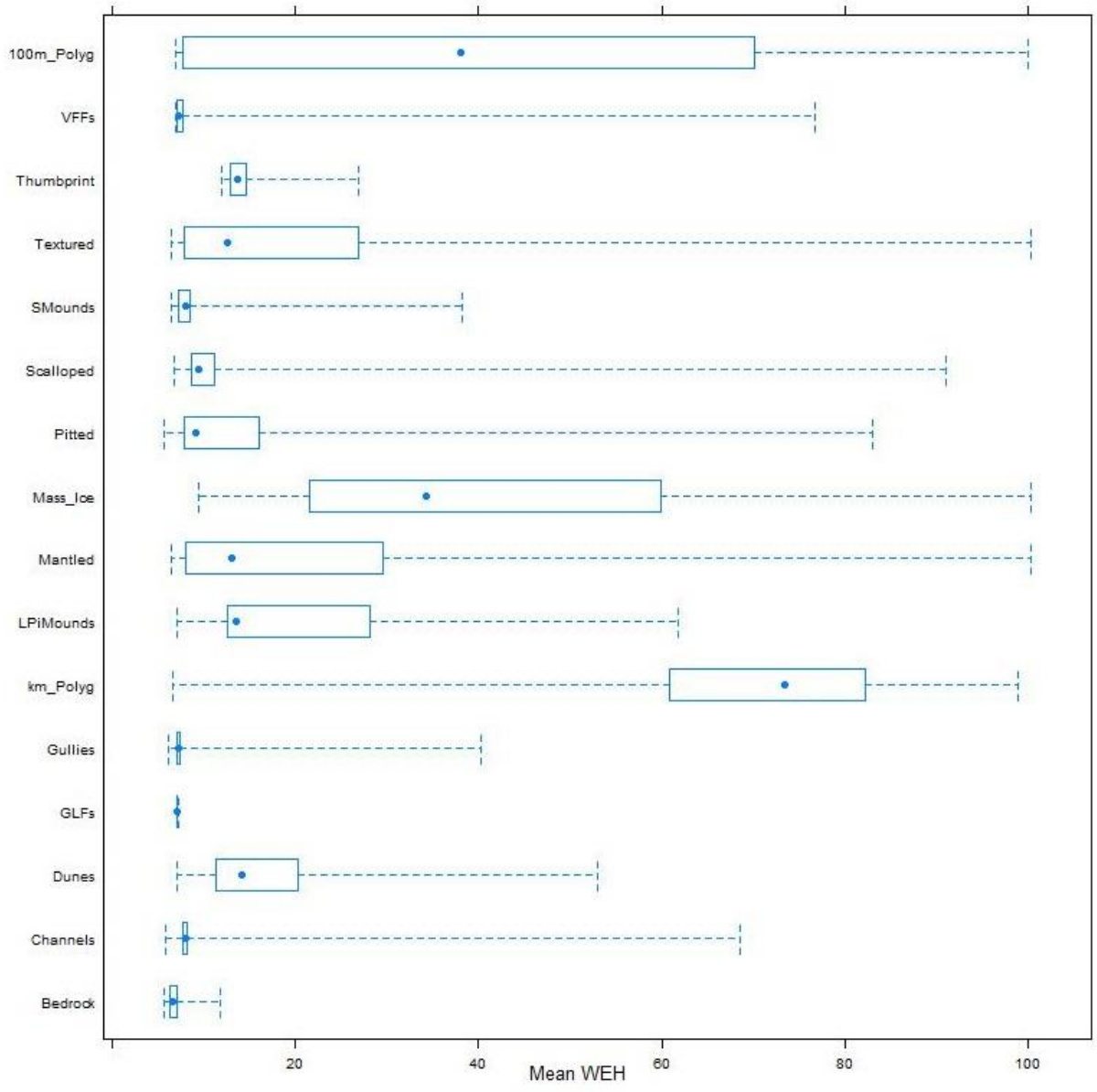

Figure 5.6 Mean WEH from Wilson (2016) by landform. The WEH values are given as percentage of water/ice content in the first 50 cm to 1 m from the surface. WEH is calculated from gamma ray spectroscopy looking at changes in the neutron flux signature returning from the martian surface as each element has a different signature. Dots show median, boxes show interquartile range, whiskers mark extremes.

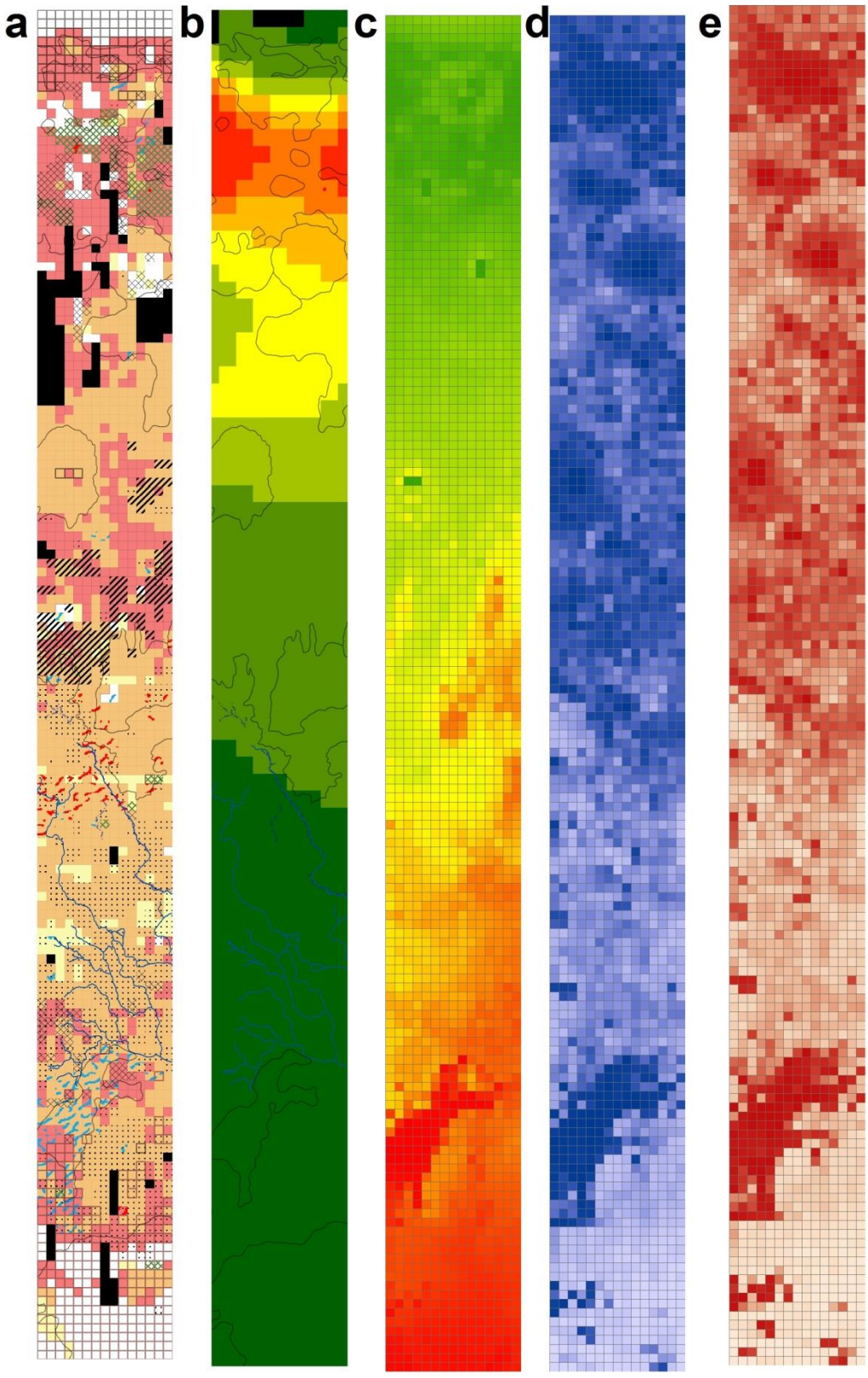

Figure 5.7 (a) Composite map showing the grid mapping results from Arcadia. Key in Figure 5.2. (b) Water Equivalent Hydrogen (WEH)data from (Wilson, 2016). (c) MOLA mean elevation ranging from ~-3000 m (red) to ~-6000 m (green). (d) MOLA mean slope

ranging from ~0.05° (white) to ~17° (blue). (e) MOLA surface area, as an approximation for roughness per grid square (Red is high roughness, white is low).

Figure 5.6 shows that kilometre-scale polygons correlate with the highest WEH values. While this could indicate that they formed by ground ice related processes, they seem to be covered by a significant and largely intact mantle that could be responsible for the high WEH values. At first glance, it may appear counter-intuitive that massive ice does not have the highest WEH values but this is likely due to proximity with the dune fields, which appear to be largely ice-free; many of the cells that contain massive ice also contain dune fields, moderating the WEH values. That the mantling signature shows slightly higher WEH values than the textured signature could indicate that some areas of LDM remain intact with less ablation, resulting in lower WEH values. This is supported by observations of a smoother, more intact mantle in the northern extent of the strip (see Figure 4.6).

For elevation, slope and surface area (as a first approximation of roughness) I have taken the mean values for each grid square to be compared against the landform grid mapping. The topography grades gently from ~ -3000 m in the south to ~ -6000 m in the north (see Figure 5.7c). Similarly to WEH, this makes it difficult to determine whether landforms are topography-dependent based on one thin strip, and will be discussed in more detail with the context of Acidalia and Utopia in Chapter 5.2. As expected, though, viscous flow features are concentrated in areas with higher relief, as they occur on or near steep slopes (see Figure 5.7). There is a significant change in both average slope and "roughness" at the north-south landform type boundary marked by the thumbprint terrain, suggesting that the thumbprint terrain might be either a topographic boundary physically dividing different processes or is a transitional landform.

The channels and small mounds appear to be confined to a much flatter and less varied surface than the landforms found to the north (see Figure 5.7). From the grid mapping alone, the causal relationship is not clear, but it could be that either (i) the processes that

formed the channels and small mound assemblages infilled, or planed the topography, removing relief, (ii) that the processes that form the landforms are slope dependent, or (iii) that these processes themselves create slopes and increase surface roughness. The channels and small mounds fall largely within the geological units Amazonis Planitia North and South. The traditional interpretation (e.g. Tanaka et al., 2005) for the Amazonis Planitia units is of voluminous lava and volcaniclastic flows, suggesting that the infilling of topography is the most likely explanation for the low roughness and slope values in the southern extent of the strip. As to whether the channels could be a source for liquid water into Arcadia Planitia, or if they are a product of volcanic/ground ice interactions, this will be a topic of discussion in Chapter 7.

Figure 5.8 displays the mean elevation for each landform type. Some landforms appear to be confined to tight elevation constraints (e.g. thumbprint terrain from -4300 to -4000). However, given that these landforms also occur within a tight latitude band, and are clustered in one location, it is difficult to determine if they are controlled by topography, latitude or neither of these. Landforms found in the south of Arcadia are naturally at a higher elevation than those found in the north, given the topographic gradient over the basin. Comparing where these landforms occur over all three strips in the northern plains will help to determine which landforms, if any, are constrained by latitude, as shown in section 5.2.

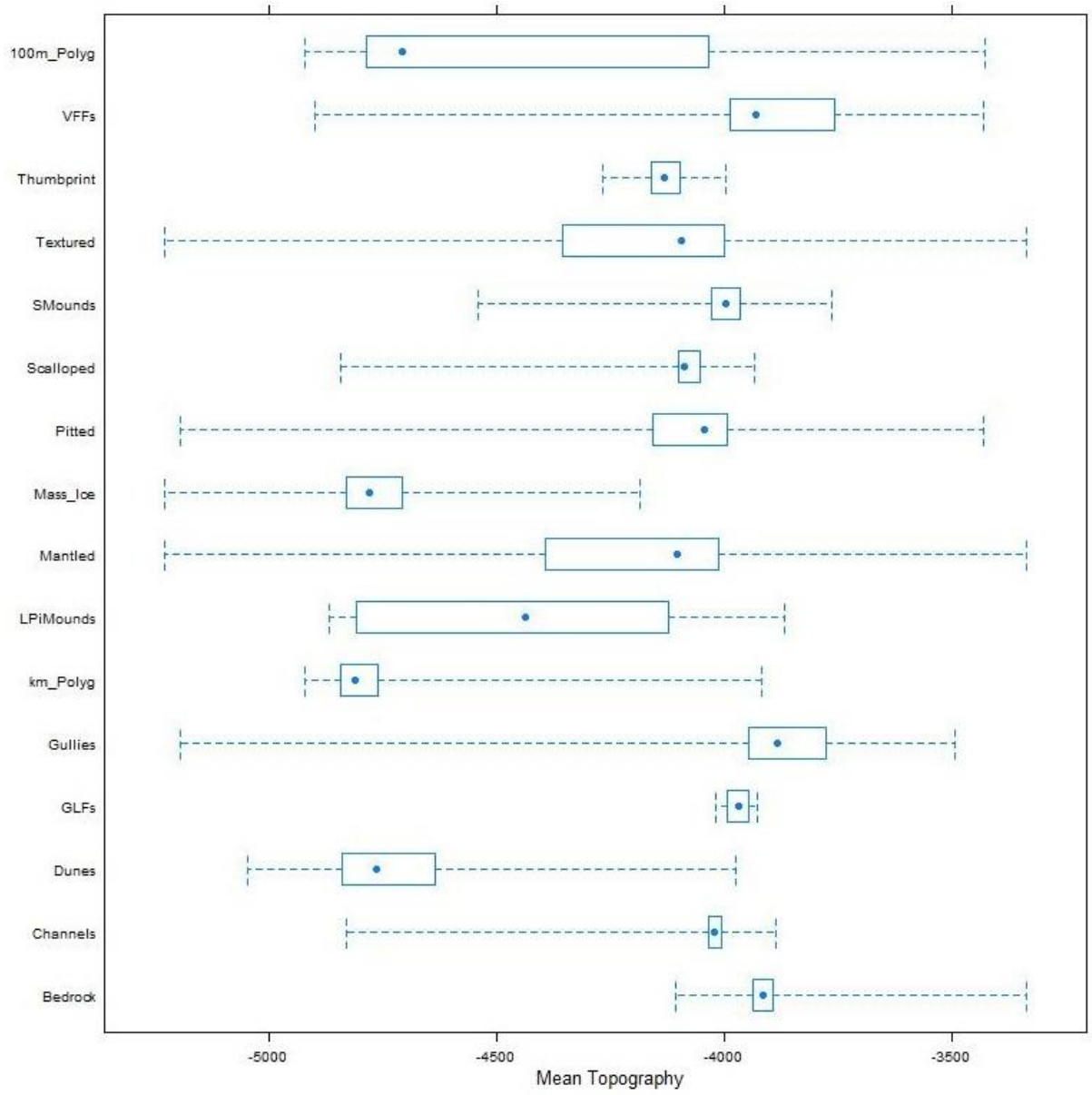

Figure 5.8 Mean topography by landform. Dots show median, boxes show interquartile range, whiskers mark extremes.

Figure 5.9 shows the mean slope for each landform. As would be expected, VFFs and putative GLFs and gullies occur in areas of higher mean average slopes. Massive ice also occurs in areas of higher mean slopes, but this is likely due to the massive ice creating higher slope values as it occurs as outlying mesas of polar cap deposits on the plains, with high slope values at its edges. Thumbprint terrain displays higher than usual minimum mean slope values: this is likely due to the thumbprint terrain itself altering the topography. These observations are consistent with the kilometre scale surface roughness values

observed in Figure 5.10, with the same landforms that occur in areas of high slopes occurring in areas with high roughness values. This suggests the areas with high slope values are areas with topography that undulates on the hundreds of metre to kilometre scale rather than one steep, consistent slope.

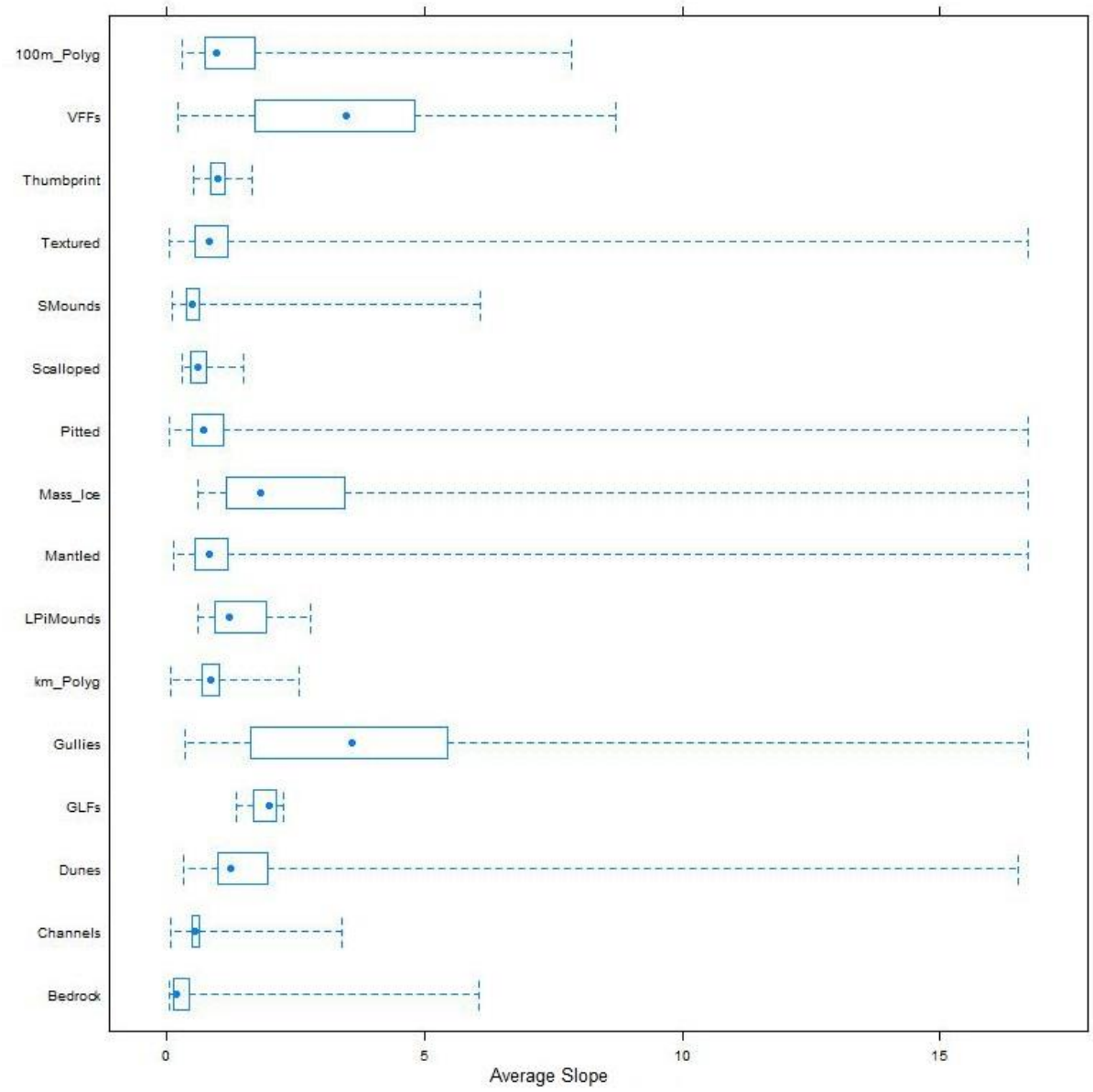

Figure 5.9 Mean slope by landform. Dots show median, boxes show interquartile range, whiskers mark extremes.

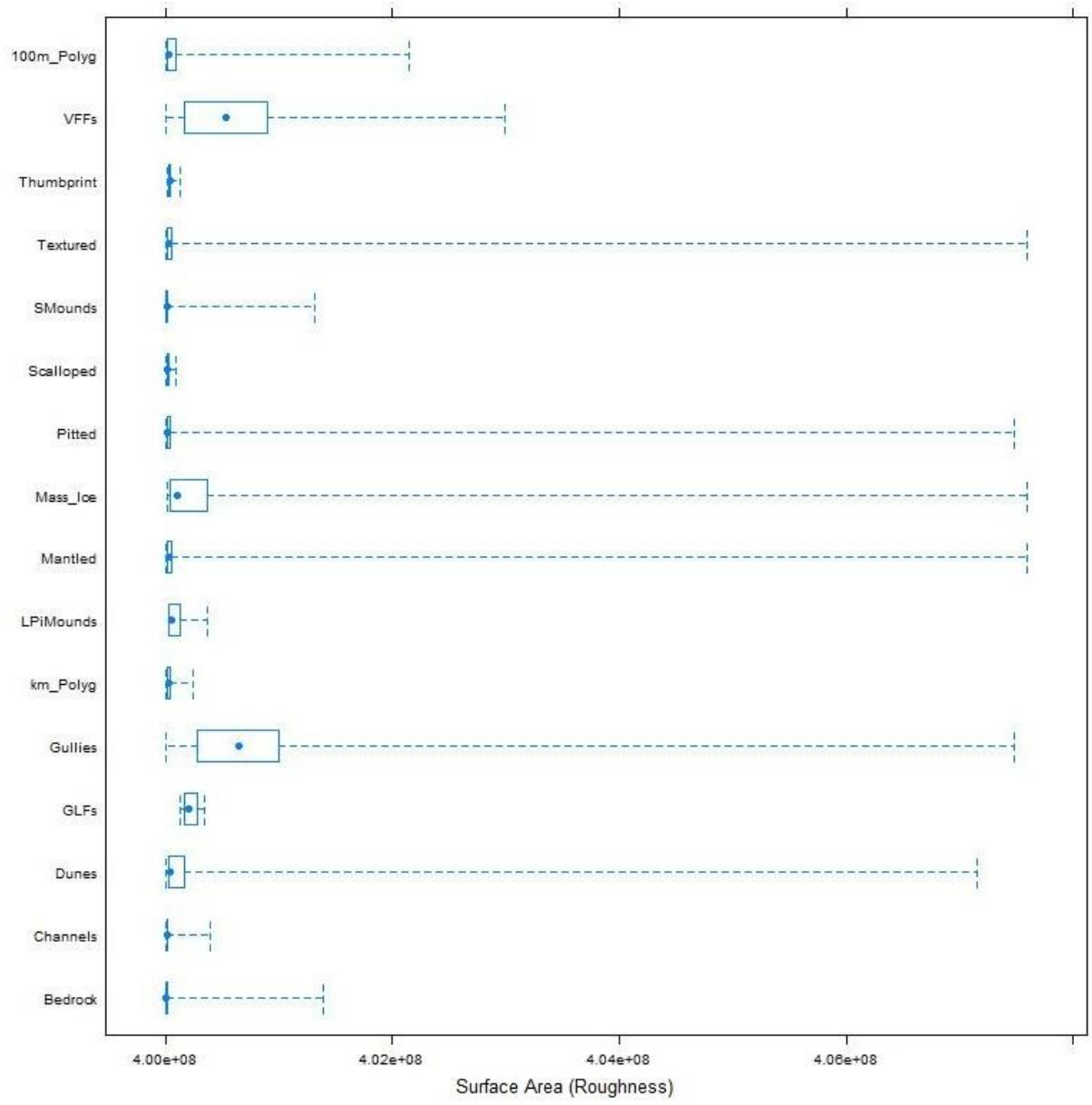

Figure 5.10 Surface area as a measure of roughness by landform. Dots show median, boxes show interquartile range, whiskers mark extremes.

5.2. **Insights to be gained from comparing results from grid mapping in Arcadia, Acidalia and Utopia and previous observations.**

The data from the three regions can be displayed collectively through box and whisker plots and composite maps (e.g. Figure 5.11 and Figure 5.12) which nicely summarise the data. However, this does not allow for easy comparisons between single landforms. Thus, as I did in Chapter 4, I will display each landform individually as I discuss them.

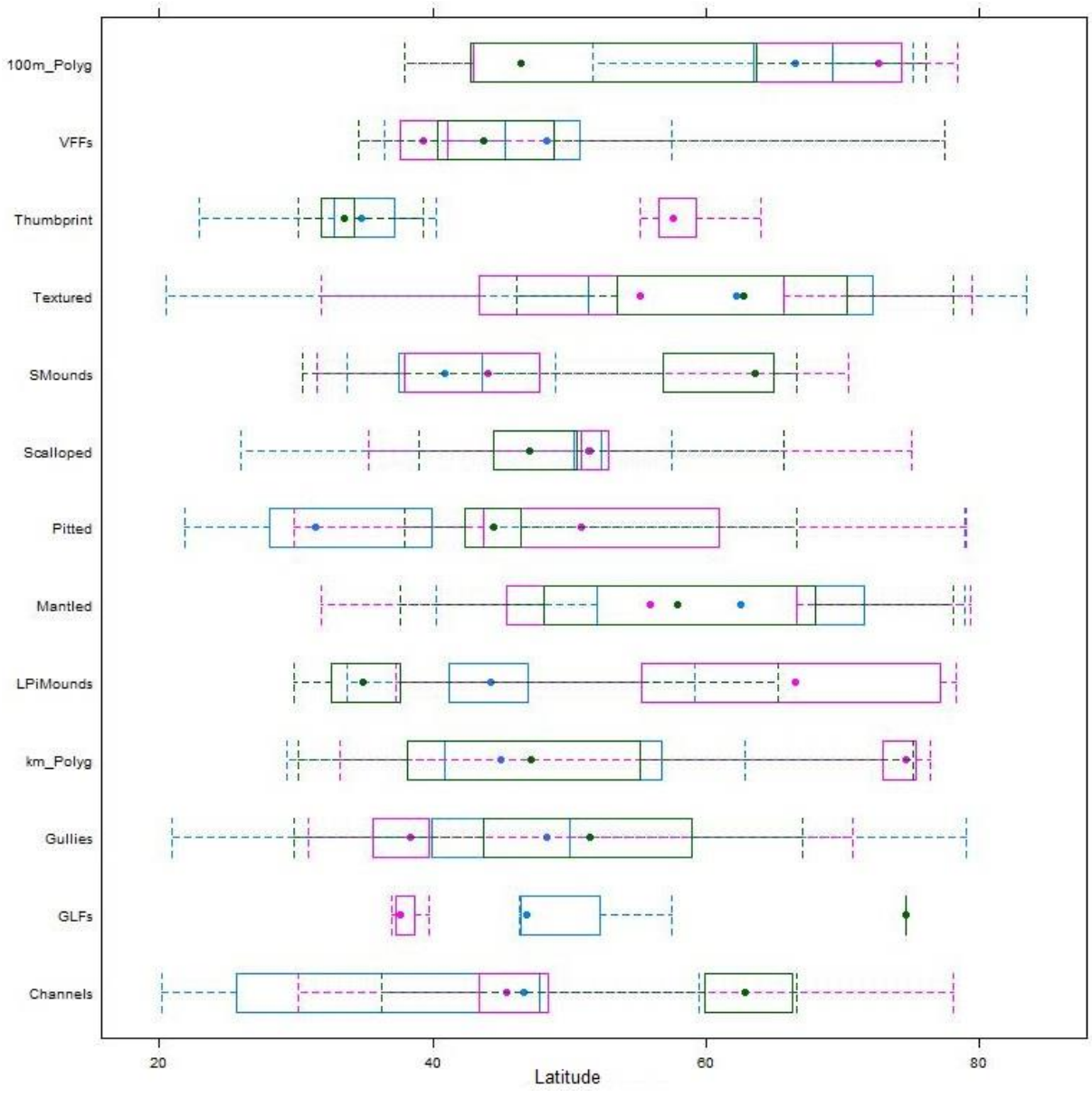

Figure 5.11 Latitude by landform. Dots show median, boxes show interquartile range, whiskers mark extremes. Pink – Arcadia, Green – Utopia, and Blue – Acidalia.

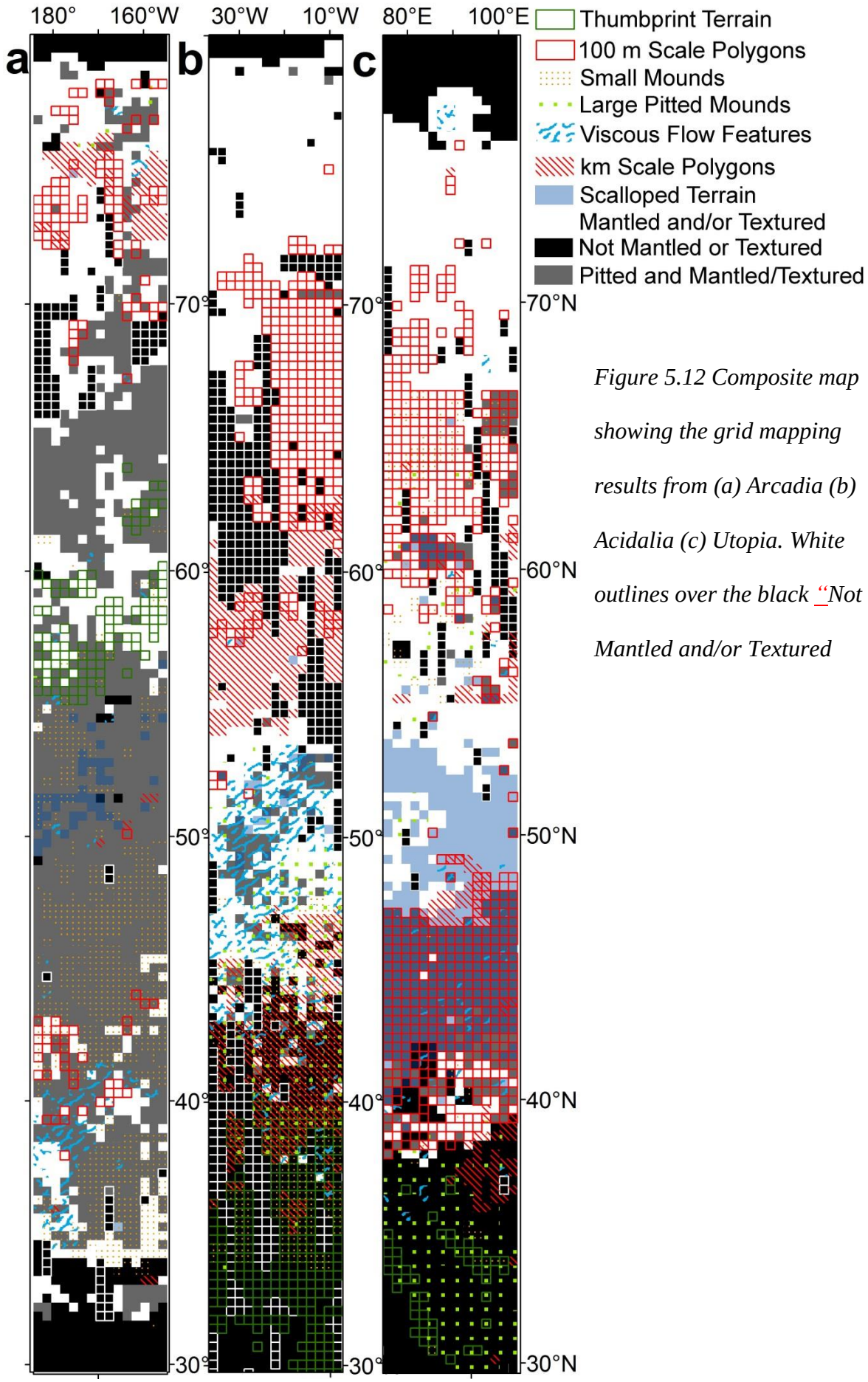

Figure 5.12 Composite map showing the grid mapping results from (a) Arcadia (b) Acidalia (c) Utopia. White outlines over the black "Not Mantled and/or Textured

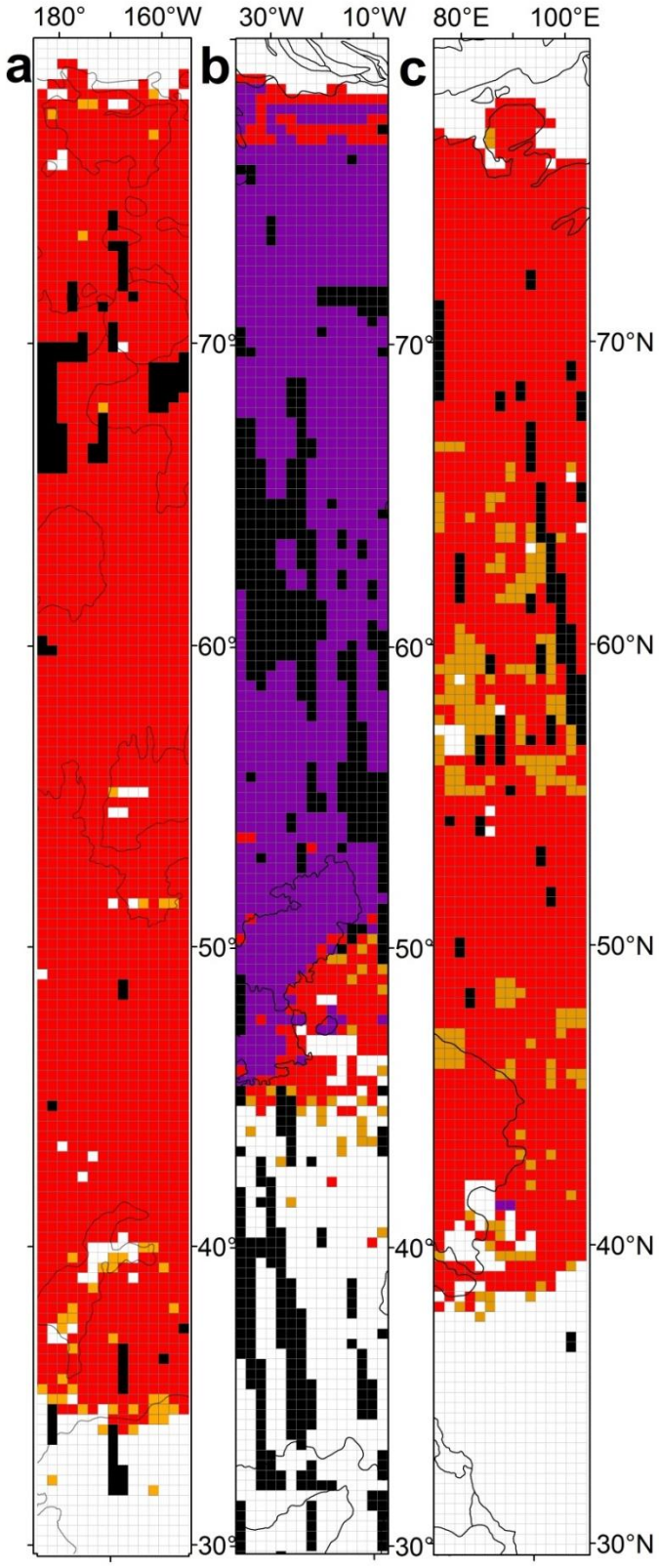

Figure 5.13 Mantled terrain from (a) Arcadia, (b) Acidalia and (c) Utopia. The group in Acidalia chose to distinguish between where the mantled terrain was present (red) and dominating (purple), orange is possible, black no data and white absent.

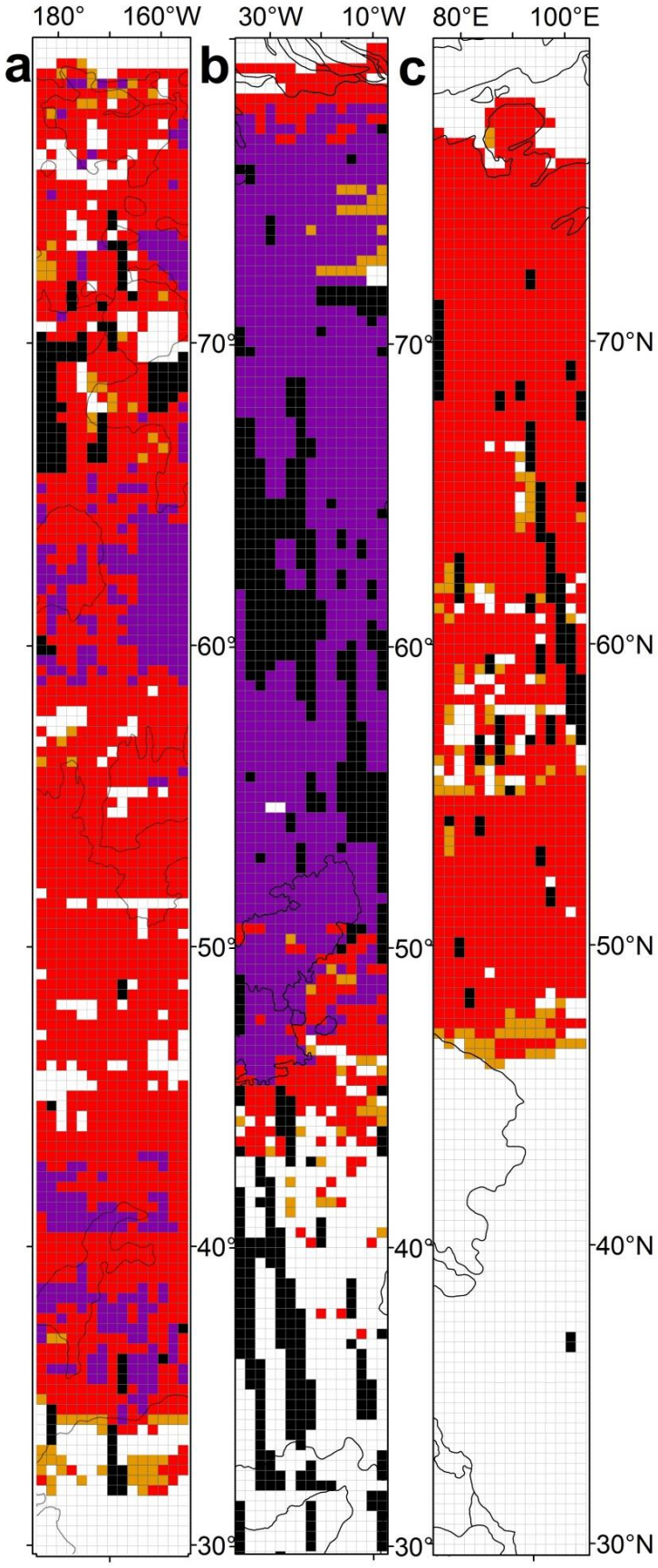

Figure 5.14 Textured terrain from (a) Arcadia, (b) Acidalia and (c) Utopia. Red is present, purple dominating, orange possible, black no data and white not present.

The mantled terrain is ubiquitous wherever CTX is available in the three regions from 78° N to around 35-45° N (see Figure 5.11 and Figure 5.13). The mantled terrain extends farthest south in Arcadia at around 35° N; 38° N in Utopia and 45° N in Acidalia (see Figure 5.11 and Figure 5.13). The biggest difference between the three strips shown in Figure 5.13 is that the mapping group in Acidalia chose to distinguish between where the mantle was present, and where it was dominating, whereas the Utopia and Arcadia groups grouped those responses as simply "present". The textured terrain in Arcadia and Acidalia overlaps with that of the mantled terrain almost entirely (see Figure 5.11, and Figure 5.13 and Figure 5.14). In Utopia, however, the textured terrain stops at around 45° N whereas the mantled terrain continues down to 38° N. The mapping group in Acidalia also found the textured terrain to be "dominating" more grid squares than in the other two areas. That the mantled and textured terrain extends further south in Arcadia matches well with what is predicted by climatic modelling (e.g. Chamberlain and Boynton, 2007). With the extent of the mantled (see Figure 5.13) and textured (see Figure 5.14) terrains correlating with predictions for the stability for ground ice at obliquities close to present (25°) conditions (see Figure 5.15), there is strong evidence for climate-dependent control of ground ice. While there do seem to be strong latitude controls over the presence of mantled and textured terrain, the consistent differences between the three areas are highly suggestive of some regional controlling factors. The prediction of stable ground ice at even lower obliquities for the northern extent of the three strips is consistent with the observations that the mantling deposits appear thicker, and there is more smoothing of topography, farther north in the strip. North of 50° N, climate models (e.g. Chamberlain and Boynton, 2007) predict that this ice could be found under stable conditions within one metre of the surface, but at lower latitudes the ice would be expected to be unstable (see Figure 5.16). However, it is important to note that, for almost the entirety of the three strips, ground ice is not expected to be stable within the uppermost few centimetres and therefore we might expect to see degradation of ice-related landforms, and this correlates

well with the presence of textured and pitted terrains being widespread, but particularly dominating, within mid- and lower latitudes.

The hypothesis that the observations of the mantle and textured terrains extending further south in Arcadia are evidence of ground ice extending further south in Arcadia is supported by WEH observations that show consistently higher WEH values in Arcadia than at the same latitudes in Utopia and Acidalia (see Figure 5.17). The main exception to this are at the very north of Arcadia where the area is dominated by dunefields overlying ground ice deposits, masking the WEH observations of the underlying ice-rich material. This indicates that the dunes have formed after or have been resurfaced since the ground ice was deposited into the regolith. The mantled and textured terrains show similar ranges in WEH values across the three strips (see Figure 5.18). This correlation between mantle and textured terrains and the climatic modelling and WEH values is consistent with a latitude-dependent mantle being comprised of both sediment and ground ice and having a climatically-controlled origin.

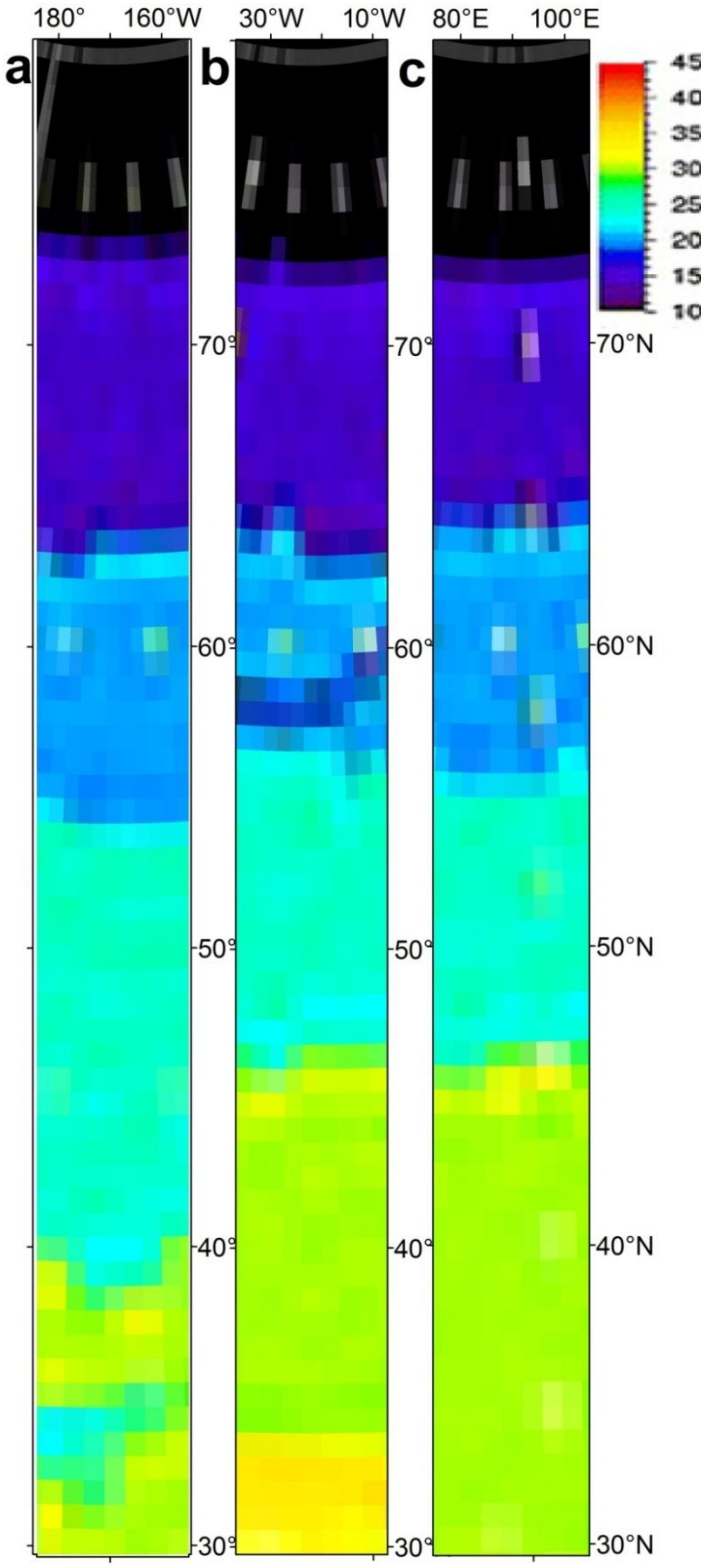

Figure 5.15 Data from Chamberlain and Boynton (2007) distribution of ground ice for different obliquities (°) with zero eccentricity plotted in ArcGIS for (a) Arcadia, (b) Acidalia and (c) Utopia.

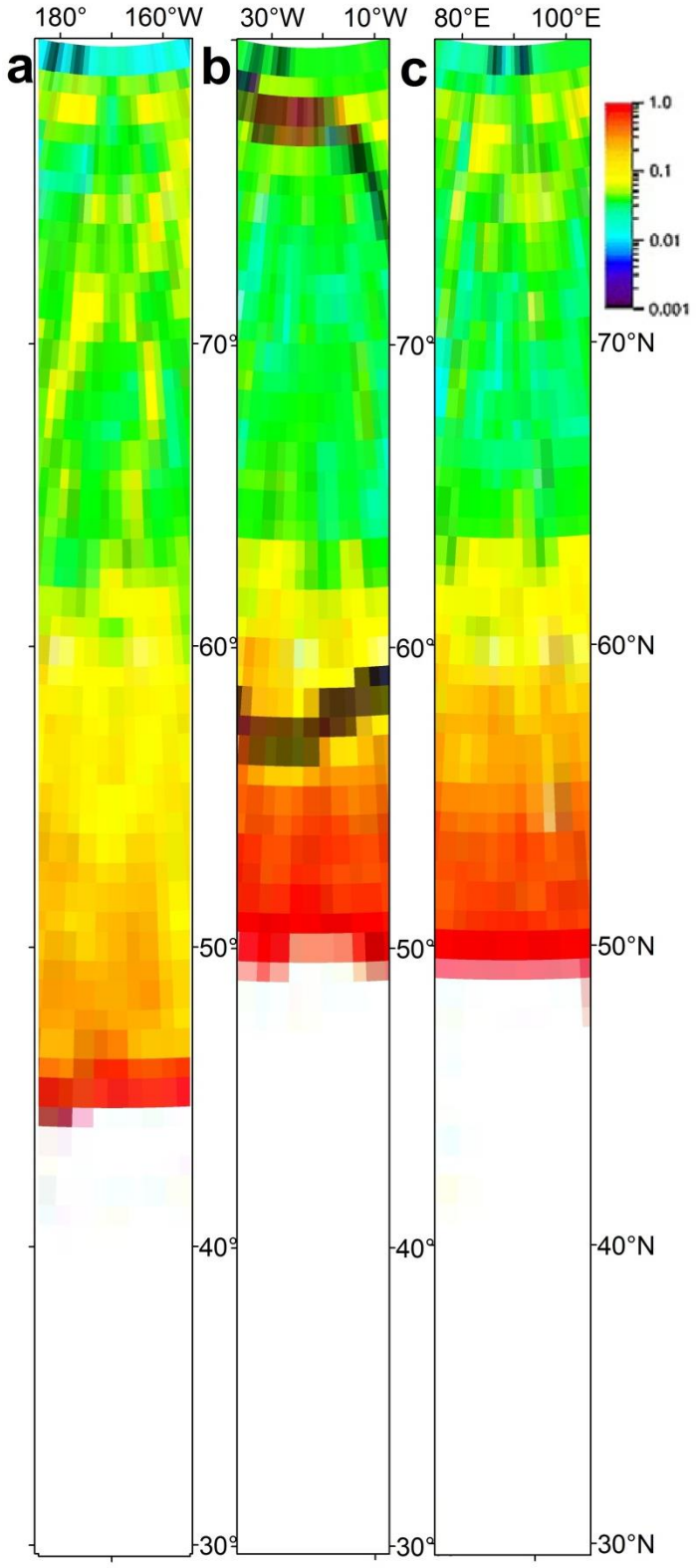

Figure 5.16 Data from Chamberlain and Boynton (2007) depth (m) to stable ground-ice under current conditions plotted in ArcGIS for (a) Arcadia, (b) Acidalia and (c) Utopia.

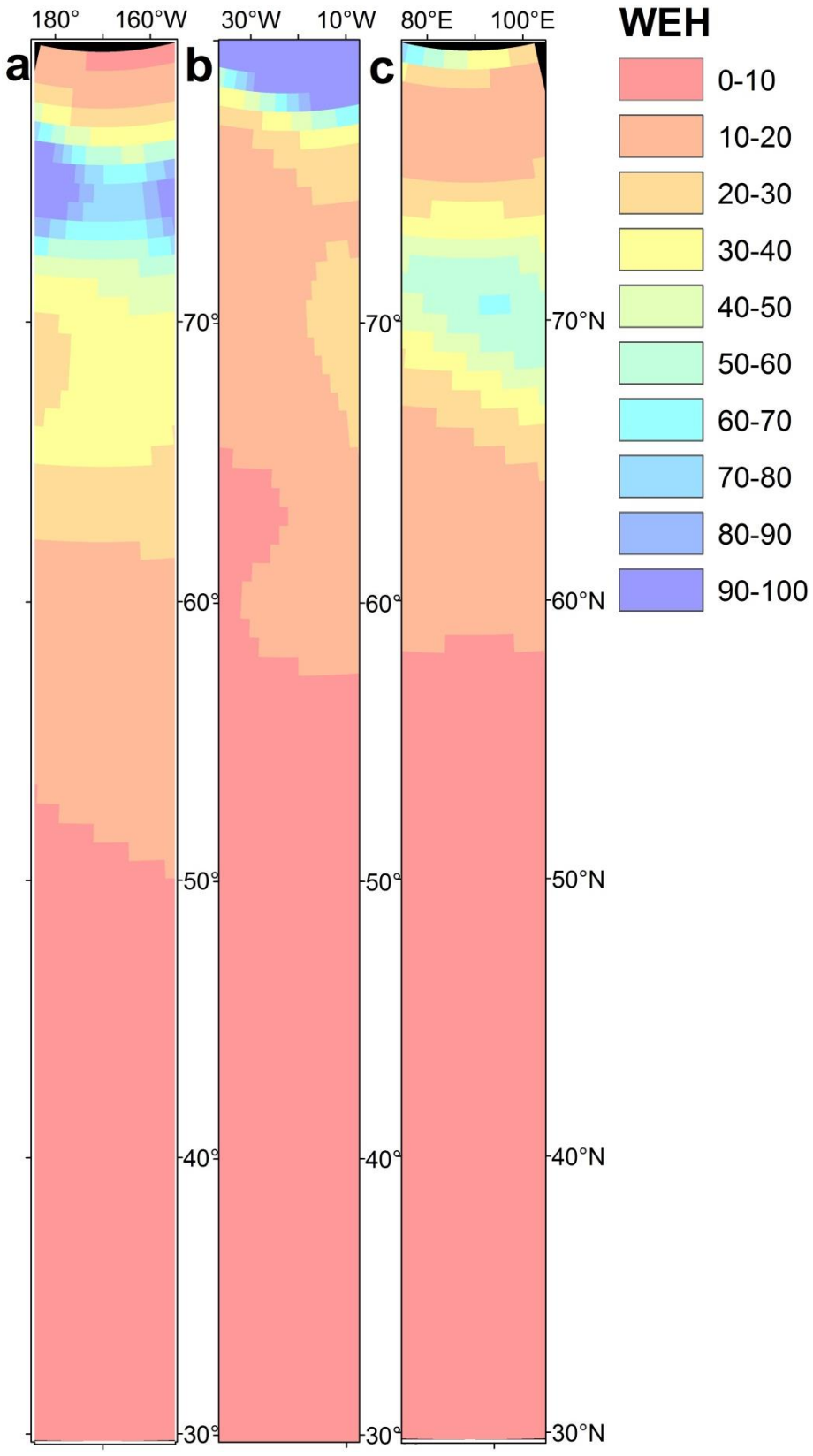

Figure 5.17 Water Equivalent Hydrogen (WEH) data from Wilson (2016) for (a) Arcadia, (b) Acidalia and (c) Utopia.

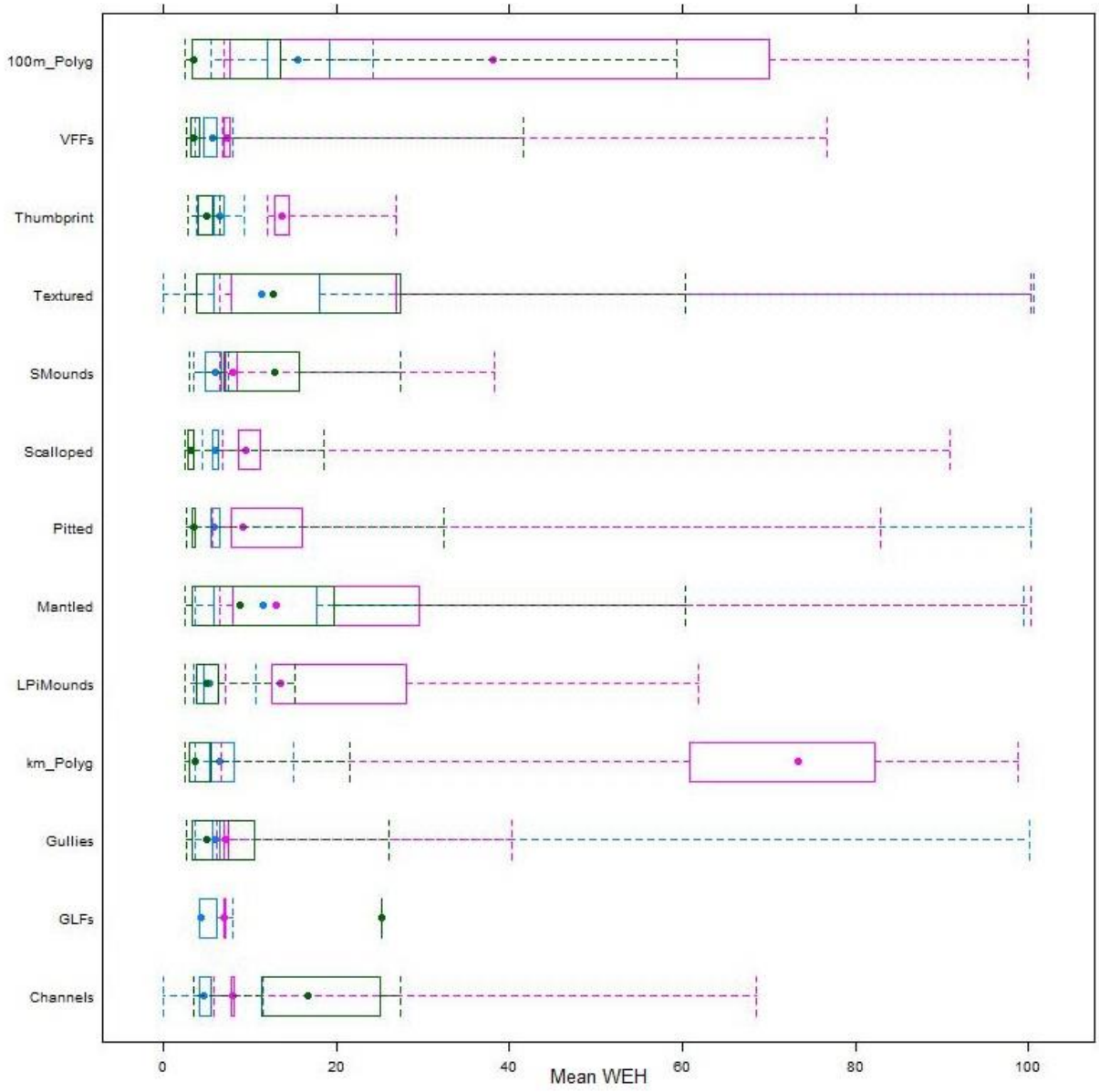

Figure 5.18 Mean WEH by landform. Dots show median, boxes show interquartile range, whiskers mark extremes. Pink – Arcadia, Green – Utopia, and Blue – Acidalia.

The northern extents of all the areas are dominated by dunes and massive ice (see Figure 5.19 and Figure 5.20). The presence of dominating massive ice and dunes in the very north of the three strips likely explains the gap in both mantled and textured terrains at the very high latitudes, as the mantle likely continues beneath these ice and dune deposits. The dune fields are most extensive in Acidalia Planitia, extending as far south as 70° N, but only as far south as 76° N in Utopia and 78° N in Arcadia. These dunes are the dark, likely basaltic, dunes mapped in the Mars global dune database (Hayward et al., 2007) and are

part of the Olympia Undae unit (Tanaka et al., 2005). Individual dunes are tens to hundreds of metres across and up to several kilometres in length and have a lower albedo than the surrounding material. The dunes tend to have crisp edges and do not appear to be mantled. In all three regions the surrounding material tends to be particularly smooth, lacking textures, and impact craters into this material tend to be subdued, suggesting that a relatively undegraded mantle could continue beneath the dunes.

The "massive ice" terrains observed are largely polar cap outliers found between 70-80° N. They range in size from tens of metres across to a few hundreds of kilometres across. The massive ice deposits are easily identified by their high albedo and smooth uncratered surfaces. These deposits do not appear to be mantled or textured and likely post-date the mantle deposits. The particularly smooth non-textured appearance of the surfaces in the northern extents of the strips could be indicative of a relatively thick and non-degraded mantle that is largely buried by the large dune fields and massive ice deposits.

The southern extent of the mantle and textured terrains is marked by the appearance of bedrock terrain across the three regions (compare Figure 5.13, Figure 5.14 and Figure 5.21). Arcadia displays the most decisive transition, where Acidalia appears to show a large area of gradation (45-55° N). Whereas the transition from ubiquitous Textured and Mantled to ubiquitous Bedrock is apparent in Arcadia 30-38° N and Acidalia 30-50° N, bedrock terrain appears patchy in Utopia, occurring sporadically between 30-40° N (see Figure 5.21).

The pitted terrain in the three regions differs quite significantly (see Figure 5.22). The pitted terrain is most pervasive in Arcadia, pitting consistently occurring from 60-68°N and from 36-56°N with one significant gap between 56-60°N, overlapping the vast majority of mantled and textured terrains. Although pitted terrain in Arcadia appears to be largely overlapping with mantled and texture terrains, the opposite seems to be true in Acidalia (compare Figure 5.13, Figure 5.14, and Figure 5.22), with the pitted terrain being concentrated at 35-30° N, where the mantled and textured terrains are not present. The

pitted terrain in Utopia is concentrated between 48-38 N, an area that is mapped as mantled but not textured, and is just north of a heavily scalloped area. While the pits in Arcadia and Utopia appear to be forming in the so called LDM, the pits in Acidalia are unrelated and appear to be a bedrock related feature.

It is not immediately clear as to why pits appear to be much more prevalent in Arcadia, and this seems to be at odds with the predictions for ground ice stability from climate modelling. At first glance, TES thermal inertia data (see Figure 5.24) appears to correlate with pitted terrain distribution (see Figure 5.22), with pitted terrain in Arcadia appearing to correlate with high thermal inertia units. However, the results from Acidalia and Utopia show pitted terrains correlating with areas of low thermal inertia, suggesting that pitted terrains occur independent of thermal inertia.

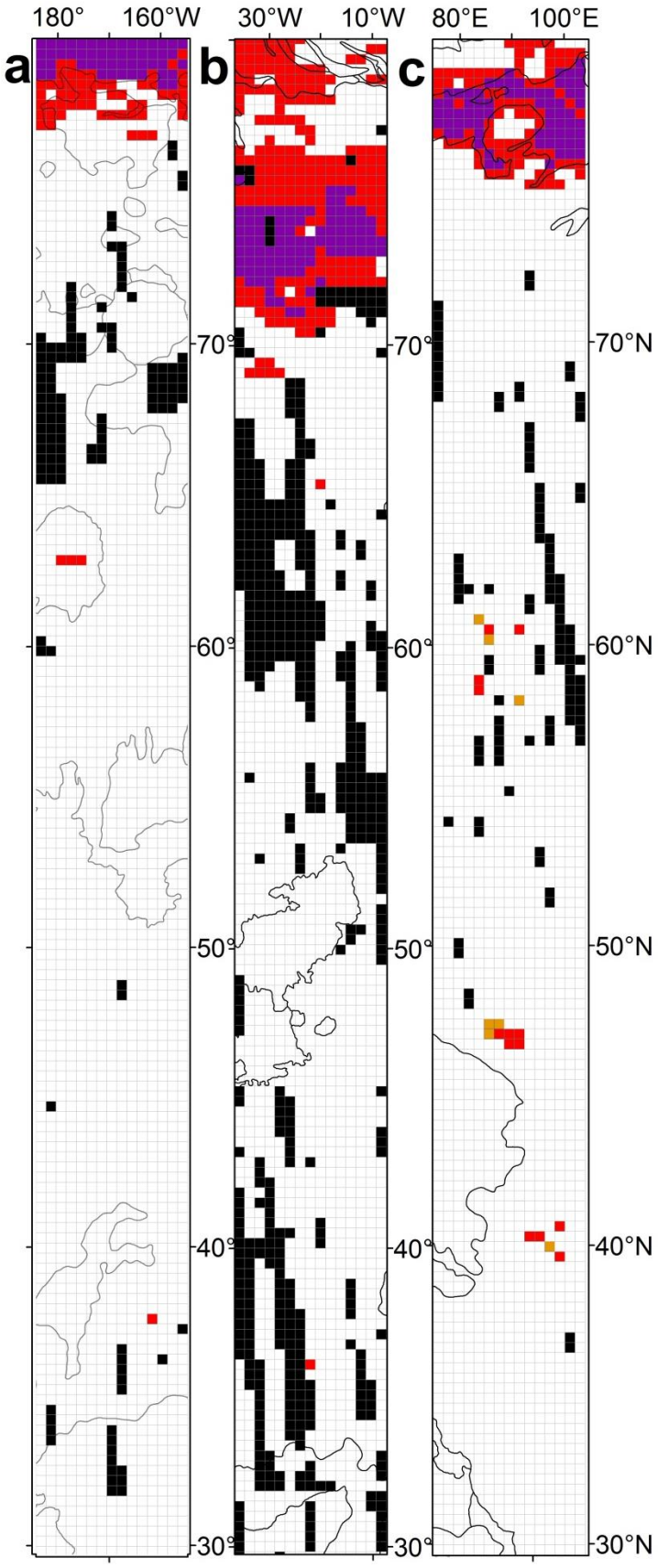

Figure 5.19 Dunes from (a) Arcadia, (b) Acidalia and (c) Utopia. Red is present, purple dominating, orange possible, black no data and white not present.

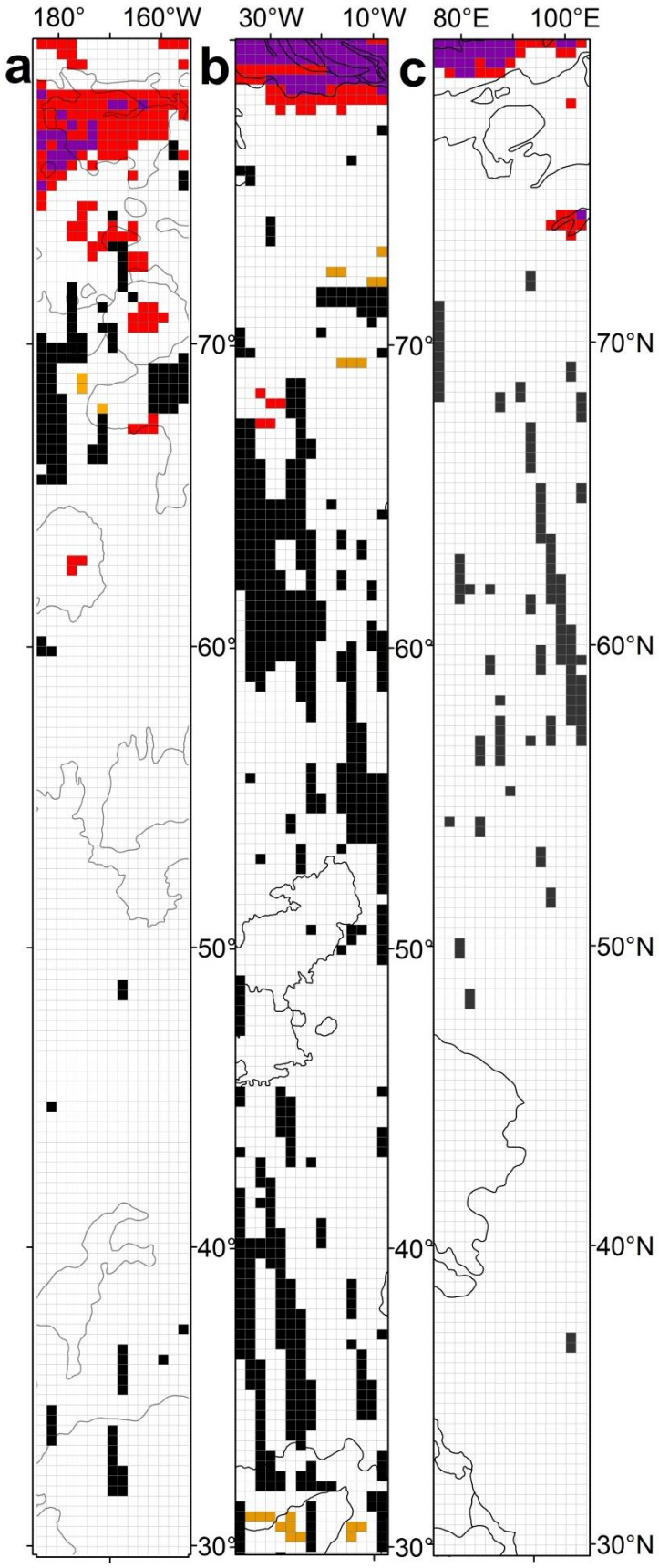

Figure 5.20 Massive Ice from (a) Arcadia, (b) Acidalia and (c) Utopia. Red is present, purple dominating, orange possible, black no data and white not present.

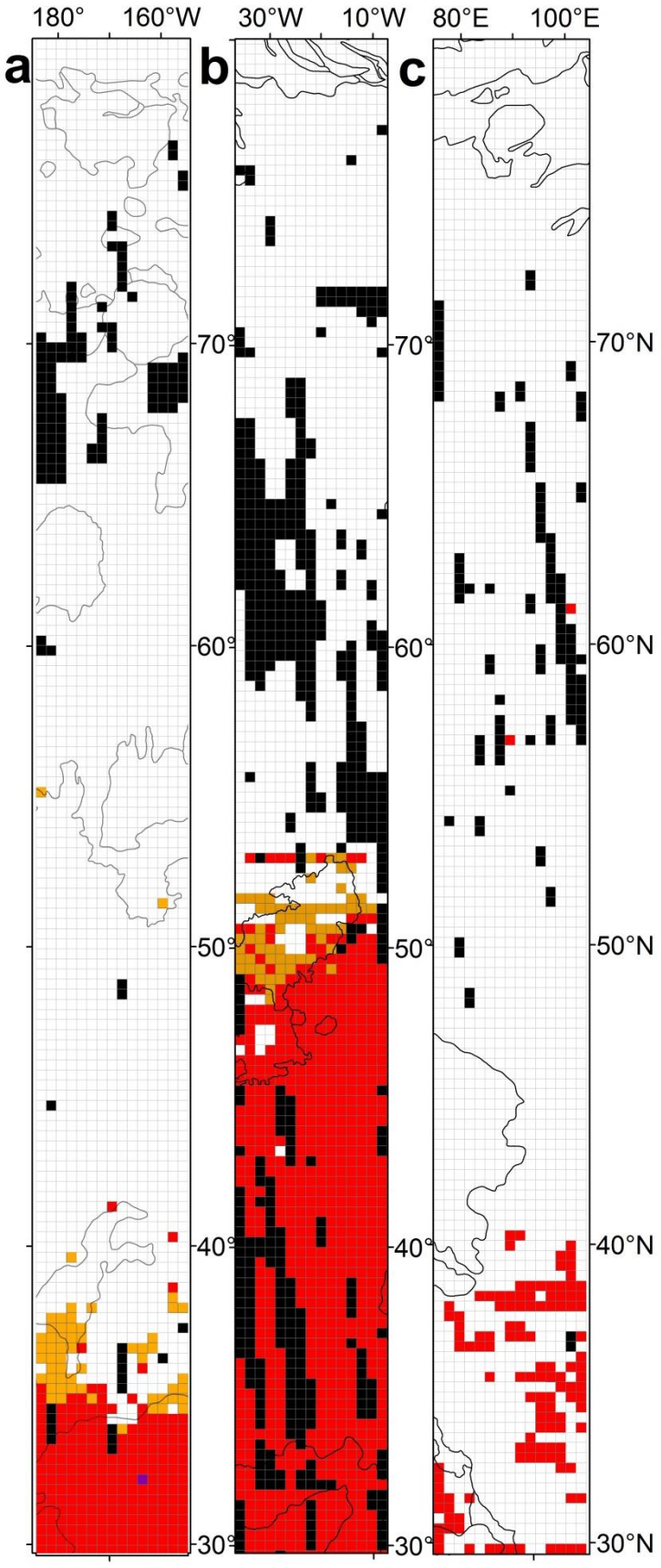

Figure 5.21 Bedrock from (a) Arcadia, (b) Acidalia and (c) Utopia. Red is present, purple dominating, orange possible, black no data and white not present.

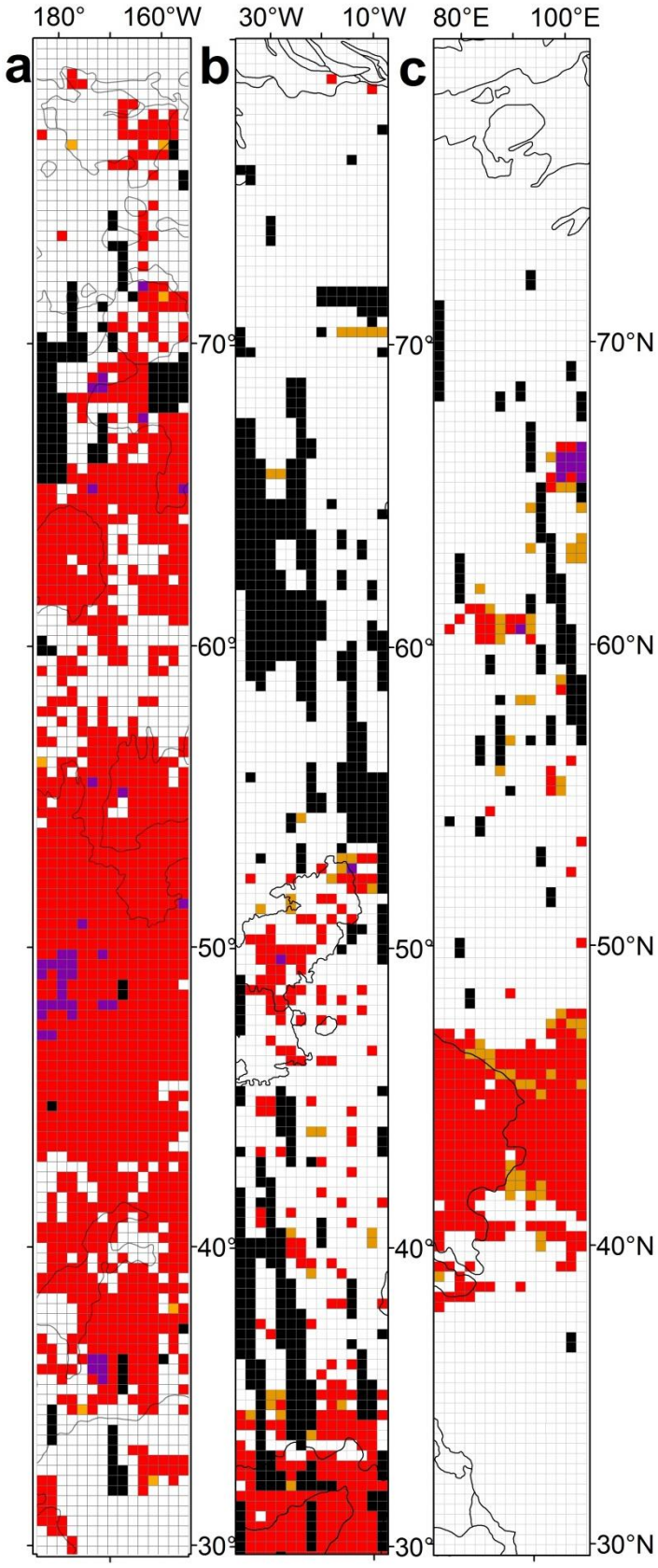

Figure 5.22 Pitted terrain from (a) Arcadia, (b) Acidalia and (c) Utopia. Red is present, purple dominating, orange possible, black no data and white not present.

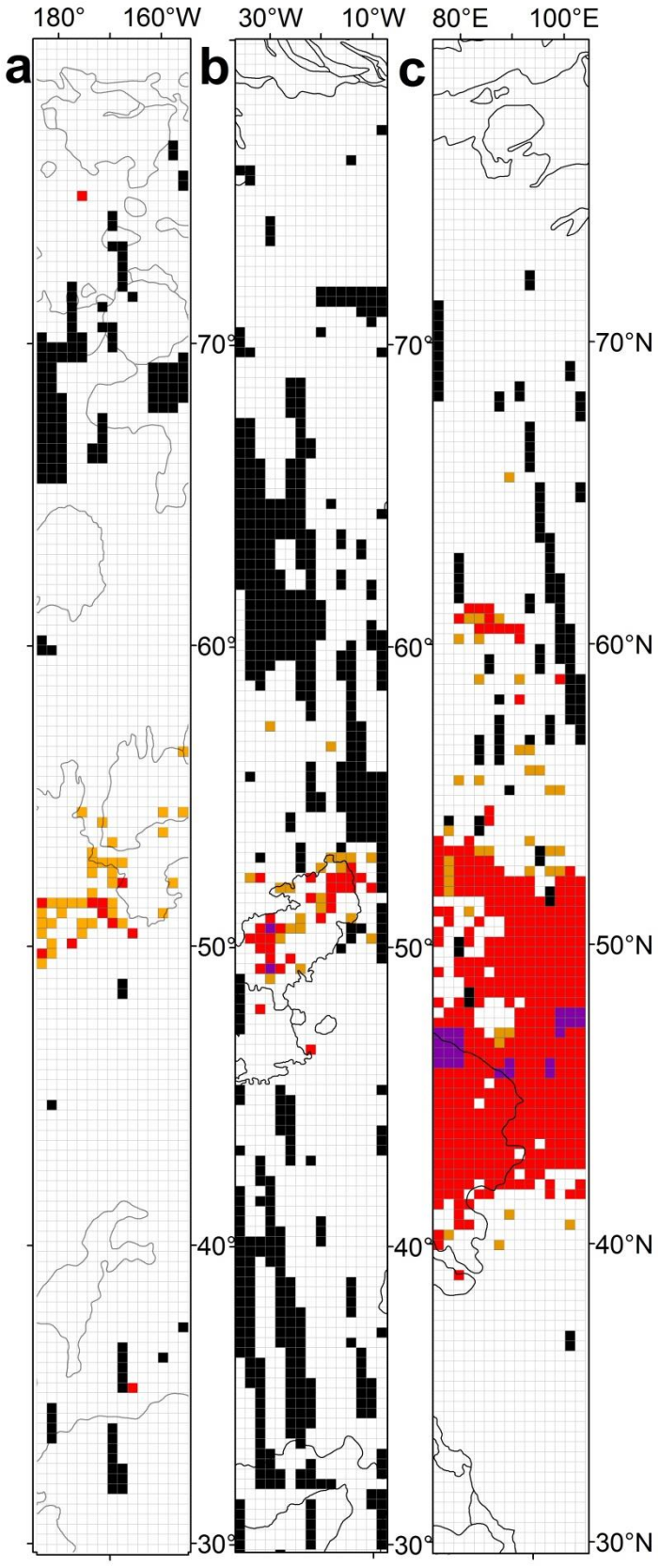

Figure 5.23 Scalloped terrain from (a) Arcadia, (b) Acidalia and (c) Utopia. Red is present, purple dominating, orange possible, black no data and white not present.

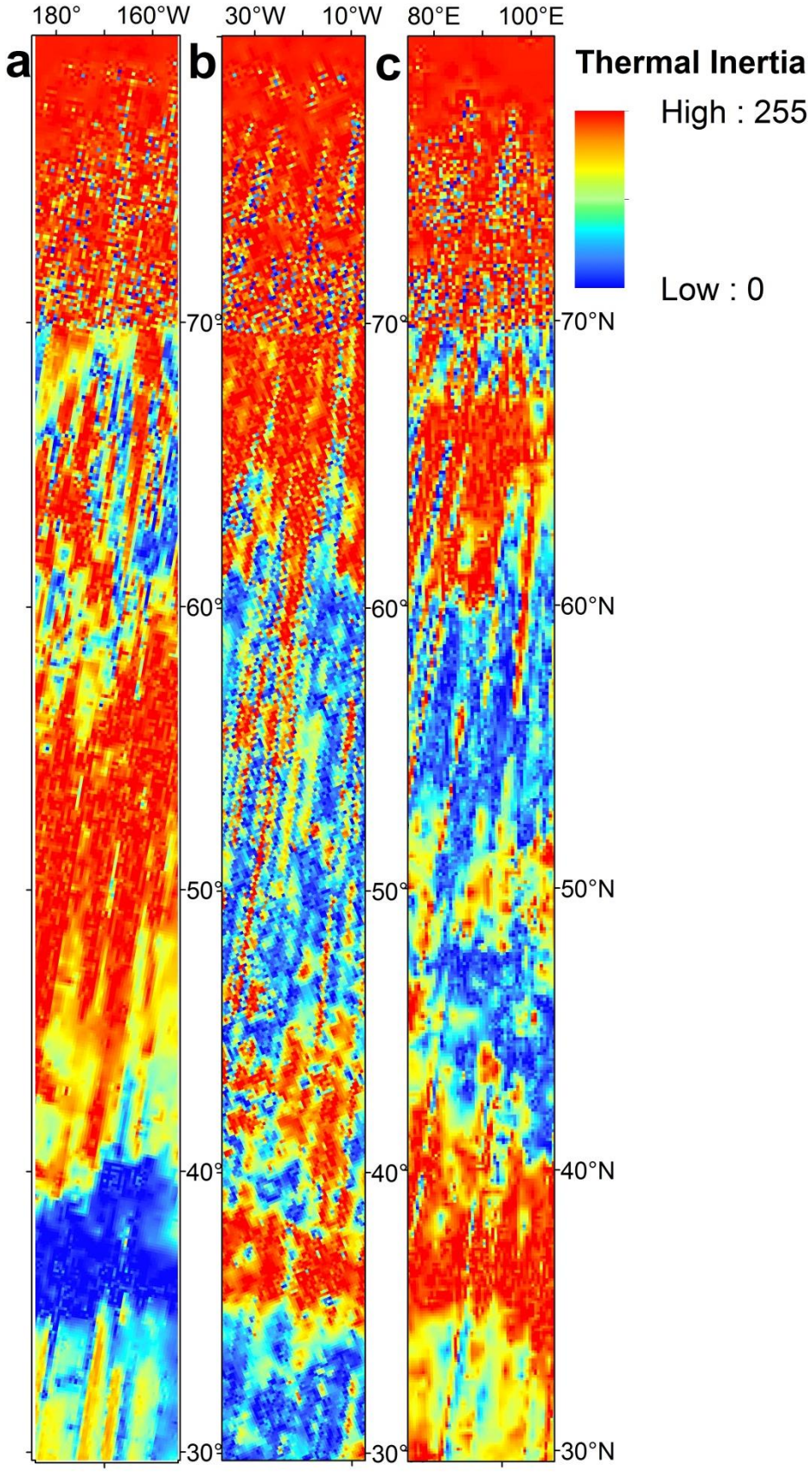

Figure 5.24 Thermal Inertia from TES (Thermal Emission Spectrometer on board Mars Global Surveyor; Christensen et al., 2001) for (a) Arcadia, (b) Acidalia and (c) Utopia.

The scalloped terrain occurs in a thin narrow band between 50-55 ° N in both Acidalia and Arcadia. The scalloped terrain in Utopia appears to be much more pervasive, with a large patch of scalloped terrain at 40-55° N. It is interesting to note that, despite the scalloped terrains occurring in a much narrower band and being much more poorly formed in Arcadia than the large assemblages described in Utopia Planitia (e.g. Séjourné et al., 2012), the areas around the scallops are heavily pitted by more generic, roughly circular depressions (see Figure 4.20). This suggests that volatiles were still present within the subsurface at the correct latitude for scallop formation. Therefore, the limitation on scallop formation in Arcadia is more likely to be due to the surface material's susceptibility to form scalloped pits of the surface material. There are numerous possible explanations for this limitation including: (i) coarser surface material, which could provide an armoring lag deposit as sublimation occurs, preventing further aeolian removal and hence further sublimation and scalloped depression formation (finer material may be more easily removed by wind and allow for further sublimation), (ii) alternatively, ice-volume, ice-depth and the form which the ice takes may control pit morphology: larger ice volumes in the shallow subsurface would lead to greater volume loss and potentially lead to larger scalloped pit formation (Séjourné et al., 2011).

The thumbprint terrain in Arcadia occurs between 55-65° N whereas in Acidalia and Utopia it is limited to between 30-40° N (see Figure 5.25). The thumbprint terrain in Arcadia coincides with mantled and textured terrain, but it does not in the other two areas. The morphology of the thumbprint terrain also differs significantly in the three areas. It is interesting to note that, despite occurring 20° further north in Arcadia, the elevation of the thumbprint terrain in Arcadia lies between that in Acidalia and Utopia (see Figure 5.26). In Arcadia, the thumbprint terrain appears to be very smooth, and appears to be made up of ridges, whereas in Acidalia and Utopia it appears to be made of individual cones. This difference could be accounted for in several ways. The first is that the various thumbprint

terrains could have formed through different processes. Alternatively, the differences in morphology could be accounted for by burial and smoothing of the thumbprint terrain in Arcadia by the LDM. Another possibility is that the LDM formed an impermeable layer and fluid or fluidised material was upwelled and trapped, forming ridges beneath the surface in Arcadia, where it was directly ejected onto the surface, forming cones in Acidalia and Utopia.

The areas that contain small mounds overlap consistently between 34-60° N in Arcadia, 34-50° N in Acidalia, but there is no overlap in Utopia, with small mounds occurring between 55-67° N (see Figure 5.27). In Arcadia, the area in which the small mounds occur overlaps that in which large scale channels are found (see Figure 5.27 and Figure 5.28). This is not the case in Acidalia and Utopia. In Acidalia, channels are confined to between 45-50° N. Channels largely do not occur within the Utopia mapping area, with the exception of some small-scale channels around the mesa and knobs of older material.

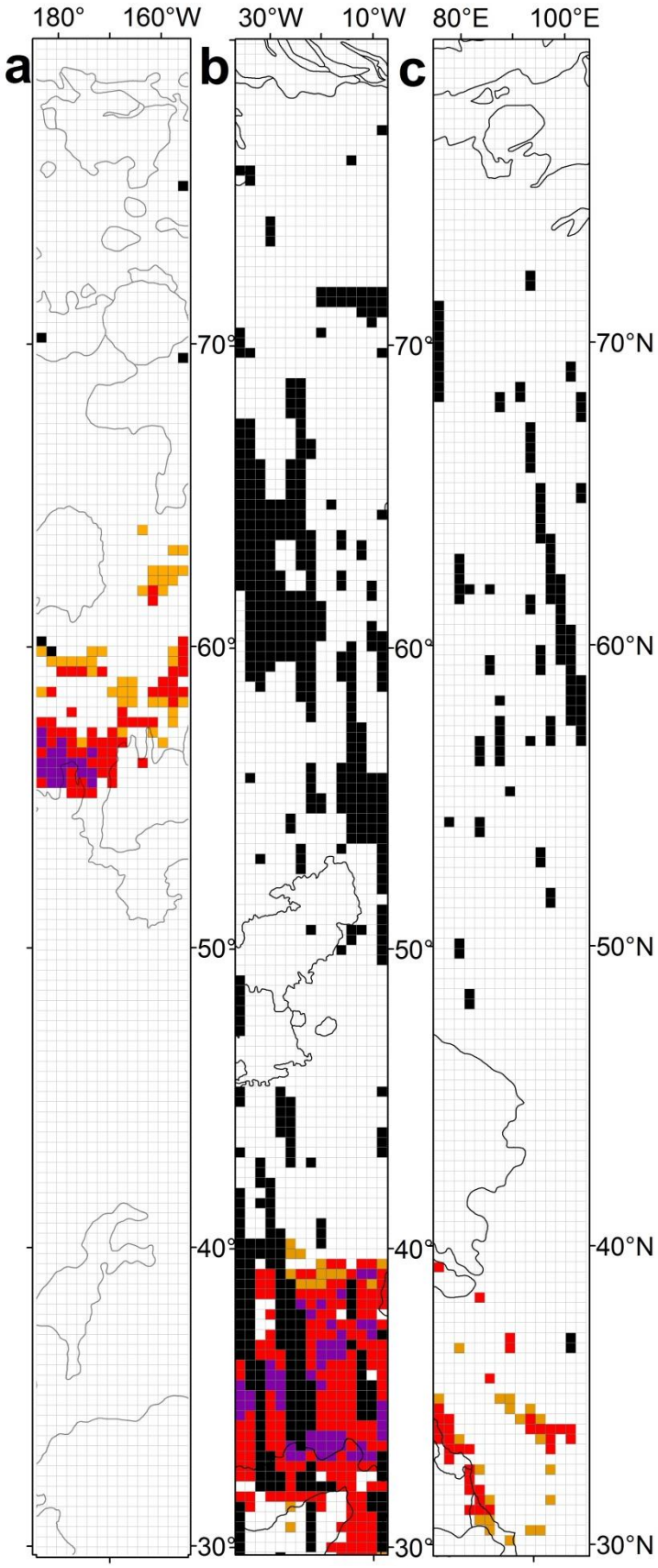

Figure 5.25 Thumbprint terrain from (a) Arcadia, (b) Acidalia and (c) Utopia. Red is present, purple dominating, orange possible, black no data and white not present.

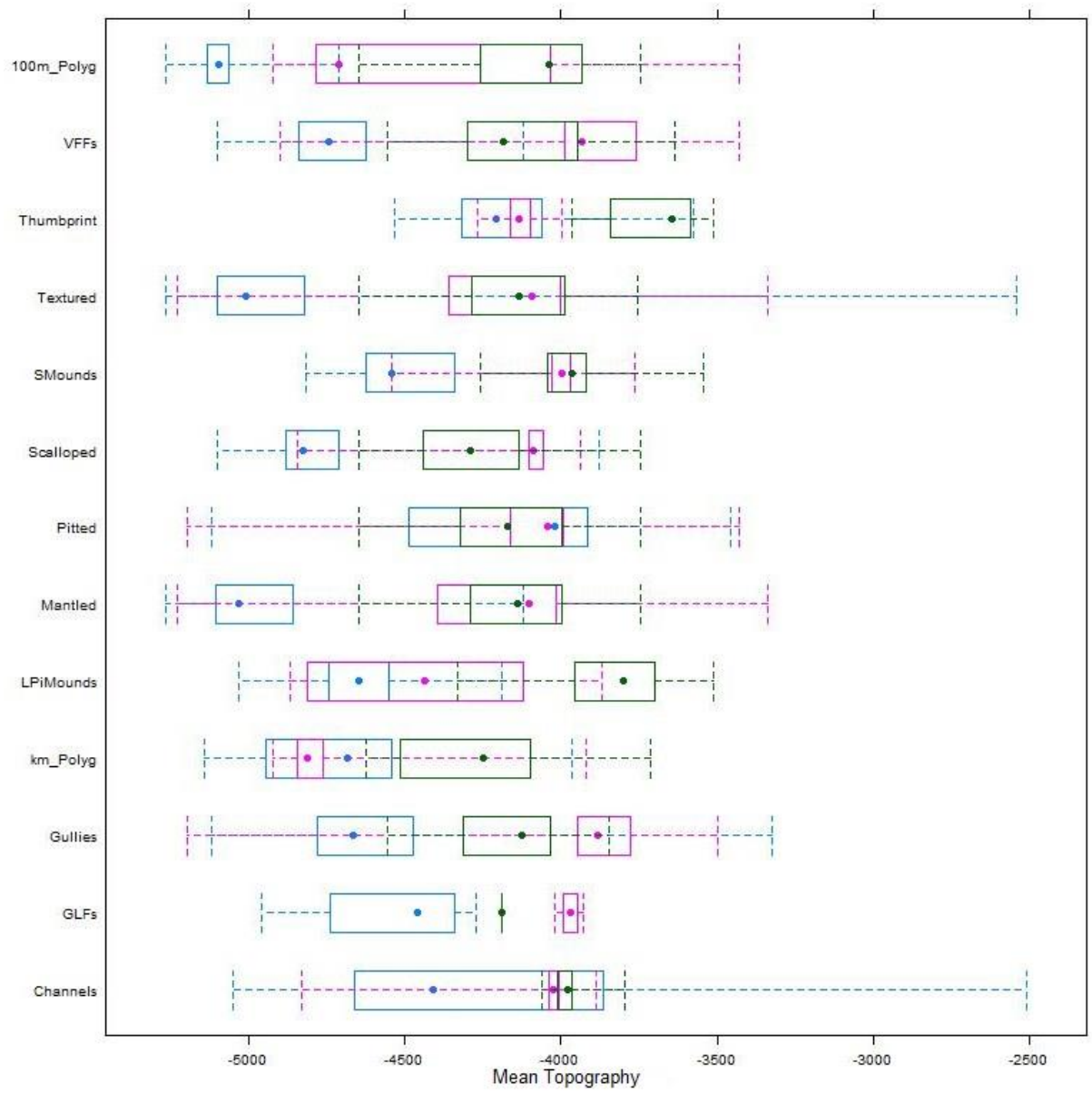

Figure 5.26 Mean Topography by landform. Dots show median, boxes show interquartile range, whiskers mark extremes. Pink – Arcadia, Green – Utopia, and Blue – Acidalia.

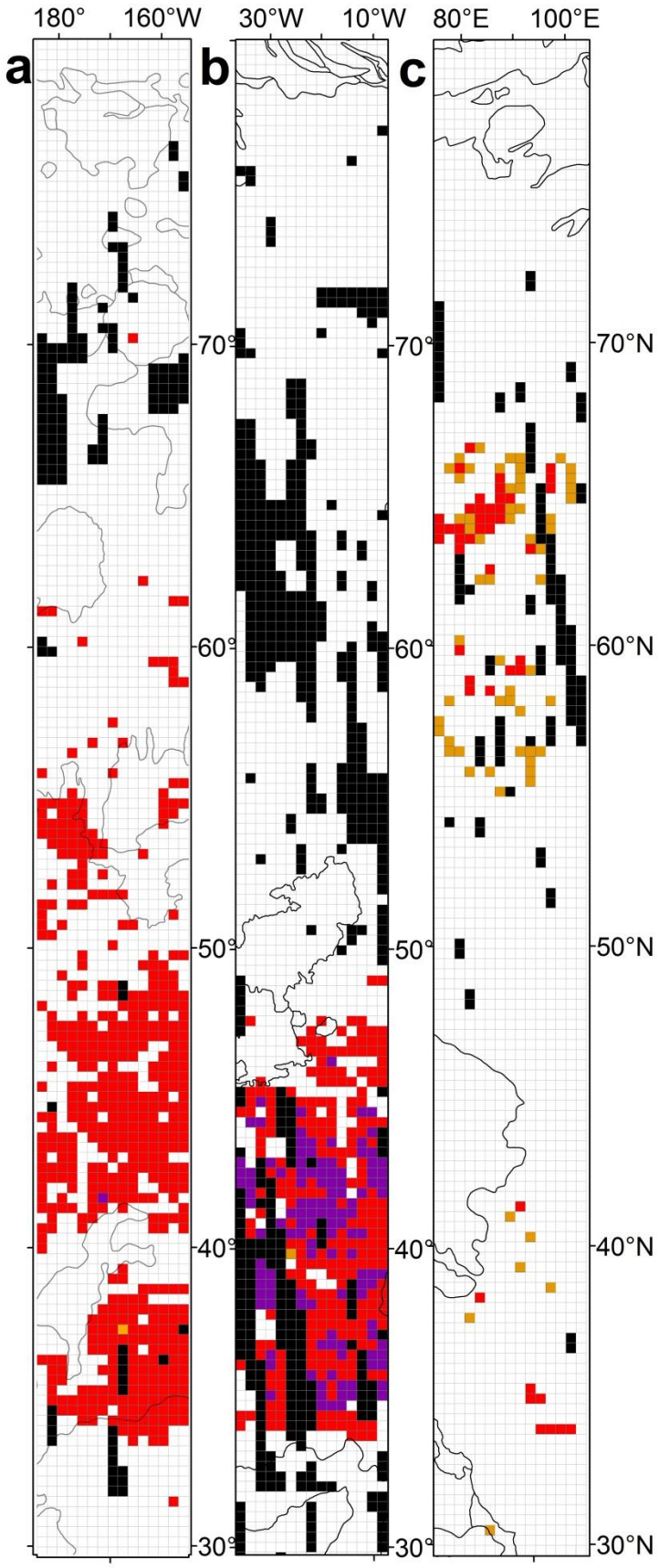

Figure 5.27 Small mounds from (a) Arcadia, (b) Acidalia and (c) Utopia. Red is present, purple dominating, orange possible, black no data and white not present.

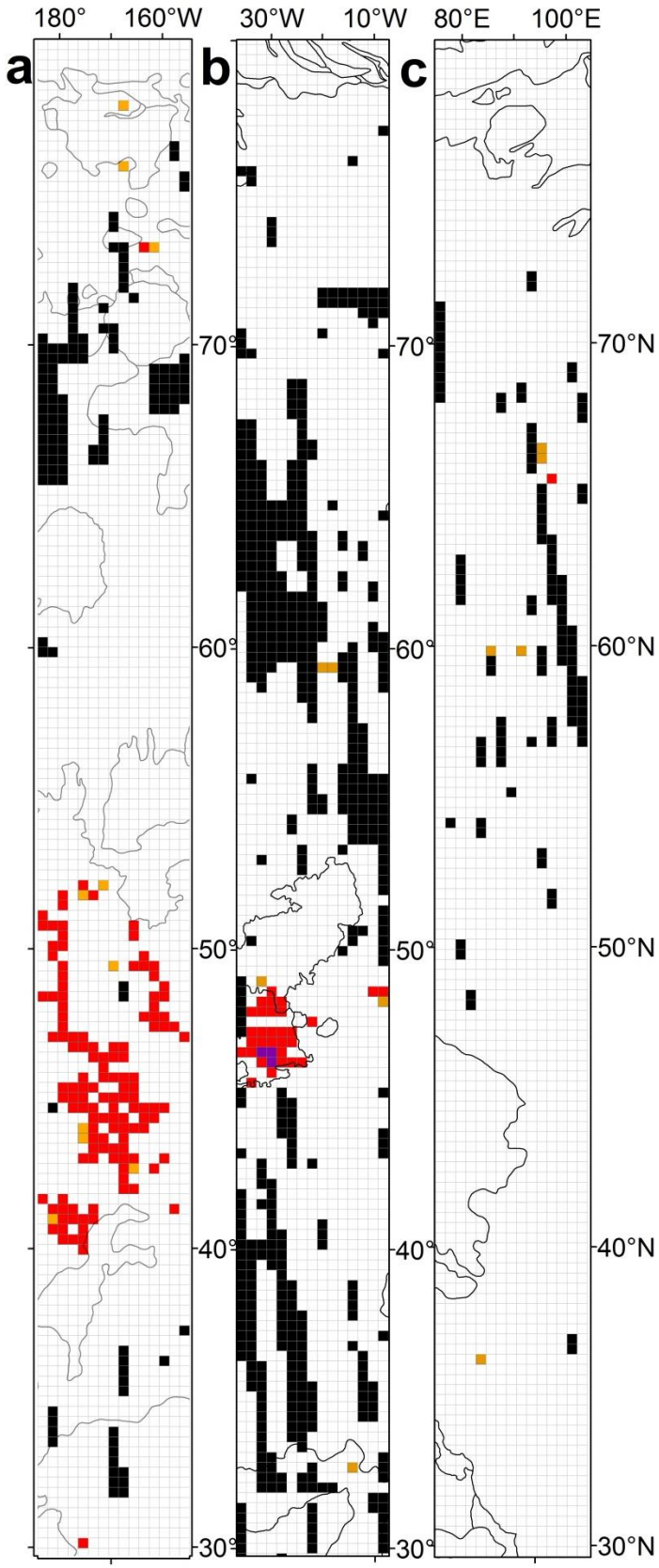

Figure 5.28 Channels from (a) Arcadia, (b) Acidalia and (c) Utopia. Red is present, purple dominating, orange possible, black no data and white not present.

Kilometre-scale polygons in Arcadia are found between 72-76° N (see Figure 5.29). In Acidalia there appear to be two groups of kilometre-scale polygons, one occurring between 54-64° N and the other from 36-48 ° N (see Figure 5.29). In Utopia, kilometre scale polygons occur in small patches between 36-64° N and appear to have a similar, but sparser, pattern to those in Utopia (see Figure 5.29). Kilometre-scale polygons occur in areas of high WEH in Arcadia (see Figure 5.18), but the opposite is true in both Acidalia and Utopia. Given that the kilometre-scale polygons in Arcadia are buried by LDM, and appear to pre-date the LDM emplacement, and thus represent underlying geology, their occurrence is almost certainly independent of ground-ice related processes, and also probably of latitude.

Whereas very few large pitted mounds were found in Arcadia, a large swathe of these features was found in Acidalia between 38-50° N, and two groups of these mounds were found in Utopia at 30-40° N and, more sparsely, at 50-65° N (see Figure 5.30). From these observations, it seems likely that the large pitted mounds are not latitude dependent and are instead a product of local basin conditions. I also see no evidence to suggest that the large pitted mounds are a product of ground-ice related processes in Arcadia as they are uncommon here, but other ground-ice related forms are not.

VFFs in Arcadia are primarily concentrated to within 35-42° N, and within 40-53° N in Acidalia. The VFFs in Arcadia are largely LDAs around inliers of the Nepenthes Mensae unit, and the same is true in Acidalia, with the majority of VFFs being LDAs around inliers of Nepenthes Mensae and Noachis Terra units. As would be expected, and as can be seen in Figure 5.33 and Figure 5.34, VFFs occur in areas with higher slope and roughness values as they need relief in order to flow, and, by definition, flow is required for their formation. Given the low relief of the northern plains in general it is not surprising that the VFFs are confined to the knobs and mesas formed from inliers of older more resistant material. At most, GLFs are found in around 0.1% of the grid squares in the three

combined regions (see Figure 5.32); this is likely at least part due to the majority of the region being flat lying with little slopes for GLFs to have formed on.

No convincing examples of gullies were found in Arcadia; however they have been identified in both Acidalia and Utopia. In Acidalia, the identified gullies are concentrated around inliers of older material that provide areas of high relief, as are the putative gullies in Arcadia (see Figure 5.35). This is similar to the VFFs, suggesting that they are somewhat collocated – although this probably reflects only the slope regimes in which they formed, and not necessarily a genetic link.

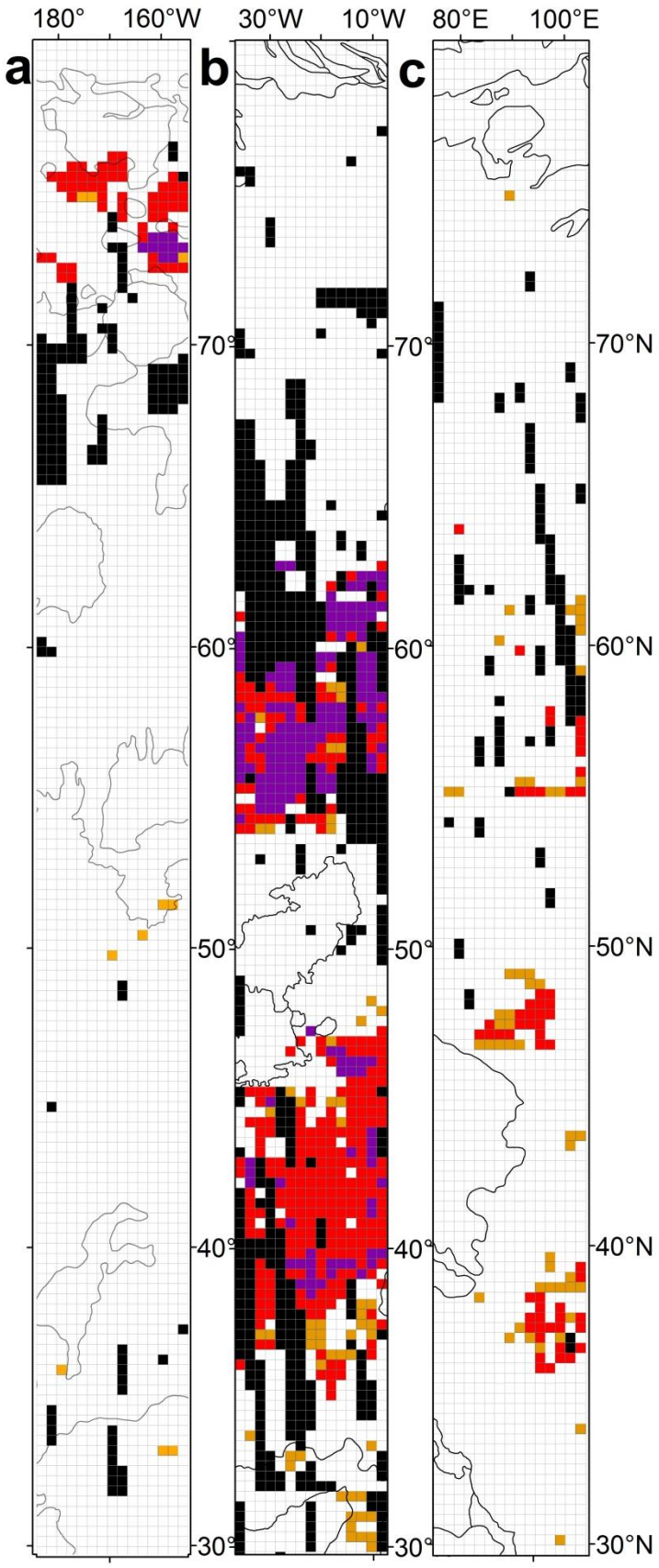

Figure 5.29 km-scale polygons from (a) Arcadia, (b) Acidalia and (c) Utopia. Red is present, purple dominating, orange possible, black no data and white not present.

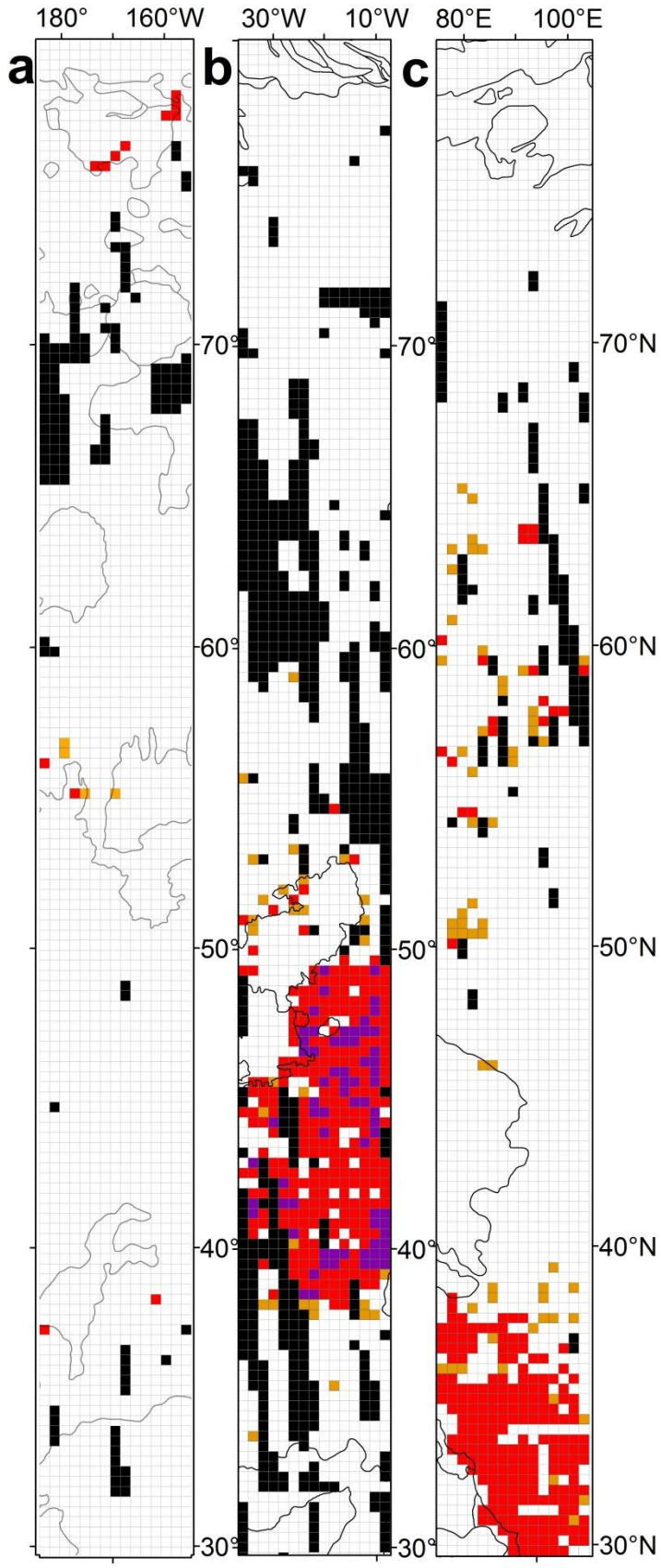

Figure 5.30 Large Pitted Mounds from (a) Arcadia, (b) Acidalia and (c) Utopia. Red is present, purple dominating, orange possible, black no data and white not present.

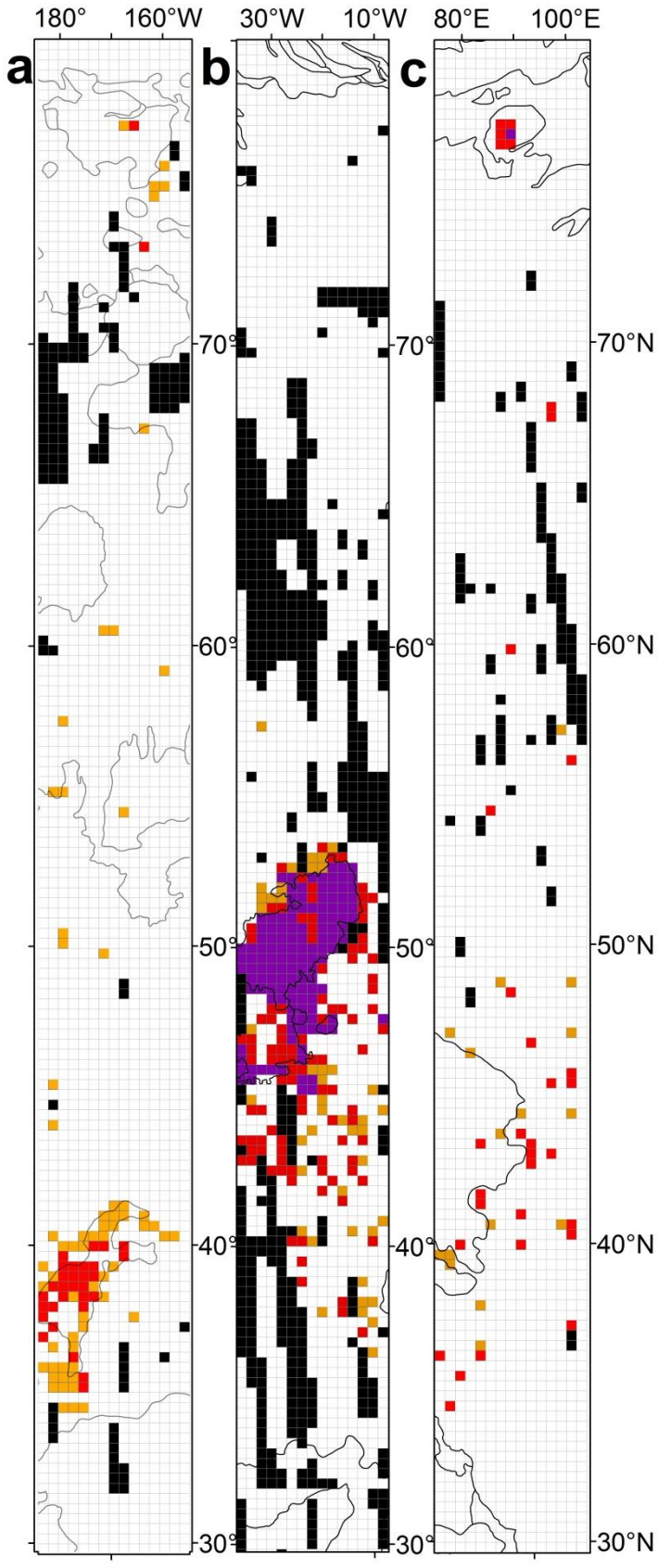

Figure 5.31 VFFs from (a) Arcadia, (b) Acidalia and (c) Utopia. Red is present, purple dominating, orange possible, black no data and white not present.

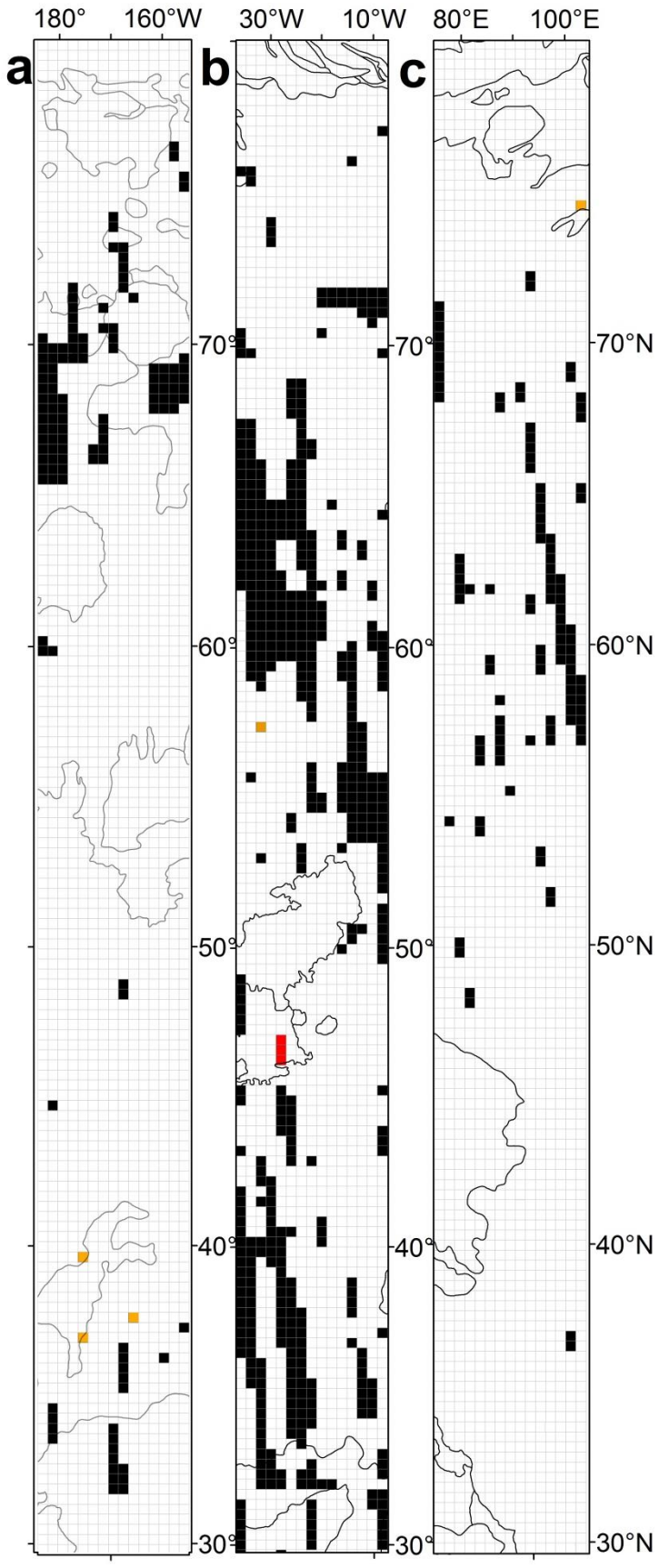

Figure 5.32 GLFs from (a) Arcadia, (b) Acidalia and (c) Utopia. Red is present, purple dominating, orange possible, black no data and white not present.

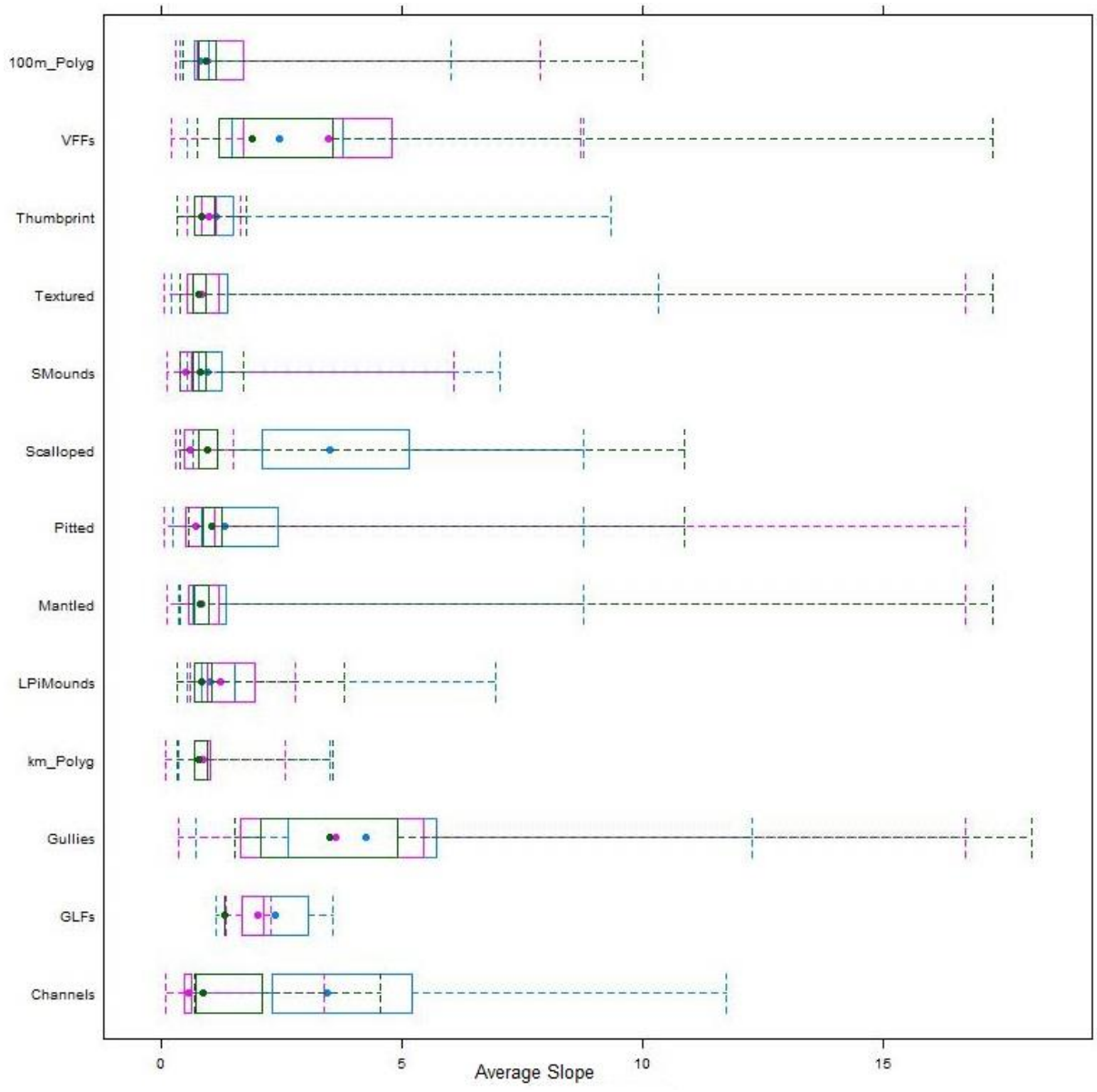

Figure 5.33 Average Slope by landform. Dots show median, boxes show interquartile range, whiskers mark extremes. Pink – Arcadia, Green – Utopia, and Blue – Acidalia.

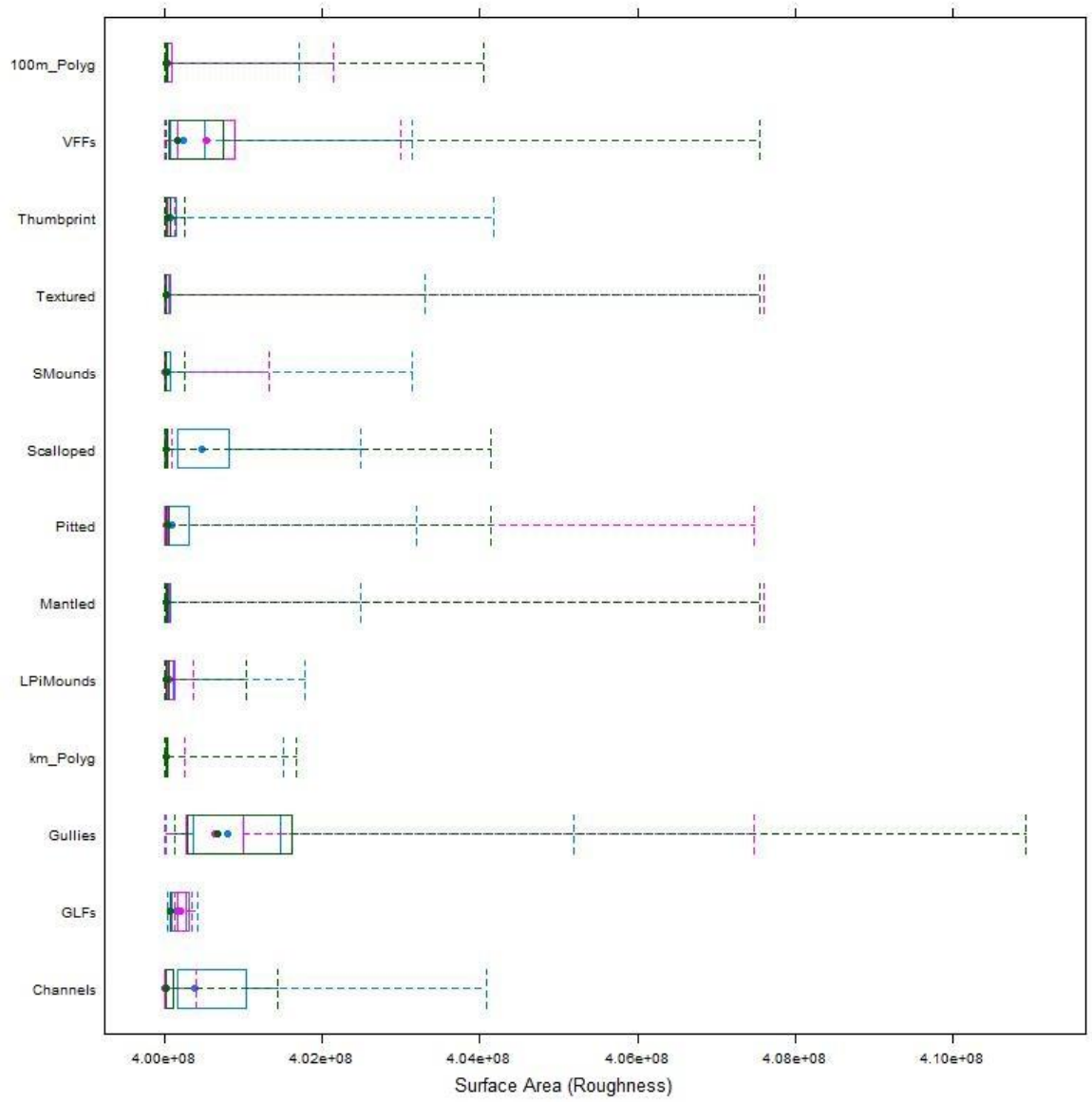

Figure 5.34 Surface area as a measure of roughness by landform. Dots show median, boxes show interquartile range, whiskers mark extremes. Pink – Arcadia, Green – Utopia, and Blue – Acidalia.

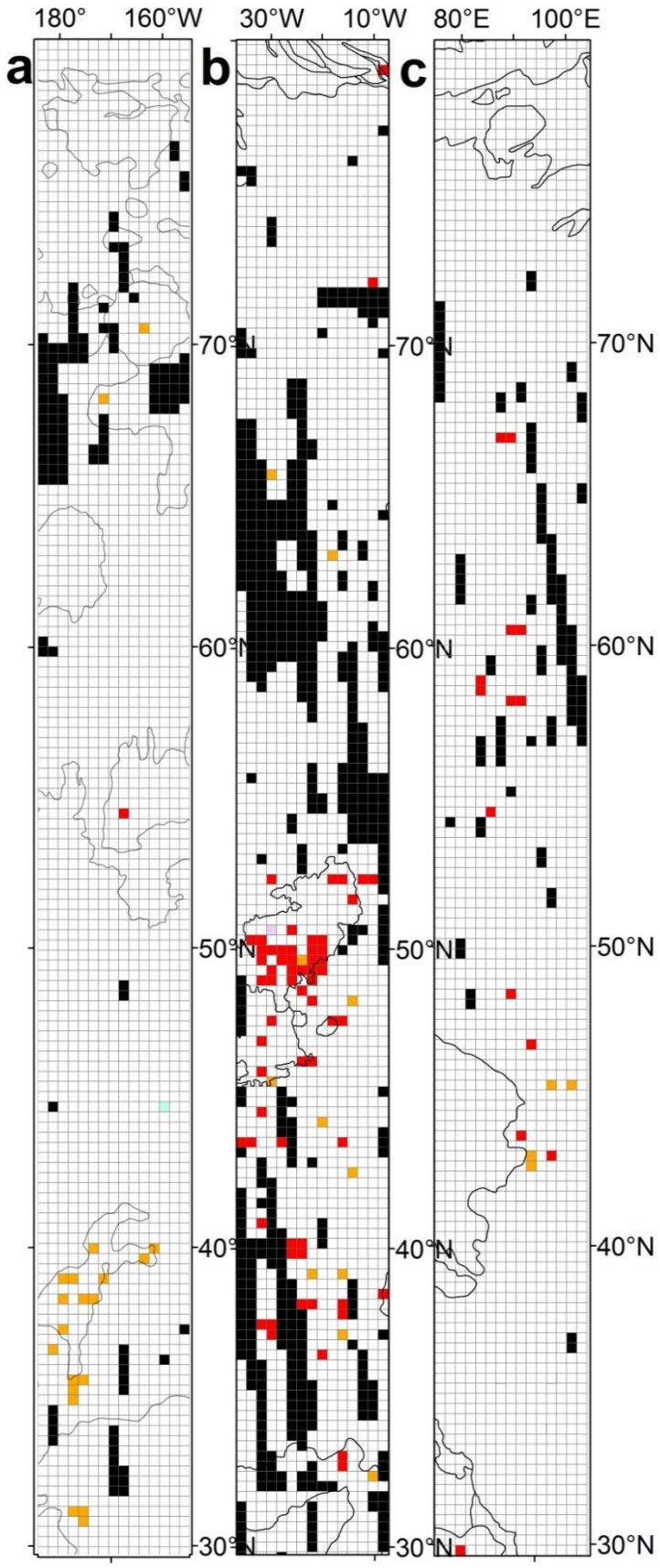

Figure 5.35 Gullies from (a) Arcadia, (b) Acidalia and (c) Utopia. Red is present, purple dominating, orange possible, black no data and white not present.

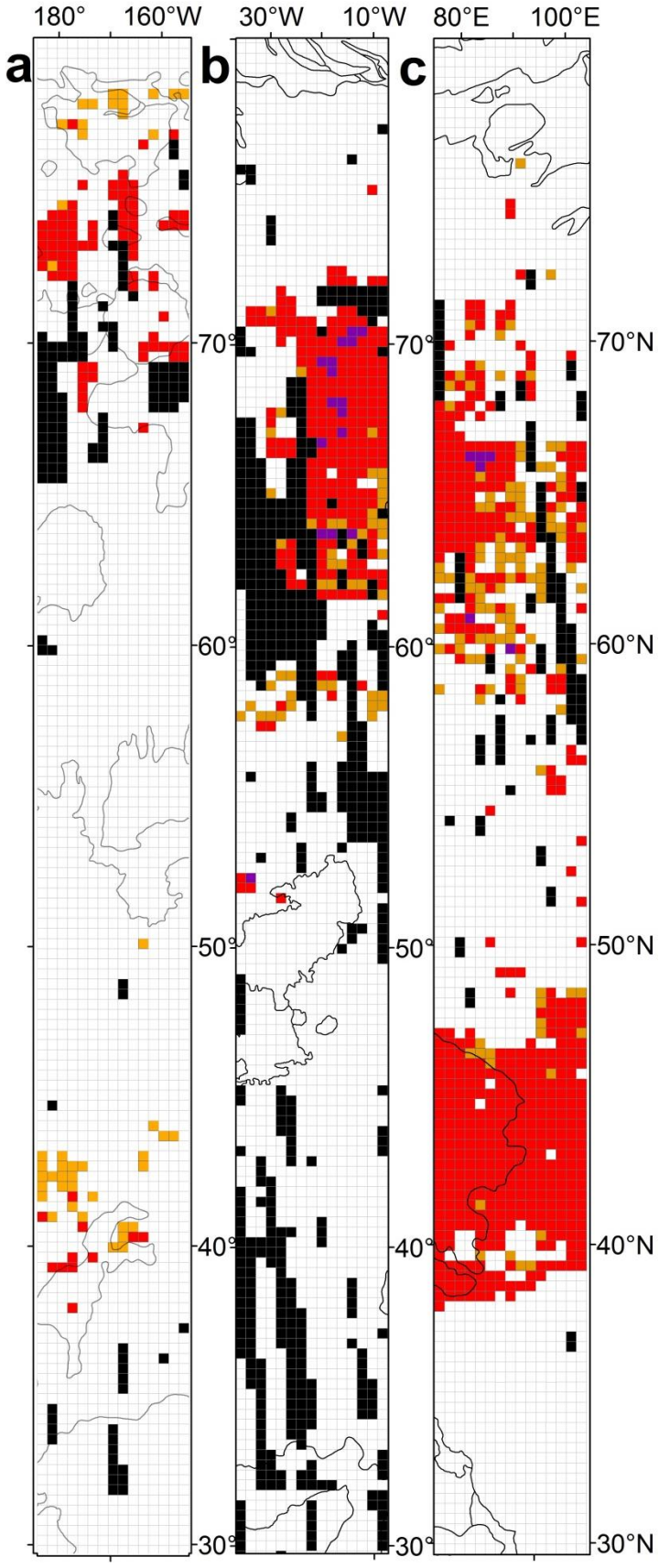

Figure 5.36 100 m-scale polygons from (a) Arcadia, (b) Acidalia and (c) Utopia. Red is present, purple dominating, orange possible, black no data and white not present.

The northern group of 100 metre-scale polygons observed in the Arcadia strip (see Figure 4.29), which appears reminiscent of ice-wedge polygons on Earth, has morphological counterparts in both Utopia and Acidalia that occur at comparable latitudes (66-78° N in Arcadia, 60-70° N in Acidalia and Utopia; see Figure 5.36). These are characterised by high albedo contracts with dark centres (see Figure 4.30b). Like in Arcadia 38-45° N, Utopia displays a southern group of polygons found between 40-50° N (see Figure 5.36). However, where the southern 100 m polygons in Arcadia (see Figure 4.29) appear more like bedrock fracture networks than clastic or ice-related polygons (see Figure 4.30a), the southern polygons in Utopia are associated with pits and scalloping and are likely a product of sublimation and thermal contraction (Séjourné et al., 2011, 2012) and thus are likely are a product of ground ice. The obvious differences in morphology between the polygons implies different modes of origin and warrants caution when interpreting the presence of 100 m scale polygons as being indicative of ground ice. For future projects, a polygon classification scheme should be used to try to distinguish between polygons with different morphologies (El Maarry et al., 2010; Levy et al., 2009; Mellon, 1997; Séjourné et al., 2011) and to better understand where polygons indicative of ground ice are located.

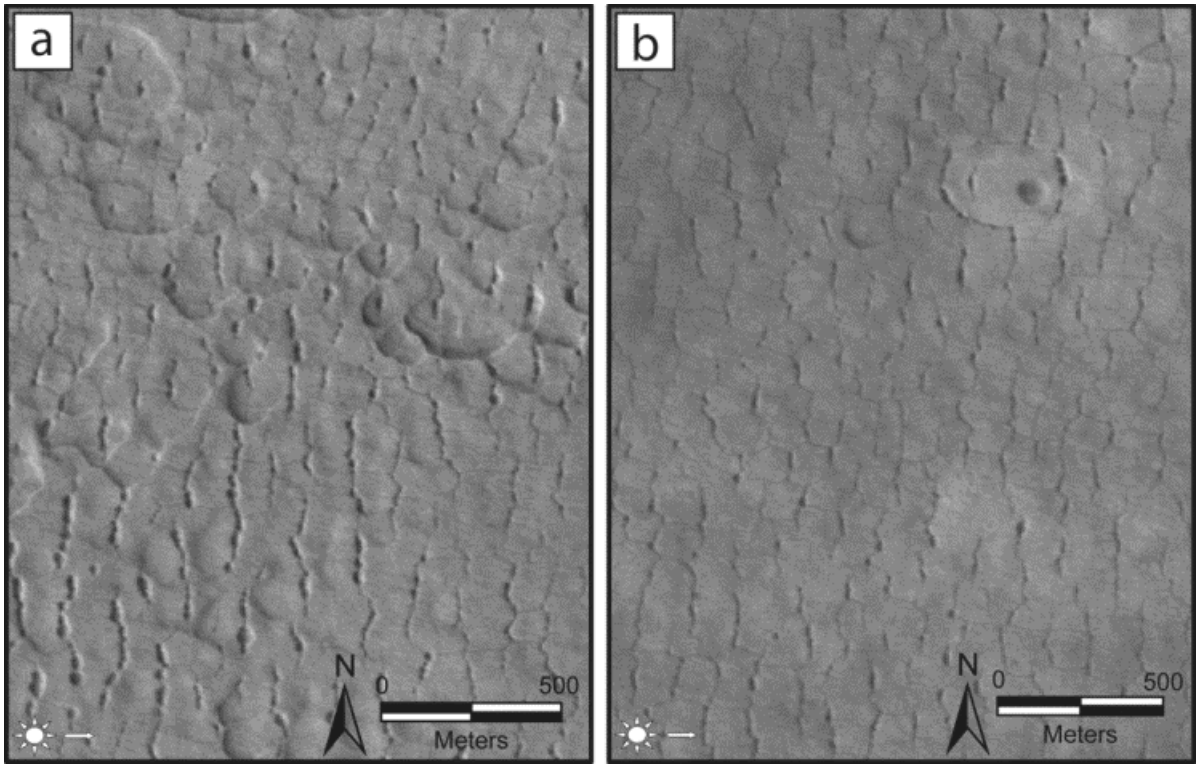

Figure 5.37 100 m Polygon and scalloped terrains from southern Utopia Planitia, after Sejourné,(2011).

5.3. **Summary of key observations**

- The distribution of the morphological "textured" designation generally matches the topographical "mantled" regions and these signatures also continue over multiple geological and topographical boundaries. These observations strongly support the presence of a ubiquitous, ice-rich airfall deposit across the northern plains.

- Large areas of the LDM in Arcadia are covered in pits, or depressions indicative of collapse, potentially as a result of the removal of volatiles and consistent with the presence of an ice-rich, ubiquitous mantle.

- The LDM in Arcadia displays significantly more pitted terrain than in both Utopia and Acidalia. Given that Arcadia tends to show comparable or high WEH values, this suggests that the LDM in Arcadia may have had higher volatile content and has subsequently been subject to higher volatile loss and more widespread pitting.

- The gradational boundary between textured and bedrock in Arcadia is supportive of an icy mantle that thins towards the south.

- VFFs occur in areas with higher slope and roughness values. This is not unexpected, as they need relief in order to flow, and, by definition, flow is required for their formation. VFFs in the northern plains are confined to the knobs and mesas formed from inliers of older more resistant material.

- GLFs are found in around 0.1% of the grid squares, making them a very minor component of possible ice-related landforms in the northern plains.

- Dunes dominate the northern extent of the three regions masking any underlying landforms indicative of ground ice, and WEH values suggest that these dunes are relatively ice-free. This in turn suggests that the dunes were emplaced well after the ice-rich regolith they sit upon, and that LDM formation has therefore not occurred recently.

- Given that the kilometre-scale polygons in Arcadia are buried by LDM, and appear to pre-date the LDM emplacement representing underlying geology, and that they occur south of the mantled and textured terrains in Acidalia and Utopia, then their formation was probably independent of both ground-ice related processes and latitude.

- The thumbprint terrain in Arcadia occurs 20° further north than in Acidalia and Utopia and is buried by LDM; this probably accounts for the smoother and more ridge-like morphology of the thumbprint terrain in Arcadia.

- 100 m Polygons can be divided into two groups in Arcadia: a northern group that are reminiscent of snow filled, ice-wedge polygons and which are likely to be a product of ground

ice processes, and a southern group which appear to be more bedrock-fracture related, and are not likely to be a product of ground ice processes.

- The northern groups of these polygons are also found in Utopia and Acidalia suggesting a widespread occurrence of ice-wedge polygons on the northern plains. Utopia also displays what appears to be a group of sublimation related polygons in association with the scalloped terrain.

- The large scale channel system and small mound assemblage in Arcadia does not have counterparts in Utopia and Acidalia suggesting regional, as opposed to latitudinal, control of these landforms.

5.3.1. **Summary**

The grid-mapping of the northern plains has allowed me to determine the distribution of ice-indicative landforms on the northern plains, with the most prominent being the mantled and textured terrains of the LDM found north of 35° N. As the LDM drapes over topographic and geological boundaries uniformly rather than collecting in topographic lows (like both ash and snow deposits) its' origin is most likely airfall. In Chapter 6 I aim to establish whether fluvial processes could have played a role in providing the water required to form the ice-indicative landforms in the northern plains by looking at Rahway Vallis, a possible source of water for the Amazonis and Arcadia Planitias.

6. Rahway Vallis

In this chapter I aim to establish whether fluvial processes could have played a role in providing the water required to form the ice-indicative landforms in the northern plains by looking at Rahway Vallis, as a possible source of water for the Amazonis and Arcadia Plantias. I published this in Icarus as first author in 2015 (DOI: 10..1016/j.icarus.2015.03.005). The contents of this manuscript remain unchanged with the exception of slight formatting alterations to allow for figure and table numbers to run consecutively with the rest of the thesis and slight changes to tense and first person singular and plurals where appropriate.

6.1. Ponding, draining and tilting of the Cerberus Plains; a cryolacustrine origin for the sinuous ridge and channel networks in Rahway Vallis, Mars.

J. D. Ramsdale [(1)], M. R. Balme [(1, 2)], S. J. Conway [(1)], C. Gallagher [(3)].

[(1)] Dept. Physical Sciences, Open University, Walton Hall, Milton Keynes, MK7 6AA (jason.ramsdale@open.ac.uk).

[(2)] Planetary Science Institute, Suite 106, 1700 East Fort Lowell, Tuscon, AZ, USA.

[(3)] UCD School of Geography, Planning & Environmental Policy, University College Dublin, Dublin, Ireland.

Keywords: Geological processes, Mars, Mars surface, Tectonics, Terrestrial planets.

6.1.1. Abstract

Rahway Vallis sits within a shallow basin (the "Rahway basin") in the Cerberus Plains of Mars containing a branching network of channels converging on the basin floor. Using topographic cross-profiles of the channels we have found that they are set within broader, subtly-expressed, valleys. These valleys are shallow (around 15 metres vertically compared to several kilometres in the horizontal) and have convex to rectilinear slope profiles that are consistent in form across the whole Rahway basin. Both channels and valleys descend and deepen consistently from west to east. The channels typically widen down-slope and

increase in width at confluences. The morphology and topology of this channel system are consistent with formation by contributory fluid flow, generated from many distributed sources. The transition between the older heavily cratered terrain and the floor of the Rahway basin is bounded by near-horizontal continuous topographic terraces. Plotting the elevation of the terraces shows that they conform to a plane with a height difference of around 100 m east to west for the 300 km width of the Rahway basin. We calculate that the volume of material needed to fill the topography up to the level of the plane best fit by the terraces is ~1500 km^3. Bordering the channels are sinuous ridges, typically several kilometres long, 20 m across, with heights on the order of 10 m. They sometimes form branching networks leading into the channels, but also occur individually and parallel to the channels. The multiple tilted terraces, the channel/valley network with many fluvial-like characteristics, and the distributed source regions, suggest that the landforms within the Rahway basin are unlikely to have formed through purely volcanic processes. Rather, the channels within the Rahway basin are consistent with a genesis requiring the flow of liquid water, and the sinuous ridges with melting of a static ice body that occupied the basin. We suggest a hypothesis of rapid basin filling by fluvial flooding, followed by lake drainage. Drainage could have occurred as a consequence of an ice or debris-dam failure within (or during the formation of) the large, nearby fluvial flood channel Marte Vallis. If the lake was partly or largely frozen prior to drainage, this offers a possible explanation for the sinuous ridge systems. Hence, although the sinuous ridges provide some of the most compelling morphological analogues of terrestrial eskers yet observed, we conclude that the contextual evidence for this interpretation in Rahway Vallis is not strong, and instead they are better explained in the context of a frozen or partially frozen lake or cryolacustrine model.

6.1.2. **Introduction**

Rahway Vallis, located at 10° N 175° E, is a valley network within the Cerberus Plains in the Elysium Planitia region of Mars (Figure 6.1). The system was described by Head and Kreslavsky (2001) , who identified shallow v-shaped valleys in the Mars Orbiter Laser Altimeter (MOLA) data of this region. Burr (2002a) and Plescia (2003) noted that several of the valleys extend westward 450 km into the late Amazonian Cerberus Fossae unit (AEc2; Tanaka et al., 2005; grouped into the late Amazonian volcanics unit, lAv, in the global map(Kenneth L. Tanaka et al., 2014) that stands around 10–20 m above a younger infilling unit (AEc3) (also grouped into the late Amazonian volcanics unit, lAv, in the global map Tanaka et al., 2014) within Marte Vallis. Plescia (2003) determined that the valley network was older than AEc3 due to cross-cutting relationships and identifies "several major branches forming a well-defined dendritic pattern". Rahway Vallis itself is therefore best described as a branching valley network that is around 450 km in length and 300 km wide and which is amongst the youngest terrain features in the area. Rahway Vallis is situated in low-lying terrain bounded to west, north and east by older highlands, and to the south by the flood-carved channel system Marte Vallis (Figure 6.1). We refer to the low-lying area in which Rahway Vallis sits as the “Rahway basin”. The majority of the boundary is determined by where the Cerberus plains meets the outliers of Nepenthes Mensae Unit (HNn; Tanaka et al., 2005; grouped into the Hesperian and Noachian transition unit, HNt, in the global map Tanaka et al., 2014); the southern boundary is defined as where Marte Vallis truncates the Rahway basin and then tracing along the Cerberus fossae. The fossae boundary is somewhat arbitrary and has been mainly used as an aid to describing this area specifically as opposed to the Cerberus plains in general.

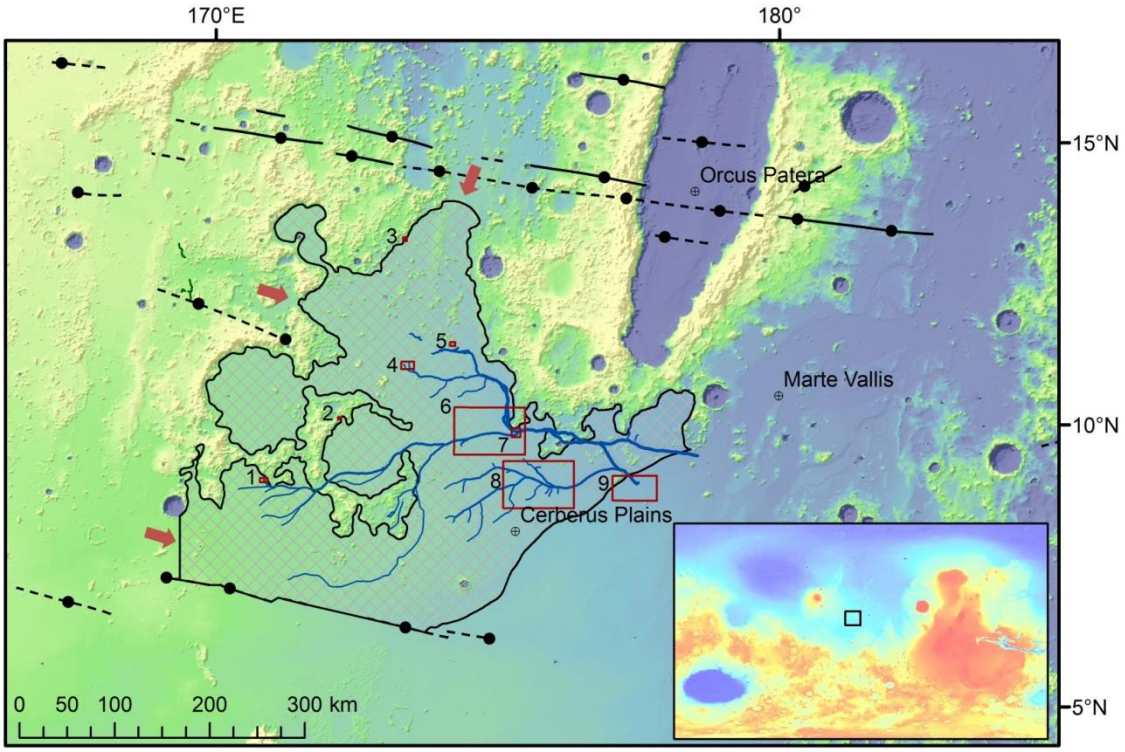

Fig 1. Regional context map of Rahway Vallis, Rahway basin and Marte Vallis with MOLA colour coded elevation in the background (blue ≈ -3000 m; yellow ≈ -2000 m). The solid black line filled with light-grey hatching represents the approximate boundary of the Rahway basin. Blue lines show the locations of the channels within Rahway Vallis identified in this study with increased thickness representing higher stream orders. The Cerberus Fossae are marked by noded lines with solid black lines where fresh and dashed black lines where subdued. The red arrows mark possible inlets for the Rahway basin. Insert: Near global MOLA elevation map (blue ≈ -5000 m; red ≈ 16000 m) showing the location of the study area; the blue crater to the south-west is Hellas. (North is up in this figure and all following figures unless otherwise stated). Box 1- Location of Figure 6.9a. Box 2- Figure 6.3a. Box 3- Figure 6.15. Box 4- Figure 6.9b. Box 5- Figure 6.3b. Box 6- Fig's 12a and 13a. Box 7- Figure 6.8. Box 8- Figure 6.14a. Box 9- Figure 6.10.

6.1.3. **Background**

The Cerberus Plains, in which the Rahway basin lies, are thought to be composed of late Amazonian lavas (Berman and Hartmann, 2002; W. L. Jaeger et al., 2010; Page, 2010; Plescia, 2003; Tanaka et al., 2005), although there have been other interpretations involving once ice-rich basaltic sediments (Brakenridge, 1993; Murray et al., 2005; Page, 2007). Prominent features of the Cerberus Plains include the "Cerberus Fossae"; extensional en-echelon fracture systems with individual factures being up to several hundred kilometres in length and a few hundred metres wide (Figure 6.1). The Cerberus Fossae have been identified as a possible source of both lava and water outbursts onto the Cerberus Plains (Balme et al., 2010; Berman and Hartmann, 2002; Burr et al., 2002a, 2002b; Head and Kreslavsky, 2001; W. L. Jaeger et al., 2010; Page, 2010; Plescia, 2003; Thomas, 2013) and hence could provide the source for the formation of Rahway Vallis, either as point sources of ground water release or vents for highly mobile lava flows. The rocks cropping out in large impact crater rims that bound the Rahway basin are mapped as the Nepenthes Mensae Unit, described as knobs and mesas of highland rocks inferred to be Early Hesperian to Early Noachian in age (Tanaka et al., 2005).

In addition to the valley and channel network, we have identified a series of sinuous ridges (*Figure 6.2*) in the Rahway basin. The branching pattern of this ridge network is reminiscent of fluvial systems on Earth, although the branching landforms are in positive relief in the case of the Rahway Vallis ridge systems. The term sinuous ridge has been used by a number of authors (e.g., Kargel and Strom, 1990) to describe elongate, positive relief landforms that occur on the Martian surface. The sinuous ridges described by Kargel and Strom (1992, 1991, 1990) in the Argyre Planitia are one of the most diagnostic glacial features found on Mars. Kargel and Strom (1992) note that the sinuous ridges are identified alongside features interpreted to be tunnel valleys, outwash plains, rock glaciers, kettle holes, kames and glacial grooves. Various other modes of origin have been proposed for

these sinuous ridges including wrinkle ridges (Tanaka and Scott, 1987), exhumed igneous (Carr et al., 1980) and clastic (Ruff and Greeley, 1990) dykes, lava flow features (Tanaka and Scott, 1987), linear sand dunes (Parker et al., 1986; Ruff, 1992), lacustrine spits or barrier bars (Parker, 1994; Parker et al., 1986; Parker and Gorsline, 1992), glacial moraines (Hiesinger and Head III, 2002; Kargel, 2004), inverted stream topography (Howard, 1981; Rice and Mollard, 1994), frozen waves within a mudflow (Jons, 1992)but the most often cited explanation is that they are eskers (Carr et al., 1980; Hiesinger and Head III, 2002; Howard, 1981; Kargel, 2004; Kargel and Strom, 1992, 1990; Metzger, 1992, 1991; Nussbaumer et al., 2000; Ruff and Greeley, 1990).

It is worth noting that the majority of interpretations were suggested during the Viking era using images with 50-100 metres per pixel resolution. Since then, higher resolution images have become available, such as the 6 metre per pixel Context Camera (CTX) and the 25 centimetre per pixel High Resolution Imaging Science Experiment Camera (HiRISE) data, from the Mars Reconnaissance Orbiter (MRO) spacecraft, which has been operational since 2006. Post 2006, the debate on the dominant active process has been centralised around the two main contrasting theories of fluvioglacial (Banks et al., 2008; Burr et al., 2009b; Fassett et al., 2010; Hubbard et al., 2011; Souness and Hubbard, 2012) and igneous hypotheses (e.g., W.L. Jaeger et al., 2010).

The Aeolis and Zephyri Plana region to the south of Marte Vallis host an extensive population of sinuous ridges (Burr et al., 2010, 2009b; Pain et al., 2007) clustered preferentially in the lower, hence older, member of the Medusa Fossae Formation around the global dichotomy boundary. Trending from high to low elevations with distinct fluvial morphologies these ridges are inferred to have been formed by flowing water (Burr et al., 2010, 2009b). The sinuous ridges in the Aeolis and Zephyri Plana region have sinuosity values up to 2.4 and are up to hundreds of kilometres in length, a kilometre in width and tens of metres in height (Burr et al., 2009b). The sinuous ridges in the Aeolis and Zephyri

Plana region have been interpreted as inverted fluvial channels (Burr et al., 2010, 2009b; Zimbelman and Griffin, 2010). The majority of these ridges are inferred to have been formed through precipitation-driven channel development with subsequent induration, burial and exhumation by aeolian abrasion resulting in inverted fluvial channels (Burr et al., 2010, 2009b; Pain et al., 2007).

Given the variety of interpretations proposed for sinuous ridges on Mars and the number of sinuous ridges identified in Rahway Vallis it is entirely possible that there could be a number of processes occurring on Mars that are producing forms that look very similar when viewed from orbit. The inability to ground-proof favours an agnostic position, when reviewing geomorphic interpretations; this means in practice landforms must be viewed in a contextual setting, whereby the interpretation of several landforms supporting the same mode of origin is more reliable than an interpretation of a single form. In this paper we document the suite of sinuous ridges associated with Rahway Vallis and the wider Rahway basin with the aim of testing the hypotheses that these ridges and associated landforms are fluvial, glaciofluvial or volcanic in origin. Finally, continuous topographic steps occur at the margins of the Rahway basin and against geological inliers; we refer to these as terraces.

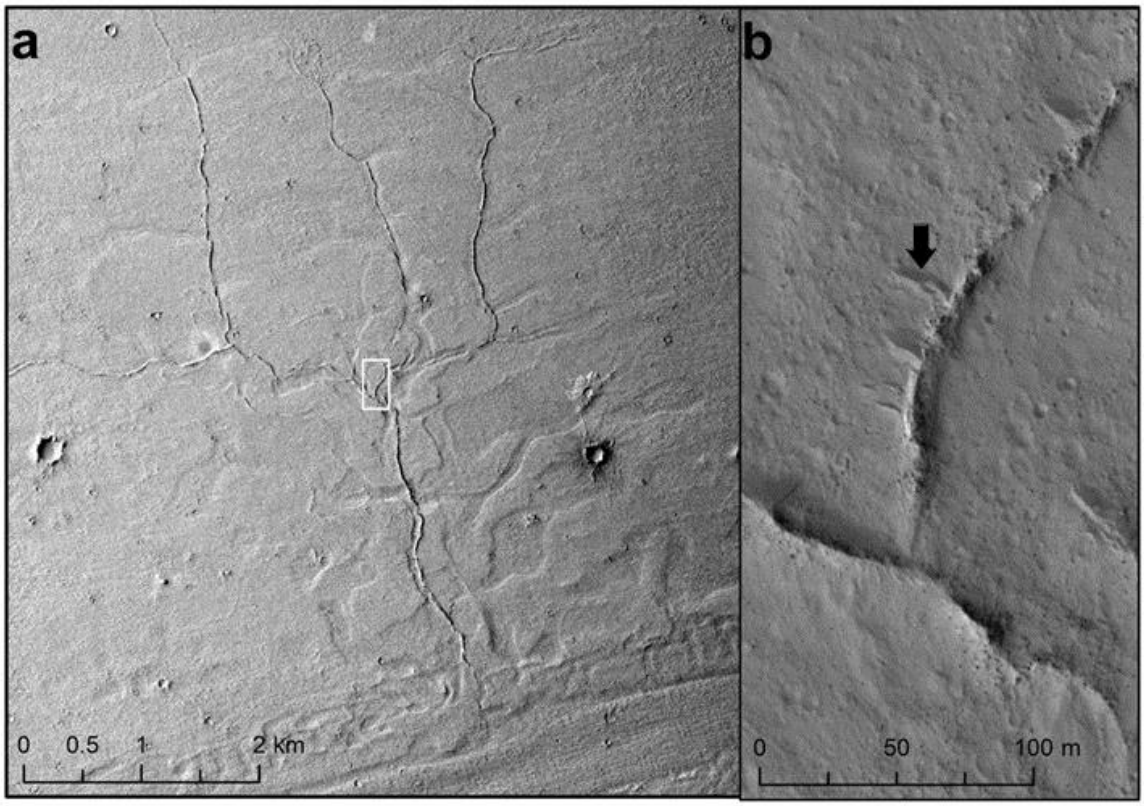

Figure 6.2 (a) CTX image G19_025538_1899_XN_09N185W showing an example of a sinuous ridge network in the Rahway basin and (b) HiRISE image ESP_025538_1900 of the same ride close-up. The white box in (a) shows the location of (b). The black arrow in (b) shows short >50 m, straighter ridges that we infer to be aeolian landforms.

6.1.4. **Data and Methods**

Geomorphological analysis and mapping were performed primarily using publically available Context Imager (CTX; ~6 m/pixel; Malin et al., 2007) and High Resolution Stereo Camera (HRSC;12 m/pixel; Neukum and Jaumann, 2004) images where possible. CTX images were downladed pre-processed directly from the Arizona State University Mars Portal and inserted into ArcGIS 10.1 software. MOLA gridded and point data, THermal EMission Imaging System (THEMIS; Christensen et al., 2004), HRSC and High Resolution Science Imaging Experiment images (HiRISE; McEwen et al., 2007) were downloaded from the Planetary Data Systems' Geosciences Node, Mars Orbital Data

Explorer (ODE). An equicylindrical projection centred on 5° N 175° E was used when digitising to minimise projection distortion across the study area.

Mars Orbiter Laser Altimeter (MOLA; Smith et al., 1993) data, with around 1 m vertical accuracy, around 150 m surface spot size point data and around 300 m along-track spacing, were used to create along track topographic profiles. Topographical analysis was done along MOLA tracks to give the maximum resolution, with around 50 points per valley profile and 10 points across wider channel profiles, and to ensure interpolated data were not used. The official MOLA gridded data set was downloaded from ODE and has a resolution of around 460 m/pixel across the Rahway basin. All elevations are presented with respect to the Mars datum**.**

We used a combination of MOLA or HRSC shaded relief maps and image data to identify and map the channel system. The whole of the Rahway basin was systematically searched for ridges in CTX or HRSC imaging data and any discrete topographical ridges and terraces were digitised in ArcGIS. Flow direction maps were made using the ArcGIS d8 single flow direction tool on the gridded MOLA topography raster.

6.1.5. **Observations**

6.1.5.1. ***Terraces***

The transition between the steep, heavily cratered Nepenthes Mensae Unit and the Rahway basin is often bounded by near-horizontal topographic steps (Figure 6.3). These steps appear continuous around the basin's margin and are present in almost all locations where CTX images of the boundary are available. These steps are at altitudes between -3108 m and -2620 m with a mean of -3000 metres and a standard deviation of 68.7 metres, forming a consistent boundary around the Rahway basin. Inliers of highland terrain within the Rahway basin often have terraces at their base (e.g. Figure 6.3b).

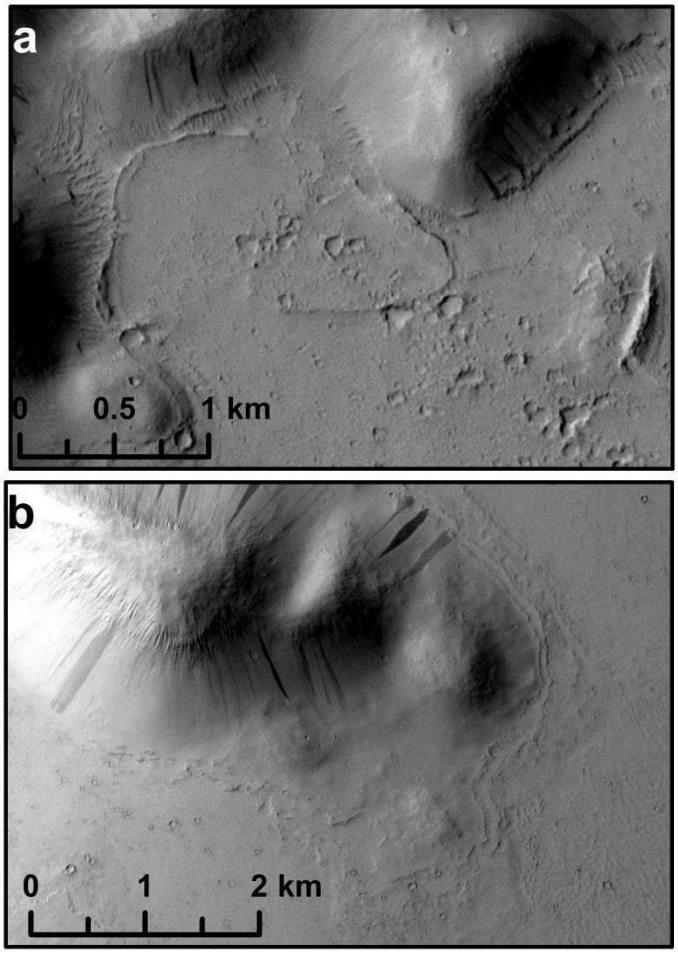

Figure 6.3 (a) CTX image P18_007882_1907_XN_10N187W showing terraces at the edge of the Rahway basin and (b) P19_008462_1896_XI_09N185W terrace around inlying hill of the Nepenthes Mensae Unit.

6.1.5.2. ***Rahway Vallis***

The term Rahway Vallis refers to the shallow v-shaped valley network in the MOLA data that lies within the area we refer to as the Rahway basin. Analysis of individual MOLA profiles shows that the well-defined channels, identifiable in CTX visible images, are themselves set within broader valleys that have almost no morphological expression, but which are apparent in derived topographic data products (Figure 6.4) and can be shown to be "v-shaped" in topographic profiles (Figs. 5, 6 and 7.). The valleys that form the Rahway Vallis network have concave-up, shallow (tens of metres deep compared to several kilometres wide) v-shaped profiles that are consistent in form across the Rahway basin.

Measured along the thalweg, the main branch of the channel and valley network is in excess of 500 kilometres long and shows an elevation drop of 200 metres from -2950 m at source to -3150 m at the point where it terminates at Marte Vallis (Figure 6.6). A plot of channel width to distance along the profile of the main channel shows a largely concave-up gradient indicating that the channel increases in width at an accelerating rate with distance, from around 100 metres at 'source' to around 4 kilometres just before it terminates (Figure 6.6). The branching patterned network has a minimum Strahler stream order of 4; finer channels may be present but are either infilled or too fine to be detectable. For ease of description, we refer to the hierarchy of the channels as stream orders; use of this term is not in itself intended to infer origin but rather give topological context. The confluence north of profile 'd' in Figure 6.5 shows the west-east branch to be infilled by a material with a depth of around 10 m where the north-south branch is relatively unfilled (Figure 6.8). The infill material also has a minor channel carved into it (Figure 6.8). The sinuosity of the channels is around 1.05 - 1.1. Junction angles between branches range from 10° to 90°, with the higher angles being consistent with fluvial networks on earth that have had insufficient time to erode shallower angled tributaries (e.g. Howard, 1971; Mosley, 1976) or are structurally controlled (Longwell et al., 1969).

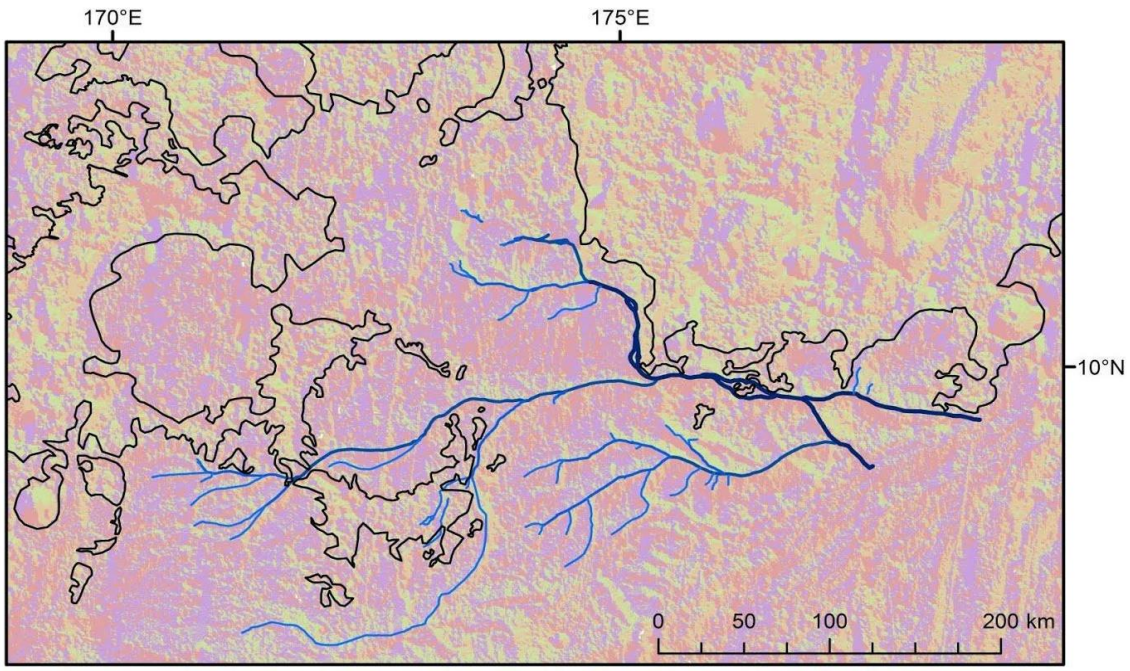

Figure 6.4 d8 single flow direction map derived from MOLA data at 460 m/pixel. The black lines represent the boundary between the Rahway basin and the steep heavily cratered Nepenthes Mensae Unit. The flow directions have been classified into four bins 45°-135° East (purple), 135°-225° South (green), 225°-315° West (red) and 315°-45° North (orange) . The blue lines show the location of Rahway Vallis, with higher Strahler stream orders having progressively darker and thicker lines. The predominantly west to east directed channels nearly always lie at the boundary between areas of northerly and southerly flow, meaning that the channels are located within topographic lows. Furthermore, the pattern of flow shows that the topography of the Rahway basin is consistent with a landscape in which non-channelized flow across the surface is contributory, and towards a well-defined (also contributory) channel network.

Figure 4 shows the mapped channel system and simulated flow directions highlighting that the valley system may continue several tens of kilometres upstream of where the visible channel terminates (especially in the south of the area).

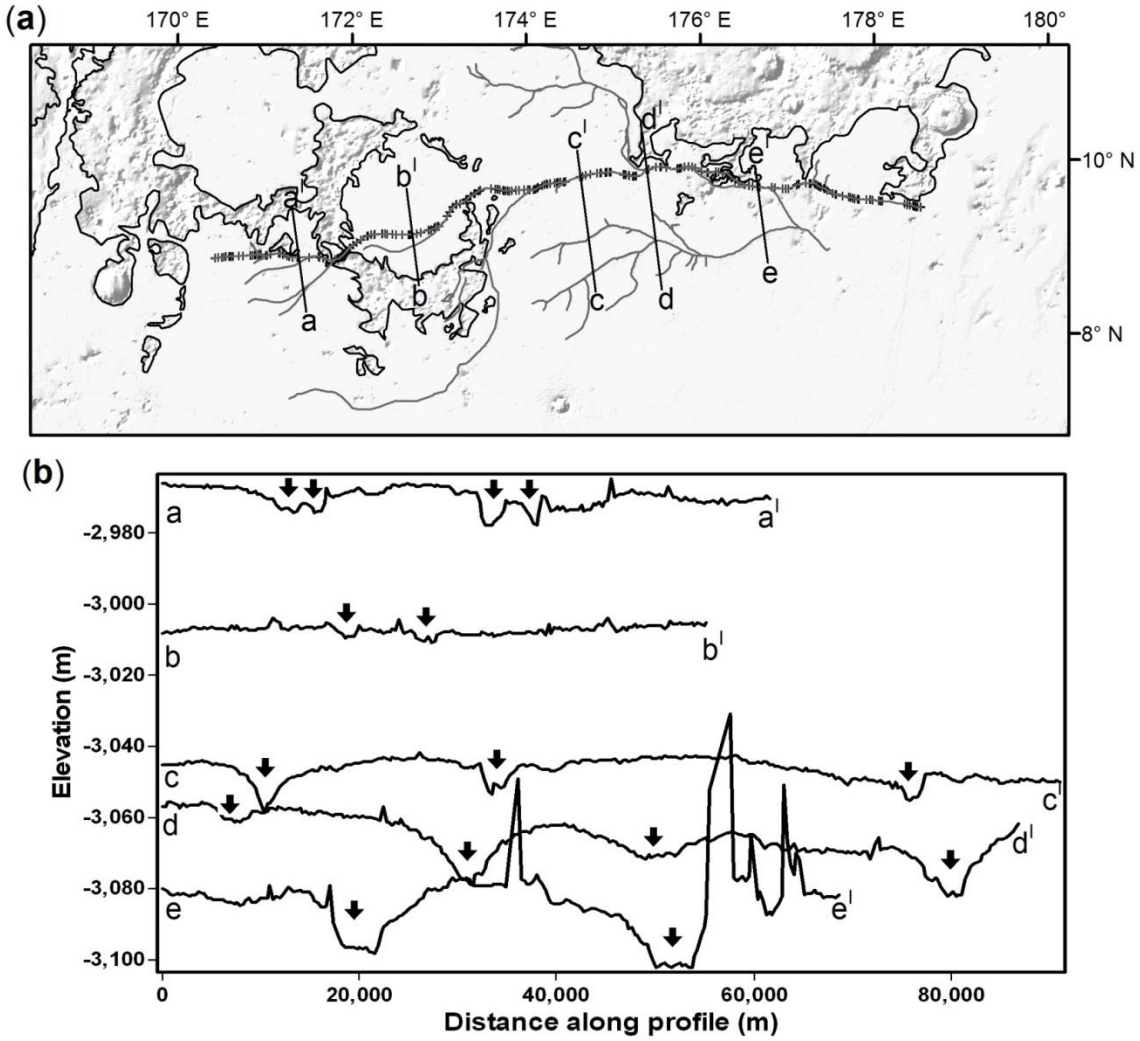

Fig 5. ***(a)*** *A map showing the channel system (grey lines). The black lines represent the boundary between the Rahway basin and the steep heavily cratered Nepenthes Mensae Unit. The black crosses (along the main channel) each mark the location of MOLA points within 100 metres of the main channel identified in Figs. 6, 7, 8. cross-channel profiles (aa' to ee') are shown in (b).*

(b) *Topographic profiles across the main branch of Rahway Vallis. Profile aa' is of orbital track 16891, profile bb' is of orbital track 18563, profile cc' is of orbital track 13533, Profile dc' is of orbital track 19945, and profile ee' is of orbital track 14690.. The major peak in profile e has been truncated to allow it to display on the scale of the graph. Black arrows mark the positions of channels in the cross-sections.*

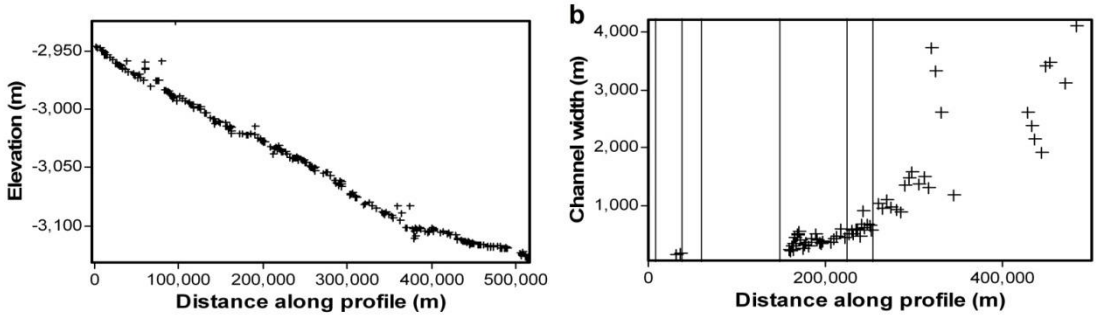

Figure 6.6 (a) Long profile of the trunk channel (marked on Fig.5 as black crosses) with each point on the graph representing a MOLA point within 100 metres of the channel centre. (b) Plot of width vs. distance west to east along the trunk channel, with each cross on the graph representing a measurement of width from CTX images. Vertical lines represent confluences along the profile.

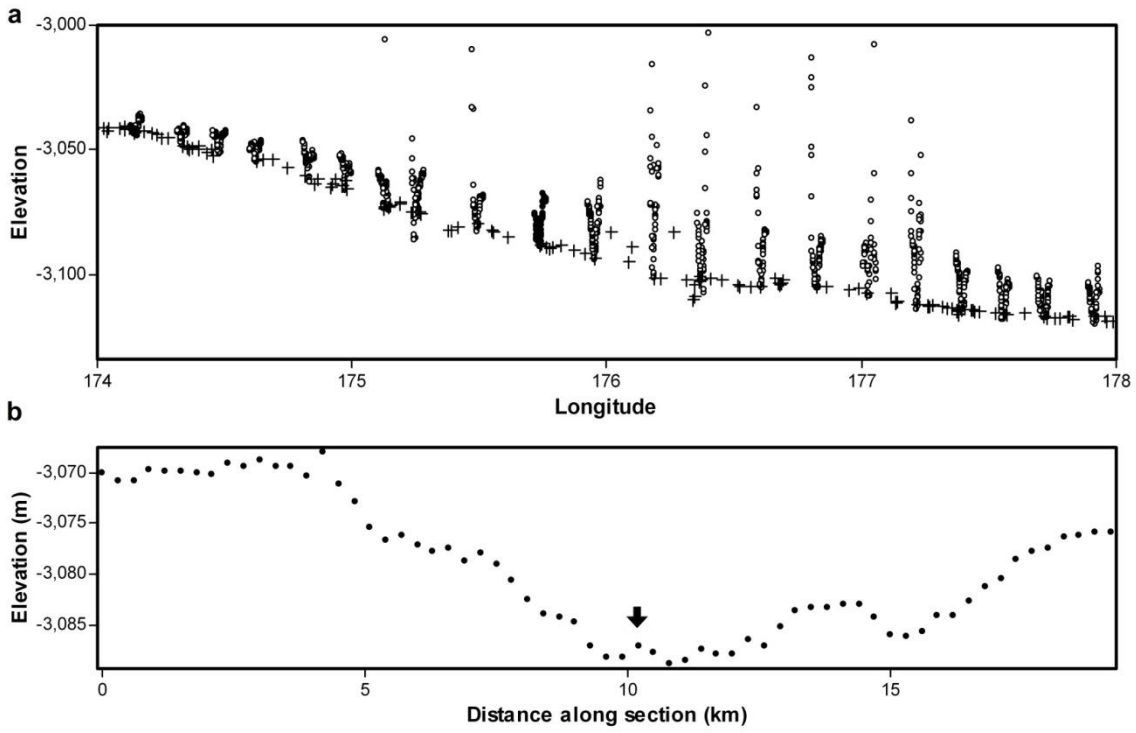

Figure 6.7 (a) Long profile of the middle and distal reaches of the main trunk channel floor compared to its banks. This plot includes all MOLA data points from a 10 km buffer either side of the channel. Data points from the buffer are shown by circles and the channel long profile data are shown with crosses and are also shown in Figure 6.5a.

Topography extracted from MOLA point data. The east-west orientation of the channel and the NNE azimuth of the MOLA tracks allow the v-shape cross sections of the valley to be seen when topography is plotted against longitude. (b) A cross profile at around ~175.8° (MOLA track: 11068) of the example channel highlighted by black circles in (a). Note the possible ridge of infilling material in the bottom of the channel marked by the black arrow.

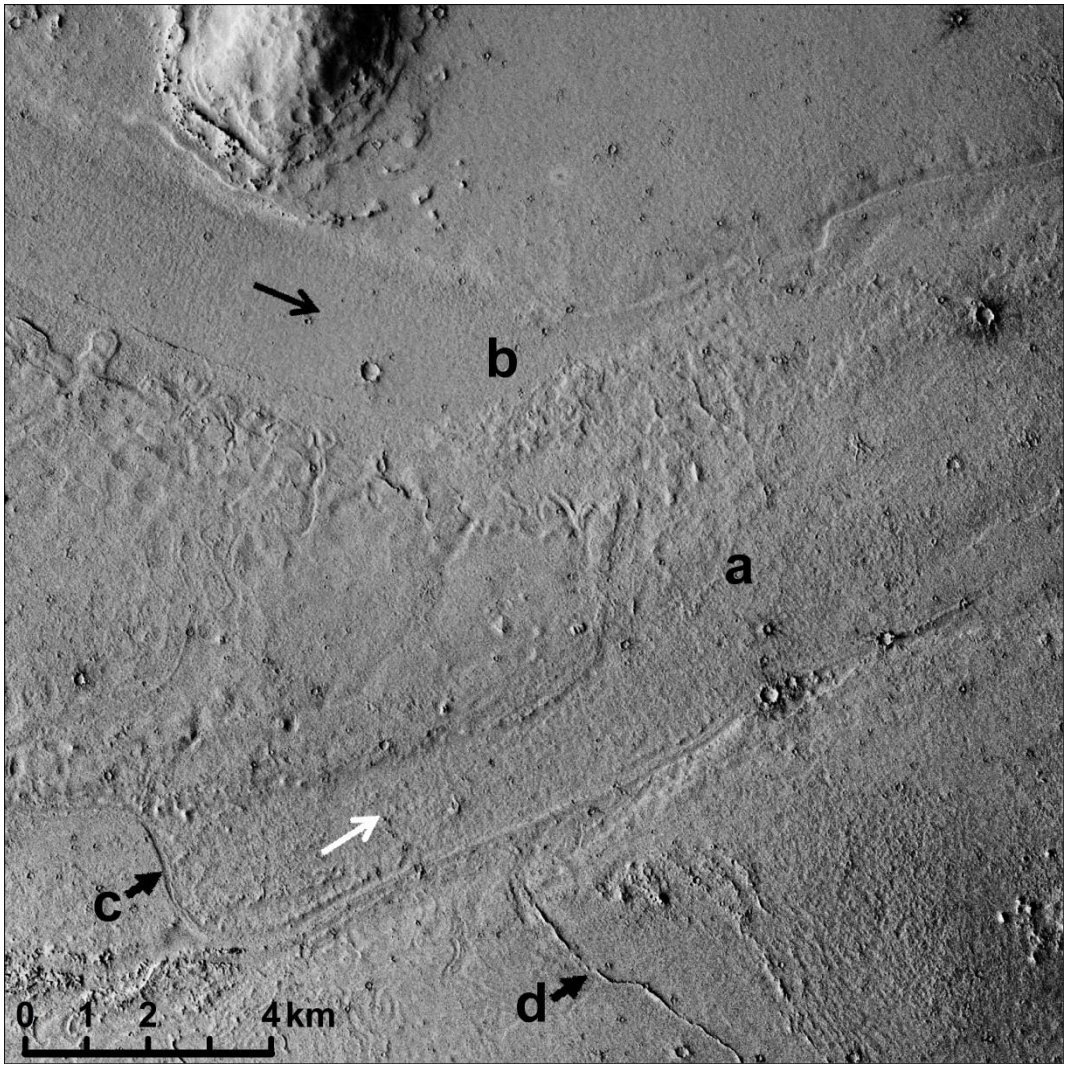

Figure 6.8 CTX Image P04_002423_1904_XI_10N184W showing the confluence north of profile 'd' in Figure 6.5. The west-east branch (white arrow) appears to be infilled by around 10 m of material (measurement derived from MOLA point data) where the north-south branch (black arrow) is relatively unfilled. (a) Infilling Material. (b) Unfilled channel. (c) Small channel carved into the infilling material. (d) Sinuous ridge.

Most of Rahway Vallis' tributaries (where the start of the channel can be identified in CTX or higher resolution imagery) have abrupt beginnings with no visible sources (Figure 6.9). In some cases, there is a gradual transition from a featureless background terrain to what seems to be quite a wide and well-developed channel. This could be due to subsequent channel fill and/or bank erosion, or, perhaps, the flow that fed into them was never properly channelised and progressed as overland flow upstream of the observed channel. For the most part, the banks either side of the channel are smooth textured (with the exception of impact craters) and have low relief.

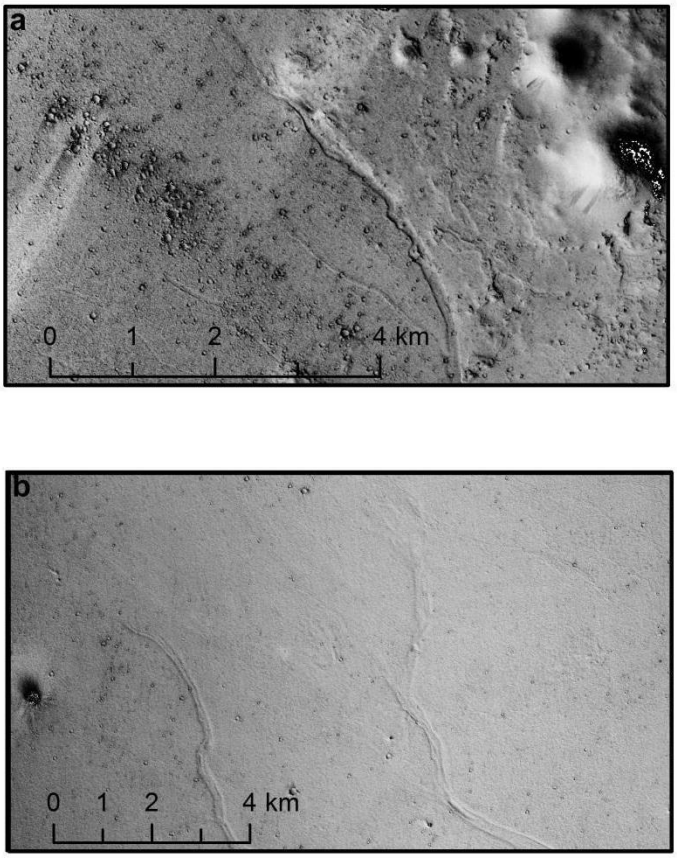

Figure 6.9 Head regions of Rahway Vallis' tributaries. (a) CTX image B10_013710_1894_XN_09N189W and (b) G23_027371_1920_XN_12N187W show examples of channel head regions where the channel has a distinct start, but with no obvious source.

The Rahway Vallis channel and valley systems terminate where two main branches meet the channel system of Marte Vallis. These terminations appear subdued due to a later event that infilled much of Marte Vallis. Some of this material seems to have back-filled part of Rahway Vallis (Figure 6.10). At its terminus the Rahway channel is around 6 km wide and only 1 m deep. The infilling material has a rough textured platy upper surface and a low albedo in comparison to the upstream portion of the channel that does not show a platy texture. The junction angles between the terminations of the channel system in Rahway Vallis and the channel in Marte Vallis are around 90°.

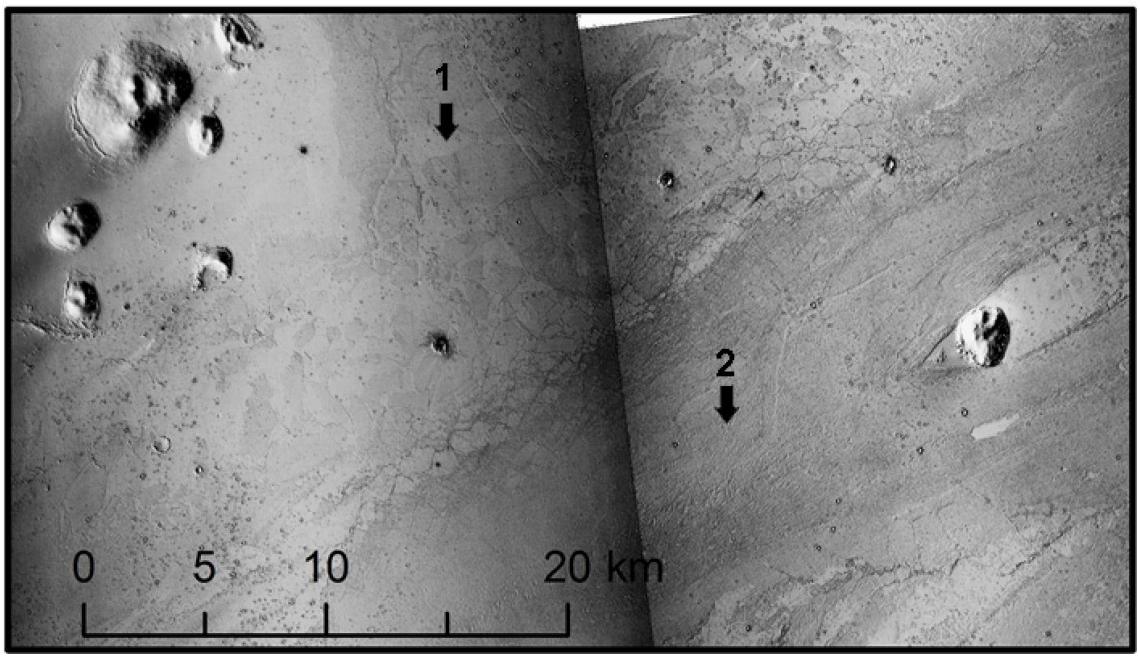

Figure 6.10 CTX images P06_003346_1874_XN_07N182W and P02_001790_1871_XN_07N182W showing the termination of Rahway Vallis (arrow 1; flow north to south) at Marte Vallis to the south (arrow 2; flow west to east). Given that this material is absent for the most part in Rahway Vallis and prominent in the majority of Marte Vallis, it seems likely that this platy-ridged material appears to have flowed northwards into the terminal regions of Rahway Vallis.

6.1.5.3. ***Sinuous Ridges***

The sinuous ridges in the Rahway basin are elongate linear to curvilinear positive-relief landforms that are distinct from the short (< 50 m), straighter features we infer to be of aeolian origin (Figure 6.2b). The locations of all the sinuous ridge landforms we have identified are shown in Figure 6.11. The vast majority of the ridges found in the Rahway basin are a few tens of metres in width and show an approximately constant width along their length. They are around 4-5 metres high based on shadow length measurements, and do not appear to change in width when they merge or where branches occur (Figure 6.12). Crest morphology is variable, displaying a continuum between sharp and rounded crests in contrast to the broad flat ridges inferred to be a result of sapping (e.g., Harrison et al., 2013) and lava/fluvial-conglomerate capped inverted channels (Burr et al., 2009b). Sinuous ridges occur throughout the Rahway basin and have not been found in the surrounding Nepenthes Mensae Unit. The sinuous ridges occur in three main settings, each of which has a distinctive ridge morphology and network topology, but they are grouped mainly for ease of description. We refer to these groups as: central Rahway, southern Rahway, and basin marginal.

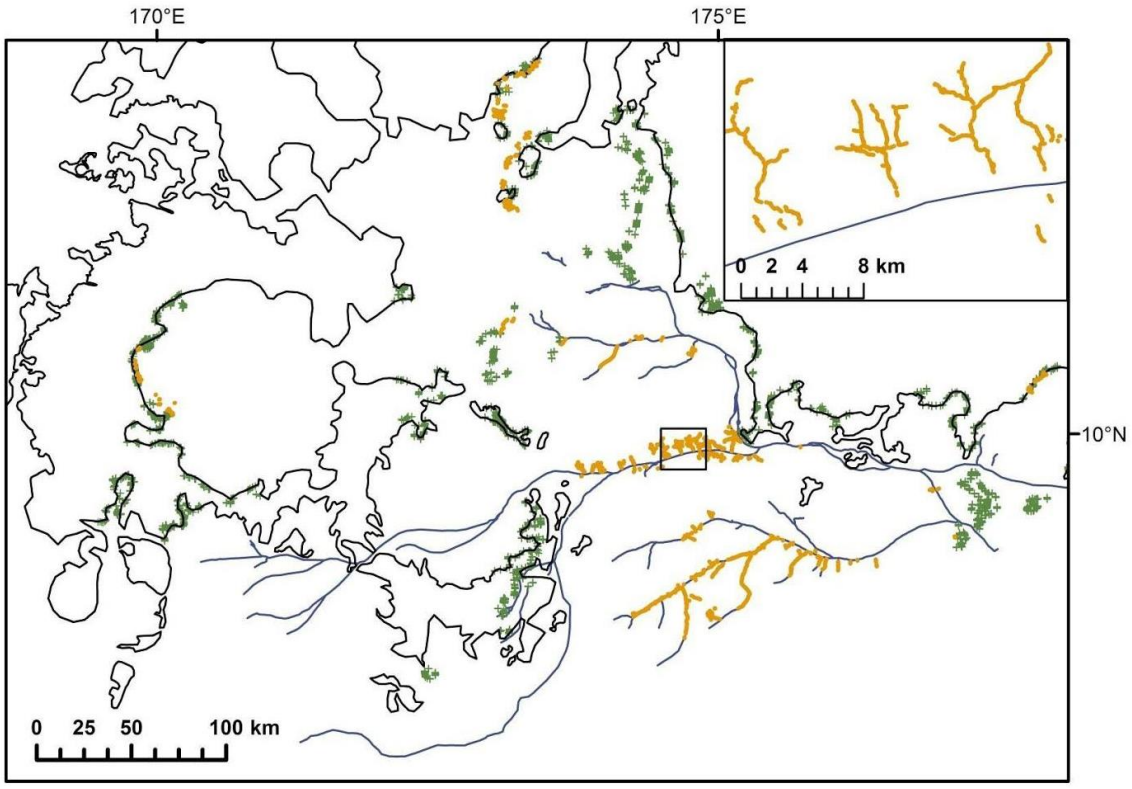

Figure 6.11 A sketch map to show the location of all sinuous ridges *in Rahway basin. The continuous black line is the outline of the Rahway basin, orange lines are the locations of the* sinuous ridges*, blue lines represent the channels and the green crosses show the locations of MOLA points where terraces have been identified. Insert shows network patterns of the central Rahway ridges.*

6.1.5.3.1. Central Rahway.

The sinuous ridges in central Rahway are curvilinear features, up to 3 km in length and around 15 m in width (Figure 6.12), that intersect at moderate to high angles and form branching patterns reminiscent of a contributory fluvial network. If this same pattern were seen in a fluvial network, the network would have a minimum Strahler stream order of 3-4 before it intersects with the main channel network. Individual ridges often seem to form en-echelon segments, and the intersections between the ridges can include gaps of tens of metres (Figure 6.12c) between sections. Individual ridges often have a higher proportion of boulder sized clasts than the surrounding materials (Figure 6.12d) but it is unclear as to

whether these boulders formed in-situ due to weathering of the ridge or were transported and deposited here.

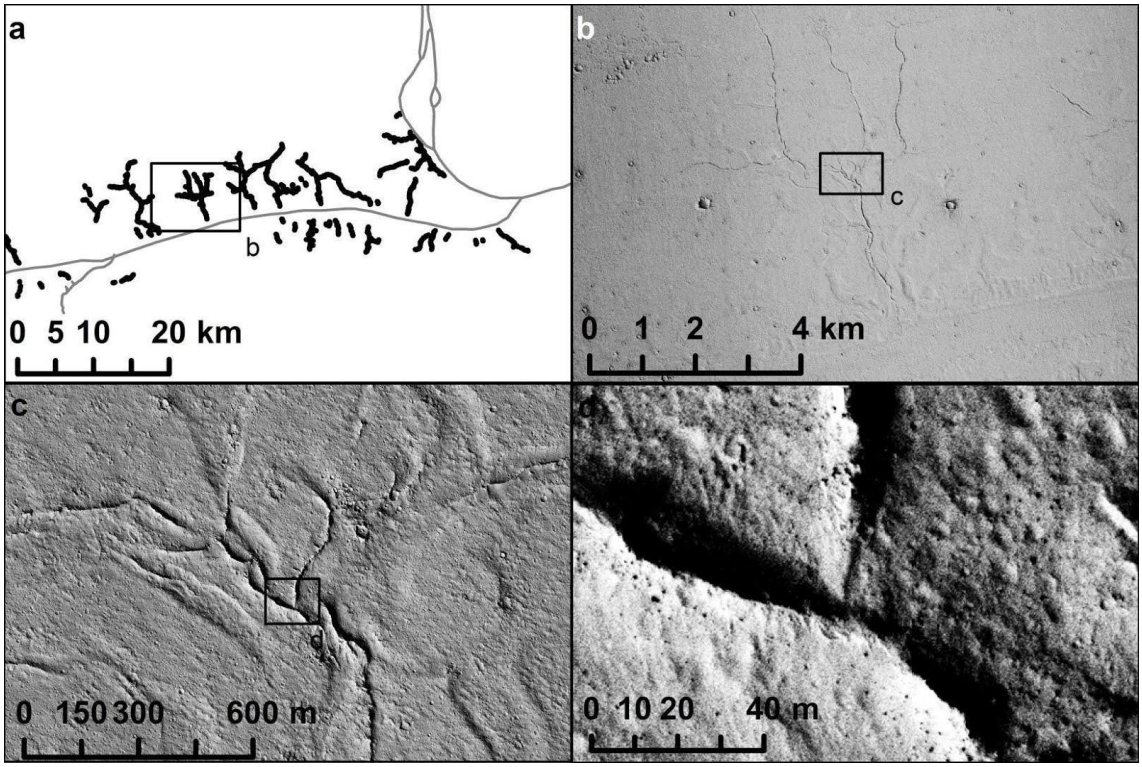

Figure 6.12 (a) is a sketch map of the locations of the ridges in central Rahway, grey lines represent channels and black lines represent sinuous ridges, (b) CTX image P07_003623_1903_XN_10N185W shows an example of the planform network, (c) HiRISE image PSP_003623_1900 shows an example with gaps between the branches, (d) HiRISE image PSP_003623_1900 shows boulders on the ridges.

Many of the branched sinuous ridges 'feed into' one of the larger Rahway tributary channels or the main trunk. The intersections with the Rahway channels are nearly always at angles close to 90° (Figure 6.13b). Although ridges can be found on both sides of Rahway channels there is no evidence that they have been crosscut by the Rahway channels, but rather they appear to be feeding into the main channel. In rare cases, a ridge makes a sudden almost 90° turn as it meets the main channel and then begins to follow the channel margin (Fig 13c) downstream. In general, the ridges tend to terminate at, or just

prior to, the channel margins (Figure 6.13a). Away from the Rahway channels, the sinuous ridges often lie within discontinuous troughs that themselves appear to have a somewhat contributory pattern similar to the sinuous ridge system (Fig 13d). Although the sinuous ridges appear to cross-cut the trough boundaries in places, it is unclear in the coarse MOLA topography whether the sinuous ridges actually cross topographic divides or whether the gradient is always downstream.

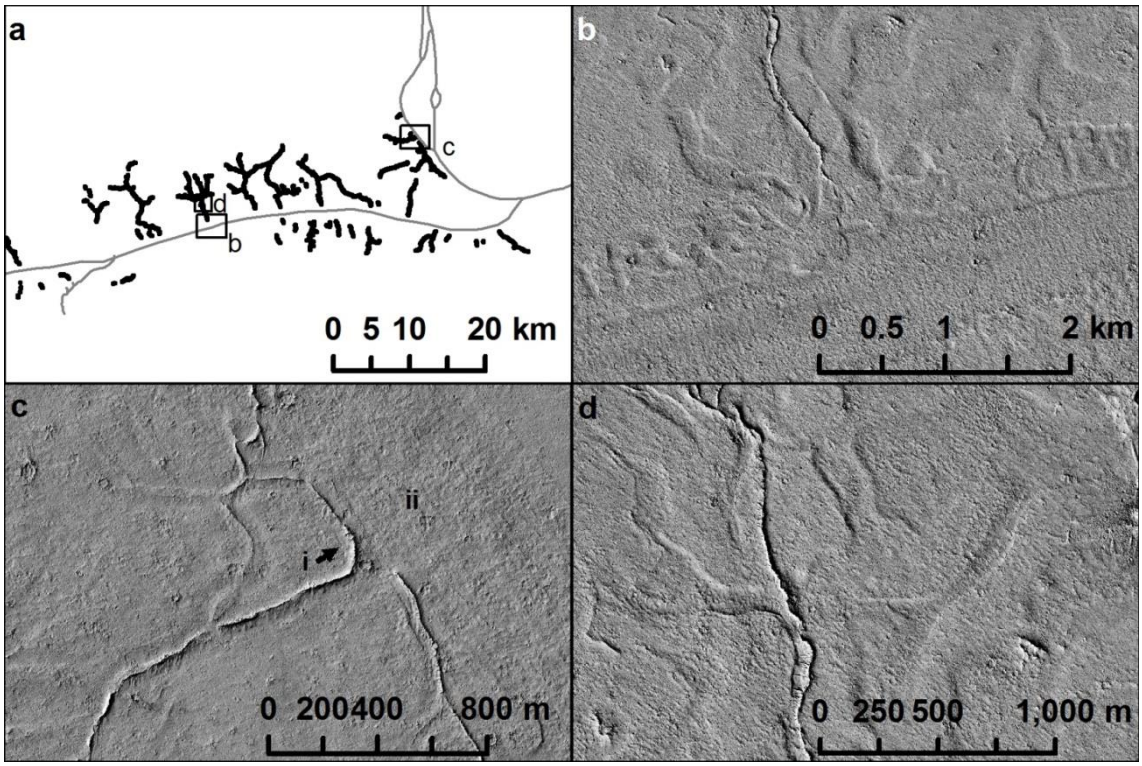

Figure 6.13 (a) is a sketch map of the locations of the ridges in central Rahway, grey lines represent channels and black lines represent sinuous ridges*, the locations of parts (b-d) are indicated by black boxes. (b), HiRISE image PSP_003623_1900 shows intersection of ridges with Rahway channel and shows some pitting on the channel margins, (c) HiRISE image PSP_003623_1900 shows a ridge (i) turning to parallel to the channel (ii), (d) HiRISE image PSP_003623_1900 shows trough examples.*

The topographic data (Figure 6.5 profile c) shows what could be a discrete, central ridge in the main channel that could not been identified in the CTX images. This ridge contains no clasts that can be seen in HiRISE images (25 cm/pixel). The inter-channels in parts of this region appears to dip away from the channel (Figure 6.5 profile c), much like terrestrial floodplains on which levees slope away from the channel (e.g. Filgueira-Rivera et al., 2007).

6.1.5.3.2. Southern Rahway.

The sinuous ridges located in the south of the Rahway basin appear to feed into wider, longer ridges that run along the low points of shallow valleys. The main ridges are around 100 km in length and around 100 m wide and unlike the lower order ridges they appear to widen noticeably at major intersections (Figure 6.14c). The individual ridges range in form from flat-topped with sharp medial edges to rounded sloping crests. The larger ridges sometimes have parallel channels on either side and often appear to grade between positive and negative relief. The largest of these features (Figure 6.14b) continues as a ridge with twin parallel channels on either side for around 100 km, displaying apparent confluences with sinuous ridges and also other larger ridges before degrading and continuing as a single channel that eventually terminates at Marte Vallis.

The lower order sinuous ridges intersect at around 60-90° to form what appears to be a contributory network (inferred downstream flow from MOLA topography) with minimum Strahler Stream orders up to 2-3. However, these branched-ridge-terminating sinuous ridge networks are less densely distributed than those in Central Rahway and usually only thin, singular, discontinuous sinuous ridges intersect with the main ridge. The confluences do not appear to be separated by a gap between the sinuous ridge and the main Rahway channel, unlike the Central Rahway sinuous ridges. Individual clasts up 6 m across can be identified on the ridge in HiRISE images. The southern Rahway sinuous ridges generally lie within continuous troughs, giving the appearance of twin parallel channels. These

sinuous ridges do not trend across troughs boundaries and do not cross topographic divides "flowing" only "downstream". These branched networks largely intersect a main ridge (also with twin parallel channels) at angles close to 90°.

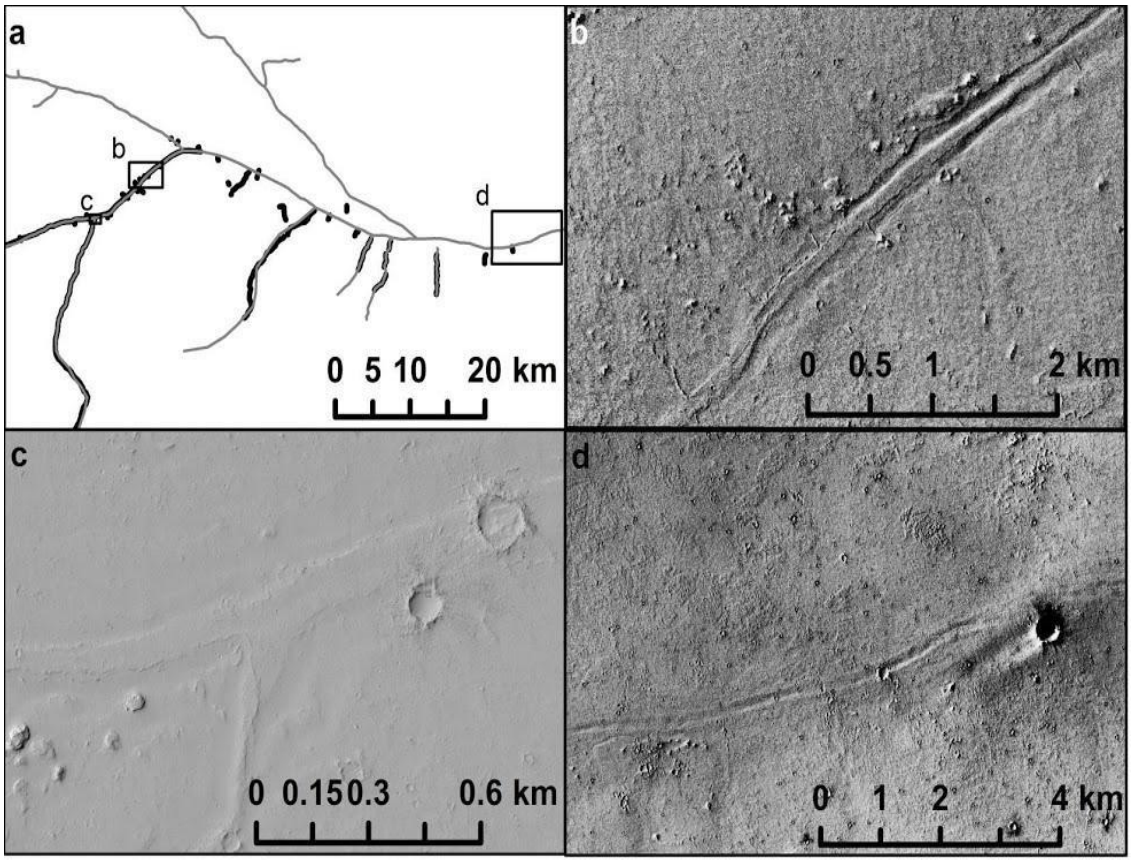

Figure 6.14 (a) Sketch map showing the ridge-terminated branched network showing the locations of parts (b-d). Grey lines represent channels and black lines sinuous ridges. *(b) CTX image P20_008897_1889_XN_08N184W showing a main ridge from the ridge-terminated branched network with associated twin parallel channels. (c) HiRISE image PSP_009253_1890 showing a confluence between two major ridges in the ridge-terminated branched network. (d) CTX image B01_009965_1889_XI_08N183W showing the negative relief that can be observed in the downstream section of the ridge-terminated branched network.*

6.1.5.3.3. Basin-marginal regions.

Sinuous ridges (Figure 15) have been observed to occur perpendicular to the strike of the slopes associated with impact craters and their ejecta, the basin-marginal terraces and outliers of the surrounding Nepenthes Mensae Unit. The ridges are on the order of 15 m across, 10 m high and around 500 m long. These sinuous ridges are narrow and largely sharp crested, and rarely branching. Some are spatially associated with dune and/or yardang fields and can often be traced into the inferred dune and/or yardang field where they become indistinguishable from the aeolian features.

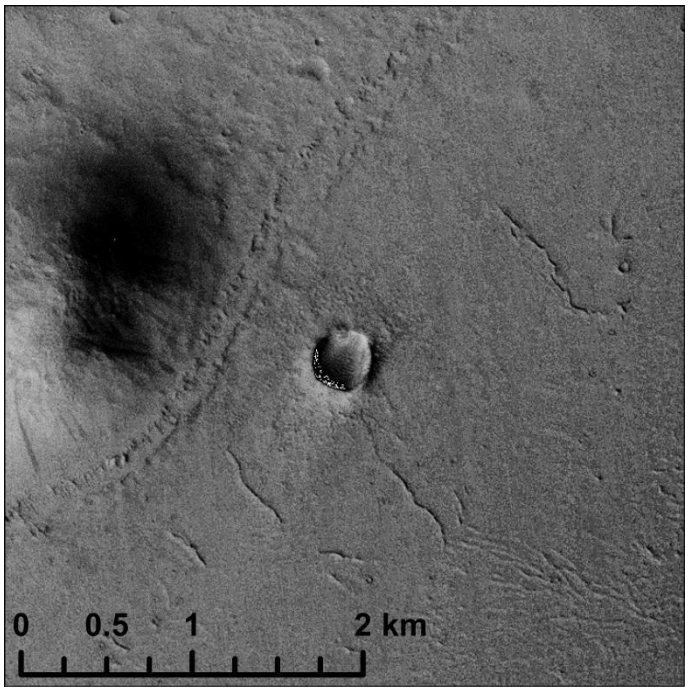

Figure 6.15 CTX image P08_004045_1921_XN_12N186W showing basin marginal ridges.

6.1.5.4. ***Bank Morphology***

For ease of description we refer to the areas between the channels within the Rahway basin as banks; use of this term is not in itself intended to infer origin but rather give topological context. The banks show three main texture types: smooth, platy-ridged (see Figure 6.10 and Balme et al., 2011; Keszthelyi et al., 2004) and pitted (see Figure 6.13b). Large areas of the Rahway basin are extremely smooth in appearance in CTX images and show very

little relief other than that of impact craters and large boulders and aeolian deposits observable in HiRISE images. The platy-ridge terrain is similar in appearance to that of the material that appears to be filling large parts of the Elysium basin (e.g. Tanaka et al., 2005) and surrounding flood channels (Keszthelyi et al., 2004, 2000) . The plates range in size from a few tens of metres to over tens of kilometres in size. The surface shows signs of breakup, rotation and collision and on the whole the present pattern can be reassembled to an unbroken form (Balme et al., 2010; Murray et al., 2005). This has been inferred to be the upper surface of a lava flow (e.g. Keszthelyi et al., 2004, 2000; Plescia, 2003) and a frozen sea (e.g. Murray et al., 2005) in the literature. Where plates have drifted into topographic obstacles, crumpled rubble piles and linear flow shadows have formed on the stoss and leeward sides respectively. This platy-ridge surface often forms the banks of the channel and ridge network in the Rahway basin suggesting that the platy-ridged material at least in part predates the valley and ridge network. If the impact crater counting dates of the platy-ridged material in the Cerberus plains are accurate (Berman and Hartmann, 2002; Vaucher et al., 2009a, 2009b) and the ridge and channel network postdates the platy ridge material the processes to have formed the ridge and channel network are likely to have occurred in the very late Amazonian. However, if the ridges were formed through exhumation the structures themselves would be difficult to date, but the exhumation must have occurred in the very late Amazonian as none of the ridges appear to be dissected by impacts.

6.1.6. **Topological analysis of the terraces.**

To characterize the mapped terraces described in section 4.1, and to help constrain their formation mechanism, we assessed their spatial elevation trends. To do this, we used a GIS to select the closest MOLA points below or on the mapped terraces. The elevations of these MOLA points show that these terraces conform to a dipping plane (Figure 6.16). The plane to which these terraces appear to conform can be expressed with a strike and dip of

170° / 0.02° ENE. Whilst this is an extremely shallow dip it equates to a height difference of around 100 m over a 300 km cross-strike transect of the Rahway basin. By extracting the values of the trend's raster to the original terrace point measurements we calculate that the standard deviation from the trend is around 16 m. The small amount of deviation from this trend over such a large distance suggests either that these terraces represent a since tilted paleoshoreline or infill of the Rahway basin with a more viscous material, perhaps lava or ice.

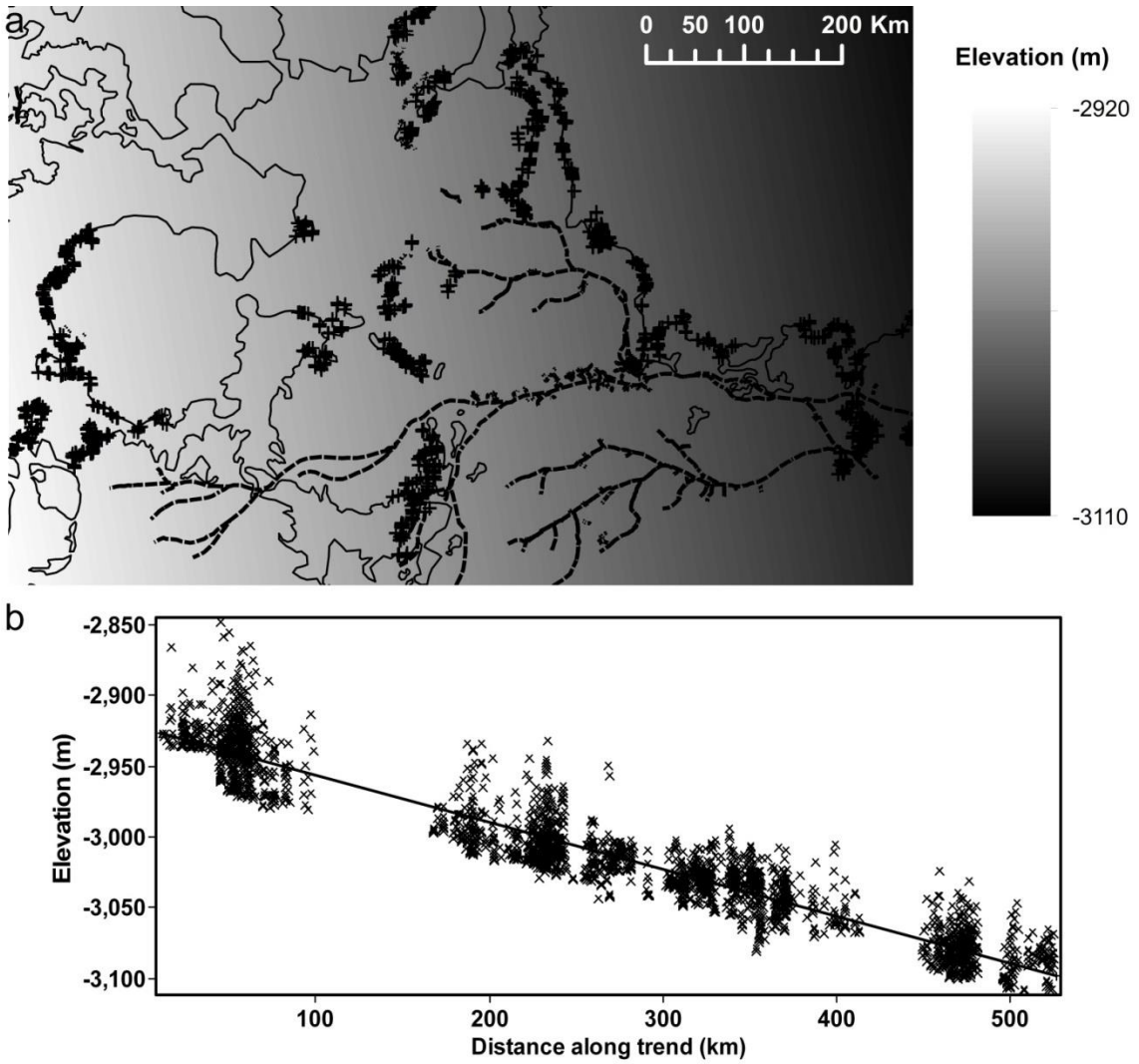

Figure 6.16 a Sketch map showing the location of the terraces (crosses), channel (dashed lines), outline of the Rahway basin (solid line) and the gradient represent the topography of the terraces' trend. b plot of MOLA topography values of the terraces (crosses) and trend height (line).

Where this trend lies above the topography we calculate the average depth to be around 18 m with a standard deviation of 8 m (Figure 6.17). To determine the volume of material needed to fill the topography up to the level of the trend we extracted trend minus topography values and multiplied the positive values (depth) by the pixel dimensions (width and length). We calculated the volume of material needed to fill the topography to the trend to be around 1500 km^3.

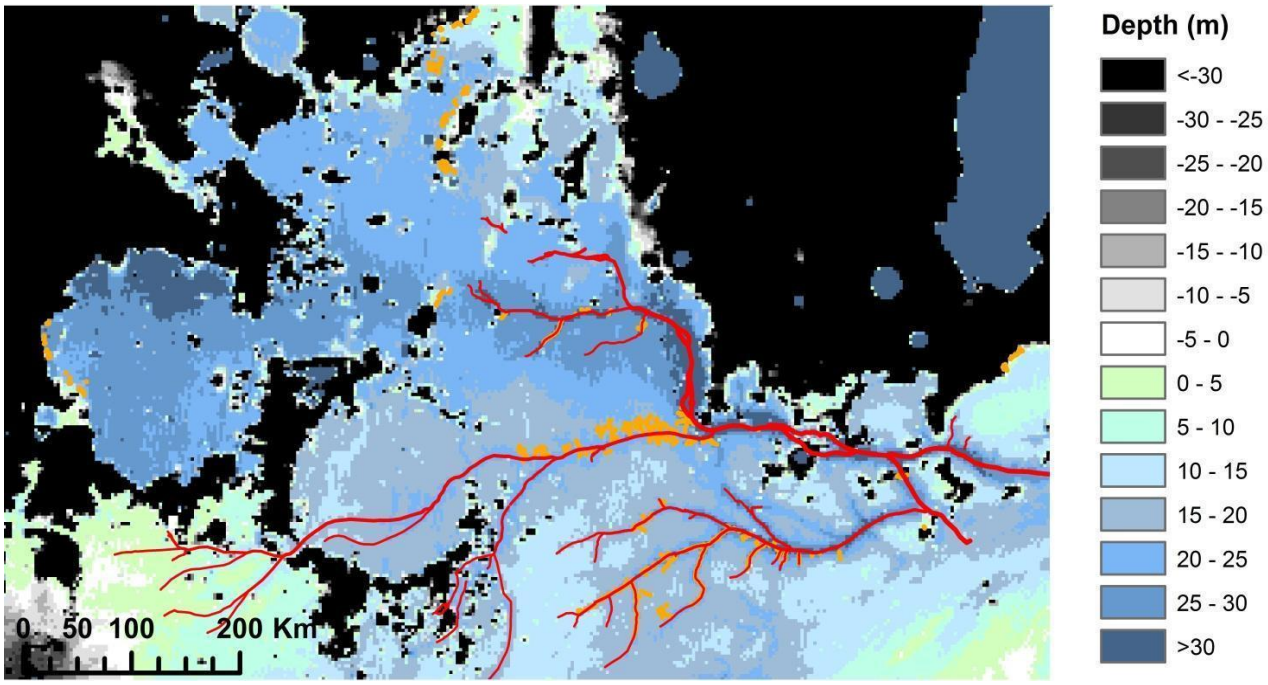

Figure 6.17 A map to show the trend of the terraces minus the topography. Red lines represent channels and orange sinuous ridges. The positive depth values represent the depth of a hypothetical equipotential body in relation the terraces; the negative values show areas above the trend.

6.1.7. **Discussion**

The Rahway Vallis system as a whole appears to be consistent in form and morphometry with it being of fluvial origin, although immature as a system compared to a terrestrial river network. Other formation hypotheses will be considered later, but there is much evidence to suggest that this is the best working hypothesis. To begin with, the overall

pattern of the network is contributory (Figure 1), with narrower channels merging to form wider ones (Figure 6a). The long profile (Figure 6b) of the main trunk is concave, and the regions between the channels slope towards the main channels to form shallow, v-shaped valleys (Figures 4 and 7). The topography is therefore representative of converging fluid flows from multiple sources, or from a continuously distributed source, that became concentrated into a single channel. Moreover, the valleys in which the channels sit have cross sectional profiles that suggest that there has been erosion and down-cutting by the flowing fluid, although in many cases this down-cutting has only been of the order of ten metres. This is shown particular clearly in Figure 7, where the banks of the channel are about 10 m higher than the thalweg for the upper reaches (longitudes 174-175° E), but are nearly 100 m higher between longitudes 176-177° E, and are again lower between latitudes 177 and 178° E. The parts of the profile with higher banks correspond to the areas closest to Nepenthes Mensae Unit outliers, suggesting that in these regions there has been significant down-cutting of the pre-existing topography.

The large junction angles between the terminations of the channel system in Rahway Vallis and the channel in Marte Vallis have at least three possible explanations. The first explanation is that the Marte Vallis system postdates and truncates the Rahway Vallis network. The second explanation is that the Rahway Vallis system was short-lived and did not have the time or hydraulic potential to erode a smoother lower angle confluence. The third explanation is that the flow between Marte and Rahway Vallis was bidirectional and that an equilibrium was reached around 90° (e.g. Langbein and Leopold, 1964).The slope of the Rahway Vallis thalweg is shallow, a drop of only ~ 200 m across a distance of ~ 500 km, equivalent to a gradient of about 0.04%, similar to large river systems on Earth (Tinkler and Wohl, 1998). Rahway Vallis is shallower than the nearby, and much deeper and larger Athabasca Vallis outflow channel (gradient of ~ 0.06%) yet steeper than the shorter, but of similar cross sectional area, Lethe Vallis (gradient of ~ 0.02%). Both these

channels occur in the same terrain types as Rahway, and contain similar platy-ridged terrain. Both are interpreted to have formed as catastrophic flood channels (Balme et al., 2011; Burr et al., 2004, 2002a, 2002b; e.g. Head et al., 2003b). No morphological evidence for catastrophic formation is seen in Rahway Vallis, however, and there is no obvious single source for any of the lower order channels. Also, Rahway Vallis formed as a contributory network, unlike the other two channels, which both have point sources. Rahway Vallis contains some small channels that are carved into deposits located within larger channels, suggesting that the channel system is time-transgressive with multiple stages of erosion and deposition. Hence, the Rahway Vallis system seems more consistent with a quiescent formation style that could occur over very shallow slopes (i.e. involving a low viscosity liquid) than with a catastrophic origin.

Fluvial formation hypotheses that could be advanced to explain these observations include precipitation as rain followed by run-off, precipitation as snow followed by melting, groundwater release, lake-drainage, or melt of a frozen, formerly ponded body of water. Of these, only the last two seem consistent with the observations. Precipitation appears unlikely, as the channels systems are constrained to lowland regions, bounded by terrace-like structures, and do not appear to originate at detectable changes in lithology or porosity differences that could account for the lack of dissection in the uplands, only a few kilometres away. Although groundwater release cannot be ruled out as a primary source of the liquid within the Rahway basin it alone does not account for the obvious widespread distribution of the channel heads. We did not find any landform (e.g. escarpments, vents, changes in lithology) which could account for the widespread channel head distribution as a product of groundwater release directly into the Rahway basin.

An alternative to a fluvial origin is a purely volcanic one (e.g. Figure 6.18a) with the channels being carved by a turbulent low viscosity lava flow. Although the source of the channel-forming fluid appears to be distributed, it could also be from many discrete

sources. However, we found no geomorphological evidence (e.g., small cones, fissures or other obvious volcanic centres) that would support multiple small volcanic centres being the source of the low order Rahway channels. Moreover, the converging flow patterns revealed in the landscape, the low slopes, and the fact that turbulent lavas are unlikely to remain hot long enough to stay fluid and turbulent over long distances (several hundred kilometres; see, for example, the arguments put forward in Balme et al., 2010). We therefore do not think that Rahway Vallis represents a network of primary lava channels, formed as lavas flowed from a series of primary sources to a single sink.

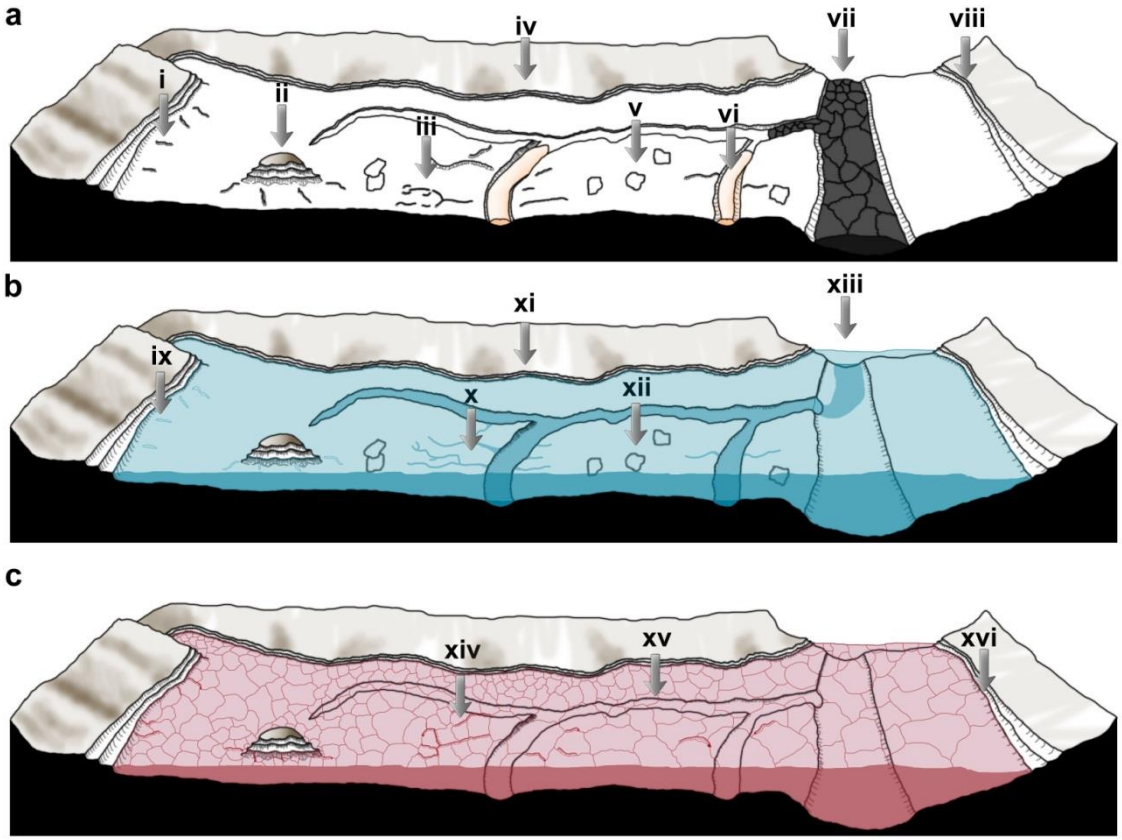

Figure 6.18 Diagrams to place the observed Rahway basin geomorphic features into geological and temporal context. ***(a)*** *The landforms currently present in the Rahway basin.* ***(b)*** *A cryolacustrine scenario.* ***(c)*** *A volcanic scenario. The following features are indicated by the roman numerals:* ***(i)*** *basin-marginal ridges,* ***(ii)*** *outliers with terraces and ridges on their margins,* ***(iii)*** *sinuous ridges on channel margins,* ***(iv)*** *basin-marginal*

*terraces which now appear to have been tilted resulting in a 100 m change in elevation over a 300 km cross-strike transect of the Rahway basin , **(v)** remnant lava plates, **(vi)** infilling material within channels, with grooves into the infilling material showing further channel development, **(vii)** infilling of Marte Vallis and backfilling into Rahway Vallis; whether Marte Vallis was carved prior to the formation of the channels, ridges and terraces within the Rahway basin is unclear, **(viii)** although it lies outside the spatial extent of this project, reconnaissance observations show that there are similar-terrace like features south of Marte Vallis, **(ix)** Crevasses with sediment fill on margins of cryolake, **(x)** sediment deposition in sub-, en- , and/or supra-ice channels, **(xi)** terraces form on the margins through deposition of sediment as the cryolake thaws and drains and/or through ice shielding the lower topography from aeolian erosion, **(xii)** remnant lava plates on the surface that likely formed synonymous with the lavas of the Cerberus Plains that the Rahway channels and valleys are carved into, **(xiii)** drainage from the Rahway basin onto Amazonis Planita through the proto-Marte Vallis, **(xiv)** push up ridges formed between lava plates, **(xv)** lava plates formed on the surface of ponded lavas and deposited on the surface as the lava is then drained, **(xvi)** terraces form on the margins of the lava lake due to erosion, deflation and/or grounding of lava plates that were attached to the basin margins.*

On the other hand, we do not rule out a scenario in which extremely low viscosity lava filled the Rahway basin and then drained rapidly to form the visible channel, terrace and ridge systems seen today. Under this scenario the sinuous ridges would have formed as part of a crust on an inflating lava's surface, with plates forming, and pulling apart before being fused and forming push-up lava ridges. Such plates could also have grounded and piled up onto the lake's margins forming the terraces. The channels could have then been formed as the lava lake drained, presumably as erosional features. However, we note again the problems that such models have in requiring lavas to remain very fluid and capable of

erosion over long distances. Some models of lava cooling can allow for this (Jaeger et al., 2007; W. L. Jaeger et al., 2010; Keszthelyi et al., 2008; e.g. Vaucher et al., 2009b) after flow from a primary vent, but for Rahway, the problem would be worse: the lava would have had to have travelled from a primary source to a spatially large, temporary sink (a lava 'lake' in the same sense as a lake of aqueous origin, rather than a lava lake above the primary source) and would then had to have remained liquid while this same lava 'lake' was breached and then drained to form the Rahway Vallis network. We suggest that this is unlikely, and that the simpler explanation is that the Rahway system is of fluvial origin.

The entire Rahway Vallis system of channels, valleys and ridges is contained within a basin bounded by terrace-like structures shown in Figures 11 and 16. These have a consistent elevation, occurring between 3100 and 2850 m below Mars datum. Moreover, when a plane is fitted to these mapped elevation points, they conform closely (+/- about 50m) to a consistent, shallow East-dipping linear trend (Figure 16). If these terrace-like structures represent the high-stand margins of what was a once-liquid, basin-filling material, then they will define an equipotential surface. The current gently tilting trend therefore implies either that (a) the material that filled the Rahway basin was of low viscosity and continuously flowing in an approximately easterly direction, or (b) that the Cerberus plains have been tectonically tilted post-formation, and that the terraces were once at the margins of an approximately level equipotential surface. Although there are some possible inlets at the north and northwest of the Rahway Basin that might support the first possibility, the ~ 150 km-diameter 'flooded' crater at the far west of the Rahway system contains terraces, but has no inlets to the west, so presumably must have been flooded from the east. In this case, the terraces should be of lower elevation than those near any proposed inlet area (such as around the main channel trunk, immediately to the south of this crater), but this is not the case. We therefore conclude that the second case, post-depositional tilting, is more likely. In light of recent observations of possible ongoing

tectonism in the Cerberus region (Taylor et al., 2013; Vetterlein and Roberts, 2003), this seems plausible.

Figure 17 shows the result of subtracting the current topography from the proposed trend, to form a 'pre-tilting' elevation map. This suggests that the original long profiles of the channels were even shallower. It should be noted that, even after this detrending, the channels still slope downstream, and none of the channels, nor the ridge systems on their margins, are above the height of the putative high stand elevation denoted by the detrended terrace heights. This observation is consistent with these features being the result of an infilling of the topography, and then removal by drainage, by a fluid. The volume beneath the trend and above the current topography is around 1500 km^3 within the area of the Rahway basin we have examined. This is a large volume, but we note that flux estimates of the catastrophic floods from the Cerberus Fossae that formed Athabasca Vallis are of the order of 2×10^6 m^3s^{-1} (Burr et al., 2002b), or equivalent to 3-5 km^3 of water per hour. Athabasca is upstream of Rahway Vallis, and is only one of several source regions for flooding in the region, so even this large volume of water could have been supplied by regional catastrophic floods lasting days or weeks. We conclude that it is likely that the Rahway Vallis network is cryolacustrine in origin, formed by the draining of a lake somehow impounded in the Rahway basin, or by the melt of ice either left as nearly pure ice within the Rahway basin after inundation, or sequestered into the sediments following flooding.

Although we believe that the evidence for Rahway Vallis being a cryolacustrine channel system is strong, the origin of the sinuous ridge systems is not so clear, although it might have a bearing on whether the better interpretation for the formation of the Rahway Vallis network was of a draining lake, or of melting of ice. The clastic appearance of the sinuous ridges and Strahler stream orders of up to four points to a fluvial or cryofluvial hypothesis rather than that of a volcanic or structural genesis. The elongate, sometimes discontinuous

curvilinear plan view morphology, the positive-relief and narrow crested cross sectional shape and the overall scale are all comparable with examples of both inverted fluvial channels (e.g. Clarke and Stoker, 2011; Williams et al., 2009) and terrestrial eskers (e.g. Flint, 1930; Gregory, 1912). The en-echelon appearance with gaps of tens of metres between ridges is particularly suggestive of post-depositional modification more indicative of terrestrial eskers than inverted fluvial channels, with the disturbance being due to the removal or flow of ice. Also, the troughs related to the sinuous ridges feed into, and slope towards, the main channel, and resemble subglacial canal systems (e.g. Walder and Hallet, 1979), shallow tunnel valleys associated with eskers (e.g. O'Cofaigh, 1996), or poorly developed channels that were carved as the material that filled the Rahway basin drained. Again, this supports a mechanism in which melting of an ice rich material occurred in the Rahway.

Based on morphology, it does not seem unreasonable to conclude that the sinuous ridges are glaciofluvial in origin. If the sinuous ridge deposits do represent eskers, then by definition sub, supra and/or englacial meltwater must have been involved in their formation, and so we should be able to identify other landforms associated with wet/warm-based glaciers. In this hypothesis, a pro-glacial lansdscape with a well-developed braided river system, outwash plains, kettle holes, glacial lakes, kames and moraines, would be expected downstream of the ridges. Also, in the upland regions around the Rahway basin – the older heavily cratered Nepenthes Mensae Unit – we might expect to find glacial accumulation zone morphologies such as cirques, arêtes, horns, hanging valleys, truncated spurs and possible remnant glacier-like forms (GLFs; e.g. Souness and Hubbard, 2012). However, after examining 260 CTX images (≈1 million km^2 at ≈6 m/px) and 51 HiRISE images (≈1,250 km^2 at ≈25 cm/px), no further evidence of landforms indicative of formation related to a moving body of ice has been found. While this does not rule out glacial activity, it does make a simple wet-based glacial hypothesis less likely. That said,

the similarity between sinuous ridge morphometry and plan-view appearance and that of terrestrial eskers encourages the consideration of a glacial hypothesis.

The absence of wet/warm-based glacial landforms leads us to suggest that, if present, any ice body was largely cold-based, and therefore unable to create landforms analogous to terrestrial polythermal or wet/warm-based glaciers. Lucchitta (2001) calculated the minimum thickness for which clean water could melt, under current heat flow and climatic conditions at equatorial regions of Mars to be around 5 km, which is around an order of magnitude thicker than the Rahway basin is deep. If we subtract the topography of the basin floor from the terrace-derived, de-trended basin-full level, we find that the maximum depth to be around 50 m, with an average 18 m. This is at least two orders of magnitude below the transition predicted by Lucchitta (2001). Therefore, if the Rahway basin was ever ice-filled, this ice was not deep enough to undergo pressure induced melting, and so the origin of the ridges as sub-glacial eskers is improbable. This does not preclude, the possibility that the ridges formed as supra-glacial eskers formed within subaerial, u-shaped channels on the ice-body (Delaney, 2001; Fitzsimons, 1991; Hambrey and Fitzsimons, 2010).

Other possibilities that might be used to explain the presence of these features include a top-down (or two-sided) freezing lake that acts like a wet based glacier due to it being drained when nearly frozen solid. In this scenario, landforms similar to eskers and tunnel valleys could potentially form as interconnected ‘taliks’ drained the system, potentially forming landforms such as the sinuous ridge, trough and channel systems. It should be noted though, that this would have to have occurred at a specific point in the freezing history of the lake (when there was ‘just enough’ unfrozen water near the base of the ice body to allow tunnel-like flow, but not so much that the whole body moved by floating) so is perhaps an unlikely scenario, or at least one that requires ‘special circumstances’. Another possibility is that partial melting of an ice body through climatic, volcanic or

impact related processes, could perhaps have provides glaciofluvial conditions in which esker-like features may have formed.

In terms of explaining the terrace morphologies, a shoreline environment on Mars (Figure 6.18b) would have considerable differences from their terrestrial comparison; the absence of a large moon and relatively weak winds would severely limit any wave or tidal erosion. However, we can envision at least two processes that could lead to the formation of terraces on a Martian shoreline. The first is similar to ice-push ramparts on earth (e.g. Butler, 1999; Kovacs and Sodhi, 1980), where sediment-rich ice is floating on the surface of a body of water and is snagged on the shallowest parts of the basin; i.e. the basin margins and "islands". This grounded ice might then melt and deposit sediment on the margins leading to terrace development. A second scenario could be that of a completely frozen body of water acting as a shield from aeolian erosion, with topography above the ice margin being exposed to aeolian erosion and the topography below the ice margin being shielded leading to terrace development. This shielding from erosion by a static body of ice can be seen on the high mountains of the Patagonian Andes that are now higher than their more northern and "wetter" counterparts due to increased protection from erosion (Thomson et al., 2010). With erosion occurring above the ice margin, we might expect to find transportation of sediment onto the surface of the ice which would likely infill any crevasses on the surface of the ice. Removal of the ice might then lead to crevasse fill ridges (e.g. Sharp, 1985) forming on the basin margins, offering a possible explanation for the basin marginal sinuous ridges. Melting and draining of the cryolake could have carved the channel network within the Rahway basin analogous to lake drain environments on Earth (e.g. Baker, 1973). In such a scenario, the sinuous ridges might have formed as inverted channels late in the process. Also, deposition into the Rahway system channels during waning flow after the main draining of the basin could have formed a lag deposit and caused the infilling of the channels that has been inferred, especially in the southern

branches of Rahway (e.g. Baker, 1973). Subsequent melting and draining events of remnant ice may have led to twin, parallel channel development (e.g. Pain et al., 2007) and partial removal of the lag deposit.

In summary, the sinuous ridges resemble eskers, possible even eskers set within subglacial canals or tunnel channels. However there is no other evidence of wet/warm based glaciation in the region. Consequently, if eskers at all, the sinuous ridges are supraglacial eskers, a type that can form on the surface of dry/cold based glaciers, or they are ridges formed in a cryolacustrine environment by thaw-water draining off the surface or from within a non-glacial ice-body that filled the Rahway basin. Both scenarios have analogues in the Antarctic (e.g. Fitzsimons, 1991; Hambrey and Fitzsimons, 2010).

The alternative to the ridge system being 'esker-like' landforms is that they are inverted channels (Clarke and Stoker, 2011; Williams et al., 2009) in which the presence of ice played little or no role. If so, they probably also formed due to draining of the Rahway basin. The troughs associated with the sinuous ridges could have formed by incision in the initial high energy stages of drainage before declining transport competence resulted in the deposition of sediment to form the ridges. However, as can be seen in Figure 13d, the ridges cross-cut the troughs, an observation that sits uncomfortably with a purely fluvial hypothesis, but which could be explained if the ridges formed by intra- or supra-ice body discharge. Figure 17 shows that the sinuous ridges occur in the topographically highest parts of the Rahway basin (after detrending) and along the basins margin. This could mean that the sinuous ridges were preserved only in these locations, where they were left abandoned by further fluvial modification (e.g. Fig.8 with the small channel incised into infilling material) as the basin drained.

To conclude, we suggest that a hypothesis of lake drainage, occurring perhaps as a consequence of an ice or debris-dam failure within (or during the formation of) Marte

Vallis, as suggested by Burr et al., (2002a, 2002b), is most consistent with the evidence, but does not offer a clear explanation for the ridge systems. Any lake forming on Mars would first freeze at its surface and, if the lake was not drained for months or years, it could have frozen to many metres deep, perhaps even to its base (Carr, 1983). It is possible that the sinuous ridges formed by sedimentation associated with draining of thaw fluids from the top of a frozen lake, or by draining of unmelted portions of the frozen body. It is unlikely that the ridges could have formed from pressure-melting at the base of an entirely frozen ice-body of such a shallow depth, so they cannot be eskers in the strict glacial sense. If the lake drain hypothesis is correct, this glaciofluvial-lacustrine activity was followed by regional tilting, leading to the trend in elevation seen in the terraces surrounding Rahway basin today. Future work that could test this hypothesis might include searching for spectral/radar evidence of any surviving ice within the Rahway basin. Additional CTX image examination might also be used to confirm that the terraced margins are indeed continuous and an additional study south of Marte Vallis might be proposed to search for a corresponding southern terraced margin that would support the large lake hypothesis.

A mechanically similar hypothesis, of very fluid lavas infilling, partially solidifying, and then draining, might also be possible. However, this mechanism is difficult to reconcile with the fact that such lavas would have had to have remained liquid while travelling extensive distances from source, to have remained liquid while forming a single, ponded body with a volume of 1500 km^3, and then to have remained liquid while flowing large distances, across very shallow slopes while at the same time carving a series of channels, as the ‘lake’ was drained.

6.1.8. **Conclusions**

The ~ 500 km long channel network within the Rahway basin is topographically and morphologically consistent with a genesis involving flowing water. The network pattern

requires a distributed source of fluid, inconsistent with these channels being of primary volcanic origin, and instead indicative of either a draining lake, or a melting ice-body.

The terraces that bound the Rahway basin conform to a slightly inclined plane, suggesting that they once defined an equipotential surface that has since been tilted. This equipotential surface is consistent with the Rahway basin having once been filled with a liquid that was later removed. This probably does not reflect a glacio-isostatic mechanism, and instead was probably due to endogenic movement related to volcanic or tectonic processes.

Subtracting the current topographic surface from the plane that fits the terrace elevation point data gives a volume of fluid infilling the basin of ~ 1500 km^3 and a maximum depth of ~ 50 m. Such a volume could be supplied from upstream fluvial floods such as those that carved the Athabasca Vallis system.

Sinuous ridges, with a branching, contributory network pattern, are found alongside the main channel networks in places, along with shallow troughs and pits. Despite these forms being morphologically very similar to terrestrial eskers and tunnel channels, no consilient evidence for them having a subglacial origin is apparent. However, because they cross-cut shallow troughs and pits, a supra-ice body interpretation involving incision from the ice surface into the substrate is possible.

Lake drainage, occurring perhaps as a consequence of an ice or debris-dam failure within (or during the formation of) Marte Vallis, is most consistent with the channel and terrace morphology, but does not offer a clear explanation for the sinuous ridge systems. Although, taken in isolation, the sinuous ridges provide some of the most compelling morphological analogues of terrestrial eskers yet observed, we conclude that contextual evidence for this interpretation in Rahway Vallis is absent. Instead, these landforms fit better into a cryolacustrine/frozen or partially frozen lake model.

6.1.9. **Acknowledgments**

JR was supported by a UK Science and Technology Facilities Council (STFC) studentship and a British Society of Geomorphology (BSG) Post Graduate Conference Grant. MB was supported for this work by grants from the UK Science and Technology Facilities Council (ST/L000776/1), and the UK Leverhulme Trust (RPG-397). SC was supported by the Leverhulme Trust (RPG-397). We thank Devon Burr and an anonymous reviewer for critical comments and ideas that significantly improved the manuscript.

6.2. **Summary**

This study of Rahway Vallis identifies sinuous ridges, a large channel network and terraces, consistent with either a draining lake, or a melting ice-body. I infer that the landforms in Rahway Vallis are relict ground ice structures and as such are evidence for at least short lived ground ice south of ~40° N in the recent (Late Amazonian) past. If this interpretation is correct, it indicates a flow of volatiles into the northern plains and is possibly, large scale shifts in ground ice stability and climate.

7. Discussion

In this chapter I will discuss the main results of the thesis and how they answer – or begin to answer – the research questions put forward in Chapter 3. I have grouped the materials into sections based upon individual research questions, and finish the chapter with a discussion of potentially fruitful future work, based on the findings of my research.

7.1. What is the evidence for ground ice in the northern plains and how do the insights from this study fit with what could be predicted from the literature?

The landforms that appear to be most indicative of ground-ice are the combination of the mantled, textured and pitted signatures, all of which appear to be ubiquitous from 35-45° N to ≈80° N (see Figure 7.1). These observations indicate that the LDM reaches further north than had been previously observed between latitudes 30° and 60° (e.g. Costard and Kargel, 1995; Mustard et al., 2001; Kreslavsky and Head, 2002), but are an observation supported by theoretical predictions of wide-scale ground ice on Mars (e.g., Mellon and Jakosky, 1993) and orbital spectrometer measurements of abundant near-surface water ice in the northern plains (e.g., Feldman et al 2007). In the Arcadia study area, the topographic signature of the mantle (M. A. Kreslavsky and Head, 2002a; Mustard et al., 2001; Schon et al., 2009) coincides with the textural signatures (Kostama et al., 2006), with an 87% overlap. Also, these features occur within 86% of the mapped area of Arcadia, irrespective of topography. This substantiates the hypothesis of a widespread, heavily weathered mantle deposit that has draped the terrain. These observations, combined with intepretations of the LDM deposits being layers of ice-cemented dust, with each layer being formed during a glacial phase (with ice being transported from the poles to the mid-latitudes when obliquity is above 30°; e.g. Head et al., 2003) and being subject to ablation during interglacial phases (e.g. Mustard et al., 2001), is evidence for widespread ground ice in the northern plains. Unlike the polar layered deposits the LDM has a high sediment/lithic content meaning that the ice is not visible through direct observation of the surface. Even at close proximity the LDM and outliers of the polar layered deposits are readily distinguished suggesting that they do not share the same origins.

The grid mapping shows that the LDM in Arcadia is pitted consistently from 60-68°N and from 36-56°N with one significant gap between 56-60°N, supporting previous surveys of the northern plains (Costard and Kargel, 1995; Lefort et al., 2009; Morgenstern et al., 2007; Zanetti et al., 2010). The pitted surfaces displayed by the LDM have been argued to suggest a cycle of dis-aggregation and re-accumulation (e.g. Carr and Head, 2010). The reasons why the pitting appears to be much more pervasive in Arcadia than other regions remain elusive. Given that the spatial distribution of pitted terrain do not correlate with variations in thermal inertia, it seems unlikely that it is explained by clast size or composition in the surficial material. As the WEH values are higher, or are comparable to Acidalia and Utopia despite higher levels of pitting in Arcadia, it could be that the Arcadia study area had a greater percentage of near-surface ground ice, and was thus more susceptible to pitting, or that the ice was less well-buried by sediments.

The scalloped depressions terrain occurs in a narrow band between 50-55 ° N in both Acidalia and Arcadia, but is more pervasive and spatially extensive in Utopia, occurring between 40-55° N. The scalloped terrain in Arcadia and Acidalia is less well developed, but it can be seen to be developing in the mantled and textured terrain, supporting the hypothesis that the scalloped pits formed through sublimation of ground ice (Lefort et al., 2009; Morgenstern et al., 2007; Séjourné et al., 2011; Ulrich et al., 2010; Zanetti et al., 2009). During grid mapping, I did not observe any runoff channels or interconnected “tapping channels” in the scalloped terrains, further supporting a hypothesis of formation by sublimation as opposed to thawing and evaporation (Séjourné et al., 2012, 2011).

While not being as ubiquitous as the mantled, textured and pitted terrains, the scalloped terrains do indicate that there was at least one episode in which ground-ice was present in these areas. That the scalloped terrain occurs only on the LDM south of 55° N is indicative of a somewhat de-volatised mantle south of 55° N and an intact ground-ice rich mantle north of 55° N. The relative lack of scalloped terrains in Arcadia and Acidalia, combined with many other seemingly contrary observations of evidence for ground ice at these latitudes in these areas, supports the hypothesis

that various factors (such as rate of exposure, or local variations in humidity) may play a role in in determining where, and to what extent, scalloped pit development occurs (Séjourné et al., 2011).

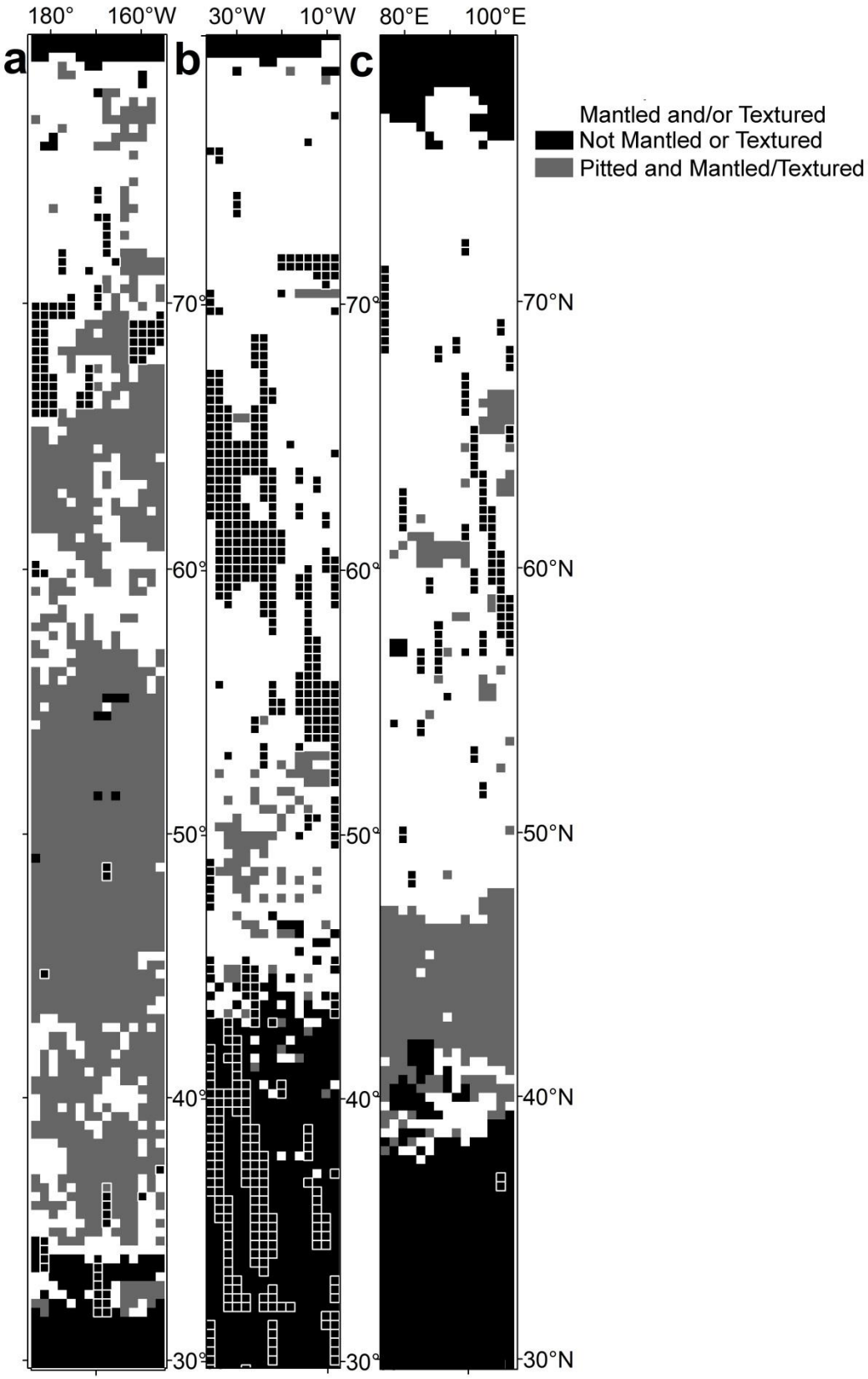

Figure 7.1 Composite map showing the grid mapping results from (a) Arcadia (b) Acidalia (c) Utopia. White outlines over the black Not Mantled and/or Textured Terrain shows CTX gaps. This map shows the extent of the LDM (white and grey) and its degradation through pitting (grey).

VFFs, thought to be landforms indicative of past or present debris-covered or debris-rich ice bodies, are primarily concentrated in the 35-42° N band in Arcadia and 40-53° N in Acidalia. This agrees with the proposed 30° to 60° latitude limits from previous studies (Head et al., 2010; Milliken et al., 2003; Souness and Hubbard, 2012; Squyres and Carr, 1986). As would be expected, VFFs occur in areas with higher slope and kilometre-scale roughness (Milliken et al., 2003; Souness and Hubbard, 2012). For this reason, it is important to note that, while VFFs are indicators of the presence of ground ice, protected from sublimation by a thick lag of dust or debris (Forget et al., 2006; Levy et al., 2009; Page et al., 2009; Souness and Hubbard, 2012), the absence of VFFs can only be inferred to be an absence for ground ice in areas of high relief: in areas of less relief, no such inference can be made. As GLFs are found in only around 0.1% of the grid squares in Arcadia, Utopia and Acidalia combined they are not a major indicator for ground ice on the northern plains.

Thumbprint terrain, kilometre-scale polygons and large pitted mounds appear to occur independent of latitude, topography and WEH values. In Arcadia, they appear to be mantled, which leads me to conclude they reflect underlying regional geology. The thumbprint terrain has been suggested to relate to glacial sediment transport and deposition (Guidat et al., 2015; Kargel et al., 1992; Lockwood et al., 1992; Rossbacher and Judson, 1981; Scott and Underwood, 1991; Tanaka et al., 2005), but the lack of other glacial landforms makes this hypothesis seem unlikely. Whether the thumbprint terrain and large pitted mounds are a relic of large scale glaciations, or a product of soft sediment deformation and mudflows (e.g. Costard et al., 2015), they do not appear to be indicative of the presence of ground ice but rather are buried by the LDM in Arcadia. While the exact origins of the kilometre scale polygons remain enigmatic, the hypotheses involving regional tectonics, sediment deformation and large scale dewatering during

compression appear likely candidates and again are not indicative of ground ice processes but also likely buried by the LDM.

Similarly, I do not see direct evidence of the small mounds in Arcadia being indicative of ground ice. They are smooth and featureless in appearance, offering little clues to their origin; however, they appear to occur in proximity to the channels system and are generally confined to the Amazonis Planitia geological units. However, the small mounds in Utopia are not confined to the same latitude, and they occur within the Vastitas Borealis unit and do not correlate with the presence of a channel system. The Amazonis Planitia unit is believed to be volcanic/volcaniclastic in origin, whereas the Vastitas Borealis unit fluviatile, associated with large outflow channels (Tanaka et al., 2005). This suggests that the small mounds are either secondary features that formed independent of the geological unit on which they occur, or that they have multiple modes of origin. Despite their differences in geological setting, both the geological units on which small mounds occur are interpreted to have undergone volatile release. Vastitas Borealis is thought to have released volatiles after being deposited as wet sediment (e.g. Kreslavsky and Head, 2002; Tanaka et al., 2005) and the Amazonis Planitia unit is thought to result from volcanic/volcaniclastic flow and ground ice interactions (perhaps similar to rootless cone formation, e.g. Lanagan et al., 2001). If the small mounds in Arcadia are mantled or eroded remnants of rootless cones then they represent evidence for ground ice at the time that the volcanic material was deposited (i.e. Middle to Late Amazonian; Tanaka et al., 2005).

While the origins of the sinuous ridges in Rahway Vallis remain enigmatic, the ~ 500 km long channel network and terraces conforming to a tilted equipotential surface within the Rahway basin are topographically and morphologically consistent with either a draining lake, or a melting, once liquid, ice-body. The landform assemblage as a whole represents evidence for massive ice or ground ice occurring at much lower latitudes in the past than can be observed or inferred today. If my interpretation of catastrophic draining of a cryolacustrine environment through a channel system feeding into Arcadia Planitia is correct, the whole landform assemblage is indicative of a

flow of volatiles into the northern plains and possibly indicative of large scale shifts in ground ice stability.

In summary, the strongest evidence for ground-ice in the northern plains is the LDM which is observed in the mantled and textured sub-categories of the grid mapping. With pitted, scalloped and 100 m polygon terrains providing supporting evidence as a result of sublimation.

7.2. What is the distribution of ground ice and can it be related to distinct latitudinal bands, different geological units, physiographic provinces, and/or topography?

7.2.1. How do the insights from this study fit with the hypotheses and the literature?

To answer this research question, I began by framing the following hypotheses in Chapter 3:

1) There is intact ground ice north of ~40° N.
2) There are relict ground ice structures south of ~40°N.
3) Latitude will be the dominant control over the distribution of landforms indicative of ground ice.
4) Evidence for thaw and sublimation will be more prevalent south of 40°N.

In this section I will attempt to substantiate or refute each hypothesis, by reference to the key new observations made in this study and within the broader context set by the literature.

7.2.1.1. *Hypothesis 1: There is intact ground ice north of ~40° N.*

The landforms that provide the most convincing evidence for ground ice in the northern plains are the mantled and textured terrains. The mantled and textured terrains have almost ubiquitous surface coverage, irrespective of topography, geology, surface roughness or thermal inertia, and are inferred to represent a latitude dependant mantle. Both in the widespread textured appearance, and in the occurrence of pitted terrain, the LDM can be shown to contain volatiles that were lost by sublimation. This study provides the first continuous mapping of these landforms at full CTX resolution, and shows that these terrains occur north of 35° N in Arcadia but

north of 40° N on average across the three grid mapping strips. This spatial distribution substantiates the hypothesis that there is ground ice north of ~40° N in the northern plains. The latitudinal gradation between (i) the mantled and textured terrains and, (ii) the non-mantled and non-textured bedrock and, (iii) the graduation from high WEH values in the north but low WEH values in the south, suggest that the ground ice within the LDM is more intact in the north, more having been lost by sublimation in the LDM close to 40° N. Additionally, where previous studies (e.g. Costard and Kargel, 1995; Mustard et al., 2001; Kreslavsky and Head, 2002) had found the LDM to occur between 30-60° N, we find that the LDM occurs up to the boundary of the northern plains, polar ice and dunes, at around 80° N.

7.2.1.2. *Hypothesis 2: There are relict ground ice structures south of ~40° N.*

The grid mapping in the three regions did not find evidence for relict ground ice south of ~40° N. The "Relict ground ice structures" were found in the form of sublimation pits north of ~40° N, but these were in what appears to be LDM that I infer to contain intact ground ice. However, the study in Rahway Vallis identifies sinuous ridges, a large channel network and terraces, consistent with either a draining lake, or a melting ice-body. Given that any large body of water on Mars is likely to have been at least partially frozen at some point, and, in order to leave significant deposits, must have supported sediment. Thus, I infer that the landforms in Rahway Vallis are relict ground ice structures and as such are evidence for at least short lived ground ice south of ~40° N in the recent (Late Amazonian) past. If this interpretation is correct, it indicates a flow of volatiles into the northern plains and is possibly, large scale shifts in ground ice stability and climate. Alternatively, the release, freezing and re-melting of such a large body of water might be related to geothermal controls.

7.2.1.3. *Hypothesis 3: The distribution of landforms indicative of ground ice will be controlled primarily by latitude.*

For the two most widespread signatures of ground ice in the northern plains (i.e. the mantle and textured signatures of the LDM), latitude appears to be the dominant control, for these signatures

occur almost ubiquitously in the three studies areas from 80° N to between 35-45° N, as described above. However, for other landforms indicative of ground ice (e.g. pitted terrain, scalloped terrain, 100 m scale polygons, VFFs, and GLFs) there are significant differences between the three grid mapping strips, suggesting that regional factors, not latitude, are the dominant control over these landforms.

An important distinction to make is that these features are all secondary degradation features of terrains containing near-surface ground ice. VFFs and GLFs, for example, are a result of deformation due to gravity, with ice flowing from high to low elevation and, as such, require relief either through topography or by uneven build-up of ice creating relief. Thus their distribution is dependent on regional topography as well as the latitudinally-controlled ability of ground ice to form and remain stable. Pitted terrain, scalloped terrain and 100 m scale polygons are all likely products of sublimation, and possibly thaw. As such, they are dependent on regional climatic conditions and processes that may increase or decrease rates of removal of the ice. These processes could include, but are not limited to: (i) deposition or removal of aeolian dust; dust deposition or removal, in turn could slow or hasten sublimation, (ii) the permeability, porosity, composition and percentage ice-content of the near surface material, (iii) regional variations in near-surface humidity which might control sublimation rate, and (iv) regional variations in insolation due to slope aspect, albedo, thermal inertia and the resulting surface and near-surface temperatures.

7.2.1.4. *Hypothesis 4: Evidence for thaw and sublimation will be more prevalent south of 40° N.*

Contrary to the hypothesis, evidence for sublimation is more prevalent north of 40° N in the form of pitted terrain, textured terrain and scalloped terrain. Although my initial prediction was for evidence of sublimation to be most prevalent where ice was not, the mapping indicates that sublimation landforms are best preserved in the surfaces containing ground ice and which are actively degrading. In the context of this work, the surfaces with evidence of sublimation (e.g. pitted terrain and scalloped depressions) are those of the LDM between 35-80° N. So, in relation

to sublimation, the hypothesis has to be rejected. However, the evidence for thaw (i.e. the origins of the channels systems in both Arcadia and Rahway Vallis and possibly the sinuous ridge networks, if eskers), is more prevalent south of 40° N. Hence, the hypothesis is substantiated with regards to thaw.

7.2.2. How effective was the grid mapping method with regards to recording the distribution of landforms indicative of ground ice?

The mapping project required the acquisition, handling and analysis of large numbers of high resolution CTX images in order to identify small landforms over large areas. I elected to use the grid mapping approach to provide an efficient, consistent and standardised approach to map the landforms indicative of ground ice in one examination of the data set, and would promote data sharing and collaboration with other ISSI team members. The speed at which the data could be recorded using the grid mapping method allowed for the first continuous, full resolution mapping of decametre-scale landforms in CTX images on hemispherical-scale maps.

Importantly, it is a scalable approach: if a landform type needs to be split into two or more sub-categories, then only those grid-squares containing the parent category need to be re-examined. Hence, if in future work more information is required for any of the landforms mapped here, a hierarchy of high spatial resolution, detailed classifications could be built up by employing smaller and smaller grids, then sub-classifying individual landform types, where needed. An example of this would be classifying the metre scale textures that can be observed in HiRISE of mantled and textured terrains mapped in CTX. A distinct advantage with the grid mapping approach is that it records negative results, making it possible to distinguish between absence of landforms and absence of data.

The discrete nature of the grid mapping allowed for easy transitions between my data and those of colleagues working on the Acidalia and Utopia strips, and allowed for efficient comparison of results. The tabular nature of the dataset allowed for efficient statistical manipulation of the spatial datasets, with summary statistics being produced procedurally using code for both new

primary data and existing secondary datasets. To ensure comparability, reconnaissance and test mapping comparisons were essential to confirm everyone involved knew what landforms were to record and under what categories.

I found that the grid mapping was both effective and efficient at identifying where specific landforms and ground-ice occur and then relating these spatial characteristics to hypothesised controls i.e. latitude, geology, physiography, and/or relief. However, the main disadvantage of grid mapping was that it did not clarify how many specific landforms are present per mapping unit. The current method assigns the same weight to one landform as it does to a hundred. This shortcoming could be removed by recording percentage of terrain in each mapping unit occupied by each landform class, which, in turn, could clarify how much ice is present.

The choice of mapping scale also influenced the effectiveness of recording certain landforms. The chosen scale as 20 km by 20 km grid-squares was very effective for identifying the smaller landforms such as the textured, pitted, mantled, and polygonal terrains. However, it was less effective in mapping landforms such as thumbprint terrain, or large (>20 km wide) channels, both of which are larger than the mapping grid squares, and was thus difficult to spot whilst "zoomed in" at CTX scale. This is something definitely worth bearing in mind when deciding the scale of mapping and additionally, when deciding upon the protocol for mapping each grid square, i.e. beginning the examination of each grid square at the lowest resolution but widest coverage before "zooming in" to higher resolutions.

7.2.1. How effective was the grid mapping method with regards to identifying the origins of the ground ice?

The grid mapping method allowed for rapid acquisition of the spatial distribution of multiple landform types over a wide area. This in turn helped to test the different hypotheses regarding the origins of the ground ice in northern plains. The method was particularly helpful in mapping the distribution of the LDM by dividing the LDM into both textured and mantled sub-classes. The mapping approach provided two lines of evidence that the LDM is (i) ubiquitous north of around

40° N and (ii) overlaps geological and topographical boundaries, an observation central to substantiating the hypothesis of an airfall origin. While the limitations discussed in Chapter 3.5.7.1 apply, the main limitation of the grid mapping with regards to answering the question about the origins of the ground ice is the areal scale of the mapping unit. Moreover, expanding the grid mapping to cover the whole of the northern plains would offer a much greater insight into both the distribution of landforms and their possible origins.

7.3. What insights can we gain from understanding the spatial distribution of the ground ice in the northern plains with regards to its origins and history?

There are three likely mechanisms to account for the ground ice observed in the northern plains: (i) the ground ice is a primordial remnant of a northern ocean; (ii) the ground ice was fluvially emplaced into the northern plains, ending up either as buried frozen seas and lakes, or as an icy component of sediments; (iii) the ground ice was emplaced by precipitation of snow or ice concurrently or alternatively with deposition of aeolian dust to produce ice-rich deposits, protected from deep sublimation by the development of auto-generated lag covers as the uppermost icy-surfaces sublimed.

7.3.1. Could the ice be the frozen remnants of a northern ocean?

The LDM mantles the vast majority of craters, meaning it is likely to be very late Amazonian in age. Hence, the landforms associated with ground ice in the northern plains are generally very young. It is extremely unlikely that a northern ocean could have occurred in Mars' most recent past given that liquid water is unstable at the martian surface under current and recent climate conditions (Forget et al., 2006; Read and Lewis, 2004). Without significant ongoing resurfacing processes that preserve the surfaces of the LDM while preserving and displaying underlying craters, it does not seem probable that the ground ice in the northern plains are remnants of a frozen ocean. An alternative hypothesis is that the ice is derived from wet sediments, deposited in a since evaporated, sublimated or concealed beneath dust on the northern ocean, buried below the surface and dewatering through diagenesis. However, this does not seem likely as the ice

appears to be smoothly distributed and not clustered around cracks or vents that would allow for upward water and sediment flux like might be expected if the ice was sourced from below.

7.3.2. **Could the ice be fluvial in origin?**

There is significant evidence for fluvial activity having transported water into the northern plains (Baker et al., 1991; Clifford and Parker, 2001; Head et al., 1999; Masursky et al., 1977). The Cerberus Fossae are believed to have outpoured water from underground onto the martian surface at the astonishing rate of 3-5 km^3 per hour (2×10^6 m^3s^{-1} ; Burr et al., 2002b). In Chapter 6, I suggested that it is this water that was likely to have once filled the Rahway basin, before spilling into Amazonis and Arcadia Planitia through the Marte Vallis channel system. In Chapter 4, I described evidence for fill and spill having occurred within Arcadia Planitia in the form of its large channel system sourced from and terminating in bodies of standing water. If channels systems such as these were the source of the ice in the northern plains we might expect to see a concentration of ice related landforms and elevated WEH signatures around the channel systems. These characteristics were not observed. Instead, in chapters 4 and 5, the channel systems occur in areas of relatively low WEH with no apparent concentration of ice related landforms around the channels. While this might be evidence against a fluvial source for the ice in the northern plains, it could also be accounted for by the widespread occurrence of pits at these latitudes, suggesting significant loss of volatiles. Given that water tends to conform to an equipotential surface infilling lows, it appears unlikely that a fluvial origin could account for the origin of the LDM that appears to drape topography; but a fluvial mechanism could account for deposition of wet sediments that have been inferred to explain the thumbprint terrain and large pitted mounds (e.g. Costard et al., 2015). It appears likely that the vast majority of water transported fluvially in to the northern plains in the recent past would have been subsequently lost to evaporation and sublimation unless it was rapidly buried. In summary, fluvial input may have been an important contributing factor to ice in the northern plains over a long period of time, however, the most recent manifestation of ground ice, i.e. the LDM, does not appear to be fluvial in origin.

7.3.1. **Could the ice be airfall in origin?**

For airfall or direct condensation of ice in the northern plains we would expect to see the distribution landforms associated with ground ice to have a positive correlation with the spatial distribution of inferred ice stability (i.e. ice related landforms occurring with latitude dependence, rather than being clustered around outflow zones). The almost ubiquitous spatial distribution of both mantled and textured terrain shows this latitude dependence. The landforms are not clustered around outflow zones (e.g. Figure 5.2). The putative sublimation features (pitting, polygons and scalloped terrain), also appear to be concentrated within distinct latitudinal bands (e.g. Figure 5.2), providing good evidence for the airfall hypothesis. It seems highly likely that the dust component of the LDM is of airfall origins, given the observations of active replenishment of the dust component of the LDM described in Chapter 4. This also lends credence to the hypothesis that, under the right conditions, ice may be deposited and rapidly buried and protected from ablation by large dust storms (Bryson et al., 2008; Fanale et al., 1986). Given that the sediment component of the LDM appears to only occur north of around 40° N (see distribution of the mantled and textured terrains in Chapters 4 and 5), then perhaps the ice component of the LDM is required to cement the deposit, as much as the sediment is required to prevent the ice from sublimating.

Whether the ice component could be a result of direct condensation into the pore-spaces within the loose surficial material (Mellon et al., 2008; Mellon and Jakosky, 1995; Mustard et al., 2001; Read and Lewis, 2004), or by snowfall that may have been possible during Mars' recent past (Forget et al., 2006; Kite et al., 2011; Levy et al., 2009, 2014; Page et al., 2009), is still open for debate. While Souness and Hubbard (2012) argued that direct condensation appears to be at odds with the results of SHARAD based studies of LDAs (Holt et al., 2008; Plaut et al., 2009), which show them to be glacial landforms comprised largely of water ice with minimal lithic content and thereby supporting the air-fall hypothesis, I find that the LDM appears to be the most widespread form of ice in the northern plains and it appears to contain large volumes of sediment and leave behind significant lag deposits post sublimation. This suggests that both airfall and direct

condensation into pore-spaces are plausible formation mechanisms for the ice component of the LDM.

7.4. **Further investigations**

At approximately six weeks per 5° longitudinal band from 30-80° N, a whole 30-80° N grid map could be completed by an individual in approximately 432 weeks or 8.3 years. This is clearly beyond the endurance of a single, normal researcher. However, as suggested in Chapter 3.5.7.4, the discrete nature of the datasets also opens up the possibility for citizen science and "crowdsourcing" the large mapping area. Similar large participant studies are being performed by NASA's "Be a Martian" and "ClickWorkers" projects and Zooniverse's "Moon Zoo" project (Joy et al., 2011). Weighting the results against "experts" using control squares (experts being members of the appropriate science community who survey a sample of the mapping area) would allow for much quicker completion of the grid mapping while maintaining reliability. The simplicity of each decision is the main strength of the grid mapping approach for a citizen science project as mappers do no need advanced GIS skills or mapping experience.

The aim of expanding the study would be to improve extent to which we can test latitude dependence hypotheses. Each grid would need to have a cropped basemap specific to that area to allow it to be "served" to each mapper without every mapper storing the entire image catalogue. A large database would need to be established to record multiple entries of each grid square recording landforms observations alongside the identity of the mapper that recorded them. Crowdsourcing would also open up the possibility of collecting additional information about landforms, such as the number of landforms in a given area, the percentage cover by that landform and other geomorphic metrics, which would be too time consuming for one individual to gather for the entire northern hemisphere at CTX resolution. Additional metrics such as the average time taken by the mapper to complete each grid-square could be recorded and provide an interesting and perhaps useful insight into the complexity of different regions and may in itself serve as a tool for identifying areas of interest to be studied in further detail.

8. **Conclusions**

The increased volume, spatial resolution, and areal coverage of high-resolution images of Mars over the past 15 years have led to an increased quantity and variety of small-scale landform identifications. Identification of many such landforms form the observational basis for developing hypotheses on the geological nature and environmental history of a study area. The combination of improved spatial resolution and near-continuous coverage significantly increases the time required to analyse the data. This thesis presents an approach for mapping small features across large areas, formulated for a project to study the northern plains of Mars, and gives insight into how it can be implemented and results that we found.

The first, and perhaps most important, output of this PhD is the development and application of a grid-based mapping approach that provides an efficient solution to the problems of mapping small landforms over large areas by providing a consistent and standardised approach to spatial data collection. The grid-based mapping approach allows the cataloguing of landform classes, of multiple sizes, efficiently in a single pass, minimising the time spent looking over the same images. The grid-based mapping is extremely scalable and workable for group efforts, requiring minimal user experience and, based on the results of testing, producing consistent and repeatable results. The speed at which the data could be recorded using the grid mapping method allowed for the first continuous, full resolution mapping of decametre-scale landforms in CTX images on hemispherical-scale maps. The discrete, tabular nature of grid mapping opens up the possibility of using citizen science techniques to leverage vast numbers of users to perform geomorphological mapping tasks from orbital data. One potential application of a "grid-based mapping by citizen science" approach would be to expand the grid mapping to cover the whole of the northern plains offering greater insight into both the distribution of landforms and their possible origins. Such a project would require considerable effort to

plan and implement, but could then be easily adopted for many similar studies on Mars or other planetary bodies. Thus, the detailed description of the grid mapping approach described in this thesis could have considerable use and impact in the future.

The main scientific goal of this thesis was to determine the distribution and origins of ice-related landforms in the northern plains, and provide insight as to whether these landforms are related to distinct geological or geomorphological units. To accomplish this, I used the grid mapping approach to explore a large tract covering the Arcadia Planitia region of the northern plains of Mars. In addition, as part of a wider consortium project, I was able to compare these results to two other sister-studies performed in the Utopia Planitia and Acidalia Planitia regions of Mars. Hence, I was able to compare the three main lowland basins in the northern plains of Mars.

The first major outcome of this grid mapping was the observation that the mantled and textured signatures occur almost ubiquitously in the three studies areas from 80° N to between 35-45° N, supporting the arguments of other workers in the field that the strongest evidence for ground-ice in the northern plains is the latitude dependent mantle (LDM; e.g. Kostama et al., 2006; Kreslavsky and Head, 2002).Where previous studies had found the LDM to occur between 30-60° N (e.g. Costard and Kargel, 1995; Mustard et al., 2001; Kreslavsky and Head, 2002), we find that the LDM occurs up to around 80° N suggesting that ground ice is even more widespread than had previously been shown. While this is not a wholly unexpected result, it demonstrates the extensive nature of this ice-rich draping mantle, and that it is older than the dunes in the northern polar region that superimpose the LDM here.

The spatial distribution of the LDM has positive correlation with the spatial distribution of inferred ice stability based on climate modelling and gamma-ray spectroscopy data, making latitude the dominant control for where ground ice occurs. The LDM and the other ice-related landforms identified in this research are not clustered around outflow zones or

tectonic features and vents, as would be expected if the ice had formed through fluvial or groundwater outburst flood processes, respectively. Instead, we find the LDM to be distributed evenly over both topographic and geological boundaries indicating that the ground ice in the northern plains has airfall origins.

Next, I have shown that landforms indicative of sublimation, i.e. pitted, scalloped and 100 m polygon terrains, provide supporting evidence for ground-ice being present north of around 35-45° N. Evidence for sublimation is greatest north of 40° N, in the form of pitted terrain, textured terrain and scalloped terrain. Pitted terrain appears much more pervasive in Arcadia than in Utopia and Acidalia suggesting that the Arcadia study area had a greater percentage of near-surface ground ice, and was thus more susceptible to pitting, or that the ice was less well-buried by sediments. As would be expected from previous studies (Milliken et al., 2003; Souness and Hubbard, 2012), the grid mapping found VFFs and GLFs to occur in areas with higher slope and kilometre-scale roughness. These results suggest that regional factors, not latitude, are the dominant control over ice deformation related landforms.

One of the key observations from the Arcadia study area is that there are extensive channel systems in the south that seem to be buried by later LDM materials. It is likely that those channels have brought large quantities of ice and sediments into southern Arcadia, but evidence for there being geomorphological evidence of this fluvial origin for the ice has since been covered by the LDM. Hence, while it is perfectly plausible that there is a significant fluvial component to the ground ice in Southern Arcadia, this cannot be easily tested using remote sensing image data. It is possible that subsurface RADAR data could be used to locate fluvial features buried in the landscape, but this must await future work.

To explore the possible source regions of ice in the southern part of the Arcadia study area, where abundant channel forms can be seen, I performed a detailed study of the Rahway Vallis system, which occurs above Marte Vallis and could be a possible source region for

this channel system. Marte Vallis is a large flood carved channel south of the Elysium volcanic rise, which debouches onto the Amazonia Planitia region, and which in turn grades into the Arcadia Planitia. Hence, it is possible that Rahway Vallis could be a source region for volatiles in Arcadia Planitia.

The assemblage of terraces, channels and sinuous ridges in Rahway Vallis are topographically and morphologically consistent with either a draining lake, or a melting, once liquid, ice-body. The evidence for thaw (i.e. the Arcadia and Rahway Vallis channel and ridge systems), is more prevalent south of 40° N where in the past ground ice may have been quasi-stable and likely melted. The landform assemblage as a whole represents evidence for massive ice or ground ice occurring at much lower latitudes in the past than can be observed or inferred today, with catastrophic draining feeding into Arcadia Planitia being indicative of a flow of volatiles into the northern plains and large scale shifts in ground ice stability.

Overall, this thesis demonstrates the dominant effects of the deposition and sublimation of the LDM in shaping the recent landscapes of the northern plains of Mars. There was little evidence for thaw-related landforms, and evidence for a fluvial origin for ice in the near surface is circumstantial, or has been erased or covered.

9. References

Alan Stern, S., 2003. The evolution of comets in the Oort cloud and Kuiper belt. Nature **424**, 639–642. doi:10.1038/nature01725

Albee, A.L., Palluconi, F.D., Arvidson, R.E., 1998. Mars Global Surveyor Mission: Overview and Status. Science **279**, 1671–1672. doi:10.1126/science.279.5357.1671

Anders, E., Owen, T., 1977. Mars and earth - Origin and abundance of volatiles. Science 198, 453–465. doi:10.1126/science.198.4316.453

Ansan, V., Mangold, N., 2013. 3D morphometry of valley networks on Mars from HRSC/MEX DEMs: Implications for climatic evolution through time. J. Geophys. Res. Planets **118**, 1873–1894. doi:10.1002/jgre.20117

Arfstrom, J., Hartmann, W.K., 2005. Martian flow features, moraine-like ridges, and gullies: Terrestrial analogs and interrelationships. Icarus **174**, 321–335. doi:10.1016/j.icarus.2004.05.026

Baker, D.M.H., Head, J.W., Marchant, D.R., 2010. Flow patterns of lobate debris aprons and lineated valley fill north of Ismeniae Fossae, Mars: Evidence for extensive mid-latitude glaciation in the Late Amazonian. Icarus **207**, 186–209. doi:10.1016/j.icarus.2009.11.017

Baker, V.R., 2001. Water and the martian landscape. Nature **412**, 228–236. doi:10.1038/35084172

Baker, V.R., 1982. The channels of Mars. University of Texas Press, Austin.

Baker, V.R., 1973. Paleohydrology and Sedimentology of Lake Missoula Flooding in Eastern Washington. Geol. Soc. Am. Spec. Pap. **144**, 1–73. doi:10.1130/SPE144-p1

Baker, V.R., Strom, R.G., Gulick, V.C., Kargel, J.S., Komatsu, G., Kale, V.S., 1991. Ancient oceans, ice sheets and the hydrological cycle on Mars. Nature 352, 589–594. doi:10.1038/352589a0

Balme, M., Berman, D.C., Bourke, M.C., Zimbelman, J.R., 2008. Transverse Aeolian Ridges (TARs) on Mars. Geomorphology **101**, 703–720. doi:10.1016/j.geomorph.2008.03.011

Balme, M., Gallagher, C., Page, D., Murray, J., Muller, J.-P., Kim, J.-R., 2010. The western Elysium Planitia palaeolake, in: Cabrol, N., Grin, E. (Eds.), Lakes on Mars. Elsevier.

Balme, M., Mangold, N., Baratoux, D., Costard, F., Gosselin, M., Masson, P., Pinet, P., Neukum, G., 2006. Orientation and distribution of recent gullies in the southern hemisphere of mars : Observations from High Resolution Stereo Camera/Mars Express (HRSC/MEX) and Mars Orbiter Camera/Mars Global Surveyor (MOC/MGS) data. J. Geophys. Res. **111**.

Balme, M.R., Gallagher, C.J., Gupta, S., Murray, J.B., 2011. Fill and spill in Lethe Vallis: a recent flood-routing system in Elysium Planitia, Mars. Geol. Soc. Lond. Spec. Publ. **356**, 203–227. doi:10.1144/SP356.11

Balme, M.R., Gallagher, C.J., Hauber, E., 2013. Morphological evidence for geologically young thaw of ice on Mars: A review of recent studies using high-resolution imaging data. Prog. Phys. Geogr. doi:10.1177/0309133313477123

Balme, M.R., Gallagher, C.J., Page, D.P., Murray, J.B., Muller, J.-P., 2009. Sorted stone circles in Elysium Planitia, Mars: Implications for recent martian climate. Icarus **200**, 30–38. doi:10.1016/j.icarus.2008.11.010

Bandfield, J.L., Hamilton, V.E., Christensen, P.R., 2000. A Global View of Martian Surface Compositions from MGS-TES. Science **287**, 1626–1630. doi:10.1126/science.287.5458.1626

Banks, M.E., McEwen, A.S., Kargel, J.S., Baker, V.R., Strom, R.G., Mellon, M.T., Gulick, V.C., Keszthelyi, L., Herkenhoff, K.E., Pelletier, J.D., Jaeger, W.L., 2008. High Resolution Imaging Science Experiment (HiRISE) observations of glacial and periglacial morphologies in the circum-Argyre Planitia highlands, Mars. J. Geophys. Res. Planets **113**. doi:10.1029/2007JE002994

Baratoux, D., Toplis, M.J., Monnereau, M., Sautter, V., 2013. The petrological expression of early Mars volcanism. J. Geophys. Res. Planets 118, 59–64. doi:10.1029/2012JE004234

Barlow, N.G., 1990. Constraints on early events in Martian history as derived from the cratering record. J. Geophys. Res. Solid Earth **95**, 14191–14201. doi:10.1029/JB095iB09p14191

Barlow, N.G., Bradley, T.L., 1990. Martian impact craters: Correlations of ejecta and interior morphologies with diameter, latitude, and terrain. Icarus **87**, 156–179. doi:10.1016/0019-1035(90)90026-6

Barlow, N.G., Perez, C.B., 2003. Martian impact crater ejecta morphologies as indicators of the distribution of subsurface volatiles. J. Geophys. Res. Planets **108**, 5085. doi:10.1029/2002JE002036

Batson, R.M., Bridges, P.M., Inge, J.L., 1979. Atlas of Mars, the 1:5,000,000 map series:

Berman, D.C., Crown, D.A., Bleamaster III, L.F., 2009. Degradation of mid-latitude craters on Mars. Icarus **200**, 77–95. doi:10.1016/j.icarus.2008.10.026

Berman, D.C., Crown, D.A., Joseph, E.C.S., 2015. Formation and mantling ages of lobate debris aprons on Mars: Insights from categorized crater counts. Planet. Space Sci. **111**, 83–99. doi:10.1016/j.pss.2015.03.013

Berman, D.C., Hartmann, W.K., 2002. Recent Fluvial, Volcanic, and Tectonic Activity on the Cerberus Plains of Mars. Icarus **159**, 1–17. doi:10.1006/icar.2002.6920

Bibring, J.-P., Langevin, Y., Gendrin, A., Gondet, B., Poulet, F., Berthé, M., Soufflot, A., Arvidson, R., Mangold, N., Mustard, J., Drossart, P., 2005. Mars Surface Diversity as Revealed by the OMEGA/Mars Express Observations. Science **307**, 1576–1581. doi:10.1126/science.1108806

Blasius, K.R., Cutts, J.A., Howard, A.D., 1982. Topography and stratigraphy of Martian polar layered deposits. Icarus **50**, 140–160. doi:10.1016/0019-1035(82)90122-1

Bleamaster, L.F., Crown, D.A., 2005. Mantle and gully associations along the walls of Dao and Harmakhis Valles, Mars. Geophys. Res. Lett. **32**, L20203. doi:10.1029/2005GL023548

Boynton, W.V., Feldman, W.C., Squyres, S.W., Prettyman, T.H., Brückner, J., Evans, L.G., Reedy, R.C., Starr, R., Arnold, J.R., Drake, D.M., Englert, P. a. J., Metzger, A.E., Mitrofanov, I., Trombka, J.I., d'Uston, C., Wänke, H., Gasnault, O., Hamara, D.K., Janes, D.M., Marcialis, R.L., Maurice, S., Mikheeva, I., Taylor, G.J., Tokar, R., Shinohara, C., 2002. Distribution of Hydrogen in the Near Surface of Mars: Evidence for Subsurface Ice Deposits. Science **297**, 81–85. doi:10.1126/science.1073722

Bradley, B.A., Sakimoto, S.E.H., Frey, H., Zimbelman, J.R., 2002. Medusae Fossae Formation: New perspectives from Mars Global Surveyor. J. Geophys. Res. Planets **107**, 2–1. doi:10.1029/2001JE001537

Bradwell, T., 2013. Identifying palaeo-ice-stream tributaries on hard beds: Mapping glacial bedforms and erosion zones in NW Scotland. Geomorphology **201**, 397–414. doi:10.1016/j.geomorph.2013.07.014

Brakenridge, G.R., 1993. Modern shelf ice, equatorial Aeolis Quadrangle, Mars, in: Lunar and Planetary Institute Science Conference Abstracts. Presented at the Lunar and Planetary Institute Science Conference Abstracts, pp. 175–176.

Brandenburg, J.E., 1987. The Paleo-ocean of Mars. Presented at the MECA Symposium on Mars: Evolution of its Climate and Atmosphere, pp. 20–22.

Bridges, J.C., Seabrook, A.M., Rothery, D.A., Kim, J.R., Pillinger, C.T., Sims, M.R., Golombek, M.P., Duxbury, T., Head, J.W., Haldemann, A.F.C., Mitchell, K.L., Muller, J.-P., Lewis, S.R., Moncrieff, C., Wright, I.P., Grady, M.M., Morley, J.G., 2003. Selection of the landing site in Isidis Planitia of Mars probe Beagle 2. J. Geophys. Res. Planets **108**, 5001. doi:10.1029/2001JE001820

Brooker, L., Balme, M., Conway, Hagermann, A., Collins, G., 2015. Preliminary grid mapping of fluvial, glacial and periglacial landforms in and around Lyot crater, Mars. Eur. Planet. Sci. Congr. 2015 Held 27 Sept. - 2 Oct. 2015 Nantes Fr. Online HttpmeetingorganizercopernicusorgEPSC2015 IdEPSC2015-810 10, EPSC2015-810.

Bruno, B.C., Fagents, S.A., Thordarson, T., Baloga, S.M., Pilger, E., 2004. Clustering within rootless cone groups on Iceland and Mars: Effect of nonrandom processes. J. Geophys. Res. E Planets **109**, E07009 1-11. doi:10.1029/2004JE002273

Bryson, K.L., Chevrier, V., Sears, D.W.G., Ulrich, R., 2008. Stability of ice on Mars and the water vapor diurnal cycle: Experimental study of the sublimation of ice through a fine-grained basaltic regolith. Icarus **196**, 446–458. doi:10.1016/j.icarus.2008.02.011

Burr, D.M., Baker, V.R., Carling, P.A., 2009a. Megaflooding on Earth and Mars. Cambridge University Press.

Burr, D.M., Bruno, B.C., Lanagan, P.D., Glaze, L.S., Jaeger, W.L., Soare, R.J., Wan Bun Tseung, J.-M., Skinner Jr., J.A., Baloga, S.M., 2009b. Mesoscale raised rim depressions (MRRDs) on Earth: A review of the characteristics, processes, and spatial distributions of analogs for Mars. Planet. Space Sci. **57**, 579–596. doi:10.1016/j.pss.2008.11.011

Burr, D.M., Carling, P.A., Beyer, R.A., Lancaster, N., 2004. Flood-formed dunes in Athabasca Valles, Mars: morphology, modeling, and implications. Icarus **171**, 68–83. doi:10.1016/j.icarus.2004.04.013

Burr, D.M., Enga, M.-T., Williams, R.M.E., Zimbelman, J.R., Howard, A.D., Brennand, T.A., 2009c. Pervasive aqueous paleoflow features in the Aeolis/Zephyria Plana region, Mars. Icarus **200**, 52–76. doi:10.1016/j.icarus.2008.10.014

Burr, D.M., Grier, J.A., McEwen, A.S., Keszthelyi, L.P., 2002a. Repeated Aqueous Flooding from the Cerberus Fossae: Evidence for Very Recently Extant, Deep Groundwater on Mars. Icarus **159**, 53–73. doi:10.1006/icar.2002.6921

Burr, D.M., McEwen, A.S., H. Sakimoto, S.E., 2002b. Recent aqueous floods from the Cerberus Fossae, Mars. Geophys. Res. Lett. 29, 13–1–13–4. doi:10.1029/2001GL013345

Burr, D.M., Tanaka, K.L., Yoshikawa, K., 2009d. Pingos on Earth and Mars. Planet. Space Sci. **57**, 541–555. doi:10.1016/j.pss.2008.11.003

Burr, D.M., Williams, R.M.E., Wendell, K.D., Chojnacki, M., Emery, J.P., 2010. Inverted fluvial features in the Aeolis/Zephyria Plana region, Mars: Formation mechanism and initial paleodischarge estimates. J. Geophys. Res. Planets **115**, E07011. doi:10.1029/2009JE003496

Butcher, F.E.G., Conway, S.J., Arnold, N.S., 2016. Are the Dorsa Argentea on Mars eskers? Icarus **275**, 65–84. doi:10.1016/j.icarus.2016.03.028

Butler, E.R.T., 1999. Process environments on modern and raised beaches in McMurdo Sound, Antarctica. Mar. Geol. **162**, 105–120. doi:10.1016/S0025-3227(99)00061-4

Byrne, S., Dundas, C.M., Kennedy, M.R., Mellon, M.T., McEwen, A.S., Cull, S.C., Daubar, I.J., Shean, D.E., Seelos, K.D., Murchie, S.L., Cantor, B.A., Arvidson, R.E., Edgett, K.S., Reufer, A., Thomas, N., Harrison, T.N., Posiolova, L.V., Seelos, F.P., 2009. Distribution of Mid-Latitude Ground Ice on Mars from New Impact Craters. Science **325**, 1674–1676. doi:10.1126/science.1175307

Carr, M.H., 2015. Roving Across Mars: Searching for Evidence of Former Habitable Environments.

Carr, M.H., 1995. The Martian drainage system and the origin of valley networks and fretted channels. J. Geophys. Res. Planets **100**, 7479–7507. doi:10.1029/95JE00260

Carr, M.H., 1989. Recharge of the early atmosphere of Mars by impact-induced release of CO2. Icarus **79**, 311–327. doi:10.1016/0019-1035(89)90080-8

Carr, M.H., 1983. Stability of streams and lakes on Mars. Icarus **56**, 476–495. doi:10.1016/0019-1035(83)90168-9

Carr, M.H., Baum, W.A., Blasius, K.R., Briggs, G.A., Cutts, J.A., Duxbury, T.C., Greeley, R., Guest, J., Masursky, H., Smith, B.A., 1980. Viking orbiter views of Mars. NASA Spec. Publ. **441**.

Carr, M.H., Head III, J.W., 2010. Geologic history of Mars. Earth Planet. Sci. Lett. **294**, 185–203. doi:10.1016/j.epsl.2009.06.042

Carr, M.H., Head, J.W., 2003. Oceans on Mars: **An** assessment of the observational evidence and possible fate. J. Geophys. Res. Planets 108, 5042. doi:10.1029/2002JE001963

Carr, M.H., Schaber, G.G., 1977. Martian permafrost features. J. Geophys. Res. **82**, 4039–4054. doi:10.1029/JS082i028p04039

Carter, J., Poulet, F., Bibring, J.-P., Murchie, S., 2010. Detection of Hydrated Silicates in Crustal Outcrops in the Northern Plains of Mars. Science **328**, 1682–1686. doi:10.1126/science.1189013

Chamberlain, M.A., Boynton, W.V., 2007. Response of Martian ground ice to orbit-induced climate change. J. Geophys. Res. Planets **112**, E06009. doi:10.1029/2006JE002801

Christensen, P.R., Bandfield, J.L., Hamilton, V.E., Ruff, S.W., Kieffer, H.H., Titus, T.N., Malin, M.C., Morris, R.V., Lane, M.D., Clark, R.L., Jakosky, B.M., Mellon, M.T., Pearl, J.C., Conrath, B.J., Smith, M.D., Clancy, R.T., Kuzmin, R.O., Roush, T., Mehall, G.L., Gorelick, N., Bender, K., Murray, K., Dason, S., Greene, E., Silverman, S., Greenfield, M., 2001. Mars Global Surveyor Thermal Emission Spectrometer experiment: Investigation description and surface science results. J. Geophys. Res. Planets **106**, 23823–23871. doi:10.1029/2000JE001370

Christensen, P.R., Jakosky, B.M., Kieffer, H.H., Malin, M.C., Jr, H.Y.M., Nealson, K., Mehall, G.L., Silverman, S.H., Ferry, S., Caplinger, M., Ravine, M., 2004. The Thermal Emission Imaging System (THEMIS) for the Mars 2001 Odyssey Mission. Space Sci. Rev. **110**, 85–130. doi:10.1023/B:SPAC.0000021008.16305.94

Chyba, C.F., 1987. The cometary contribution to the oceans of primitive Earth. Nature **330**, 632–635.

Clarke, J.D.A., Stoker, C.R., 2011. Concretions in exhumed and inverted channels near Hanksville Utah: implications for Mars. Int. J. Astrobiol. **10**, 161–175. doi:10.1017/S1473550411000048

Clifford, S.M., Parker, T.J., 2001. The Evolution of the Martian Hydrosphere: Implications for the Fate of a Primordial Ocean and the Current State of the Northern Plains. Icarus **154**, 40–79. doi:10.1006/icar.2001.6671

Cofaigh, C.Ó., 1996. Tunnel valley genesis. Prog. Phys. Geogr. **20**, 1–19. doi:10.1177/030913339602000101

Conway, S.J., Balme, M.R., Murray, J.B., Towner, M.C., Okubo, C.H., Grindrod, P.M., 2011. The indication of Martian gully formation processes by slope–area analysis. Geol. Soc. Lond. Spec. Publ. **356**, 171–201. doi:10.1144/SP356.10

Costard, F., Forget, F., Mangold, N., Peulvast, J.P., 2002. Formation of Recent Martian Debris Flows by Melting of Near-Surface Ground Ice at High Obliquity. Science **295**, 110–113. doi:10.1126/science.1066698

Costard, F., Sejourne, A., Rygaloff, A., 2015. Evidence of recent flow activity in Acidalia Planitia, Mars. Presented at the EGU General Assembly Conference Abstracts, p. 3842.

Costard, F.M., Kargel, J.S., 1995. Outwash Plains and Thermokarst on Mars. Icarus **114**, 93–112. doi:10.1006/icar.1995.1046

Craddock, R.A., Howard, A.D., 2002. The case for rainfall on a warm, wet early Mars. J. Geophys. Res. Planets **107**, 5111. doi:10.1029/2001JE001505

Davis, P.A., Tanaka, K.L., 1995. Curvilinear ridges in Isidis Planitia, Mars-the result of mud volcanism. Lunar Planet Sci Conf 321–322.

Delaney, C., 2001. Esker formation and the nature of deglaciation: the Ballymahon esker, Central Ireland [WWW Document]. URL http://e-space.openrepository.com/e-space/handle/2173/7887 (accessed 6.16.14).

Di Achille, G., Hynek, B.M., 2010. Ancient ocean on Mars supported by global distribution of deltas and valleys. Nat. Geosci. **3**, 459–463. doi:10.1038/ngeo891

DiBiase, R.A., Limaye, A.B., Scheingross, J.S., Fischer, W.W., Lamb, M.P., 2013. Deltaic deposits at Aeolis Dorsa: Sedimentary evidence for a standing body of water on the northern plains of Mars. J. Geophys. Res. Planets **118**, 1285–1302. doi:10.1002/jgre.20100

Dickson, J.L., Fassett, C.I., Head, J.W., 2009. Amazonian-aged fluvial valley systems in a climatic microenvironment on Mars: Melting of ice deposits on the interior of Lyot Crater. Geophys. Res. Lett. **36**, L08201. doi:10.1029/2009GL037472

Dickson, J.L., Head, J.W., Kreslavsky, M., 2007. Martian gullies in the southern mid-latitudes of Mars: Evidence for climate-controlled formation of young fluvial features based upon local and global topography. Icarus **188**, 315–323. doi:10.1016/j.icarus.2006.11.020

Diniega, S., Byrne, S., Bridges, N.T., Dundas, C.M., McEwen, A.S., 2010. Seasonality of present-day Martian dune-gully activity. Geology **38**, 1047–1050. doi:10.1130/G31287.1

El Maarry, M.R., Markiewicz, W.J., Mellon, M.T., Goetz, W., Dohm, J.M., Pack, A., 2010. Crater floor polygons: Desiccation patterns of ancient lakes on Mars? J. Geophys. Res. Planets **115**, E10006. doi:10.1029/2010JE003609

Endal, A.S., Schatten, K.H., 1982. The faint young sun-climate paradox: Continental influences. J. Geophys. Res. Oceans **87**, 7295–7302. doi:10.1029/JC087iC09p07295

Ewing, R.C., Peyret, A.-P.B., Kocurek, G., Bourke, M., 2010. Dune field pattern formation and recent transporting winds in the Olympia Undae Dune Field, north polar region of Mars. J. Geophys. Res. Planets **115**, E08005. doi:10.1029/2009JE003526

Fanale, F.P., 1971. History of Martian volatiles: Implications for organic synthesis. Icarus **15**, 279–303. doi:10.1016/0019-1035(71)90080-7

Fanale, F.P., Salvail, J.R., Zent, A.P., Postawko, S.E., 1986. Global distribution and migration of subsurface ice on mars. Icarus **67**, 1–18. doi:10.1016/0019-1035(86)90170-3

Farrand, W.H., Gaddis, L.R., Keszthelyi, L., 2005. Pitted cones and domes on Mars: Observations in Acidalia Planitia and Cydonia Mensae using MOC, THEMIS, and TES data. J. Geophys. Res. Planets **110**, E05005. doi:10.1029/2004JE002297

Fassett, C.I., Dickson, J.L., Head, J.W., Levy, J.S., Marchant, D.R., 2010. Supraglacial and proglacial valleys on Amazonian Mars. Icarus **208**, 86–100. doi:10.1016/j.icarus.2010.02.021

Fassett, C.I., Head, J.W., 2005. Fluvial sedimentary deposits on Mars: Ancient deltas in a crater lake in the Nili Fossae region. Geophys. Res. Lett. **32**. doi:10.1029/2005GL023456

Fawdon, P., 2016. Understanding the Volcanic Evolution of Syrtis Major Planum, Mars. Ph.D Thesis, Open University.

Feldman, W. c., Boynton, W. v., Tokar, R. l., Prettyman, T. h., Gasnault, O., Squyres, S. w., Elphic, R. c., Lawrence, D. j., Lawson, S. l., Maurice, S., McKinney, G. w., Moore, K. r., Reedy, R. c., 2002. Global Distribution of Neutrons from Mars: Results from Mars Odyssey. Science **297**, 75.

Feulner, G., 2012. The faint young Sun problem. Rev. Geophys. **50**, RG2006. doi:10.1029/2011RG000375

Filgueira-Rivera, M., Smith, N.D., Slingerland, R.L., 2007. Controls on natural levée development in the Columbia River, British Columbia, Canada. Sedimentology **54**, 905–919. doi:10.1111/j.1365-3091.2007.00865.x

Fitzsimons, S.J., 1991. Supraglacial eskers in Antarctica. Geomorphology **4**, 293–299. doi:10.1016/0169-555X(91)90011-X

Flamini, E., Capaccioni, F., Colangeli, L., Cremonese, G., Doressoundiram, A., Josset, J.L., Langevin, Y., Debei, S., Capria, M.T., De Sanctis, M.C., Marinangeli, L., Massironi, M., Mazzotta Epifani, E., Naletto, G., Palumbo, P., Eng, P., Roig, J.F., Caporali, A., Da Deppo, V., Erard, S., Federico, C., Forni, O., Sgavetti, M., Filacchione, G., Giacomini, L., Marra, G., Martellato, E., Zusi, M., Cosi, M., Bettanini, C., Calamai, L., Zaccariotto, M., Tommasi, L., Dami, M., Ficai Veltroni, J., Poulet, F., Hello, Y., 2010. SIMBIO-SYS: The spectrometer and imagers integrated observatory system for the BepiColombo planetary orbiter. Planet. Space Sci., Comprehensive Science Investigations of Mercury: The scientific goals of the joint ESA/JAXA mission BepiColombo **58**, 125–143. doi:10.1016/j.pss.2009.06.017

Flint, R.F., 1930. The Origin of the Irish “Eskers.” Geogr. Rev. 20, 615. doi:10.2307/209015

Forget, F., Haberle, R.M., Montmessin, F., Levrard, B., Head, J.W., 2006. Formation of Glaciers on Mars by Atmospheric Precipitation at High Obliquity. Science **311**, 368–371. doi:10.1126/science.1120335

Frey, H., Lowry, B.L., Chase, S.A., 1979. Pseudocraters on Mars. J. Geophys. Res. Solid Earth **84**, 8075–8086. doi:10.1029/JB084iB14p08075

Frey, H., Schultz, R.A., 1988. Large impact basins and the mega-impact origin for the crustal dichotomy on Mars. Geophys. Res. Lett. **15**, 229–232. doi:10.1029/GL015i003p00229

Frey, H.V., Schultz, R.A., 1990. Speculations on the origin and evolution of the Utopia-Elysium Lowlands of Mars. J. Geophys. Res. Solid Earth **95**, 14203–14213. doi:10.1029/JB095iB09p14203

Gallagher, C., Balme, M., 2015. Eskers in a complete, wet-based glacial system in the Phlegra Montes region, Mars. Earth Planet. Sci. Lett. **431**, 96–109. doi:10.1016/j.epsl.2015.09.023

Gallagher, C., Balme, M.R., Conway, S.J., Grindrod, P.M., 2011. Sorted clastic stripes, lobes and associated gullies in high-latitude craters on Mars: Landforms indicative of very recent, polycyclic ground-ice thaw and liquid flows. Icarus 211, 458–471. doi:10.1016/j.icarus.2010.09.010

Gallagher, C.J., Balme, M.R., 2011. Landforms indicative of ground-ice thaw in the northern high latitudes of Mars. Geol. Soc. Lond. Spec. Publ. **356**, 87–110. doi:10.1144/SP356.6

Gasselt, D.S. van, Neukum, D.G., 2011. Chronology, Cratering and Stratography, in: Gargaud, M., Amils, P.R., Quintanilla, J.C., II, H.J. (Jim) C., Irvine, W.M., Pinti, P.D.L., Viso, M. (Eds.), Encyclopedia of Astrobiology. Springer Berlin Heidelberg, pp. 304–313. doi:10.1007/978-3-642-11274-4_294

Ghent, R.R., Anderson, S.W., Pithawala, T.M., 2012. The formation of small cones in Isidis Planitia, Mars through mobilization of pyroclastic surge deposits. Icarus **217**, 169–183. doi:10.1016/j.icarus.2011.10.018

Gierasch, P., 2002. Planetary science: The north–south martian divide. Nature **416**, 269–270. doi:10.1038/416269a

Gough, D.O., 1981. Solar Interior Structure and Luminosity Variations, in: Domingo, V. (Ed.), Physics of Solar Variations. Springer Netherlands, pp. 21–34. doi:10.1007/978-94-010-9633-1_4

Greeley, R., Guest, J.E., 1987. Geologic map of the eastern equatorial region of Mars.

Greene, D.R., Hudlow, M.D., 1982. Hydrometeorologic grid mapping procedures, in: AWRA Int. Symp. on Hydrometeorology, Denver, CO.

Gregory, J.W., 1912. The Relations of Kames and Eskers. Geogr. J. **40**, 169. doi:10.2307/1778463

Grizzaffi, P., Schultz, P.H., 1989. Isidis basin: Site of ancient volatile-rich debris layer. Icarus **77**, 358–381. doi:10.1016/0019-1035(89)90094-8

Grotzinger, J.P., Crisp, J., Vasavada, A.R., Anderson, R.C., Baker, C.J., Barry, R., Blake, D.F., Conrad, P., Edgett, K.S., Ferdowski, B., Gellert, R., Gilbert, J.B., Golombek, M., Gómez-Elvira, J., Hassler, D.M., Jandura, L., Litvak, M., Mahaffy, P., Maki, J., Meyer, M., Malin, M.C., Mitrofanov, I., Simmonds, J.J., Vaniman, D., Welch, R.V., Wiens, R.C., 2012. Mars Science Laboratory Mission and Science Investigation. Space Sci. Rev. **170**, 5–56. doi:10.1007/s11214-012-9892-2

Guidat, T., Pochat, S., Bourgeois, O., Souček, O., 2015. Landform assemblage in Isidis Planitia, Mars: Evidence for a 3 Ga old polythermal ice sheet. Earth Planet. Sci. Lett. **411**, 253–267. doi:10.1016/j.epsl.2014.12.002

Gulick, V.C., 2001. Origin of the valley networks on Mars: a hydrological perspective. Geomorphology 37, 241–268. doi:10.1016/S0169-555X(00)00086-6

Hambrey, M.J., Fitzsimons, S.J., 2010. Development of sediment–landform associations at cold glacier margins, Dry Valleys, Antarctica. Sedimentology **57**, 857–882. doi:10.1111/j.1365-3091.2009.01123.x

Hamilton, C.W., Fagents, S.A., Wilson, L., 2010. Explosive lava-water interactions in Elysium Planitia, Mars: Geologic and thermodynamic constraints on the formation of the Tartarus Colles cone groups. J. Geophys. Res. Planets **115**, E09006. doi:10.1029/2009JE003546

Hansen, C.J., Bourke, M., Bridges, N.T., Byrne, S., Colon, C., Diniega, S., Dundas, C., Herkenhoff, K., McEwen, A., Mellon, M., Portyankina, G., Thomas, N., 2011. Seasonal Erosion and Restoration of Mars' Northern Polar Dunes. Science **331**, 575–578. doi:10.1126/science.1197636

Harrison, S.K., Balme, M.R., Hagermann, A., Murray, J.B., Muller, J.-P., Wilson, A., 2013. A branching, positive relief network in the middle member of the Medusae Fossae Formation, equatorial Mars - Evidence for sapping? Planet. Space Sci. **85**, 142–163. doi:10.1016/j.pss.2013.06.004

Harrison, T.N., Osinski, G.R., Tornabene, L.L., Jones, E., 2015. Global documentation of gullies with the Mars Reconnaissance Orbiter Context Camera and implications for their formation. Icarus **252**, 236–254. doi:10.1016/j.icarus.2015.01.022

Hartmann, W.K., 2005. Martian cratering 8: Isochron refinement and the chronology of Mars. Icarus **174**, 294–320. doi:10.1016/j.icarus.2004.11.023

Hartmann, W.K., 2001. Martian Seeps and Their Relation to Youthful Geothermal Activity, in: Kallenbach, R., Geiss, J., Hartmann, W.K. (Eds.), Chronology and Evolution of Mars, Space Sciences Series of ISSI. Springer Netherlands, pp. 405–410. doi:10.1007/978-94-017-1035-0_15

Hartmann, W.K., Neukum, G., 2001. Cratering Chronology and the Evolution of Mars. Space Sci. Rev. **96**, 165–194. doi:10.1023/A:1011945222010

Hartmann, W.K., Thorsteinsson, T., Sigurdsson, F., 2003. Martian hillside gullies and icelandic analogs. Icarus 162, 259–277. doi:10.1016/S0019-1035(02)00065-9

Hartmann, W.K., Werner, S.C., 2010. Martian Cratering 10. Progress in use of crater counts to interpret geological processes: Examples from two debris aprons. Earth Planet. Sci. Lett. **294**, 230–237. doi:10.1016/j.epsl.2009.10.001

Hauber, E., Reiss, D., Ulrich, M., Preusker, F., Trauthan, F., Zanetti, M., Hiesinger, H., Jaumann, R., Johansson, L., Johnsson, A., Gasselt, S.V., Olvmo, M., 2011. Landscape evolution in Martian mid-latitude regions: insights from analogous periglacial landforms in Svalbard. Geol. Soc. Lond. Spec. Publ. **356**, 111–131. doi:10.1144/SP356.7

Hayward, R.K., Mullins, K.F., Fenton, L.K., Hare, T.M., Titus, T.N., Bourke, M.C., Colaprete, A., Christensen, P.R., 2007. Mars Global Digital Dune Database and initial science results. J. Geophys. Res. Planets **112**, E11007. doi:10.1029/2007JE002943

Head, J.W., 2007. The geology of Mars: new insights and outstanding questions. Geol. Mars Evid. Earth-Based Analog **1**, 1.

Head, J.W., Hiesinger, H., Ivanov, M.A., Kreslavsky, M.A., Pratt, S., Thomson, B.J., 1999. Possible Ancient Oceans on Mars: Evidence from Mars Orbiter Laser Altimeter Data. Science **286**, 2134–2137. doi:10.1126/science.286.5447.2134

Head, J.W., Kreslavsky, M., Hiesinger, H., Ivanov, M., Pratt, S., Seibert, N., Smith, D.E., Zuber, M.T., 1998. Oceans in the past history of Mars: Tests for their presence using Mars Orbiter Laser Altimeter (MOLA) data. Geophys. Res. Lett. **25**, 4401–4404. doi:10.1029/1998GL900116

Head, J.W., Kreslavsky, M.A., 2001. Plains in Eastern Elysium Planitia, Mars: Topographic Evidence for Aqueous Channels and Lava Flows, in: Lunar and Planetary Science Conference. Presented at the Lunar and Planetary Science Conference, p. 1002.

Head, J.W., Marchant, D.R., Dickson, J.L., Kress, A.M., Baker, D.M., 2010. Northern mid-latitude glaciation in the Late Amazonian period of Mars: Criteria for the recognition of debris-covered glacier and valley glacier landsystem deposits. Earth Planet. Sci. Lett. **294**, 306–320. doi:10.1016/j.epsl.2009.06.041

Head, J.W., Mustard, J.F., Kreslavsky, M.A., Milliken, R.E., Marchant, D.R., 2003a. Recent ice ages on Mars. Nature **426**, 797–802. doi:10.1038/nature02114

Head, J.W., Neukum, G., Jaumann, R., Hiesinger, H., Hauber, E., Carr, M., Masson, P., Foing, B., Hoffmann, H., Kreslavsky, M., Werner, S., Milkovich, S., van Gasselt, S., Team, T.H.C.-I., 2005. Tropical to mid-latitude snow and ice accumulation, flow and glaciation on Mars. Nature **434**, 346–351. doi:10.1038/nature03359

Head, J.W., Wilson, L., Mitchell, K.L., 2003b. Generation of recent massive water floods at Cerberus Fossae, Mars by dike emplacement, cryospheric cracking, and confined aquifer groundwater release. Geophys. Res. Lett. 30. doi:10.1029/2003GL017135

Heldmann, J.L., Carlsson, E., Johansson, H., Mellon, M.T., Toon, O.B., 2007. Observations of martian gullies and constraints on potential formation mechanisms: II. The northern hemisphere. Icarus **188**, 324–344. doi:10.1016/j.icarus.2006.12.010

Heldmann, J.L., Mellon, M.T., 2004. Observations of martian gullies and constraints on potential formation mechanisms. Icarus **168**, 285–304. doi:10.1016/j.icarus.2003.11.024

Hiesinger, H., Head III, J.W., 2002. Topography and morphology of the Argyre Basin, Mars: implications for its geologic and hydrologic history. Planet. Space Sci. **50**, 939–981. doi:10.1016/S0032-0633(02)00054-5

Holt, J.W., Safaeinili, A., Plaut, J.J., Head, J.W., Phillips, R.J., Seu, R., Kempf, S.D., Choudhary, P., Young, D.A., Putzig, N.E., Biccari, D., Gim, Y., 2008. Radar Sounding Evidence for Buried Glaciers in the Southern Mid-Latitudes of Mars. Science **322**, 1235–1238. doi:10.1126/science.1164246

Hoogenboom, T., Smrekar, S.E., 2006. Elastic thickness estimates for the northern lowlands of Mars. Earth Planet. Sci. Lett. **248**, 830–839. doi:10.1016/j.epsl.2006.06.035

Howard, A.D., 1981. Etched plains and braided ridges of the south polar region of Mars: features produced by basal melting of ground ice? Rep. Planet. Geol. Program 1, 286–288.

Howard, A.D., 1971. Optimal Angles of Stream Junction: Geometric, Stability to Capture, and Minimum Power Criteria. Water Resour. Res. **7**, 863–873. doi:10.1029/WR007i004p00863

Howard, A.D., Moore, J.M., 2011. Late Hesperian to early Amazonian midlatitude Martian valleys: Evidence from Newton and Gorgonum basins. J. Geophys. Res. Planets **116**, E05003. doi:10.1029/2010JE003782

Hubbard, B., Milliken, R.E., Kargel, J.S., Limaye, A., Souness, C., 2011. Geomorphological characterisation and interpretation of a mid-latitude glacier-like form: Hellas Planitia, Mars. Icarus **211**, 330–346. doi:10.1016/j.icarus.2010.10.021

Hynek, B.M., Beach, M., Hoke, M.R.T., 2010. Updated global map of Martian valley networks and implications for climate and hydrologic processes. J. Geophys. Res. Planets **115**, E09008. doi:10.1029/2009JE003548

Hynek, B.M., Phillips, R.J., 2003. New data reveal mature, integrated drainage systems on Mars indicative of past precipitation. Geology **31**, 757–760. doi:10.1130/G19607.1

Ingersoll, A.P., Svitek, T., Murray, B.C., 1992. Stability of polar frosts in spherical bowl-shaped craters on the Moon, Mercury, and Mars. Icarus **100**, 40–47. doi:10.1016/0019-1035(92)90016-Z

Jaeger, W.L., Keszthelyi, L.P., McEwen, A.S., Dundas, C.M., Russell, P.S., 2007. Athabasca Valles, Mars: A Lava-Draped Channel System. Science **317**, 1709–1711. doi:10.1126/science.1143315

Jaeger, W.L., Keszthelyi, L.P., Skinner Jr., J.A., Milazzo, M.P., McEwen, A.S., Titus, T.N., Rosiek, M.R., Galuszka, D.M., Howington-Kraus, E., Kirk, R.L., 2010. Emplacement of the youngest flood lava on Mars: A short, turbulent story. Icarus, MRO/HiRISE Studies of Mars **205**, 230–243. doi:10.1016/j.icarus.2009.09.011

Jaeger, W.L., Keszthelyi, L.P., Skinner Jr., J.A., Milazzo, M.P., McEwen, A.S., Titus, T.N., Rosiek, M.R., Galuszka, D.M., Howington-Kraus, E., Kirk, R.L., 2010. Emplacement of the youngest flood lava on Mars: A short, turbulent story. Icarus **205**, 230–243. doi:10.1016/j.icarus.2009.09.011

Jakosky, B.M., Ahrens, T.J., 1979. The history of an atmosphere of impact origin. Presented at the Lunar and Planetary Science Conference Proceedings, pp. 2727–2739.

Jakosky, B.M., Carr, M.H., 1985. Possible precipitation of ice at low latitudes of Mars during periods of high obliquity. Nature **315**, 559–561. doi:10.1038/315559a0

James, P.B., Kieffer, H.H., Paige, D.A., 1992. The seasonal cycle of carbon dioxide on Mars, in: Mars. pp. 934–968.

Johnsson, A., Reiss, D., Hauber, E., Hiesinger, H., Zanetti, M., 2014. Evidence for very recent melt-water and debris flow activity in gullies in a young mid-latitude crater on Mars. Icarus **235**, 37–54. doi:10.1016/j.icarus.2014.03.005

Johnsson, A., Reiss, D., Hauber, E., Zanetti, M., Hiesinger, H., Johansson, L., Olvmo, M., 2012. Periglacial mass-wasting landforms on Mars suggestive of transient liquid water in the recent past: Insights from solifluction lobes on Svalbard. Icarus **218**, 489–505. doi:10.1016/j.icarus.2011.12.021

Jones, A.P., McEwen, A.S., Tornabene, L.L., Baker, V.R., Melosh, H.J., Berman, D.C., 2011. A geomorphic analysis of Hale crater, Mars: The effects of impact into ice-rich crust. Icarus **211**, 259–272. doi:10.1016/j.icarus.2010.10.014

Jons, H.-P., 1992. Fossil Glaciations in the Environs of the South Pole, Mars? Presented at the Lunar and Planetary Institute Science Conference Abstracts, p. 633.

Joy, K., Crawford, I., Grindrod, P., Lintott, C., Bamford, S., Smith, A., Cook, A., Zoo, M., 2011. Moon Zoo: citizen science in lunar exploration. Astron. Geophys. **52**, 2.10-2.12. doi:10.1111/j.1468-4004.2011.52210.x

Kadish, S.J., Head, J.W., Barlow, N.G., Marchant, D.R., 2008. Martian pedestal craters: Marginal sublimation pits implicate a climate-related formation mechanism. Geophys. Res. Lett. **35**, n/a–n/a. doi:10.1029/2008GL034990

Kargel, J.S., 2004. Mars - A Warmer, Wetter Planet. Springer.

Kargel, J.S., Baker, V.R., Begét, J.E., Lockwood, J.F., Péwé, T.L., Shaw, J.S., Strom, R.G., 1995. Evidence of ancient continental glaciation in the Martian northern plains. J. Geophys. Res. Planets **100**, 5351–5368. doi:10.1029/94JE02447

Kargel, J.S., Strom, R.G., 1992. Ancient glaciation on Mars. Geology **20**, 3–7. doi:10.1130/0091-7613(1992)020<0003:AGOM>2.3.CO;2

Kargel, J.S., Strom, R.G., 1991. Terrestrial glacial eskers: Analogs for Martian sinuous ridges. Bibliogr. Planet. Geol. Geophys. Princ. Investig. Their Assoc. 1990 - 1991 1, 129–130.

Kargel, J.S., Strom, R.G., 1990. Ancient glaciation on Mars. In Mars: Evolution of Volcanism, Techtonics, and Volatiles.

Kargel, J.S., Strom, R.G., Lockwood, J., Shaw, J., 1992. Subglacial and Glaciomarine Processes in the Martian Northern Plaints. Presented at the Lunar and Planetary Science Conference.

Keszthelyi, L., Jaeger, W., McEwen, A., Tornabene, L., Beyer, R.A., Dundas, C., Milazzo, M., 2008. High Resolution Imaging Science Experiment (HiRISE) images of volcanic terrains from the first 6 months of the Mars Reconnaissance Orbiter Primary Science Phase. J. Geophys. Res. Planets **113**. doi:10.1029/2007JE002968

Keszthelyi, L., McEwen, A.S., Thordarson, T., 2000. Terrestrial analogs and thermal models for Martian flood lavas. J. Geophys. Res. Planets **105**, 15027–15049. doi:10.1029/1999JE001191

Keszthelyi, L., Thordarson, T., McEwen, A., Haack, H., Guilbaud, M.-N., Self, S., Rossi, M.J., 2004. Icelandic analogs to Martian flood lavas. Geochem. Geophys. Geosystems **5**, Q11014. doi:10.1029/2004GC000758

Kieffer, H.H., 1979. Mars south polar spring and summer temperatures: A residual CO2 frost. J. Geophys. Res. Solid Earth **84**, 8263–8288. doi:10.1029/JB084iB14p08263

Kite, E.S., Michaels, T.I., Rafkin, S., Manga, M., Dietrich, W.E., 2011. Localized precipitation and runoff on Mars. J. Geophys. Res. Planets **116**. doi:10.1029/2010JE003783

Kneissl, T., Reiss, D., van Gasselt, S., Neukum, G., 2010. Distribution and orientation of northern-hemisphere gullies on Mars from the evaluation of HRSC and MOC-NA data. Earth Planet. Sci. Lett., Mars Express after 6 Years in Orbit: Mars Geology from Three-Dimensional Mapping by the High Resolution Stereo Camera (HRSC) Experiment **294**, 357–367. doi:10.1016/j.epsl.2009.05.018

Kostama, V.-P., Kreslavsky, M.A., Head, J.W., 2006. Recent high-latitude icy mantle in the northern plains of Mars: Characteristics and ages of emplacement. Geophys. Res. Lett. **33**, L11201. doi:10.1029/2006GL025946

Kovacs, A., Sodhi, D.S., 1980. Shore ice pile-up and ride-up: Field observations, models, theoretical analyses. Cold Reg. Sci. Technol., The Seasonal Sea Ice Zone Proceedings International Workshop **2**, 210–288. doi:10.1016/0165-232X(80)90076-2

Kreslavsky, M.A., Head, J.W., 2002a. Mars: Nature and evolution of young latitude-dependent water-ice-rich mantle. Geophys. Res. Lett. **29**, 14–1–14–4. doi:10.1029/2002GL015392

Kreslavsky, M.A., Head, J.W., 2002b. Mars: Nature and evolution of young latitude-dependent water-ice-rich mantle. Geophys. Res. Lett. **29**, 14–1. doi:10.1029/2002GL015392

Kreslavsky, M.A., Head, J.W., 2002. Fate of outflow channel effluents in the northern lowlands of Mars: The Vastitas Borealis Formation as a sublimation residue from frozen ponded bodies of water. J. Geophys. Res. Planets **107**, 4–1–4–25. doi:10.1029/2001JE001831

Kreslavsky, M.A., Head, J.W., 2000. Kilometer-scale roughness of Mars: Results from MOLA data analysis. J. Geophys. Res. Planets **105**, 26695–26711. doi:10.1029/2000JE001259

Kuhn, W.R., Atreya, S.K., 1979. Ammonia photolysis and the greenhouse effect in the primordial atmosphere of the earth. Icarus **37**, 207–213. doi:10.1016/0019-1035(79)90126-X

Kuhn, W.R., Atreya, S.K., Postawko, S.E., 1979. The influence of ozone on Martian atmospheric temperature. J. Geophys. Res. **84**, 8341. doi:10.1029/JB084iB14p08341

Lachenbruch, A.H., 1962. Mechanics of Thermal Contraction Cracks and Ice-Wedge Polygons in Permafrost. Geol. Soc. Am. Spec. Pap. 70, 1–66. doi:10.1130/SPE70-p1

Lanagan, P.D., McEwen, A.S., Keszthelyi, L.P., Thordarson, T., 2001. Rootless cones on Mars indicating the presence of shallow equatorial ground ice in recent times. Geophys. Res. Lett. **28**, 2365–2367. doi:10.1029/2001GL012932

Lancaster, N., Greeley, R., 1990. Sediment volume in the north polar sand seas of Mars. J. Geophys. Res. Solid Earth **95**, 10921–10927. doi:10.1029/JB095iB07p10921

Langbein, W.B., Leopold, L.B., 1964. Quasi-equilibrium states in channel morphology. Am. J. Sci. 262, 782–794. doi:10.2475/ajs.262.6.782

Laskar, J., Correia, A.C.M., Gastineau, M., Joutel, F., Levrard, B., Robutel, P., 2004. Long term evolution and chaotic diffusion of the insolation quantities of Mars. Icarus **170**, 343–364. doi:10.1016/j.icarus.2004.04.005

Laskar, J., Levrard, B., Mustard, J.F., 2002. Orbital forcing of the martian polar layered deposits. Nature **419**, 375–377. doi:10.1038/nature01066

Lee, S.W., Thomas, P.C., Cantor, B.A., 2013. Disappearance of the Propontis Regional Dark Albedo Feature on Mars. Presented at the AAS/Division for Planetary Sciences Meeting Abstracts, p. 400.01.

Lefort, A., Russell, P.S., Thomas, N., McEwen, A.S., Dundas, C.M., Kirk, R.L., 2009. Observations of periglacial landforms in Utopia Planitia with the High Resolution Imaging Science Experiment (HiRISE). J. Geophys. Res. Planets **114**, E04005. doi:10.1029/2008JE003264

Leovy, C., 2001. Weather and climate on Mars. Nature **412**, 245–249. doi:10.1038/35084192

Leverington, D.W., 2004. Volcanic rilles, streamlined islands, and the origin of outflow channels on Mars. J. Geophys. Res. Planets **109**, E10011. doi:10.1029/2004JE002311

Levy, J., Head, J., Marchant, D., 2009. Thermal contraction crack polygons on Mars: Classification, distribution, and climate implications from HiRISE observations. J. Geophys. Res. Planets **114**. doi:10.1029/2008JE003273

Levy, J.S., Fassett, C.I., Head, J.W., 2016. Enhanced erosion rates on Mars during Amazonian glaciation. Icarus **264**, 213–219. doi:10.1016/j.icarus.2015.09.037

Levy, J.S., Fassett, C.I., Head, J.W., Schwartz, C., Watters, J.L., 2014. Sequestered glacial ice contribution to the global Martian water budget: Geometric constraints on the volume of remnant, midlatitude debris-covered glaciers. J. Geophys. Res. Planets **119**, 2014JE004685. doi:10.1002/2014JE004685

Levy, J.S., Head, J.W., Marchant, D.R., 2007. Lineated valley fill and lobate debris apron stratigraphy in Nilosyrtis Mensae, Mars: Evidence for phases of glacial modification of the dichotomy boundary. J. Geophys. Res. Planets **112**, E08004. doi:10.1029/2006JE002852

Levy, J.S., Marchant, D.R., Head, J.W., 2010. Thermal contraction crack polygons on Mars: A synthesis from HiRISE, Phoenix, and terrestrial analog studies. Icarus **206**, 229–252. doi:10.1016/j.icarus.2009.09.005

Lingenfelter, R.E., Schubert, G., 1973. Evidence for convection in planetary interiors from first-order topography. The moon **7**, 172–180. doi:10.1007/BF00578814

Lockwood, J.F., Kargel, J.S., Strom, R.B., 1992. Thumbprint Terrain on the Northern Plains: A Glacial Hypothesis. Presented at the Lunar and Planetary Science Conference, p. 795.

Longwell, C.R., Flint, R.F., Sanders, J.E., 1969. Physical geology. Wiley, New York.

Lorenz, R.D., 2009. Power law of dust devil diameters on Mars and Earth. Icarus **203**, 683–684. doi:10.1016/j.icarus.2009.06.029

Lucchitta, B.K., 2001. Antarctic ice streams and outflow channels on Mars. Geophys. Res. Lett. **28**, 403–406. doi:10.1029/2000GL011924

Lucchitta, B.K., 1982. Ice sculpture in the Martian outflow channels. J. Geophys. Res. Solid Earth **87**, 9951–9973. doi:10.1029/JB087iB12p09951

Lucchitta, B.K., 1981. Mars and Earth: Comparison of cold-climate features. Icarus **45**, 264–303. doi:10.1016/0019-1035(81)90035-X

Lucchitta, B.K., Ferguson, H.M., Summers, C., 1986. Sedimentary deposits in the Northern Lowland Plains, Mars. J. Geophys. Res. Solid Earth **91**, E166–E174. doi:10.1029/JB091iB13p0E166

Madeleine, J.-B., Forget, F., Head, J.W., Levrard, B., Montmessin, F., Millour, E., 2009. Amazonian northern mid-latitude glaciation on Mars: A proposed climate scenario. Icarus **203**, 390–405. doi:10.1016/j.icarus.2009.04.037

Malin, M.C., Bell, J.F., Cantor, B.A., Caplinger, M.A., Calvin, W.M., Clancy, R.T., Edgett, K.S., Edwards, L., Haberle, R.M., James, P.B., Lee, S.W., Ravine, M.A., Thomas, P.C., Wolff, M.J.,

2007. Context Camera Investigation on board the Mars Reconnaissance Orbiter. J. Geophys. Res. Planets **112**,. doi:10.1029/2006JE002808

Malin, M.C., Edgett, K.S., 2000. Evidence for Recent Groundwater Seepage and Surface Runoff on Mars. Science **288**, 2330–2335. doi:10.1126/science.288.5475.2330

Malin, M.C., Edgett, K.S., 1999. Oceans or seas in the Martian northern lowlands: High resolution imaging tests of proposed coastlines. Geophys. Res. Lett. **26**, 3049–3052. doi:10.1029/1999GL002342

Mangold, N., 2005. High latitude patterned grounds on Mars: Classification, distribution and climatic control. Icarus **174**, 336–359. doi:10.1016/j.icarus.2004.07.030

Mangold, N., Maurice, S., Feldman, W.C., Costard, F., Forget, F., 2004. Spatial relationships between patterned ground and ground ice detected by the Neutron Spectrometer on Mars. J. Geophys. Res. Planets **109**, E08001. doi:10.1029/2004JE002235

Masursky, H., Batson, R.M., McCauley, J.F., Soderblom, L.A., Wildey, R.L., Carr, M.H., Milton, D.J., Wilhelms, D.E., Smith, B.A., Kirby, T.B., Robinson, J.C., Leovy, C.B., Briggs, G.A., Duxbury, T.C., Acton, C.H., Murray, B.C., Cutts, J.A., Sharp, R.P., Smith, S., Leighton, R.B., Sagan, C., Veverka, J., Noland, M., Lederberg, J., Levinthal, E., Pollack, J.B., Moore, J.T., Hartmann, W.K., Shipley, E.N., Vaucouleurs, G.D., Davies, M.E., 1972. Mariner 9 Television Reconnaissance of Mars and Its Satellites: Preliminary Results. Science **175**, 294–305. doi:10.1126/science.175.4019.294

Masursky, H., Boyce, J.M., Dial, A.L., Schaber, G.G., Strobell, M.E., 1977. Classification and time of formation of Martian channels based on Viking data. J. Geophys. Res. **82**, 4016–4038. doi:10.1029/JS082i028p04016

McCauley, J.F., Carr, M.H., Cutts, J.A., Hartmann, W.K., Masursky, H., Milton, D.J., Sharp, R.P., Wilhelms, D.E., 1972. Preliminary mariner 9 report on the geology of Mars. Icarus **17**, 289–327. doi:10.1016/0019-1035(72)90003-6

McElroy, M.B., Kong, T.Y., Yung, Y.L., 1977. Photochemistry and evolution of Mars' atmosphere: A Viking perspective. J. Geophys. Res. **82**, 4379–4388. doi:10.1029/JS082i028p04379

McEwen, A.S., 2007. Mars reconnaissance orbiter's high resolution imaging science experiment (HiRISE). J. Geophys. Res. 112.

McEwen, A.S., Eliason, E.M., Bergstrom, J.W., Bridges, N.T., Hansen, C.J., Delamere, W.A., Grant, J.A., Gulick, V.C., Herkenhoff, K.E., Keszthelyi, L., Kirk, R.L., Mellon, M.T., Squyres, S.W., Thomas, N., Weitz, C.M., 2007. Mars Reconnaissance Orbiter's High Resolution Imaging Science Experiment (HiRISE). J. Geophys. Res. Planets **112**, E05S02. doi:10.1029/2005JE002605

McGill, G.E., 1989. Buried topography of Utopia, Mars: persistence of a giant impact depression. J. Geophys. Res. **94**, 2753–2759.

McGill, G.E., 1989. Buried topography of Utopia, Mars: Persistence of a giant impact depression. J. Geophys. Res. Solid Earth **94**, 2753–2759. doi:10.1029/JB094iB03p02753

McGill, G.E., Hills, L.S., 1992. Origin of giant Martian polygons. J. Geophys. Res. Planets **97**, 2633–2647. doi:10.1029/91JE02863

McKay, D.S., Gibson, E.K., Thomas-Keprta, K.L., Vali, H., Romanek, C.S., Clemett, S.J., Chillier, X.D.F., Maechling, C.R., Zare, R.N., 1996. Search for Past Life on Mars: Possible Relic Biogenic Activity in Martian Meteorite ALH84001. Science **273**, 924–930.

Mellon, M.T., 1997. Small-scale polygonal features on Mars: Seasonal thermal contraction cracks in permafrost. J. Geophys. Res. Planets **102**, 25617–25628. doi:10.1029/97JE02582

Mellon, M.T., Arvidson, R.E., Marlow, J.J., Phillips, R.J., Asphaug, E., 2008. Periglacial landforms at the Phoenix landing site and the northern plains of Mars. J. Geophys. Res. Planets **113**. doi:10.1029/2007JE003039

Mellon, M.T., Arvidson, R.E., Sizemore, H.G., Searls, M.L., Blaney, D.L., Cull, S., Hecht, M.H., Heet, T.L., Keller, H.U., Lemmon, M.T., Markiewicz, W.J., Ming, D.W., Morris, R.V., Pike, W.T., Zent, A.P., 2009. Ground ice at the Phoenix Landing Site: Stability state and origin. J. Geophys. Res. Planets **114**, E00E07. doi:10.1029/2009JE003417

Mellon, M.T., Jakosky, B.M., 1995. The distribution and behavior of Martian ground ice during past and present epochs. J. Geophys. Res. Planets **100**, 11781–11799. doi:10.1029/95JE01027

Mellon, M.T., Phillips, R.J., 2001. Recent gullies on Mars and the source of liquid water. J. Geophys. Res. Planets **106**, 23165–23179. doi:10.1029/2000JE001424

Melosh, H.J., Vickery, A.M., 1989. Impact erosion of the primordial atmosphere of Mars. Nature **338**, 487–489. doi:10.1038/338487a0

Metzger, S.M., 1992. The Eskers of New York State: Formation Process Implications and Esker-like Features on the Planet Mars. Presented at the Lunar and Planetary Institute Science Conference Abstracts, p. 901.

Metzger, S.M., 1991. A Survey of Esker Morphometries, the Connection to New York State Glaciation and Criteria for Subglacial Melt-Water Channel Deposits on the Planet Mars. Presented at the Lunar and Planetary Institute Science Conference Abstracts, p. 891.

Michael, G.G., 2013. Planetary surface dating from crater size–frequency distribution measurements: Multiple resurfacing episodes and differential isochron fitting. Icarus **226**, 885–890. doi:10.1016/j.icarus.2013.07.004

Milliken, R.E., Mustard, J.F., Goldsby, D.L., 2003. Viscous flow features on the surface of Mars: Observations from high-resolution Mars Orbiter Camera (MOC) images. J. Geophys. Res. Planets **108**. doi:10.1029/2002JE002005

Milton, D.J., 1973. Water and processes of degradation in the Martian landscape. J. Geophys. Res. **78**, 4037–4047. doi:10.1029/JB078i020p04037

Morgan, G.A., Head III, J.W., Marchant, D.R., 2009. Lineated valley fill (LVF) and lobate debris aprons (LDA) in the Deuteronilus Mensae northern dichotomy boundary region, Mars: Constraints on the extent, age and episodicity of Amazonian glacial events. Icarus **202**, 22–38. doi:10.1016/j.icarus.2009.02.017

Morgenstern, A., Hauber, E., Reiss, D., van Gasselt, S., Grosse, G., Schirrmeister, L., 2007. Deposition and degradation of a volatile-rich layer in Utopia Planitia and implications for climate history on Mars. J. Geophys. Res. Planets 112, E06010. doi:10.1029/2006JE002869

Mosley, M.P., 1976. An Experimental Study of Channel Confluences. J. Geol. **84**, 535–562. doi:10.1086/628230

Mouginot, J., Pommerol, A., Beck, P., Kofman, W., Clifford, S.M., 2012. Dielectric map of the Martian northern hemisphere and the nature of plain filling materials. Geophys. Res. Lett. **39**, L02202. doi:10.1029/2011GL050286

Murray, J.B., Muller, J.-P., Neukum, G., Werner, S.C., van Gasselt, S., Hauber, E., Markiewicz, W.J., Head, J.W., Foing, B.H., Page, D., Mitchell, K.L., Portyankina, G., Team, T.H.C.-I., 2005. Evidence from the Mars Express High Resolution Stereo Camera for a frozen sea close to Mars' equator. Nature **434**, 352–356. doi:10.1038/nature03379

Musselwhite, D.S., Swindle, T.D., Lunine, J.I., 2001. Liquid CO2 breakout and the formation of recent small gullies on Mars. Geophys. Res. Lett. **28**, 1283–1285. doi:10.1029/2000GL012496

Mustard, J.F., Cooper, C.D., Rifkin, M.K., 2001. Evidence for recent climate change on Mars from the identification of youthful near-surface ground ice. Nature **412**, 411–414. doi:10.1038/35086515

Mutch, T.A., Arvidson, R.E., Head, J.W., III, Jones, K.L., Saunders, R.S., 1976. The geology of Mars.

Mutch, T.A., Saunders, R.S., 1976. The geologic development of Mars: A review. Space Sci. Rev. **19**, 3–57. doi:10.1007/BF00215628

Neukum, G., Jaumann, R., 2004. HRSC: the High Resolution Stereo Camera of Mars Express, in: Mars Express: The Scientific Payload. Presented at the Mars Express: the Scientific Payload, pp. 17–35.

Neukum, G., Jaumann, R., Hoffmann, H., Hauber, E., Head, J.W., Basilevsky, A.T., Ivanov, B.A., Werner, S.C., Gasselt, S. van, Murray, J.B., McCord, T., Team, T.H.C.-I., 2004. Recent and episodic volcanic and glacial activity on Mars revealed by the High Resolution Stereo Camera. Nature **432**, 971–979. doi:10.1038/nature03231

Nummedal, D., Prior, D.B., 1981. Generation of Martian chaos and channels by debris flows. Icarus **45**, 77–86. doi:10.1016/0019-1035(81)90007-5

Nussbaumer, J., Jaumann, R., Hauber, E., 2000. Evidence for a Surging Ice-Sheet in Elysium Planitia, Mars, in: Second International Conference on Mars Polar Science and Exploration. Presented at the Second International Conference on Mars Polar Science and Exploration, p. 137.

Oehler, D.Z., Allen, C.C., 2010. Evidence for pervasive mud volcanism in Acidalia Planitia, Mars. Icarus **208**, 636–657. doi:10.1016/j.icarus.2010.03.031

Orgel, C., Hauber, E., van Gasselt, S., Pozzobon, R., Skinner, J., Jr., 2016. Distribution, origin and evolution of hypothesized mud volcanoes, thumbprint terrain, small mounds and giant polygons: Implications for sedimentary processes in the northern lowlands of Mars: Case study from the Acidalia Planitia. Presented at the EGU General Assembly Conference Abstracts, p. 1038.

Orloff, T.C., 2012. Geomorphological analysis of boulders and polygons on martian periglacial patterned ground terrains.

Owen, T., 1992. The composition and early history of the atmosphere of Mars, in: Mars. pp. 818–834.

Page, D.P., 2010. Resolving the Elysium Controversy: An open invitation to explain the evidence. Planet. Space Sci. **58**, 1406–1413. doi:10.1016/j.pss.2010.06.010

Page, D.P., 2007. Recent low-latitude freeze–thaw on Mars. Icarus **189**, 83–117. doi:10.1016/j.icarus.2007.01.005

Page, D.P., Balme, M.R., Grady, M.M., 2009. Dating martian climate change. Icarus **203**, 376–389. doi:10.1016/j.icarus.2009.05.012

Pain, C.F., Clarke, J.D.A., Thomas, M., 2007. Inversion of relief on Mars. Icarus, Deep Impact Mission to Comet 9P/Tempel 1, Part 2 190, 478–491. doi:10.1016/j.icarus.2007.03.017

Parker, T.J., 1994. Martian Paleolakes and Oceans. Thesis PHD--Univ. South. Calif. 1994Source Diss. Abstr. Int. Vol. 56-09 Sect. B Page 4789.

Parker, T.J., Gorsline, D.S., 1992. Preliminary Geologic Mapping of the MTM-55036 and 55043 Quadrangles, Southern Argyre Planitia, Mars. Presented at the Lunar and Planetary Institute Science Conference Abstracts, p. 1031.

Parker, T.J., Gorsline, D.S., Saunders, R.S., Pieri, D.C., Schneeberger, D.M., 1993. Coastal geomorphology of the Martian northern plains. J. Geophys. Res. Planets **98**, 11061–11078. doi:10.1029/93JE00618

Parker, T.J., Stephen Saunders, R., Schneeberger, D.M., 1989. Transitional morphology in West Deuteronilus Mensae, Mars: Implications for modification of the lowland/upland boundary. Icarus **82**, 111–145. doi:10.1016/0019-1035(89)90027-4

Parker, T.J.D.C., Pieri, D.C., Saunders, R.S., 1986. Morphology and distribution of sinuous ridges in central and southern Argyre. NASA Tech Memo **8**, 468–470.

Pasquon, K., Gargani, J., Massé, M., Conway, S.J., 2016. Present-day formation and seasonal evolution of linear dune gullies on Mars. Icarus **274**, 195–210. doi:10.1016/j.icarus.2016.03.024

Pathare, A.V., Paige, D.A., Turtle, E., 2005. Viscous relaxation of craters within the martian south polar layered deposits. Icarus **174**, 396–418. doi:10.1016/j.icarus.2004.10.031

Pechmann, J.C., 1980. The origin of polygonal troughs on the Northern Plains of Mars. Icarus **42**, 185–210. doi:10.1016/0019-1035(80)90071-8

Perron, J.T., Mitrovica, J.X., Manga, M., Matsuyama, I., Richards, M.A., 2007. Evidence for an ancient martian ocean in the topography of deformed shorelines. Nature **447**, 840–843. doi:10.1038/nature05873

Peulvast, J.-P., Mège, D., Chiciak, J., Costard, F., Masson, P.L., 2001. Morphology, evolution and tectonics of Valles Marineris wallslopes (Mars). Geomorphology **37**, 329–352. doi:10.1016/S0169-555X(00)00085-4

Picardi, G., Plaut, J.J., Biccari, D., Bombaci, O., Calabrese, D., Cartacci, M., Cicchetti, A., Clifford, S.M., Edenhofer, P., Farrell, W.M., Federico, C., Frigeri, A., Gurnett, D.A., Hagfors, T., Heggy, E., Herique, A., Huff, R.L., Ivanov, A.B., Johnson, W.T.K., Jordan, R.L., Kirchner, D.L., Kofman, W., Leuschen, C.J., Nielsen, E., Orosei, R., Pettinelli, E., Phillips, R.J., Plettemeier, D., Safaeinili, A., Seu, R., Stofan, E.R., Vannaroni, G., Watters, T.R., Zampolini, E., 2005. Radar Soundings of the Subsurface of Mars. Science **310**, 1925–1928. doi:10.1126/science.1122165

Pieri, D.C., 1980. Martian valleys - Morphology, distribution, age, and origin. Science 210, 895–897. doi:10.1126/science.**210**.4472.895

Pilorget, C., Forget, F., 2016. Formation of gullies on Mars by debris flows triggered by CO2 sublimation. Nat. Geosci. 9, 65–**69**. doi:10.1038/ngeo2619

Plaut, J.J., Safaeinili, A., Holt, J.W., Phillips, R.J., Head, J.W., Seu, R., Putzig, N.E., Frigeri, A., 2009. Radar evidence for ice in lobate debris aprons in the mid-northern latitudes of Mars. Geophys. Res. Lett. **36**. doi:10.1029/2008GL036379

Plescia, J.B., 2003. Cerberus Fossae, Elysium, Mars: a source for lava and water. Icarus **164**, 79–95. doi:10.1016/S0019-1035(03)00139-8

Plescia, J.B., 1980. Cinder cones of Isidis and Elysium. Rep. Planet. Geol. Program 1, 263–265.

Rampey, M.L., Milam, K.A., McSween, H.Y., Moersch, J.E., Christensen, P.R., 2007. Identity and emplacement of domical structures in the western Arcadia Planitia, Mars. J. Geophys. Res. Planets **112**, E06011. doi:10.1029/2006JE002750

Read, P.L., Lewis, S.R., 2004. The Martian Climate Revisited: Atmosphere and Environment of a Desert Planet. Springer.

Rice, J.W., Mollard, J.D., 1994. Analogs and Interpretations for the Martian Thumbprint Terrain and Sinuous Ridges. Presented at the Lunar and Planetary Institute Science Conference Abstracts, p. 1127.

Rignot, E., Hallet, B., Fountain, A., 2002. Rock glacier surface motion in Beacon Valley, Antarctica, from synthetic-aperture radar interferometry. Geophys. Res. Lett. **29**, 48–1–48–4. doi:10.1029/2001GL013494

Robbins, S.J., Hynek, B.M., 2012. A new global database of Mars impact craters ≥1 km: 1. Database creation, properties, and parameters. J. Geophys. Res. Planets **117**, E05004. doi:10.1029/2011JE003966

Rodriguez, J.A.P., Fairén, A.G., Tanaka, K.L., Zarroca, M., Linares, R., Platz, T., Komatsu, G., Miyamoto, H., Kargel, J.S., Yan, J., Gulick, V., Higuchi, K., Baker, V.R., Glines, N., 2016. Tsunami waves extensively resurfaced the shorelines of an early Martian ocean. Sci. Rep. **6**. doi:10.1038/srep25106

Rossbacher, L.A., Judson, S., 1981. Ground ice on Mars: Inventory, distribution, and resulting landforms. Icarus **45**, 39–59. doi:10.1016/0019-1035(81)90005-1

Ruff, S.W., 1992. Dorsa Argentea type sinuous ridges, Mars: Evidence for linear dune hypothesis. Presented at the Martian Surface and Atmosphere Through Time, p. 126.

Ruff, S.W., Greeley, R., 1990. Sinuous Ridges of the South Polar Region, Mars: Possible Origins. Presented at the Mars: Evolution of Volcanism, Techtonics, and Volatiles, p. 253.

Sagan, C., Mullen, G., 1972. Earth and Mars: Evolution of Atmospheres and Surface Temperatures. Science **177**, 52–56. doi:10.1126/science.177.4043.52

Schaefer, M.W., 1993. The thumbprint terrain: What will Mars Observer tell us?

Schiaparelli, G.V., 1882. Decouvertes Nouvelles sur la Planete Mars. L'Astronomie 1, 216–221.

Schon, S.C., Head, J.W., 2012. Gasa impact crater, Mars: Very young gullies formed from impact into latitude-dependent mantle and debris-covered glacier deposits? Icarus **218**, 459–477. doi:10.1016/j.icarus.2012.01.002

Schon, S.C., Head, J.W., Milliken, R.E., 2009. A recent ice age on Mars: Evidence for climate oscillations from regional layering in mid-latitude mantling deposits. Geophys. Res. Lett. **36**. doi:10.1029/2009GL038554

Scott, D.H., Carr, M.H., 1978. Geologic Map of Mars.

Scott, D.H., Tanaka, K.L., 1986. Geologic map of the western equatorial region of Mars.

Scott, D.H., Underwood, J.R., Jr., 1991. Mottled terrain - A continuing Martian enigma. Presented at the Lunar and Planetary Science Conference Proceedings, pp. 627–634.

Seibert, N.M., Kargel, J.S., 2001. Small-scale Martian polygonal terrain: Implications for liquid surface water. Geophys. Res. Lett. **28**, 899–902. doi:10.1029/2000GL012093

Séjourné, A., Costard, F., Gargani, J., Soare, R.J., Fedorov, A., Marmo, C., 2011. Scalloped depressions and small-sized polygons in western Utopia Planitia, Mars: A new formation hypothesis. Planet. Space Sci. **59**, 412–422. doi:10.1016/j.pss.2011.01.007

Séjourné, A., Costard, F., Gargani, J., Soare, R.J., Marmo, C., 2012. Evidence of an eolian ice-rich and stratified permafrost in Utopia Planitia, Mars. Planet. Space Sci. **60**, 248–254. doi:10.1016/j.pss.2011.09.004

Sharp, M., 1985. "Crevasse-Fill" Ridges: A Landform Type Characteristic of Surging Glaciers? Geogr. Ann. Ser. Phys. Geogr. **67**, 213. doi:10.2307/521099

Sharp, R.P., 1973. Mars: Fretted and chaotic terrains. J. Geophys. Res. **78**, 4073–4083. doi:10.1029/JB078i020p04073

Sharp, R.P., Malin, M.C., 1975. Channels on Mars. Geol. Soc. Am. Bull. **86**, 593–609. doi:10.1130/0016-7606(1975)86<593:COM>2.0.CO;2

Skinner, J.A., Tanaka, K.L., 2007. Evidence for and implications of sedimentary diapirism and mud volcanisn in the southern Utopia highland-lowland boundary plain, Mars. Icarus **186**, 41–59.

Skinner, J.A., Tanaka, K.L., Platz, T., 2012. Widespread loess-like deposit in the Martian northern lowlands identifies Middle Amazonian climate change. Geology **40**, 1127–1130. doi:10.1130/G33513.1

Skinner Jr., J.A., Hare, T.M., Tanaka, K.L., 2006. Digital renovation of the Atlas of Mars 1:15,000,000-scale global Geologic Series maps. Lunar Planet. Sci. Conf. **37**, #2331(abstract)(online).

Skinner Jr., J.A., Mazzini, A., 2009. Martian mud volcanism: Terrestrial analogs and implications for formational scenarios. Mar. Pet. Geol., Mud Volcanism: Processes and Implications **26**, 1866–1878. doi:10.1016/j.marpetgeo.2009.02.006

Smith, D.E., Zuber, M.T., Abshire, J.B., 1993. Mars Observer laser altimeter investigation. pp. 14–18. doi:10.1117/12.157137

Smith, D.E., Zuber, M.T., Frey, H.V., Garvin, J.B., Head, J.W., Muhleman, D.O., Pettengill, G.H., Phillips, R.J., Solomon, S.C., Zwally, H.J., Banerdt, W.B., Duxbury, T.C., Golombek, M.P., Lemoine, F.G., Neumann, G.A., Rowlands, D.D., Aharonson, O., Ford, P.G., Ivanov, A.B., Johnson, C.L., McGovern, P.J., Abshire, J.B., Afzal, R.S., Sun, X., 2001. Mars Orbiter Laser Altimeter: Experiment summary after the first year of global mapping of Mars. J. Geophys. Res. Planets **106**, 23689–23722. doi:10.1029/2000JE001364

Smith, P.H., Tamppari, L.K., Arvidson, R.E., Bass, D., Blaney, D., Boynton, W.V., Carswell, A., Catling, D.C., Clark, B.C., Duck, T., DeJong, E., Fisher, D., Goetz, W., Gunnlaugsson, H.P., Hecht, M.H., Hipkin, V., Hoffman, J., Hviid, S.F., Keller, H.U., Kounaves, S.P., Lange, C.F., Lemmon, M.T., Madsen, M.B., Markiewicz, W.J., Marshall, J., McKay, C.P., Mellon, M.T.,

Ming, D.W., Morris, R.V., Pike, W.T., Renno, N., Staufer, U., Stoker, C., Taylor, P., Whiteway, J.A., Zent, A.P., 2009. H2O at the Phoenix Landing Site. Science **325**, 58–61. doi:10.1126/science.1172339

Smoluchowski, R., 1968. Mars: Retention of Ice. Science **159**, 1348–1350. doi:10.1126/science.159.3821.1348

Soare, R.J., Kargel, J.S., Osinski, G.R., Costard, F., 2007. Thermokarst processes and the origin of crater-rim gullies in Utopia and western Elysium Planitia. Icarus **191**, 95–112. doi:10.1016/j.icarus.2007.04.018

Soare, R.J., Osinski, G.R., 2009. Stratigraphical evidence of late Amazonian periglaciation and glaciation in the Astapus Colles region of Mars. Icarus **202**, 17–21. doi:10.1016/j.icarus.2009.02.009

Soare, R.J., Osinski, G.R., Roehm, C.L., 2008. Thermokarst lakes and ponds on Mars in the very recent (late Amazonian) past. Earth Planet. Sci. Lett. **272**, 382–393. doi:10.1016/j.epsl.2008.05.010

Souness, C., Hubbard, B., 2012. Mid-latitude glaciation on Mars. Prog. Phys. Geogr. **36**, 238–261. doi:10.1177/0309133312436570

Souness, C., Hubbard, B., Milliken, R.E., Quincey, D., 2012. An inventory and population-scale analysis of martian glacier-like forms. Icarus **217**, 243–255. doi:10.1016/j.icarus.2011.10.020

Squyres, S.W., 1979. The distribution of lobate debris aprons and similar flows on Mars. J. Geophys. Res. Solid Earth 84, 8087–8096. doi:10.1029/JB084iB14p08087

Squyres, S.W., 1978. Martian fretted terrain: Flow of erosional debris. Icarus **34**, 600–613. doi:10.1016/0019-1035(78)90048-9

Squyres, S.W., Carr, M.H., 1986. Geomorphic Evidence for the Distribution of Ground Ice on Mars. Science **231**, 249–252. doi:10.2307/1696642

Squyres, S.W., Kasting, J.F., 1994. Early Mars: How Warm and How Wet? Science **265**, 744–749. doi:10.1126/science.265.5173.744

Stern, S.A., 1992. The Pluto-Charon system. Annu. Rev. Astron. Astrophys. 30, 185–233. doi:10.1146/annurev.aa.30.090192.001153

Tanaka, K.L., 1997. Sedimentary history and mass flow structures of Chryse and Acidalia Planitiae, Mars. J. Geophys. Res. Planets **102**, 4131–4149. doi:10.1029/96JE02862

Tanaka, K.L., 1986. The stratigraphy of Mars. J. Geophys. Res. Solid Earth **91**, E139–E158. doi:10.1029/JB091iB13p0E139

Tanaka, K.L., Banerdt, W.B., Kargel, J.S., Hoffman, N., 2001. Huge, CO2-charged debris-flow deposit and tectonic sagging in the northern plains of Mars. Geology **29**, 427–430. doi:10.1130/0091-7613(2001)029<0427:HCCDFD>2.0.CO;2

Tanaka, K.L., Carr, M.H., Skinner, J.A., Gilmore, M.S., Hare, T.M., 2003. Geology of the MER 2003 "Elysium" candidate landing site in southeastern Utopia Planitia, Mars. J. Geophys. Res. Planets 108, 8079. doi:10.1029/2003JE002054

Tanaka, K.L., Isbell, N.K., Scott, D.H., Greeley, R., Guest, J.E., 1988. The resurfacing history of Mars: a synthesis of digitized, Viking-based geology. Lunar Planet. Sci. Conf. 18, 665–678.

Tanaka, K.L., Robbins, S.J., Fortezzo, C.M., Skinner Jr., J.A., Hare, T.M., 2014. The digital global geologic map of Mars: Chronostratigraphic ages, topographic and crater morphologic characteristics, and updated resurfacing history. Planet. Space Sci., Planetary Geology Field Symposium, Kitakyushu, Japan, 2011: Planetary Geology and Terrestrial Analogs 95, 11–24. doi:10.1016/j.pss.2013.03.006

Tanaka, K.L., Scott, D.H., 1987a. Geologic map of the polar regions of Mars.

Tanaka, K.L., Skinner, J.A., Hare, T.M., 2005. Geologic map of the northern plains of Mars.

Tanaka, K.L., Skinner, J.A., Hare, T.M., Joyal, T., Wenker, A., 2003. Resurfacing history of the northern plains of Mars based on geologic mapping of Mars Global Surveyor data. J. Geophys. Res. Planets **108**, 8043. doi:10.1029/2002JE001908

Tanaka, K.L., Skinner Jr., J.A., Dohm, J.M., Rossman, R.I.I., Kolb, E.J., Fortezzo, C.M., Platz, T., Michael, G.G., Hare, T.M., 2014. Geologic map of Mars.

Taylor, J., Teanby, N.A., Wookey, J., 2013. Estimates of seismic activity in the Cerberus Fossae region of Mars. J. Geophys. Res. Planets **118**, 2570–2581. doi:10.1002/2013JE004469

Thomas, R.J., 2013. Identification of possible recent water/lava source vents in the Cerberus plains: Stratigraphic and crater count age constraints. J. Geophys. Res. Planets **118**, 789–802. doi:10.1002/jgre.20071

Thomson, S.N., Brandon, M.T., Tomkin, J.H., Reiners, P.W., Vásquez, C., Wilson, N.J., 2010. Glaciation as a destructive and constructive control on mountain building. Nature **467**, 313–317. doi:10.1038/nature09365

Tinkler, K.J., Wohl, E., 1998. Rivers Over Rock: Fluvial Processes in Bedrock Channels. American Geophysical Union.

Torre, J.R. de la, Goebel, B.M., Friedmann, E.I., Pace, N.R., 2003. Microbial Diversity of Cryptoendolithic Communities from the McMurdo Dry Valleys, Antarctica. Appl. Environ. Microbiol. **69**, 3858–3867. doi:10.1128/AEM.69.7.3858-3867.2003

Touma, J.R., Wisdom, J., 1993. The chaotic obliquity of Mars.

Treiman, A.H., 2003. Geologic settings of Martian gullies: Implications for their origins. J. Geophys. Res. Planets **108**, 8031. doi:10.1029/2002JE001900

Turtle, E.P., Pathare, A.V., Crown, D.A., Chuang, F.C., Hartmann, W.K., Heinze, J.C., Bueno, N.F., 2003. Modeling the Deformation of Lobate Debris Aprons on Mars by Creep of Ice-rich Permafrost. AGU Fall Meet. Abstr. 1, 0830.

Ulrich, M., Hauber, E., Herzschuh, U., Härtel, S., Schirrmeister, L., 2011. Polygon pattern geomorphometry on Svalbard (Norway) and western Utopia Planitia (Mars) using high-resolution stereo remote-sensing data. Geomorphology **134**, 197–216. doi:10.1016/j.geomorph.2011.07.002

Ulrich, M., Morgenstern, A., Günther, F., Reiss, D., Bauch, K.E., Hauber, E., Rössler, S., Schirrmeister, L., 2010. Thermokarst in Siberian ice-rich permafrost: Comparison to asymmetric scalloped depressions on Mars. J. Geophys. Res. Planets **115**, E10009. doi:10.1029/2010JE003640

Ulrich, M., Wagner, D., Hauber, E., de Vera, J.-P., Schirrmeister, L., 2012. Habitable periglacial landscapes in martian mid-latitudes. Icarus **219**, 345–357. doi:10.1016/j.icarus.2012.03.019

Ulrich, R.K., 1975. Solar Neutrinos and Variations in the Solar Luminosity. Presented at the The Solar Constant and the Earth's Atmosphere, p. 263.

van Gasselt, S., Hauber, E., Neukum, G., 2010. Lineated valley fill at the Martian dichotomy boundary: Nature and history of degradation. J. Geophys. Res. Planets **115**. doi:10.1029/2009JE003336

Vaucher, J., Baratoux, D., Mangold, N., Pinet, P., Kurita, K., Grégoire, M., 2009a. The volcanic history of central Elysium Planitia: Implications for martian magmatism. Icarus **204**, 418–442. doi:10.1016/j.icarus.2009.06.032

Vaucher, J., Baratoux, D., Toplis, M.J., Pinet, P., Mangold, N., Kurita, K., 2009b. The morphologies of volcanic landforms at Central Elysium Planitia: Evidence for recent and fluid lavas on Mars. Icarus **200**, 39–51. doi:10.1016/j.icarus.2008.11.005

Vetterlein, J., Roberts, G.P., 2003. Cracking up: faulting on Earth and Mars. Astron. Geophys. **44**, 4.22-4.22. doi:10.1046/j.1468-4004.2003.44422.x

Villanueva, G.L., Mumma, M.J., Novak, R.E., Käufl, H.U., Hartogh, P., Encrenaz, T., Tokunaga, A., Khayat, A., Smith, M.D., 2015. Strong water isotopic anomalies in the martian atmosphere: Probing current and ancient reservoirs. Science **348**, 218–221. doi:10.1126/science.aaa3630

Vincendon, M., Forget, F., Mustard, J., 2010a. Water ice at low to midlatitudes on Mars. J. Geophys. Res. **115**. doi:10.1029/2010JE003584

Vincendon, M., Mustard, J., Forget, F., Kreslavsky, M., Spiga, A., Murchie, S., Bibring, J.-P., 2010b. Near-tropical subsurface ice on Mars. Geophys. Res. Lett. **37**. doi:10.1029/2009GL041426

Voelker, M., Hauber, E., van Gasselt, S., Jaumann, R., 2015. Grid Mapping of Hellas Planitia - Preliminary Results from the Northern Impact Rim, in: European Planetary Science Congress 10. Presented at the European and Planetary Science Congress, Nantes, Frankreich.

Walder, J., Hallet, B., 1979. Geometry of former subglacial water channels and cavities. J. Glaciol. 23, 335–346.

Ward, W.R., 1992. Long-term orbital and spin dynamics of Mars. Mars **1**, 298–320.

Wilhelms, D.E., Squyres, S.W., 1984. The martian hemispheric dichotomy may be due to a giant impact. Nature **309**, 138–140. doi:10.1038/309138a0

Williams, R.M.E., Irwin III, R.P., Zimbelman, J.R., 2009. Evaluation of paleohydrologic models for terrestrial inverted channels: Implications for application to martian sinuous ridges. Geomorphology **107**, 300–315. doi:10.1016/j.geomorph.2008.12.015

Wilson, J., 2016. Image reconstruction of remotely-sensed planetary data. Ph.D Thesis.

Wilson, L., Mouginis-Mark, P.J., 2003. Phreatomagmatic explosive origin of Hrad Vallis, Mars. J. Geophys. Res. Planets **108**, 5082. doi:10.1029/2002JE001927

Wilson, S.A., Zimbelman, J.R., 2004. Latitude-dependent nature and physical characteristics of transverse aeolian ridges on Mars. J. Geophys. Res. Planets **109**, E10003. doi:10.1029/2004JE002247

Wise, D.U., Golombek, M.P., McGill, G.E., 1979. Tharsis province of Mars: Geologic sequence, geometry, and a deformation mechanism. Icarus **38**, 456–472. doi:10.1016/0019-1035(79)90200-8

Zanetti, M., Hiesinger, H., Reiss, D., Hauber, E., Neukum, G., 2010. Distribution and evolution of scalloped terrain in the southern hemisphere, Mars. Icarus, Cassini at Saturn **206**, 691–706. doi:10.1016/j.icarus.2009.09.010

Zanetti, M., Hiesinger, H., Reiss, D., Hauber, E., Neukum, G., 2009. Scalloped Depression Development on Malea Planum and the Southern Wall of the Hellas Basin, Mars. Presented at the Lunar and Planetary Science Conference, p. 2178.

Zimbelman, J.R., Griffin, L.J., 2010. HiRISE images of yardangs and sinuous ridges in the lower member of the Medusae Fossae Formation, Mars. Icarus, MRO/HiRISE Studies of Mars **205**, 198–210. doi:10.1016/j.icarus.2009.04.003